Dynamic organization of bacterial chromatin by DNA bridging proteins
Qin, L.

Citation
Qin, L. (2020, September 22). *Dynamic organization of bacterial chromatin by DNA bridging proteins*. Retrieved from https://hdl.handle.net/1887/136909

Version:	Publisher's Version
License:	[Licence agreement concerning inclusion of doctoral thesis in the Institutional Repository of the University of Leiden](#)
Downloaded from:	[https://hdl.handle.net/1887/136909](#)

Note: To cite this publication please use the final published version (if applicable).

Cover Page

Universiteit Leiden

Leiden University Repository

The handle http://hdl.handle.net/1887/136909 holds various files of this Leiden University dissertation.

Author: Qin, L.
Title: Dynamic organization of bacterial chromatin by DNA bridging proteins
Issue Date: 2020-09-22

Dynamic organization of bacterial chromatin by DNA bridging proteins

Proefschrift

ter verkrijging van

de graad van Doctor aan de Universiteit Leiden,

op gezag van Rector Magnificus prof.mr. C.J.J.M. Stolker,

volgens besluit van het College voor Promoties

te verdedigen op dinsdag 22 september 2020

klokke 11:15

door

Liang Qin

geboren te Liaoning, China in 1990

Dynamic organization of bacterial chromatin by DNA bridging proteins

Liang Qin

Doctoral thesis, Leiden University, 2020

Cover design: Liang Qin

If we knew what we were doing, it wouldn't be called research, would it?

- Albert Einstein

To my family and friends

Table of contents

Chapter 1

Introduction

Part of this chapter is based on the following review article:

Qin, L., Erkelens, A. M., Ben Bdira, F., & Dame, R. T. (2019). The architects of bacterial DNA bridges: a structurally and functionally conserved family of proteins. Open Biology, 9(12), 190223.

The chapter was jointly written by L.Q. and A.M.E.. F.B.B. performed protein structural analysis and contributed to writing.

Abstract

Every organism across the tree of life compacts and organizes its genome with architectural chromatin proteins. While eukaryotes and archaea express histone proteins, the organization of bacterial chromosomes is dependent on nucleoid-associated proteins (NAPs). In *Escherichia coli* and other proteobacteria, the histone-like nucleoid structuring protein (H-NS) acts as a global genome organizer and gene regulator. Functional analogs of H-NS have been found in other bacterial species: MvaT in *Pseudomonas* species, Lsr2 in actinomycetes and Rok in *Bacillus* species. These proteins complement *hns⁻* phenotypes and have similar DNA-binding properties, despite their lack of sequence homology. In this review, we focus on the structural and functional characteristics of these four architectural proteins. They are able to bridge DNA duplexes, which is key to genome compaction and gene regulation and their response to changing conditions in the environment. Structurally the domain organization and charge distribution of these proteins is conserved, which we suggest is at the basis of their conserved environment responsive behavior. These observations could be used to find and validate new members of this protein family and to predict their response to environmental changes.

1. Introduction

All organisms compact and organize their genomic DNA. Structuring of the genome is achieved by the action of small, basic architectural proteins that interact with DNA. These proteins wrap, bend and bridge DNA duplexes. Despite the lack of both sequence and structural homology between architectural proteins in species across the tree of life, the basic concepts appear conserved, with all organisms harboring functional analogs[1]. An essential feature of genome organization is its intrinsic coupling to genome transactions, such that a process like gene expression is both dependent upon chromatin structure and a driving factor in chromatin (re)organization[2]. The structure of chromatin is affected by environmental signals, which can be translated in altered gene expression[3].

No doubt the best known architectural proteins are the histones expressed by eukaryotes. Binding of these proteins yields nucleosomes in which DNA is wrapped around an octameric histone protein core. Aided by other architectural proteins these nucleosomal fibers are further organized into higher order structures[1,4–6]. Histone H1 and BAF (barrier-to-autointegration factor) are examples of eukaryotic architectural proteins that are capable of bridging DNA[7,8]. In addition, Structural Maintenance of Chromosome (SMC) proteins (e.g. cohesin and condensin) act upon chromatin, forming large chromatin loops by bridging, at the expense of ATP[9]. SMC proteins are the only chromatin proteins that are universally conserved[10,11]. Finally, eukaryotes express small proteins that bend DNA, such as HMG-box proteins[12]. Archaea also express histones. Different from their eukaryotic counterparts, archaeal histones assemble into oligomeric filaments along DNA, yielding hypernucleosomes[13–16]. In addition they express DNA bridging proteins such as Alba (acetylation lowers binding affinity), which can both form nucleofilaments and bridge DNA, depending on the protein:DNA stoichiometry[17,18]. Some archaeal species lack histones and these express DNA bending proteins instead, like Cren7 and Sul7[19].

Bacteria lack homologues of the histone proteins expressed by eukaryotes and archaea. The organization of bacterial genomes is dependent on a group of architectural proteins collectively referred to as nucleoid-associated proteins (NAPs). At least 12 NAPs have been described for *Escherichia coli* and closely related species[20–22]. A shared feature of many of these proteins is their ability to bend DNA. Examples include the histone-like protein from strain U93

11

(HU), integration host factor (IHF) and the factor for inversion stimulation (Fis)[23–25]. The histone-like nucleoid structuring protein (H-NS) has an overarching role in organization of the *E. coli* genome and acts as a global regulator of gene expression: 5-10% of *E. coli* genes are affected, mostly repressed, by H-NS[26]. Due to its preference for A/T-rich DNA, it specifically targets and silences horizontally acquired genes, a process referred to as xenogeneic silencing[27]. Key to the role of H-NS in both processes is the formation of nucleofilaments along the DNA and protein-mediated DNA-DNA bridges[28–30]. H-NS like proteins are passive DNA bridgers in contrast to SMC proteins which are active, ATP-driven DNA bridgers (figure 1.1).
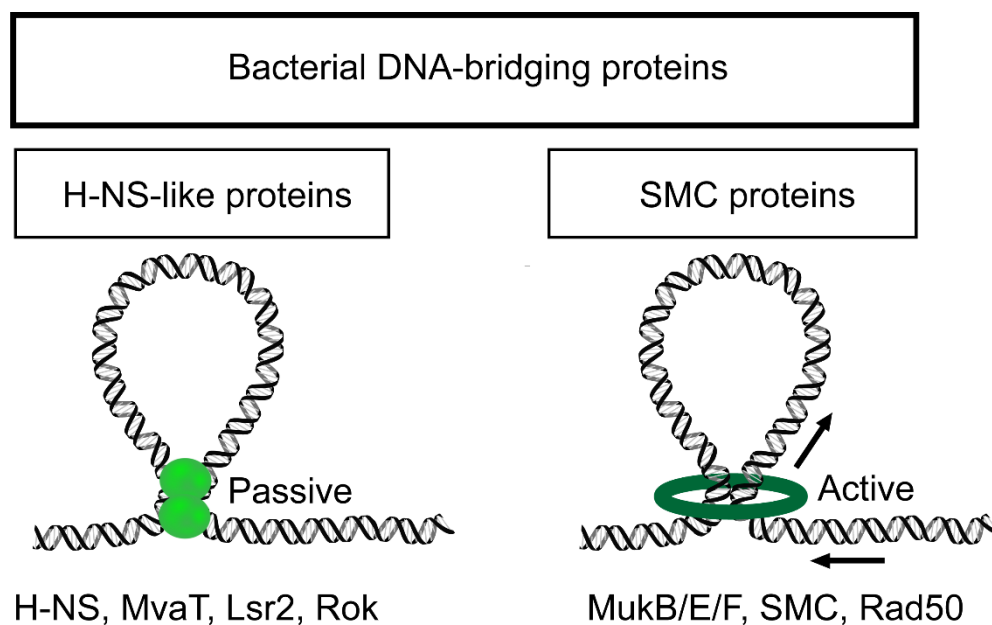

Figure 1.1: Bacterial DNA-bridging proteins. Two types can be distinguished: passive DNA bridgers such as H-NS-like proteins (light green), which bind distant segments of DNA duplexes and bring them together, and active DNA bridgers such as SMC proteins (dark green), that are able to connect two double stranded DNA segments, translocating along the DNA molecule with motor activity resulting from ATP hydrolysis. Note that the exact molecular mechanisms by which SMC proteins operate and are involved in loop formation only start to be defined and are a topic of much discussion.

Over the last two decades functional homologs of H-NS have been identified in other bacterial species. Despite low sequence similarity, these proteins have similar DNA binding properties, resulting in the formation of structurally and functionally similar protein-DNA complexes. This ability is elegantly demonstrated by the genetic complementation of *hns*⁻ phenotypes (like mucoidy, motility and β-glucoside utilization) in *E. coli* by MvaT from *Pseudomonas* species and

Lsr2 from *Mycobacterium* and related actinomycetes[31,32]. *In vitro* both proteins are also able to bridge DNA in a manner similar to H-NS[28,33,34] (figure 1.1). MvaT regulates hundreds of genes in *P. aeruginosa* and Lsr2 binds to one fifth of the *M. tuberculosis* genome, especially to horizontally acquired genes[35–38]. These properties endow them with functions as global gene regulators and spatial chromatin organizers. A newly proposed functional homolog of H-NS is the repressor of *comK* protein (Rok) of *Bacillus subtilis.* This classification is primarily based on the observation that Rok binds extended regions of the *B. subtilis* genome and especially A/T rich regions acquired by horizontal gene transfer, which it aids to repress[39]. This specific property of silencing foreign genes makes Rok, just like H-NS, MvaT and Lsr2, a xenogeneic silencer. It is also associated with a large subset of chromosomal domain boundaries identified in *B. subtilis* by Hi-C[40]. As such boundaries might involve genome loop formation, this could imply a role as DNA bridging architectural protein.

In this review we focus on the properties of DNA bridging proteins in bacteria with a proposed role in genome architecture and gene regulation: H-NS, MvaT, Lsr2 and Rok. We describe and compare their structure and function to define conserved features. Also, we discuss the mechanisms by which the architectural and regulatory properties of these proteins are modulated.

2. Fold topology of H-NS-like proteins

Structural studies have revealed that H-NS, Lsr2 and MvaT harbor similar functional modules: 1) an N-terminal oligomerization domain consisting of two dimerization sites, 2) a C-terminal DNA binding domain and 3) an unstructured linker region (figure 1.2 a,b and c)[41–45]. For Rok a similar overall domain architecture has been found: the C-terminal domain is capable of DNA binding and the N-terminal domain is responsible for oligomerization (figure 1.2d)[46].

a. The N-terminal domain

The N-terminal domain of H-NS and MvaT is involved in the formation of oligomers, which is a property essential for gene repression[37,47]. Both Lsr2 and Rok are capable of oligomerization, but it is currently unknown whether oligomerization is required for gene regulation[41,46]. As the N-terminal structure of most of these DNA bridging proteins is known, differences and similarities in

the mechanism of forming high-order complexes have become evident. H-NS of *Salmonella typhymurium* has two dimerization sites in the N-terminal domain (1-83)[42]. The N-terminal dimerization domain (site 1, 1-40) is formed by a "hand-shake" topology between α1 and α2 and part of α3. The central dimerization domain (site 2, 57–83), has two α-helices α3 and α4 that form a helix-turn-helix dimerization interface. H-NS dimers are formed via site 1 in a tail-to-tail manner, which can oligomerize via site 2 via head-to-head association (figure 1.2a). The resulting crystal structure is superhelical. Therefore, it was proposed that DNA-H-NS-DNA filaments involve superhelical wrapping of DNA around an oligomeric protein core. However, apart from the X-ray crystal structure[42], there is no evidence for this type of H-NS nucleofilaments organization.

The crystal structure of the MvaT homologue, TurB from *Pseudomonas putida,* revealed a similar fold topology of the N-terminal dimerization site 2 as that of H-NS [43]. In contrast, site 1 exhibits a standard "coiled-coil" architecture in MvaT/TurB, whereas H-NS due to the presence of two additional N-terminal helices (α1 and α2 in H-NS) compared to TurB/MvaT exhibits a "hand-shake" topology (figure 1.2). Despite this difference in site 1, both proteins form a head-head and tail-tail dimers organization in their protein filaments.

The N-terminal structure of Lsr2 from *Mycobacterium tuberculosis*, however, is completely different from that of H-NS and MvaT[41]. The flexible N-terminus is followed by a β-sheet formed by two anti-parallel β-strands and a kinked α-helix. When forming dimers, the two β-sheets of the monomers align to form a four-stranded antiparallel β-sheet with an antiparallel arrangement of the α-helices on the opposite sides of the sheet (figure 1.2c). Notably, oligomerization does not occur with the first four amino acids of Lsr2 of *M. tuberculosis* present, but is triggered by trypsin cleavage, removing these residues [41]. The oligomerization between Lsr2 dimers occurs through an antiparallel association between two N-terminal β-strands from adjacent monomers (figure 1.2c). The triggering of Lsr2 oligomerization by proteolysis indicates that this process is possibly controlled via protease-activity *in vivo*, offering a mechanism for genome protection by Lsr2 under stress conditions[48]. Note, however, that these four amino acids are not highly conserved and for example are lacking in *Mycobacterium sinensis* Lsr2 (Genbank: AEF37887.1)*.

Although the 3D-structure of Rok's N-terminal domain has not been experimentally determined, it is predicted to contain two α-helices (α1 and α2) and a part of the first α-helix (residues 1-43) is predicted to form a "coiled coil" dimerization motif [49,50] (figure 1.2d), similar to

MvaT. Based on these secondary structure predictions it is plausible that Rok exhibits higher order oligomerization with a structural organization resembling that of TurB/MvaT.

b. The C-terminal domain

The C-terminal domain of all four proteins recognizes and binds to DNA. *In vivo* the DNA segments bound are generally AT-rich compared to other parts of the genome. Although H-NS and Lsr2 differ in overall structure of the C-terminal domain, both proteins recognize the minor groove of DNA with a similar 'AT-hook-like' motif composed of three consecutive residues 'Q/RGR'[44] (figure 1.2a,c). H-NS and Lsr2 generally favor similar AT-rich DNA target sequences, both with a preference for TpA steps over A-tracts[44]. This can be related to the width of the minor groove. A-tracts narrow the minor groove in comparison to TpA steps, while GC-rich sequences result in a wider minor groove. TpA steps result in a favorable width for H-NS and Lsr2 binding to the DNA[44].

The C-terminal domain of MvaT exhibits a similar overall fold as H-NS, but has a different DNA binding mechanism[45] (figure 1.2b). The C-terminus of MvaT recognizes AT-rich DNA via both the "AT-pincer" motif consisting of three non-continuous residues 'R-G-N' targeting minor groove DNA, and a "lysine network" interacting with the DNA backbone by multiple positive charges. In general, MvaT has similar preferences in binding DNA sequences as H-NS and Lsr2, preferring TpA steps over A-tracts[45]. MvaT is however more tolerant to G/C interruptions in the DNA sequence than H-NS and Lsr2.

Binding of the C-terminal domain of H-NS and Lsr2 to DNA causes no notable changes in DNA conformation[36,44], whereas the C-terminus of MvaT triggers significant distortions in the DNA molecule[45]. It is likely that the 'AT-hook motif' of H-NS and Lsr2 forms a narrow crescent shaped structure that inserts into the minor groove without significantly interrupting the DNA helical trajectory. When bound by the C-terminal domain of MvaT, the minor groove of DNA is expanded leading to a significant rearrangement in base-stacking[45]. Therefore, binding of full length MvaT dimers to DNA results in DNA bending (see Chapter 2) [51].
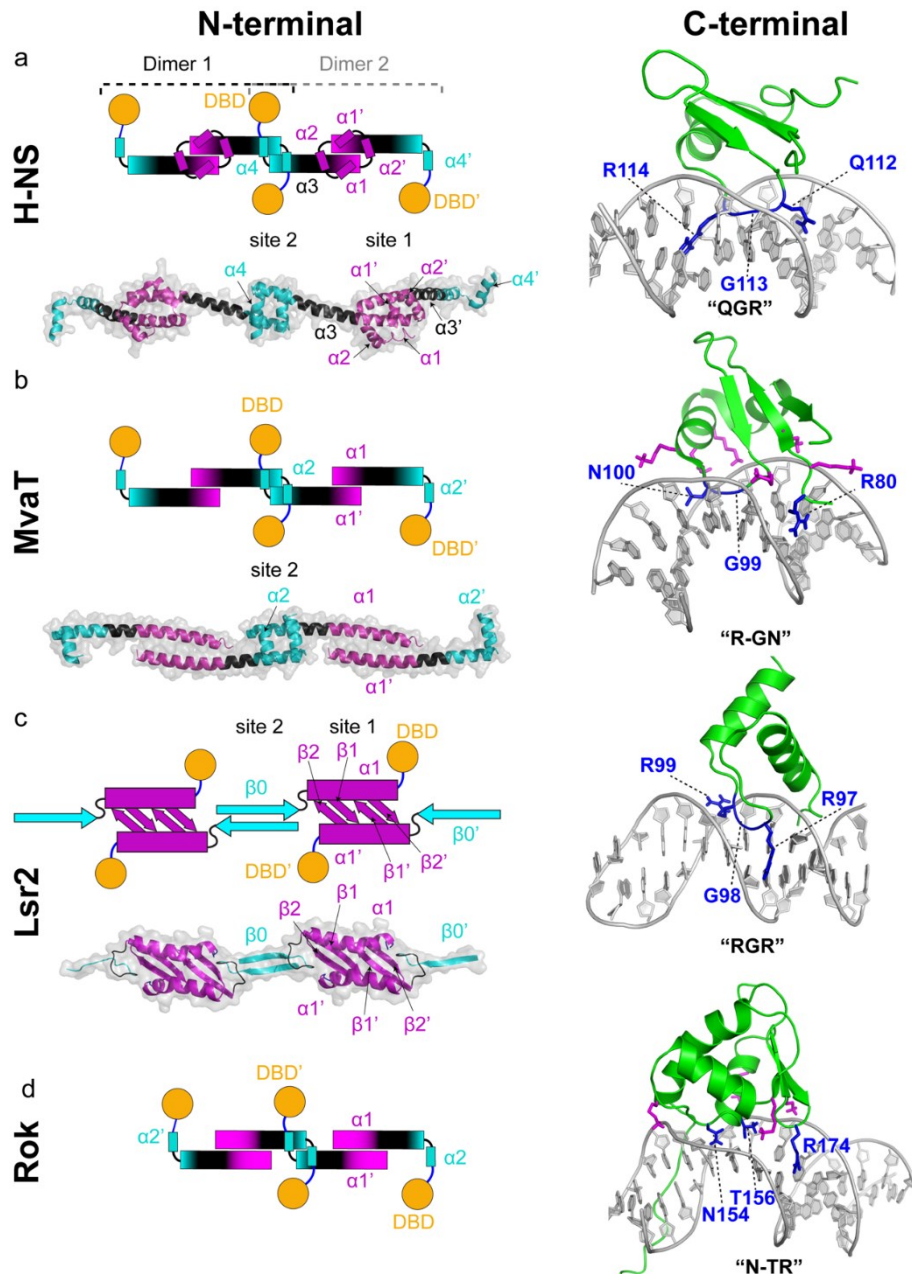
Figure 1.2: Fold topology and oligomerization states of H-NS like proteins. Left panels show models of the structures of the N-terminal oligomerization domains of (a) H-NS[42], (b) MvaT[43] and (c) Lsr2[41] as determined by crystallography. A schematic representation of the higher order oligomerization states of H-NS like proteins is shown above the crystal structures of the N-terminal domains. For Rok (d) the schematic representation of its higher order oligomerization state is based on secondary structure prediction. The dimerization sites (site 1) are shown in magenta and the oligomerization sites (site 2) in cyan. The DNA binding domains are shown in orange spheres and the linker regions in blue lines. Right panels show the NMR structures of the DNA binding domains of H-NS like proteins and their DNA recognition mechanisms[46].

The loops of the DNA binding motif are shown in blue and the residues involved in the direct interactions to the DNA minor groove and in the complex stabilization are shown in sticks.

The structure of the C-terminal DNA-binding domain of Rok reveals that it employs a winged helix domain fold utilizing a unique DNA recognition mechanism different from the other three proteins[46] (figure 1.2d). Rather than using an 'AT-hook-like' motif or 'AT-pincer' motif, the C-terminus of Rok targets the DNA minor groove via the three non-continuous residues N-T-R. As in the case of MvaT, DNA binding is stabilized by a hydrogen bond network between several lysine residues and the phosphate groups of the DNA backbone[46]. Similar to H-NS, Lsr2 and MvaT, Rok interacts with AT-rich DNA sequences with a preference for TpA steps[46]. Rok has selectivity towards some specific DNA sites, comparable with the affinity of H-NS for its high-affinity sites, where the highest affinity is noticed for AACTA and TACTA sequences [52]. Compared to MvaT, Rok induces a more pronounced conformational change in its target DNA substrate. Rok binding leads to bending of DNA by ~25 degrees[46].

The function of the conformational changes in target DNA induced by MvaT and Rok binding is unknown, but the changes may be of importance in gene regulation, where often multiple architectural proteins operate in concert. An example of this is the reversion of Rok repression by ComK at the *comK* promotor[53]. It has been suggested that the DNA-bending by Comk reverses the conformational changes in the DNA induced by Rok.

3. Protein-DNA complexes formed by H-NS like proteins

Two types of protein-DNA complexes can be formed by H-NS like proteins: 1) nucleoprotein filaments and 2) bridged complexes. Assembly of protein-DNA complexes by H-NS, MvaT and Lsr2 is believed to proceed via a multi-step process (figure 1.3). First, the C-terminal DNA-binding domain directs the protein to a high-affinity site (nucleation) [52]. This step is likely assisted by the positively charged amino acid residues of the linker region which interact with the DNA and recruit H-NS to bind non-specifically [54–56]. This then allows H-NS to scan on DNA to search for the specific site where the C-terminal domain can engage with a higher affinity. Next, the proteins spread cooperatively along the DNA forming a nucleoprotein filament by oligomerization through their N-terminal domains. If the surrounding conditions are favorable,

these nucleoprotein filaments can interact with another DNA duplex to form a bridge. Both types of protein-DNA complexes are thought to play important roles in genome structuring and gene silencing. Evidence in support of formation of nucleoprotein filaments comes from atomic force microscopy (AFM) and single-molecule studies which revealed that H-NS, Lsr2 and MvaT all form rigid protein-DNA filaments, suggestive of protein oligomerization along DNA[30,57–60]. DNA-DNA bridging has been visualized *in vitro* using microscopy[28,33,34] and corroborated using solution based assays[29,61]. The ability to oligomerize is important for the function of these proteins in chromosome organization and gene regulation[37,59,60]. To date, there are no indications that Rok rigidifies DNA suggesting that this protein might not be able to oligomerize along DNA. Nevertheless, the protein induces DNA compaction and is capable of DNA-DNA bridging (see Chapter 4) [62].
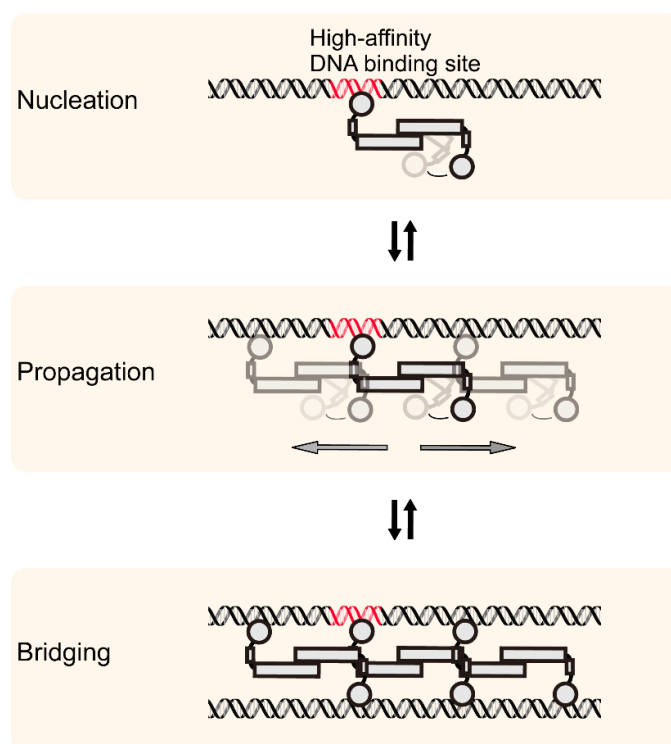
Figure 1.3: Assembly of functional protein-DNA complexes by H-NS-like proteins. DNA binding of H-NS-like proteins initiates at a nucleation site (high affinity binding site, red) in the genome; H-NS-like proteins propagate along DNA in a cooperative way due to protein-protein interactions; DNA-protein-DNA bridging complex can be formed under favorable bridging conditions, bringing distant DNA duplexes together. Further propagation (not indicated in the figure) may occur in the bridged complex due to both protein-

protein interactions and high effective local DNA concentration. Note that all steps are reversible, which is important for modulation of the function of these proteins (section 5).

Following the initial observations that two types of complexes can be formed[34,37,58,60,63], the mechanism that drives the switch between these two DNA binding modes has long been elusive. Two recent studies on H-NS have provided the first mechanistic insights into this process [61,64]. The switch between the two DNA binding modes[58] involves a conformational change of the H-NS dimers from a half-open to an open conformation driven by Mg^{2+} [61]. These conformational changes are modulated by the interactions between the N-terminal domain of H-NS and its C-terminal DNA binding domain. Mutagenesis at the interface of these domains generated an H-NS variant no longer sensitive to Mg^{2+}, which can form filaments and bridge DNA[61]. Recently, these interactions were confirmed by Arold and co-workers using H-NS truncated domains[64]. The linker of H-NS was shown to be essential for the interdomain interaction between the N-terminal and C-terminal domain[64]. Studies on MvaT in our lab further support a model in which both an increase in ionic strength and the DNA substrate additively destabilize these interdomain interactions, inducing the dimers to release their second DNA binding domain to bind and bridge a second DNA molecule in trans (figure 1.4a, see Chapter 2) [51].

The interdomain interactions described above for H-NS and MvaT might be driven by the asymmetrical charge distribution within the protein sequence: the N-terminal domain is mainly negatively charged, while the linker and the DNA-binding motif are positively charged (figure 1.4b, c). Analysis of the average charge of the primary sequences of H-NS like proteins revealed that this characteristic is a conserved feature among H-NS/MvaT proteins across species and extends to Lsr2 (figure 1.4b, c, d and supplementary figure, see Chapter 2)[51]. The conserved asymmetrical charge distribution might provide an explanation for how H-NS, MvaT and Lsr2 act as sensors of environmental changes. For Rok this asymmetrical charge distribution between its folded domains is less pronounced (figure 1.4e). In addition to that, Rok contains a neutral Q linker instead of the basic linker integrated in H-NS, MvaT and Lsr2 polypeptide chains. Previously, the Q linker was defined as a widespread structural element connecting distinct functional domains in bacterial regulatory proteins[65]. Thus, the difference in charge distribution and the linker region between Rok and the other proteins could have functional implications (see section 5).
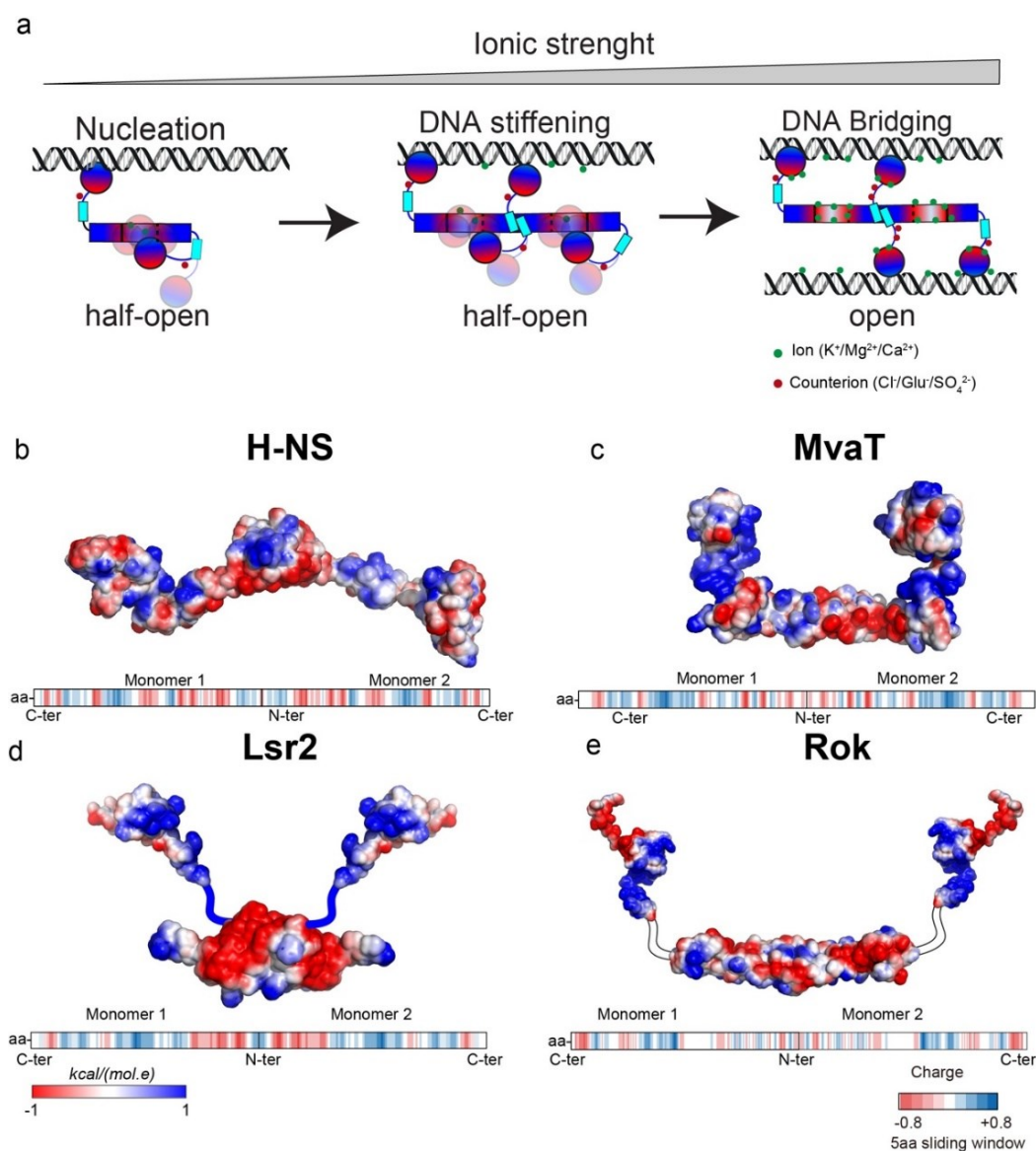
Figure 1.4: H-NS like proteins DNA binding modes and Electrostatics: (a) Schematic representation of the switching mechanism between H-NS like proteins DNA binding modes. The red/blue gradient represents the electrostatics of H-NS like protein surfaces (see Chapter 2) [51,61]. The red and blue are for negatively and positively charged surface regions, respectively. The electrostatic potential surface of (b) H-NS, (c) MvaT, (d) Lsr2 and (e) Rok are depicted on full-length protomer structural models of the proteins using a red/white/blue color gradient. The missing linkers in the structural models of Lrs2 and Rok are shown in blue (positively charged) and white (neural), respectively. In the lower panel the five amino acid sliding window averaged charge of the proteins protomers primary sequences generated by EMBOSS charge is shown. Positive, negative and neutral charged amino acid fragments are shown in blue, red and white bars, respectively.

4. Functional properties

a. genome organization

The chromosomal DNA of *E.coli* is structured into domains of various sizes[66]. The first layer of organization involves division in four macrodomains (Ori, Ter, Right and Left) of about 1 Mb in size[67–70]. Although it is not completely clear how the borders of these domains are formed, several *E. coli* DNA-binding proteins (e.g. SeqA, SlmA and MatP) are associated with certain macrodomains only [70–73]. One scale smaller, microdomains have been described of roughly 10 kb in size, which are attributed to loop formation in *E.coli* [74–77]. H-NS is important for domain formation *in vivo* and the distribution of H-NS along the chromosome is suggestive of a role in establishing microdomains[75,78]. Recently, it was shown with Hi-C that H-NS mediates short range contacts along the chromosome[79]. The DNA bridging ability of H-NS matches well with the structural properties detected *in vivo*. Genome-wide 3C-based studies reveal chromosomal interaction domains (CIDs) along the chromosome in *Caulobacter crescentus, B. subtilis* and *Vibrio cholerae*[40,80,81]. These domains are tens to hundreds kb in size and the boundaries of CIDs are often formed by highly transcribed genes[80].

It is likely that the other DNA bridging proteins organize the bacterial genome in similar ways. The genome of *B. subtilis* consists of three global domains and local smaller domains[40]. A subset of the barriers between local domains corresponds to genomic positions bound by Rok[39,40]. This suggests a role for Rok in the genome organization of *B. subtilis.* For *Pseudomonas* and *Mycobacterium* species, such studies have not been done yet. But ChIP-on-chip data shows that MvaT and Lsr2 bind to defined regions throughout the whole genome[35,36], in support of a similar role in genome organization as H-NS and Rok.

b. gene regulation by H-NS-like proteins

There has been a lot of discussion in the field as to which DNA binding mode is relevant *in vivo* and which of the two modes is needed for gene silencing. The short answer is that both modes of binding could explain gene repression. H-NS-DNA filament formation at or across a promotor region potentially occludes RNA polymerase (RNAP), preventing the initiation of gene transcription. H-NS mutants that are incapable of gene silencing were indeed found *in vitro* to be

defective for nucleofilament formation[59]. Note, however, that oligomerization is essential to both filament formation and bridging and that also transcription can be affected by failed assembly of both types of complexes, if oligomerization is perturbed. Data from a lot of recent *in vitro* studies indeed favors models in which DNA bridging plays a key role. Promotors that are sensitive to local DNA topology might be inactivated by H-NS due to its ability to constrain supercoils.[82] Generally, these promotors are affected at a distance and H-NS mediated bridging could also constrain supercoils by generation of a diffusion barrier. Bridge formation in promotor regions not only has the potential to occlude RNAP, but also to physically trap RNAP, thereby preventing promoter escape and silencing the associated gene[83–85]. Evidence from genome-wide binding profiles and a protein-protein interactions study indicates that H-NS and RNAP colocalize at some promotors, which is compatible with a trapping mechanism[86,87]. *In vitro* transcription studies show that whilst bridged H-NS-DNA complexes can inhibit progression of the elongating RNAP, the H-NS-DNA filament cannot, highlighting the importance of H-NS' DNA bridging activity[88,89]. Further mechanistic dissection of the repressive role of H-NS in transcription awaits single molecule *in vitro* transcription experiments and the application of novel approaches permitting structural investigation of the process *in vivo.* Much less mechanistic information is available for the other architectural DNA bridging proteins. Lsr2 can inhibit transcription *in vitro* and inhibits topoisomerase I, thereby introducing supercoils into the DNA[38]. Rok reduces the binding of RNAP at the promotor of *comK*[53]. Rok is antagonized at this promotor by ComK itself and, although their binding sites partially overlap[90–92], this occurs without preventing Rok binding[53]. It was postulated that anti-repression is achieved through modulation of DNA topology, which would imply that Rok itself also has impact on DNA topology[53]. In *P. aeruginosa,* MvaT is known to repress the *cupA* gene, which is important in biofilm formation. Mutants that were unable to silence *cupA*, could not form a nucleofilament[57]. For these three proteins, it remains to be investigated if DNA bridging is as important for gene silencing as in the case of H-NS.

5. Functional regulation

a. environmental conditions

Bacteria need to respond fast to environmental changes to be able to adapt to diverse living conditions. The bacterial genome operates as an information processing machine, translating environmental cues into altered transcription of specific genes required for adaptation and survival[3]. Key to this process is the dynamic organization of the bacterial genome driven by such cues[2].

The role of temperature

Change in temperature is one of the many environmental changes encountered by bacteria that need altered gene expression for adaptation. H-NS regulates the expression of many genes responsive to changes in environment. In *E. coli* H-NS controls more than 60% of the temperature-regulated genes: they have higher expression at 37°C than at 23°C[93–95]. These genes are involved in the nutrient, carbohydrate, and iron utilization systems and their changes in expression at 37°C may be of advantage for host colonization[96–98]. The involvement of H-NS in temperature regulation is corroborated by *in vitro* transcription studies, which indicate that H-NS is no longer able to pause elongating RNAP at 37°C (see section 4)[89]. The underlying mechanism may be an increased off-rate of H-NS, or a reduced propensity to oligomerize at the high temperature as observed *in vitro*[29,30,88,93].

Analogous to the situation for H-NS, also Lsr2-DNA filament formation is sensitive to temperature changes *in vitro*: the rigidity of Lsr2–DNA complexes is lower at 37°C than at 23°C[60]. This can be due to either a change in the ability of Lsr2 to oligomerize along DNA or a change in Lsr2 DNA-binding affinity at 37°C compared to 23°C. Qualitatively, Lsr2 induced DNA folding seems insensitive to change in temperature, suggesting but not conclusively proving that, DNA bridging by Lsr2 is not affected by temperature[60]. However, if the general binding scheme depicted in figure 1.3 applies, the effects of temperature on protein-DNA filament may translate into effects on DNA-protein-DNA bridging activity. Thus, taken together, it might very well be that Lsr2 is involved in regulating thermosensitive genes in *Mycobacteria*.

Unlike the protein-DNA filaments formed by H-NS and Lsr2, the stiffness of MvaT-DNA filaments is not altered in the range of 23°C to 37°C[57]. In the same temperature range an increase in DNA compaction was observed with increasing temperature. Such a switch between bridging and non-bridging modes is suggestive of temperature controlled gene regulation at MvaT-bridged genes in *Pseudomonas*. DNA bridging by Rok is not sensitive to changes in temperature from 25°C to 37°C, suggesting that genes in *B. subtilis* that are repressed by Rok are not regulated by temperature (see Chapter 4) [62].

The role of salt

H-NS has also been shown to regulate genes that are sensitive to salt stress. The *proU* (*proVWX*) operon is one of the best studied operons that is osmoregulated by H-NS. The expression of *proU* is significantly upregulated by high osmolarity[99,100]. *In vitro*, the stiffness of the nucleoprotein filament formed by H-NS and Lsr2 is sensitive to change in salt concentration from 50 mM to 300 mM KCl [58,63]: the rigidity of the protein-DNA complexes decreased as salt concentration increased. However, the stiffness of the MvaT-DNA filament is not affected by salt over the same concentration range[57]. The formation of DNA-DNA bridges by H-NS and MvaT is sensitive to both $MgCl_2$ and KCl (see Chapter 2) [51,58,101]. Changes in $MgCl_2$ (0-10 mM) or KCl concentration (50-300 mM) drive a switch between the DNA stiffening mode and bridging mode. This structural switch could be the mechanism underlying regulation of osmoregulated genes by H-NS and MvaT. Qualitatively, Lsr2 induced DNA folding seems insensitive to change in salt, suggesting that formation of the Lsr2-DNA bridged complex is not affected by salt[60]. However, the salt effects on the structure of the Lsr2-DNA filament could alter the activity of DNA-Lsr2-DNA bridging. DNA bridging by Rok is independent of and not sensitive to both $MgCl_2$ (0-60 mM) and KCl (35-300 mM) concentration (see Chapter 4) [62]. This insensitivity to changes in salt concentration may be related to the different charge distribution of Rok compared to the other H-NS like proteins (figure 1.4), where the lack of charges may lead to less interdomain interactions. In this way, Rok could be always in an open conformation, suitable for DNA bridging.

The role of pH

H-NS has been reported to be involved pH-dependent gene regulation[102]. *In vitro*, the rigidity of H-NS-DNA nucleofilaments is shown to be sensitive to changes in pH[58]. A reduction in stiffness of the protein-DNA complex was observed with increasing pH from 6.5 to 8. The formation of the bridged DNA-H-NS-DNA complex might be insensitive to pH changes as H-NS induced DNA folding was unaffected over the same range of pH values[58].

Different from the pH-sensitivity observed for H-NS-DNA filaments, Lsr2-DNA nucleofilaments were shown to be insensitive to changes in pH from 6.8 to 8.8. Similar to H-NS, DNA-folding by Lsr2 is not sensitive to pH changes in the same range[60]. Also the MvaT-DNA nucleoprotein filament is not sensitive to pH changes from 6.5 to 8.5, but DNA compaction is affected[57]: MvaT induced stronger folding at pH 6.5 than pH 8.5. Note that the DNA folding induced by H-NS, MvaT and Lsr2 was detected by a qualitative 'folding assay', in which observed DNA folding does not necessarily result from DNA bridging. A quantitative assay such as the 'bridging assay', developed by van der Valk et al. (see Chapter 5) [103], is essential to better determine the sensitivity of DNA-protein-DNA bridging to changes in environmental conditions. With this bridging assay, DNA bridging by Rok was shown to be insensitive to pH changes from 6.0 to 10.0. Strikingly, even crossing the pI of Rok (9.31) did not affect its bridging capacities, indicating that charge interactions are unlikely to play a role in DNA bridging by Rok (see Chapter 4) [62].

For H-NS, Lsr2 and MvaT, the sensitivity of protein-DNA nucleofilaments or bridged complexes to environmental changes *in vitro* is in agreement with the proposed role in regulation of genes sensitive to changes in the environment. However, the involvement in the physiological response to changes remains to be established for Lsr2 and MvaT.

b. binding-partners / antagonists

Not only physico-chemical conditions regulate the DNA binding and gene regulation properties of the four proteins. To date such binding partners (paralogs, truncated derivatives, and non-related modulators and inhibitors) have been primarily identified for H-NS, but some modulators were also identified for MvaT, Lsr2 and Rok. They are summarized in table 1.1, together with the characteristics of the four proteins.

Table 1.1: Characteristics of bacterial DNA-bridging proteins

	H-NS	MvaT	Lsr2	Rok
Bacteria	*Enterobacteriaceae* Gram-negative	*Pseudomonas sp.* Gram-negative	*Actinomycetes* Gram-positive	*Bacillus sp.* Gram-positive
Size	15.5 kDa	14.2 kDa	12.0 kDa	21.8 kDa
Protomer size	Dimer	Dimer	Dimer	Unknown
Oligomerization	Yes	Yes	Yes	Yes
Nucleofilament	Yes	Yes	Yes	N.D.
DNA-bridging	Yes	Yes	Yes	Yes
DNA-bending	No	Yes	No	Yes
Heteromers	Yes	Yes	Predicted	Predicted
Modulators				
Paralogues	StpA, Hfp, H-NS2, H-NS$_{R27}$, Sfh	MvaU, Pmr	Predicted	Unidentified
Truncated derivatives	H-NST	Unidentified	Unidentified	sRok
Non-related interaction partners	Hha, YdgT, gp5.5, Ocr, Arn	Mip	HU	DnaA

Paralogs

The H-NS paralog StpA shares 58% sequence identity. Expression of StpA partially complements an *hns*[-] phenotype of *E.coli*[104,105]. H-NS and StpA show negative autoregulation and repress transcription of each other's genes[106,107]. StpA is upregulated during growth at elevated temperature and high osmolarity[108,109]. Similar to H-NS, StpA can form dimers and higher order oligomers *in vitro*[110]. *In vivo* it is believed to exist only as heteromer with H-NS as it is otherwise susceptible to Lon degradation[111,112]. The structural effects of StpA binding to DNA *in vitro* are rather similar to H-NS: StpA can bridge DNA and forms protein filaments along DNA[33,113]. Despite the large similarities between the two proteins, H-NS, StpA and H-NS-StpA heteromers exhibit functionally distinct behavior. At 20°C H-NS mediated DNA-DNA bridges induce transcriptional pausing, whereas they do not at 37°C. (see section 5a)[88]. The upregulation of StpA during growth at higher temperature might be explained by H-NS being unable to repress StpA at this temperature. At both 20°C and 37°C, StpA does increase the pausing of RNAP, thereby

repressing transcription[89]. StpA filaments on DNA are mostly present in a bridged conformation[89]. Also, bridged DNA-DNA complexes built using StpA-H-NS heteromers are capable of inducing RNAP pausing at 37°C[89]. This robustness of StpA could contribute to gene silencing under stress conditions, forming an extra layer of gene regulation by H-NS. The presence of a third H-NS paralogue has been reported for several strains: the uropathogenic *E. coli* strain 536 expresses Hfp (also calles H-NSB[114]) which is primarily expressed at 25°C and could thus be specifically implicated in regulating gene expression outside the host.[109] Heteromerization of Hfp with H-NS occurs, but, different from StpA this is not required for the stability of the protein[109]. The enteroaggregative *E. coli* strain 042 and several other *Enterobacteriaceae* also carry a second H-NS gene (or third in e.g. strain 536 besides H-NS and Hfp) which can partially complement the *hns-* phenotype[115]. This H-NS2 is expressed at significantly lower levels than H-NS during exponential growth, but the expression increases in the stationary phase[109]. Also, expression of H-NS2 is higher at 37°C than at 25°C which could relate to the pathogenic nature of the investigated *E. coli* strains[109]. When comparing the amino acid sequences of all above mentioned H-NS paralogs, it becomes apparent that the N-terminal and C-terminal domain are quite conserved, particularly the DNA binding domain (figure 1.5a). Because of this, the charge distribution of these proteins is also conserved, which makes it likely that they are similarly regulated by environmental conditions (supplementary figure). The differences in expression levels and thermal stability is most likely responsible for their different regulons.

Several plasmids have also been reported to encode H-NS paralogs. Often these proteins have distinct functional properties. The conjugative IncHI1 plasmid pSfR27 encodes the H-NS paralogue Sfh[116,117]. It was proposed that the plasmid moves from one host to another without causing a large change in host gene expression, because the binding of Sfh to pSfR27 prevents H-NS being titrated away from the chromosome [118]. Sfh can form homodimers and heterodimers with H-NS and StpA *in vivo*, but the DNA binding properties of these complexes are still unknown[117]. The IncHI plasmid R27 encodes an H-NS variant that can partially complement the *hns-* phenotype[119]. This H-NS$_{R27}$ binds to horizontally acquired DNA, but not to the core genes regulated by chromosomal H-NS[119]. The difference is encoded in the linker region, which is hypothesized to be more rigid in H-NS$_{R27}$[120]. Both Sfh and H-NS$_{R27}$ are quite conserved in N- and

C-terminal domain compared to H-NS and also the charge distribution is conserved (figure 1.5a and supplementary figure S1.1), which likely accounts for their "stealth" function. These plasmid-borne H-NS homologues help the plasmid to stay unnoticed by the host cell upon entry. By silencing horizontally acquired DNA (including the plasmid itself) they prevent H-NS from relieving its chromosomal targets and binding to the plasmid. This allows the plasmid to be transmitted without fitness costs for the host.

In *Pseudomonas aeruginosa,* MvaU was identified as a paralogue of MvaT. The two proteins occupy the same chromosomal regions and work coordinately[35]. They are able to form heteromers, but this is not necessary for gene regulation[35,121]. Under conditions of fast growth, they are functionally redundant, becoming only essential when the other partner is deleted from the chromosome[35]. Uncharacterized paralogues of MvaT/U are present in several *Pseudomonas* genomes. For example, in *P. alcaligenes* strain RU36E four MvaT/U proteins are present (figure 1.5b). They share residues in the N-terminal domain and the AT-pincer motif. One of these is closely related to MvaT (Mva2: 81.7% sequence identity). The homology for the other three proteins is not that clear as the sequence identities to MvaT and MvaU are comparable (1: 54.7% and 52.1% 3: 54.0% and 53.7% 4: 53.2% and 54.1%). Another paralogue was found on the IncP-7 plasmid pCAR1 in *P. putida*[122]. The protein Pmr (plasmid-encoded MvaT-like regulator) shares 58% sequence identity with MvaT and *in vitro* forms homodimers and heteromers with MvaT-like proteins[123]. This is not surprising as many residues and the charge distribution are conserved between Pmr, MvaT and MvaU (figure 1.5b and supplementary figure S1.1). Pmr is able to regulate genes both on the plasmid and on the host chromosome[124]. Whereas the expression levels of the chromosomally encoded MvaT-like proteins alter between log and stationary phase, the level of Pmr is constant during different growth phases[125]. The regions on the chromosomes bound by Pmr and MvaT are identical, but their regulons differ[124]. This may be attributed to the formation of different heteromers between Pmr and the two MvaT-like proteins with slightly different functions. Therefore, it remains unsure if Pmr is able to complement a *mvaT* phenotype in *P. putida*.

For Lsr2, several candidate paralogs have been identified so far. Several genomes of *Mycobacterium* species harbor two genes encoding for Lsr2 (e.g. *Mycobacterium smegmatis*) or carry a plasmid with an Lsr2 gene (e.g. *Mycobacterium gilvum*)[41]. In the case of *M. smegmatis* MKD8 some features of Lsr2, like its DNA binding motif, are conserved between the two proteins,

but the second Lsr2 has a much longer linker domain (figure 1.5c). It enlarges the positive patch already present in the Lsr2 linker, so it may provide the protein with extra charged surface for interdomain interactions (supplementary figure S1.1). It was noticed that all *Streptomycetes* carry a second Lsr2[126], although a recent study shows that Lsr2 is more important than the second, Lsr2-like protein[127]. They appear to be similar in charge distribution (supplementary figure S1.1). The DNA binding modes of these candidate paralogs or the formation of heteromers with Lsr2 has not been investigated.
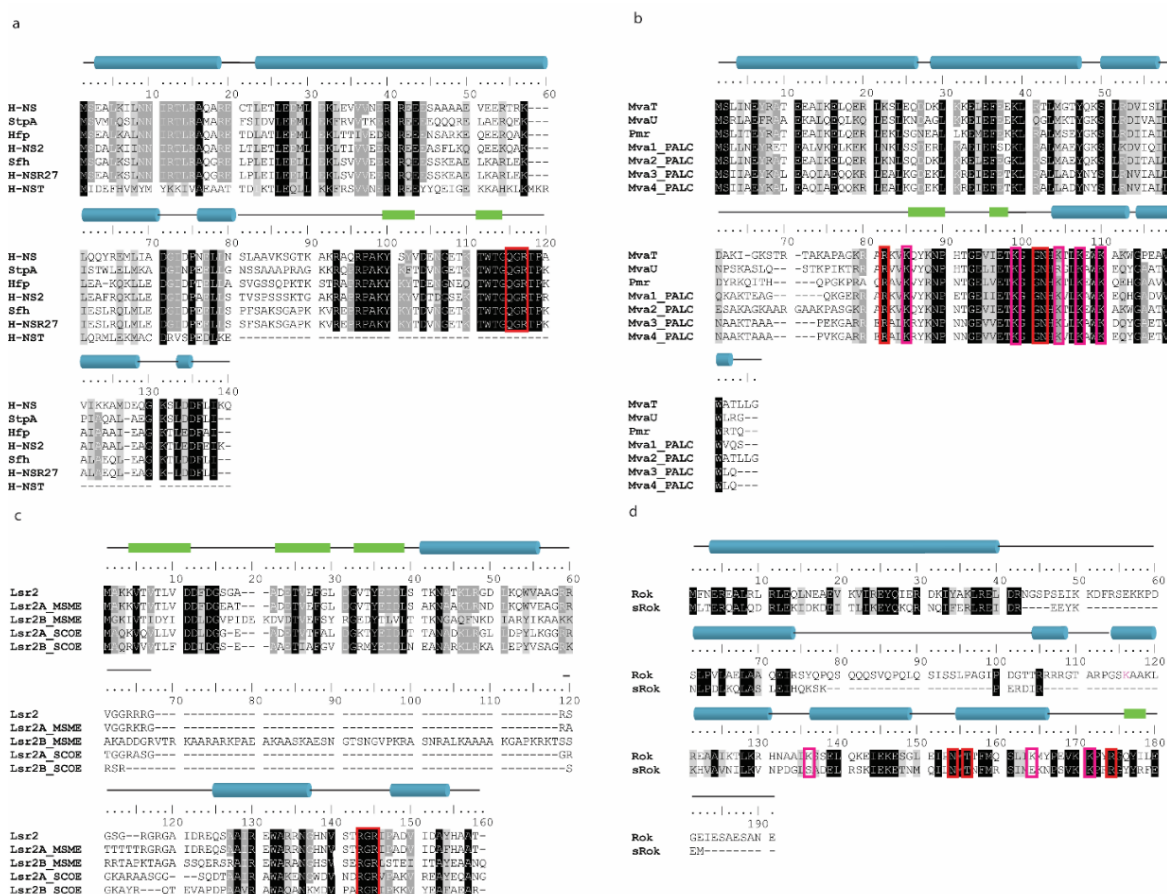

Figure 1.5: Comparison of H-NS like architectural proteins and their structurally related protein-protein interaction partners. Alignment of identified paralogues and truncated derivatives of H-NS (a), MvaT (b), Lsr2 (c) and Rok (d). Identical residues in all sequences are highlighted in black, identical residues in >75% of the sequences are highlighted in dark grey and conserved residues are highlighted in light grey. The DNA binding motif is highlighted in red and the lysine network of MvaT and Rok in magenta. α-Helices are indicated with blue cylinders and β-sheets with green boxes. The indicated structure corresponds to the most upper sequence. H-NS, *E. coli* strain K-12, NP_415753.1; StpA, *E. coli* strain K-12, NP_417155.1;

Hfp, *E. coli* strain 536, ABG69928.1; H-NS2, *E. coli* strain 042, CBG35667.1; Sfh, *Shigella flexneri* 2a, AAN38840.1; H-NSR27, *Salmonella enterica subsp. enterica serovar Typhi* strain CT18, NP_569380.1; H-NST, *Escherichia coli* CFT073, NP_754305; MvaT, *P. aeruginosa* PAO1, NP_253005.1; MvaU, *P. aeruginosa* CLJ1, PTC37345.1; Pmr, *P. resinovorans*, NP_758612.1; Mva1/2/3/4_PALC, *P. alcaligenes* RU36E SIQ98833.1, SIQ72658.1, SIP93681.1 and SIP94365.1; Lsr2_MTUB, *M. tuberculosis* H37Rv, NP_218114.1; Lsr2A/B_MSMEG, *M. smegmatis* MKD8, AWT56911.1 and AWT52048.1; Lsr2A/B_SCOEL, *S. coelicolor* A(3)2 , CAB40875.1 and CAB56356.1; Rok, *B. subtilis* strain 168, NP_389307.1; sRok, *B. subtilis subsp. natto*, YP_004243533.1

Truncated derivatives

Some pathogenic *E. coli* strains, like uropathogenic *E. coli* strain CFT073, encode a truncated version of H-NS: H-NST[114]. It lacks the DNA binding domain and the oligomerization site (figure 1.5a). H-NST is able to counteract gene silencing by H-NS, which was proposed to occur by interfering with its oligomerization[114]. This model is supported by truncated H-NS products , mimicking H-NST, that are also able to perturb DNA bridging[61].

A small Rok variant (sRok) was identified on the *B. subtilis* plasmid pLS20[128]. sRok can complement the *rok* phenotype in the competence pathway and associates genome-wide with the host chromosome. The DNA binding motif in the C-terminal domain and parts of the N-terminal domain are conserved, suggesting that the function of these domains is also conserved (figure 1.5d). The difference between the two proteins is mostly the length of the linker. The neutral Q-linker of Rok is absent in sRok, which could lead to differences in DNA binding and responsiveness to changes in environmental conditions (figure 1.5d and supplementary figure S1.1). In contrast to *B. subtilis* that carries the *srok* gene nearly always on a plasmid, the *srok* gene is present on the chromosome of *B. licheniformis* and *B. paralicheniformis*. Possibly, the gene was transferred to the chromosome from the pLS20 plasmid. The *rok gene* is not present in all *Bacillus* species and its introduction has been attributed to a horizontal gene transfer event.[92] The absence of *rok* in several *Bacillus* species means that its proposed genome organizing function is redundant and can be compensated for by other proteins. So far, it is unknown if Rok and sRok can form heteromers and how that would change their function in gene silencing and genome organization.

Non-related modulators and inhibitors

Hha and YdgT are members of the Hha/YmoA family acting as modulators of H-NS activity and function[129]. Different from H-NS truncated derivatives, these proteins have very limited sequence identity with H-NS. Hha is involved in co-regulation of a subset of known H-NS regulated genes, especially in silencing of horizontally acquired genes[119,130,131]. It is therefore not obvious *a priori* how these proteins would modulate the DNA binding properties of H-NS. Hha was found to interact with the N-terminal domain of H-NS, specifically with the first two helices[132,133]. The H-NS-Hha co-crystal structure shows two Hha monomers binding to either site of the H-NS dimer, exposing two positively charged Hha surfaces per H-NS dimer[134]. Based on this structure, it was proposed that Hha affects H-NS mediated DNA bridging and thus coregulates specific genes with H-NS[134]. Indeed, it was shown that both Hha and YdgT enhance DNA bridging by H-NS[61]. Mechanistically, this could be explained in two ways: 1) Hha provides additional electrostatic interactions with DNA[134] or 2) the H-NS dimer 'opens' upon Hha binding, resulting in a conformation capable of DNA bridging[61]. In the latter scenario, Hha could additionally stabilize the complex by the interactions implied in the first scenario. Hha has also been shown to enhance pausing of RNAP by H-NS and H-NS:Hha complexes preferentially bridge DNA[89]. In this manner, Hha could help with silencing a subset of H-NS regulated genes. Genomes of a wide-range of pathogenic *E. coli* strains also contain two extra *hha* genes: *hha2* and *hha3*[135] in addition to the H-NS paralogues as described above. The presence of the extra *hha* genes is correlated to duplication of gene clusters that are regulated by H-NS and Hha and may be important for virulence[136]. Also the *hha2* gene is present in one of the duplicated regions, meaning that it originates from a duplication event. This shows a relation between duplicated virulence regions and extra genes encoding for regulators like H-NS and Hha. A gene encoding for Hha is also present on several plasmids, including the R27 plasmid described above[137,138].

H-NS can be inhibited by several phage-encoded proteins to counteract gene silencing. Gp5.5 from phage T7 interacts for example with the oligomerization domain of H-NS[139,140], thereby inhibiting oligomerization and gene silencing by H-NS. Another strategy used for counteracting gene silencing by H-NS is mimicking DNA, thereby competing with H-NS' genomic targets.[141–143]. This strategy is used by Ocr from phage T7 and Arn from phage T4[141–143]. Both strategies result

in relieve of gene silencing by H-NS and making H-NS unable to bind to the genetic material of the phage. Lack of repression could lead to replication of the phage and entering of the lytic cycle to kill the host cell. Also MvaT can be inhibited by a protein encoded by a phage. The phage LUZ24 in *P. aeruginosa* expresses a protein called Mip (MvaT inhibiting protein), which was shown to perturb DNA binding of MvaT and proposed to inhibit the silencing of virus genes by MvaT[144].

Lsr2 of M. tuberculosis binds to the architectural protein HU [145]. This interaction involves the N-terminal domain of Lsr2 and the C-terminal tail of HU, which has (P)AKKA repeat motifs and thereby resembles histone tails. This tail is absent in HU of other bacteria discussed in this review (*E. coli, B. subtilis* and *Pseudomonas* species). The Lsr2-HU complex binds DNA, creating thick linear filaments instead of DNA bridges as seen for Lsr2 alone, or DNA compaction as seen for HU[145].

Rok interacts with bacterial replication initiator and transcription factor DnaA and jointly the two proteins interact with a subset of Rok-bound genes[146]. DnaA enhances gene repression by Rok for this subset of Rok-bound genes. DnaA binding to these genes is dependent on Rok and the DNA binding domain of DnaA is neither necessary for this interaction, nor does it bind DNA in the Rok:DnaA complex. This is consistent with a model in which DnaA modulates the function of Rok. Because DnaA is an ATPase and its activity levels change during the cell cycle[147,148], it may be an indirect way to modulate the activity of Rok according to the cell cycle or energy status of the cell.

c. Post-translational modifications

The post-translational modification (PTMs) of eukaryotic histones has been studied for years and the functional significance of these modifications in biological processes including DNA repair, gene regulation and cell division is well established[149]. Although PTMs have been identified in recent years on NAPs in bacteria, their functional importance remains unclear.

H-NS has been found to undergo many PTMs which potentially add an extra layer to its function in chromatin organization and regulation [150]. PTMs discovered for H-NS include acetylation and succinylation of lysines, methylation of arginines, phosphorylation of serines, tyrosines and threonines, deamidation of asparagines and oxidation of methionines[150]. These modifications may influence diverse functional properties of H-NS such as DNA binding,

oligomerization, and interaction with other proteins. Acetylation or succinylation occurs on Lys96 and Lys121 near to the H-NS DNA-binding motif[151]. These modifications could reduce the DNA binding affinity due to the change from positive to neutral or negative charge[152,153]. Acetylation at Lys83 and Lys87 located in the linker region has been identified[152,153]. This could decrease the H-NS DNA binding affinity since the positive charge residues of the linker region are important for the DNA binding[55]. The identified phosphorylation on Tyr61 induces a negative charge and could interfere with H-NS oligomerization[154]. Indeed, the phosphorylation-mimicking mutation Y61D was shown to be important in H-NS dimer-dimer interaction. Lys6 has been shown to be involved in the interaction between Hha and H-NS[134]. Succinylation of Lys6 may reduce the strength of Hha binding by inducing steric hindrance, which could act in regulation silencing of genes by H-NS at which Hha is involved as a co-partner[153].

Lsr2 of *M. tuberculosis* has been found to be phosphorylated at Thr112, located near the DNA binding motif[155]. A recent study shows that phosphorylation of this residue decreases DNA binding by Lsr2, thus resulting in altered expression of genes important for *M. tuberculosis* growth and survival[156]. Some residues (Thr8, Thr22 and Thr31) in the N-terminal domain of Lsr2 were also found to be phosphorylated *in vitro*[156]. All these residues are located at β-sheets which are important for the formation of dimers or oligomers[41]. The PTMs on these residues could influence the dimerization or oligomerization of Lsr2 by the addition of negative charges. Also the interaction with HU, which involves the N-terminal domain of Lsr2[145], could be regulated by phosphorylation.

In MvaT from *P. aeruginosa PA01* several residues located at the N-terminal domain and linker region are acetylated and succinylated and at the C-terminal domain succinylated[157]. MvaT Lys86 is directly adjacent to Lys85 which is involved in DNA binding[45]. Lys86 is succinylated, leading to charge inversion and thereby a decrease in DNA binding affinity[157]. Acetylation occurs on Lys22 and Lys31 located in the dimerization domain. On Lys39, shown to be important for oligomerization by forming hydrogen bonds[43], both acetylation and succinylation can occur. By altering positive charge to neutral or negative charge, these PTMs could affect the dimerization or oligomerization of MvaT. In addition, phosphorylation occurs at S2 in *P. putida PNL-MK25* MvaT, which may also affect its dimerization properties[158]. The linker region has been found to be important for H-NS interdomain interaction between C-terminal and N-terminal domain, which

plays a role in H-NS controlling genes sensitive to temperature[64]. For the MvaT linker region, acetylation of Lys63 and succinylation of Lys72 was discovered. These PTMs, by changing positive charge to neutral or negative charge, could interfere with the intradomain interaction and modulate the function of MvaT in gene regulation.

Proteome analyses of *B. amyloliquefaciens* and *B. subtilis* show that Rok can be acetylated on residues K51 and K142[159,160]. K51 is present in an (predicted) unstructured part of the N-terminal domain. Because it is currently unknown which residues are important for dimer- and oligomerization of Rok, we cannot predict what the effect of acetylation on K51 would be. K142 is close to the DNA binding motif of Rok and, while it was not identified as being directly involved, could affect the strength of the 'lysine network'[46]. Nevertheless, it could have an effect on the DNA binding affinity of Rok by changing the charge of K142 from positive to neutral.

PTMs that lead to changes in charge, could affect the charge distribution of H-NS-like proteins. This may alter the proteins' response to environmental changes, which is important for their role in gene regulation. Functional studies on PTMs on these proteins are currently lacking, but they will prove essential in better understanding the function of PTMs in global gene regulation and physiological adaptation.

6. Conclusion and perspectives

The architectural chromatin proteins H-NS, MvaT, Lsr2 and the newly proposed functional homologue Rok play important roles in the organization and regulation of the bacterial genome. Although their sequence similarity is low, their domain organization is the same: the N-terminal domain functions in dimerization and oligomerization, the C-terminal domain binds DNA and the two are connected by a flexible linker. Except for Rok, the charge distribution of these proteins along the sequence is highly conserved. The four proteins are all capable of bridging DNA duplexes, which is important for both spatial genome organization and gene regulation (figure 1.6). Although a vast amount of research is done on gene regulation by H-NS, it remains to be investigated if the other three proteins regulate genes in similar ways. To decipher mechanistically how H-NS represses genes, more advanced single-molecule and *in vivo* experiments are needed.
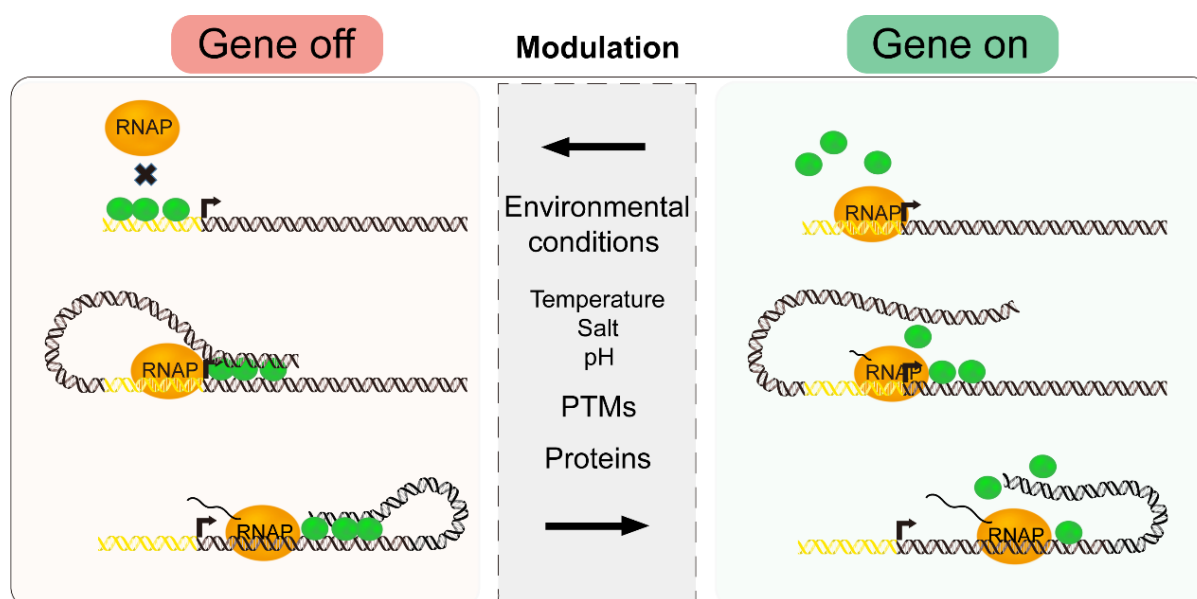
Figure 1.6: H-NS-like proteins functional regulation in gene silencing by different factors. The activity of RNAP transcription may be inhibited by H-NS-like proteins in three ways: 1) RNAP binding to promotor region can be inhibited by protein-DNA filaments or bridge complexes; 2) RNAP elongation can be trapped and inhibited by DNA-protein-DNA bridge complexes. 3) Elongating RNAP can be paused by DNA-protein-DNA complexes. The inhibition of RNAP by H-NS-like proteins may be modulated by factors such as environmental conditions (temperature, salt and pH), proteins and post-translational modifications (PTMs), allowing genes to be expressed.

H-NS, MvaT and Lsr2 are functionally modulated by changes in environmental conditions, protein partners and PTMs (figure 1.6). PTMs are to date poorly explored and could be a completely new field of research. The first functional study for phosphorylation of Lsr2 shows that PTMs can indeed be important for the DNA binding properties of these chromatin organizing proteins and could be a new, uncharacterized way of regulation.

We propose that the shared domain organization and asymmetric charge distribution of the H-NS like proteins is key to their response to changes in environmental conditions. This information could be used to predict a protein's behavior and may be employed in fighting pathogenic strains by either activating or repressing specific gene transcription.

Thesis outline

Every organism across the tree of life compacts and organizes its genome with architectural chromatin proteins. In *Escherichia coli* and other proteobacteria, the histone-like nucleoid structuring protein (H-NS) acts as a global genome organizer and gene regulator. Functional analogs of H-NS have been found in other bacterial species: MvaT in *Pseudomonas* species, Lsr2 in actinomycetes and Rok in *Bacillus* species. In this chapter, we described and compared their structure and function to define conserved features. Also, we discussed the mechanisms by which the architectural and regulatory properties of these proteins are modulated. In **Chapter 2**, we combine integrative structural biology methods and (single-molecule) biochemical assays to decipher the structural changes in the H-NS family protein MvaT that drive the switch between its DNA stiffening and bridging activities under influence of different salt conditions. In **Chapter 3**, we investigate how the DNA binding properties of MvaT are affected by Mip. Also, we define how Mip interacts with MvaT and how this translates into altered DNA structuring properties. In **Chapter 4**, we investigate the DNA binding properties of Rok and determine the effects of physico-chemical conditions on these properties. In **Chapter 5** and **Chapter 6**, we describe two methods well-suited to the analysis of the interaction between DNA and H-NS family proteins, a DNA bridging assay and Acoustic Force Spectroscopy (AFS). These techniques are helpful in understanding how proteins or other molecules interfere with the DNA binding functionality of H-NS family proteins. **Chapter 7** provides a general summary and perspectives in relation to the work described in this thesis.

Supplementary figure S1.1
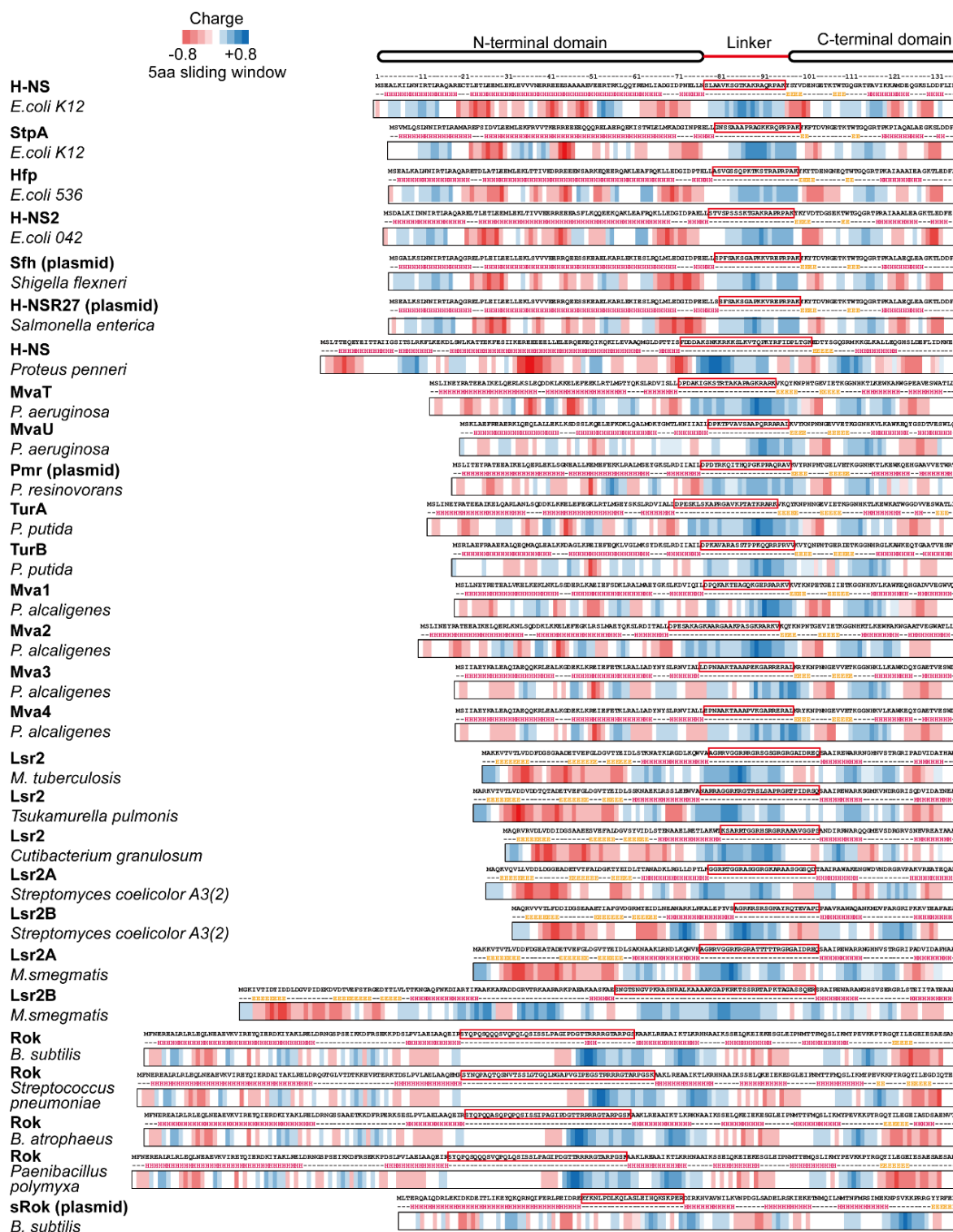
Supplementary figure S1.1: Electrostatics and fold topology of H-NS-like proteins. Comparison of the charge distribution of the four families of H-NS like protein across a range of species. The average charge of a five-amino acid window as analyzed with EMBOSS charge. Positively and negatively charged regions

are colored blue and red respectively. Unknown secondary structures were predicted using JPRED[49]. α-Helices are represented with (H) in pink, β-sheets with (E) in yellow and random coils with (-) in black. The linker domain is indicated with a red box. H-NS, *E. coli* strain K-12, NP_415753.1; StpA*, E. coli* strain K-12, NP_417155.1; Hfp, *E. coli* strain 536, ABG69928.1; H-NS2, *E. coli* strain 042, CBG35667.1; Sfh, *Shigella flexneri 2a*, AAN38840.1; H-NSR27, *Salmonella enterica subsp. enterica serovar Typhi* strain CT18, NP_569380.1; H-NS, *Proteus penneri*, SUB98598.1; MvaT, *P. aeruginosa* PAO1, NP_253005.1; MvaU, *P. aeruginosa* CLJ1, PTC37345.1; Pmr, *P. resinovorans*, NP_758612.1; TurA, *P. putida*, SUD72464.1; TurB, *P. putida*, VEE40761.1; Mva1/2/3/4_PALC, *P. alcaligenes* RU36E SIQ98833.1, SIQ72658.1, SIP93681.1 and SIP94365.1; Lsr2_MTUB, *M. tuberculosis* H37Rv, NP_218114.1; Lsr2, *Tsukamurella pulmonis*, SUP14481.1; Lsr2, *Cutibacterium granulosum*, SNV28945.1; Lsr2A/B_SCOEL, *S. coelicolor* A(3)2 , CAB40875.1 and CAB56356.1; Lsr2A/B_MSMEG, *M. smegmatis* MKD8, AWT56911.1 and AWT52048.1; Rok, *B. subtilis* strain 168, NP_389307.1; Rok, *Streptococcus pneumonia*, CVM76913.1; Rok, *B. atrophaeus*, KFK83781.1; Rok, *Paenibacillus polymyxa*, SPY12450.1; sRok, *B. subtilis subsp. natto*, YP_004243533.1.

References

1. Luijsterburg, M. S., White, M. F., Van Driel, R. & Dame, R. T. The major architects of chromatin: Architectural proteins in bacteria, archaea and eukaryotes. *Crit. Rev. Biochem. Mol. Biol.* **43**, 393–418 (2008).

2. Felsenfeld, G., Boyes, J., Chung, J., Clark, D. & Studitsky, V. Chromatin structure and gene expression. *Proc. Natl. Acad. Sci. U. S. A.* **93**, 9384 (1996).

3. Mekalanos, J. J. Environmental signals controlling expression of virulence determinants in bacteria. *J. Bacteriol.* **174**, 1–7 (1992).

4. Dorigo, B., Schalch, T., Bystricky, K. & Richmond, T. J. Chromatin fiber folding: Requirement for the histone H4 N-terminal tail. *J. Mol. Biol.* **327**, 85–96 (2003).

5. Dorigo, B. *et al.* Nucleosome arrays reveal the two-start organization of the chromatin fiber. *Science (80-.).* **306**, 1571–1573 (2004).

6. Hansen, J. C. & Luger, K. Nucleosome and chromatin fiber dynamics. *Curr. Opin. Struct. Biol.* **15**, 188–96 (2005).

7. Clark, D. J. & Thomas, J. O. Differences in the binding of H1 variants to DNA: Cooperativity and linker-length related distribution. *Eur. J. Biochem.* **178**, 225–233 (1988).

8. Zheng, R. *et al.* Barrier-to-autointegration factor (BAF) bridges DNA in a discrete, higher-order nucleoprotein complex. *Proc. Natl. Acad. Sci. U. S. A.* **97**, 8997–9002 (2000).

9. Hirano, M., Anderson, D. E., Erickson, H. P. & Hirano, T. Bimodal activation of SMC ATPase by intra-

and inter-molecular interactions. *EMBO J.* **20**, 3238–3250 (2001).

10. Hirano, T. Condensin-Based Chromosome Organization from Bacteria to Vertebrates. *Cell* **164**, 847–857 (2016).

11. Cobbe, N. & Heck, M. M. S. The Evolution of SMC Proteins: Phylogenetic Analysis and Structural Implications. *Mol. Biol. Evol.* **21**, 332–347 (2004).

12. Thomas, J. O. & Travers, A. A. HMG1 and 2, and related 'architectural' DNA-binding proteins. *Trends in Biochemical Sciences* vol. 26 167–174 (2001).

13. Henneman, B. & T. Dame, R. Archaeal histones: dynamic and versatile genome architects. *AIMS Microbiol.* **1**, 72–81 (2015).

14. Mattiroli, F. *et al.* Structure of histone-based chromatin in Archaea. *Science (80-.).* **357**, 609–612 (2017).

15. Henneman, B., van Emmerik, C., van Ingen, H. & Dame, R. T. Structure and function of archaeal histones. *PLoS Genetics* vol. 14 e1007582 (2018).

16. Henneman, B. *et al.* Mechanical and structural properties of archaeal hypernucleosomes. (2019).

17. Jelinska, C. *et al.* Obligate heterodimerization of the archaeal Alba2 protein with Alba1 provides a mechanism for control of DNA Packaging. *Structure* **13**, 963–971 (2005).

18. Laurens, N. *et al.* Alba shapes the archaeal genome using a delicate balance of bridging and stiffening the DNA. *Nat. Commun.* **3**, 1328 (2012).

19. Driessen, R. P. C. & Dame, R. T. Structure and dynamics of the crenarchaeal nucleoid. *Biochem. Soc. Trans.* **41**, 321–5 (2013).

20. Azam, T. A. & Ishihama, A. Twelve species of the nucleoid-associated protein from Escherichia coli. Sequence recognition specificity and DNA binding affinity. *J. Biol. Chem.* **274**, 33105–13 (1999).

21. Dillon, S. C. & Dorman, C. J. Bacterial nucleoid-associated proteins, nucleoid structure and gene expression. *Nat. Rev. Microbiol.* **8**, 185–195 (2010).

22. Tendeng, C. & Bertin, P. N. H-NS in Gram-negative bacteria: a family of multifaceted proteins. *Trends Microbiol.* **11**, 511–518 (2003).

23. Pan, C. Q. *et al.* Variable Structures of Fis-DNA Complexes Determined by Flanking DNA – Protein Contacts. *J. Mol. Biol.* **264**, 675–695 (1996).

24. Rice, P. A., Yang, S., Mizuuchi, K. & Nash, H. A. Crystal structure of an IHF-DNA complex: a protein-induced DNA U-turn. *Cell* **87**, 1295–306 (1996).

25. Swinger, K. K., Lemberg, K. M., Zhang, Y. & Rice, P. A. Flexible DNA bending in HU-DNA cocrystal structures. *EMBO J.* **22**, 3749–60 (2003).

26. Hommais, F. *et al.* Large-scale monitoring of pleiotropic regulation of gene expression by the prokaryotic nucleoid-associated protein, H-NS. *Mol. Microbiol.* **40**, 20–36 (2001).

27. Navarre, W. W. *et al.* Selective silencing of foreign DNA with low GC content by the H-NS protein in Salmonella. *Science (80-.).* **313**, 236–238 (2006).

28. Dame, R. T., Wyman, C. & Goosen, N. H-NS mediated compaction of DNA visualised by atomic force microscopy. *Nucleic Acids Res.* **28**, 3504–3510 (2000).

29. Dame, R. T., Noom, M. C. & Wuite, G. J. L. Bacterial chromatin organization by H-NS protein unravelled using dual DNA manipulation. *Nature* **444**, 387–390 (2006).

30. Amit, R., Oppenheim, A. B. & Stavans, J. Increased bending rigidity of single DNA molecules by H-NS, a temperature and osmolarity sensor. *Biophys. J.* **84**, 2467–2473 (2003).

31. Tendeng, C., Soutourina, O. A., Danchin, A. & Bertin, P. N. MvaT proteins in Pseudomonas spp.: A novel class of H-NS-like proteins. *Microbiology* vol. 149 3047–3050 (2003).

32. Gordon, B. R. G., Imperial, R., Wang, L., Navarre, W. W. & Liu, J. Lsr2 of Mycobacterium represents a novel class of H-NS-like proteins. *J. Bacteriol.* **190**, 7052–7059 (2008).

33. Dame, R. T. *et al.* DNA Bridging: a Property Shared among H-NS-Like Proteins. *J. Bacteriol.* **187**, 1845–1848 (2005).

34. Chen, J. M. *et al.* Lsr2 of Mycobacterium tuberculosis is a DNA-bridging protein. *Nucleic Acids Res.* **36**, 2123–2135 (2008).

35. Castang, S., McManus, H. R., Turner, K. H. & Dove, S. L. H-NS family members function coordinately in an opportunistic pathogen. *Proc. Natl. Acad. Sci.* **105**, 18947–18952 (2008).

36. Gordon, B. R. G. *et al.* Lsr2 is a nucleoid-associated protein that targets AT-rich sequences and virulence genes in Mycobacterium tuberculosis. *Proc. Natl. Acad. Sci.* **107**, 5154–5159 (2010).

37. Castang, S. & Dove, S. L. High-order oligomerization is required for the function of the H-NS family member MvaT in Pseudomonas aeruginosa. *Mol. Microbiol.* **78**, 916–931 (2010).

38. Colangeli, R. *et al.* Transcriptional regulation of multi-drug tolerance and antibiotic-induced responses by the histone-like protein Lsr2 in M. tuberculosis. *PLoS Pathog.* **3**, e87 (2007).

39. Smits, W. K. & Grossman, A. D. The transcriptional regulator Rok binds A+T-rich DNA and is involved in repression of a mobile genetic element in Bacillus subtilis. *PLoS Genet.* **6**, 1001207 (2010).

40. Marbouty, M. *et al.* Condensin- and Replication-Mediated Bacterial Chromosome Folding and Origin Condensation Revealed by Hi-C and Super-resolution Imaging. *Mol. Cell* **59**, 588–602 (2015).

41. Summers, E. L. *et al.* The Structure of the Oligomerization Domain of Lsr2 from Mycobacterium tuberculosis Reveals a Mechanism for Chromosome Organization and Protection. *PLoS One* **7**, 38542 (2012).

42. Arold, S. T., Leonard, P. G., Parkinson, G. N. & Ladbury, J. E. H-NS forms a superhelical protein scaffold for DNA condensation. *Proc. Natl. Acad. Sci.* **107**, 15728–15732 (2010).

43. Suzuki-Minakuchi, C. *et al.* Structural similarities and differences in H-NS family proteins revealed by the N-terminal structure of TurB in Pseudomonas putida KT2440. *FEBS Letters* vol. 590 3583–3594 (2016).

44. Gordon, B. R. G. *et al.* Structural basis for recognition of AT-rich DNA by unrelated xenogeneic silencing proteins. *Proc. Natl. Acad. Sci.* **108**, 10690–10695 (2011).

45. Ding, P. *et al.* A Novel AT-Rich DNA Recognition Mechanism for Bacterial Xenogeneic Silencer MvaT. *PLoS Pathog.* **11**, 1004967 (2015).

46. Duan, B. *et al.* How bacterial xenogeneic silencer rok distinguishes foreign from self DNA in its resident genome. *Nucleic Acids Res.* **46**, 10514–10529 (2018).

47. Ueguchi, C., Suzuki, T., Yoshida, T., Tanaka, K. I. & Mizuno, T. Systematic mutational analysis revealing the functional domain organization of Escherichia coli nucleoid protein H-NS. *J. Mol. Biol.* **263**, 149–162 (1996).

48. Ribeiro-Guimarães, M. L. & Pessolani, M. C. V. Comparative genomics of mycobacterial proteases. *Microb. Pathog.* **43**, 173–178 (2007).

49. Drozdetskiy, A., Cole, C., Procter, J. & Barton, G. J. JPred4: a protein secondary structure prediction server. *Nucleic Acids Res.* **43**, W389–W394 (2015).

50. Lupas, A., Dyke, M. Van & Stock, J. Predicting coiled coils from protein sequences. *Science (80-.).* **252**, 1162–1164 (1991).

51. Qin, L. *et al.* Structural basis for osmotic regulation of the DNA binding properties of H-NS proteins. *Nucleic Acids Res.* (2020) doi:10.1093/nar/gkz1226.

52. Bouffartigues, E., Buckle, M., Badaut, C., Travers, A. & Rimsky, S. H-NS cooperative binding to high-

affinity sites in a regulatory element results in transcriptional silencing. *Nat. Struct. Mol. Biol.* **14**, 441–448 (2007).

53. Smits, W. K., Hoa, T. T., Hamoen, L. W., Kuipers, O. P. & Dubnau, D. Antirepression as a second mechanism of transcriptional activation by a minor groove binding protein. *Mol. Microbiol.* **64**, 368–81 (2007).

54. Halford, S. E. & Marko, J. F. How do site-specific DNA-binding proteins find their targets? *Nucleic Acids Research* vol. 32 3040–3052 (2004).

55. Gao, Y. *et al.* Charged residues in the H-NS linker drive DNA binding and gene silencing in single cells. *Proc. Natl. Acad. Sci.* **114**, 12560–12565 (2017).

56. Gulvady, R., Gao, Y., Kenney, L. J. & Yan, J. A single molecule analysis of H-NS uncouples DNA binding affinity from DNA specificity. *Nucleic Acids Res.* **46**, 10216–10224 (2018).

57. Winardhi, R. S. *et al.* Higher order oligomerization is required for H-NS family member MvaT to form gene-silencing nucleoprotein filament. *Nucleic Acids Res.* **40**, 8942–8952 (2012).

58. Liu, Y., Chen, H., Kenney, L. J. & Yan, J. A divalent switch drives H-NS/DNA-binding conformations between stiffening and bridging modes. *Genes Dev.* **24**, 339–44 (2010).

59. Lim, C. J., Lee, S. Y., Kenney, L. J. & Yan, J. Nucleoprotein filament formation is the structural basis for bacterial protein H-NS gene silencing. *Sci. Rep.* **2**, (2012).

60. Qu, Y., Lim, C. J., Whang, Y. R., Liu, J. & Yan, J. Mechanism of DNA organization by Mycobacterium tuberculosis protein Lsr2. *Nucleic Acids Res.* **41**, 5263–5272 (2013).

61. van der Valk, R. A. *et al.* Mechanism of environmentally driven conformational changes that modulate H-NS DNA-Bridging activity. *Elife* **6**, (2017).

62. Qin, L., Erkelens, A. M., Markus, D. & Dame, R. T. The B. subtilis Rok protein compacts and organizes DNA by bridging. *bioRxiv* https://doi.org/10.1101/769117 (2019) doi:https://doi.org/10.1101/769117.

63. Dame, R. T. The role of nucleoid-associated proteins in the organization and compaction of bacterial chromatin. *Molecular Microbiology* vol. 56 858–870 (2005).

64. Shahul Hameed, U. F. *et al.* H-NS uses an autoinhibitory conformational switch for environment-controlled gene silencing. *Nucleic Acids Res.* **1**, 23955–6900 (2018).

65. Wootton, J. C. & Drummond, M. H. The Q-linker: a class of interdomain sequences found in bacterial multidomain regulatory proteins. *Protein Eng.* **2**, 535–43 (1989).

66. Dame, R. T., Rashid, F. Z. & Grainger, D. C. Chromosome organization in bacteria: mechanistic insights into genome structure and function. *Nat. Rev. Genet.* https://doi.org/10.1038/s41576-019-0185-4 (2019).

67. Valens, M., Penaud, S., Rossignol, M., Cornet, F. & Boccard, F. Macrodomain organization of the Escherichia coli chromosome. *EMBO J.* **23**, 4330–4341 (2004).

68. Valens, M., Thiel, A. & Boccard, F. The MaoP/maoS Site-Specific System Organizes the Ori Region of the E. coli Chromosome into a Macrodomain. *PLOS Genet.* **12**, e1006309 (2016).

69. Duigou, S. & Boccard, F. Long range chromosome organization in Escherichia coli: The position of the replication origin defines the non-structured regions and the Right and Left macrodomains. *PLoS Genet.* **13**, e1006758 (2017).

70. Mercier, R. *et al.* The MatP/matS site-specific system organizes the terminus region of the E. coli chromosome into a macrodomain. *Cell* **135**, 475–85 (2008).

71. Sánchez-Romero, M. A. *et al.* Dynamic Distribution of SeqA Protein across the Chromosome of Escherichia coli K-12. *MBio* **1**, (2010).

72. Tonthat, N. K. *et al.* Molecular mechanism by which the nucleoid occlusion factor, SlmA, keeps cytokinesis in check. *EMBO J.* **30**, 154–64 (2011).

73. Dame, R. T., Kalmykowa, O. J. & Grainger, D. C. Chromosomal macrodomains and associated proteins: Implications for DNA organization and replication in gram negative bacteria. *PLoS Genetics* vol. 7 (2011).

74. Deng, S., Stein, R. A. & Higgins, N. P. Organization of supercoil domains and their reorganization by transcription. *Mol. Microbiol.* **57**, 1511–21 (2005).

75. Hardy, C. D. & Cozzarelli, N. R. A genetic selection for supercoiling mutants of Escherichia coli reveals proteins implicated in chromosome structure. *Mol. Microbiol.* **57**, 1636–52 (2005).

76. Postow, L., Hardy, C. D., Arsuaga, J. & Cozzarelli, N. R. Topological domain structure of the Escherichia coli chromosome. *Genes Dev.* **18**, 1766–1779 (2004).

77. Worcel, A. & Burgi, E. On the structure of the folded chromosome of Escherichia coli. *J. Mol. Biol.* **71**, 127–47 (1972).

78. Noom, M. C., Navarre, W. W., Oshima, T., Wuite, G. J. L. & Dame, R. T. H-NS promotes looped domain formation in the bacterial chromosome. *Curr. Biol.* **17**, R913-4 (2007).

79. Lioy, V. S. *et al.* Multiscale Structuring of the E. coli Chromosome by Nucleoid-Associated and Condensin Proteins Escherichia coli Article Multiscale Structuring of the E. coli Chromosome by Nucleoid-Associated and Condensin Proteins. *Cell* **172**, 771-783.e18 (2018).

80. Le, T. B. K., Imakaev, M. V., Mirny, L. A. & Laub, M. T. High-Resolution Mapping of the Spatial Organization of a Bacterial Chromosome. *Science (80-.).* **342**, 731–734 (2013).

81. Val, M.-E. *et al.* A checkpoint control orchestrates the replication of the two chromosomes of *Vibrio cholerae*. *Sci. Adv.* **2**, e1501914 (2016).

82. Blot, N., Mavathur, R., Geertz, M., Travers, A. & Muskhelishvili, G. Homeostatic regulation of supercoiling sensitivity coordinates transcription of the bacterial genome. *EMBO Rep.* **7**, 710–5 (2006).

83. Shin, M. *et al.* DNA looping-mediated repression by histone-like protein H-NS: specific requirement of E 70 as a cofactor for looping. (2005) doi:10.1101/gad.1316305.

84. Dame, R. T., Wyman, C., Wurm, R., Wagner, R. & Goosen, N. Structural Basis for H-NS-mediated Trapping of RNA Polymerase in the Open Initiation Complex at the rrnB P1. *J. Biol. Chem.* **277**, 2146–2150 (2001).

85. Schröder, O. & Wagner, R. The bacterial DNA-binding protein H-NS represses ribosomal RNA transcription by trapping RNA polymerase in the initiation complex. *J. Mol. Biol.* **298**, 737–748 (2000).

86. Grainger, D. C., Hurd, D., Goldberg, M. D. & Busby, S. J. W. Association of nucleoid proteins with coding and non-coding segments of the Escherichia coli genome. *Nucleic Acids Res.* **34**, 4642–4652 (2006).

87. Butland, G. *et al.* Interaction network containing conserved and essential protein complexes in Escherichia coli. *Nature* **433**, 531–537 (2005).

88. Kotlajich, M. V *et al.* Bridged filaments of histone-like nucleoid structuring protein pause RNA polymerase and aid termination in bacteria. **4**, 4970 (2015).

89. Boudreau, B. A. *et al.* StpA and Hha stimulate pausing by RNA polymerase by promoting DNA–DNA bridging of H-NS filaments. *Nucleic Acids Res.* **46**, gky265–gky265 (2018).

90. Hamoen, L. W., Van Werkhoven, A. F., Bijlsma, J. J. E., Dubnau, D. & Venema, G. The competence transcription factor of Bacillus subtilis recognizes short A/T-rich sequences arranged in a unique, flexible pattern along the DNA helix. *Genes Dev.* **12**, 1539–1550 (1998).

91.   Hamoen, L. W., Van Werkhoven, A. F., Venema, G. & Dubnau, D. The pleiotropic response regulator DegU functions as a priming protein in competence development in Bacillus subtilis. *Proc. Natl. Acad. Sci.* **97**, 9246–9251 (2002).

92.   Albano, M. *et al.* The Rok protein of Bacillus subtilis represses genes for cell surface and extracellular functions. *J. Bacteriol.* **187**, 2010–9 (2005).

93.   Ono, S. *et al.* H-NS is a part of a thermally controlled mechanism for bacterial gene regulation. *Biochem. J.* **391**, 203–13 (2005).

94.   Göransson, M. *et al.* Transcriptional silencing and thermoregulation of gene expression in Escherichia coli. *Nature* **344**, 682–685 (1990).

95.   White-Ziegler, C. A. & Davis, T. R. Genome-wide identification of H-NS-controlled, temperature-regulated genes in Escherichia coli K-12. *J. Bacteriol.* **191**, 1106–10 (2009).

96.   Lease, R. A. & Belfort, M. A trans-acting RNA as a control switch in Escherichia coli: DsrA modulates function by forming alternative structures. *Proc. Natl. Acad. Sci. U. S. A.* **97**, 9919–24 (2000).

97.   Jordi, B. J. *et al.* The positive regulator CfaD overcomes the repression mediated by histone-like protein H-NS (H1) in the CFA/I fimbrial operon of Escherichia coli. *EMBO J.* **11**, 2627–32 (1992).

98.   Han, Y. *et al.* Microarray Analysis of Temperature-Induced Transcriptome of *Yersinia pestis*. *Microbiol. Immunol.* **48**, 791–805 (2004).

99.   Ueguchi, C. & Mizuno, T. The Escherichia coli nucleoid protein H-NS functions directly as a transcriptional repressor. *EMBO J.* **12**, 1039 (1993).

100. Nagarajavel, V., Madhusudan, S., Dole, S., Rahmouni, A. R. & Schnetz, K. Repression by binding of H-NS within the transcription unit. *J. Biol. Chem.* **282**, 23622–23630 (2007).

101. Winardhi, R. S., Yan, J. & Kenney, L. J. Biophysical Perspective H-NS Regulates Gene Expression and Compacts the Nucleoid: Insights from Single-Molecule Experiments. *Biophysj* **109**, 1321–1329 (2015).

102. Atlung, T., Knudsen, K., Heerfordt, L. & BrØndsted, L. Effects of σ(s) and the transcriptional activator AppY on induction of the Escherichia coli hya and cbdAB-appA operons in response to carbon and phosphate starvation. *J. Bacteriol.* **179**, 2141–2146 (1997).

103. van der Valk, R. A., Qin, L., Moolenaar, G. F. & Dame, R. T. Quantitative Determination of DNA Bridging Efficiency of Chromatin Proteins. in *Bacterial Chromatin. Methods in Molecular Biology, vol 1837* (ed. Dame R.T.) 199–209 (Humana Press, New York, NY, 2018). doi:10.1007/978-1-4939-8675-0_12.

104. Zhang, A. & Belfort, M. *Nucleotide sequence of a newly-identified Escherichia coli gene, stpA, encoding an H-NS-like protein. Nucleic Acids Research* vol. 20 (1992).

105. Shi, X. & Bennett, G. N. Plasmids bearing hfq and the hns-like gene stpA complement hns mutants in modulating arginine decarboxylase gene expression in Escherichia coli. *J. Bacteriol.* **176**, 6769–75 (1994).

106. Zhang, A., Rimsky, S., Reaban, M. E., Buc, H. & Belfort, M. Escherichia coli protein analogs StpA and H-NS: regulatory loops, similar and disparate effects on nucleic acid dynamics. *EMBO J.* **15**, 1340–9 (1996).

107. Sonden, B. & Uhlin, B. E. Coordinated and differential expression of histone-like proteins in Escherichia coli: regulation and function of the H-NS analog StpA. *EMBO J.* **15**, 4970–80 (1996).

108. Free, A. & Dorman, C. J. The Escherichia coli stpA gene is transiently expressed during growth in rich medium and is induced in minimal medium and by stress conditions. *J. Bacteriol.* **179**, 909–18 (1997).

109. Müller, C. M. *et al.* Differential effects and interactions of endogenous and horizontally acquired H-NS-like proteins in pathogenic *Escherichia coli*. *Mol. Microbiol.* **75**, 280–293 (2010).

110. Leonard, P. G., Ono, S., Gor, J., Perkins, S. J. & Ladbury, J. E. Investigation of the self-association and hetero-association interactions of H-NS and StpA from *Enterobacteria*. *Mol. Microbiol.* **73**, 165–179 (2009).

111. Johansson, J. & Uhlin, B. E. Differential protease-mediated turnover of H-NS and StpA revealed by a mutation altering protein stability and stationary-phase survival of Escherichia coli. *Proc. Natl. Acad. Sci. U. S. A.* **96**, 10776–81 (1999).

112. Johansson, J., Eriksson, S., Sondén, B., Sun Nyunt Wai & Uhlin, B. E. Heteromeric interactions among nucleoid-associated bacterial proteins: Localization of StpA-stabilizing regions in H-NS of Escherichia coli. *J. Bacteriol.* **183**, 2343–2347 (2001).

113. Lim, C. J., Whang, Y. R., Kenney, L. J. & Yan, J. Gene silencing H-NS paralogue StpA forms a rigid protein filament along DNA that blocks DNA accessibility. *Nucleic Acids Res.* **40**, 3316–28 (2012).

114. Williamson, H. S. & Free, A. A truncated H-NS-like protein from enteropathogenic Escherichia coli acts as an H-NS antagonist. *Mol. Microbiol.* **55**, 808–827 (2005).

115. Prieto, A. *et al.* Evolution of Bacterial Global Modulators: Role of a Novel H-NS Paralogue in the Enteroaggregative Escherichia coli Strain 042. *mSystems* **3**, (2018).

116. Beloin, C., Deighan, P., Doyle, M. & Dorman, C. J. Shigella flexneri 2a strain 2457T expresses three members of the H-NS-like protein family: characterization of the Sfh protein. *Mol. Genet. Genomics* **270**, 66–77 (2003).

117. Deighan, P., Beloin, C. & Dorman, C. J. Three-way interactions among the Sfh, StpA and H-NS nucleoid-structuring proteins of Shigella flexneri 2a strain 2457T. *Mol. Microbiol.* **48**, 1401–1416 (2003).

118. Doyle, M. *et al.* An H-NS-like stealth protein aids horizontal DNA transmission in bacteria. *Science* **315**, 251–2 (2007).

119. Baños, R. C. *et al.* Differential Regulation of Horizontally Acquired and Core Genome Genes by the Bacterial Modulator H-NS. *PLoS Genet.* **5**, e1000513 (2009).

120. Fernández-De-Alba, C., Berrow, N. S., Garcia-Castellanos, R., García, J. & Pons, M. On the Origin of the Selectivity of Plasmidic H-NS towards Horizontally Acquired DNA: Linking H-NS Oligomerization and Cooperative DNA Binding. *J. Mol. Biol.* **425**, 2347–2358 (2013).

121. Vallet-Gely, I., Donovan, K. E., Fang, R., Joung, J. K. & Dove, S. L. Repression of phase-variable cup gene expression by H-NS-like proteins in Pseudomonas aeruginosa. *Proc. Natl. Acad. Sci. U. S. A.* **102**, 11082–7 (2005).

122. Suzuki, C. *et al.* Oligomerization and DNA-Binding Capacity of Pmr, a Histone-Like Protein H1 (H-NS) Family Protein Encoded on IncP-7 Carbazole-Degradative Plasmid pCAR1. *Biosci. Biotechnol. Biochem.* **75**, 711–717 (2011).

123. Suzuki, C. *et al.* Oligomerization Mechanisms of an H-NS Family Protein, Pmr, Encoded on the Plasmid pCAR1 Provide a Molecular Basis for Functions of H-NS Family Members. *PLoS One* **9**, e105656 (2014).

124. Yun, C.-S. *et al.* MvaT Family Proteins Encoded on IncP-7 Plasmid pCAR1 and the Host Chromosome Regulate the Host Transcriptome Cooperatively but Differently. *Appl. Environ. Microbiol.* **82**, 832–42 (2016).

125. Sun, Z. *et al.* Growth phase-dependent expression profiles of three vital H-NS family proteins encoded on the chromosome of Pseudomonas putida KT2440 and on the pCAR1 plasmid. *BMC*

Microbiol. **17**, (2017).

126. Chandra, G. & Chater, K. F. Developmental biology of Streptomyces from the perspective of 100 actinobacterial genome sequences. *FEMS Microbiology Reviews* vol. 38 345–379 (2014).

127. Gehrke, E. J. *et al.* Silencing cryptic specialized metabolism in Streptomyces by the nucleoid-associated protein Lsr2. *Elife* **8**, (2019).

128. Singh, P. K. *et al.* Inhibition of *Bacillus subtilis* natural competence by a native, conjugative plasmid-encoded *comK* repressor protein. *Environ. Microbiol.* **14**, 2812–2825 (2012).

129. Madrid, C., Balsalobre, C., García, J. & Juárez, A. The novel Hha/YmoA family of nucleoid-associated proteins: use of structural mimicry to modulate the activity of the H-NS family of proteins. *Mol. Microbiol.* **63**, 7–14 (2007).

130. Nieto, J. M. *et al.* Expression of the hemolysin operon in Escherichia coli is modulated by a nucleoid-protein complex that includes the proteins Hha and H-NS. *Mol. Gen. Genet.* **263**, 349–58 (2000).

131. Ueda, T. *et al.* Functions of the Hha and YdgT Proteins in Transcriptional Silencing by the Nucleoid Proteins, H-NS and StpA, in Escherichia coli. *DNA Res.* **20**, 263–271 (2013).

132. García, J. *et al.* Interaction between the bacterial nucleoid associated proteins Hha and H-NS involves a conformational change of Hha. *Biochem. J.* **388**, 755–762 (2005).

133. García, J., Madrid, C., Juárez, A. & Pons, M. New Roles for Key Residues in Helices H1 and H2 of the Escherichia coli H-NS N-terminal Domain: H-NS Dimer Stabilization and Hha Binding. *J. Mol. Biol.* **359**, 679–689 (2006).

134. Ali, S. S. *et al.* Structural Insights into the Regulation of Foreign Genes in Salmonella by the Hha/H-NS Complex. *J Biol Chem* **288**, 13356–13369 (2013).

135. Prieto, A. *et al.* Tracking bacterial virulence: Global modulators as indicators. *Sci. Rep.* **6**, 25973 (2016).

136. Bernabeu, M. *et al.* Gene duplications in the E. coli genome: Common themes among pathotypes. *BMC Genomics* **20**, (2019).

137. Forns, N., Baños, R. C., Balsalobre, C., Juárez, A. & Madrid, C. Temperature-dependent conjugative transfer of R27: Role of chromosome- and plasmid-encoded Hha and H-NS proteins. *J. Bacteriol.* **187**, 3950–3959 (2005).

138. Shintani, M., Suzuki-Minakuchi, C. & Nojiri, H. Nucleoid-associated proteins encoded on plasmids: Occurrence and mode of function. *Plasmid* **80**, 32–44 (2015).

139. Liu, Q. & Richardson, C. C. Gene 5.5 protein of bacteriophage T7 inhibits the nucleoid protein H-NS of Escherichia coli. *Proc. Natl. Acad. Sci. U. S. A.* **90**, 1761–5 (1993).

140. Ali, S. S., Beckett, E., Bae, S. J. & Navarre, W. W. The 5.5 protein of phage T7 inhibits H-NS through interactions with the central oligomerization domain. *J. Bacteriol.* **193**, 4881–92 (2011).

141. Walkinshaw, M. D. *et al.* Structure of Ocr from bacteriophage T7, a protein that mimics B-form DNA. *Mol. Cell* **9**, 187–94 (2002).

142. Ho, C.-H., Wang, H.-C., Ko, T.-P., Chang, Y.-C. & Wang, A. H.-J. The T4 phage DNA mimic protein Arn inhibits the DNA binding activity of the bacterial histone-like protein H-NS. *J. Biol. Chem.* **289**, 27046–54 (2014).

143. Melkina, O. E., Goryanin, I. I. & Zavilgelsky, G. B. The DNA–mimic antirestriction proteins ArdA ColIB-P9, Arn T4, and Ocr T7 as activators of H-NS-dependent gene transcription. *Microbiol. Res.* **192**, 283–291 (2016).

144. Wagemans, J. *et al.* Antibacterial phage ORFans of Pseudomonas aeruginosa phage LUZ24 reveal a novel MvaT inhibiting protein. *Front. Microbiol.* **6**, 1242 (2015).

145. Datta, C. *et al.* Physical and functional interaction between nucleoid-associated proteins HU and Lsr2 of *Mycobacterium tuberculosis* : altered DNA binding and gene regulation. *Mol. Microbiol.* (2019) doi:10.1111/mmi.14202.

146. Seid, C. A., Smith, J. L. & Grossman, A. D. Genetic and biochemical interactions between the bacterial replication initiator DnaA and the nucleoid-associated protein Rok in Bacillus subtilis. *Mol. Microbiol.* **103**, 798–817 (2017).

147. Kurokawa, K., Nishida, S., Emoto, A., Sekimizu, K. & Katayama, T. Replication cycle-coordinated change of the adenine nucleotide-bound forms of DnaA protein in Escherichia coli. *EMBO J.* **18**, 6642–6652 (1999).

148. Burkholder, W. F., Kurtser, I. & Grossman, A. D. Replication Initiation Proteins Regulate a Developmental Checkpoint in Bacillus subtilis. *Cell* **104**, 269–279 (2001).

149. Bannister, A. J. & Kouzarides, T. Regulation of chromatin by histone modifications. *Cell Res.* **21**, 381–395 (2011).

150. Dilweg, I. W. & Dame, R. T. Post-translational modification of nucleoid-associated proteins: an extra layer of functional modulation in bacteria? *Biochem. Soc. Trans.* **46**, 1381–1392 (2018).

151. Schmidt, A. *et al.* The quantitative and condition-dependent Escherichia coli proteome. *Nat. Biotechnol.* **34**, 104–10 (2016).

152. Kuhn, M. L. *et al.* Structural, Kinetic and Proteomic Characterization of Acetyl Phosphate-Dependent Bacterial Protein Acetylation. *PLoS One* **9**, e94816 (2014).

153. Weinert, B. T. *et al.* Lysine Succinylation Is a Frequently Occurring Modification in Prokaryotes and Eukaryotes and Extensively Overlaps with Acetylation. *Cell Rep.* **4**, 842–851 (2013).

154. Hansen, A.-M. *et al.* The Escherichia coli Phosphotyrosine Proteome Relates to Core Pathways and Virulence. *PLoS Pathog.* **9**, e1003403 (2013).

155. Turapov, O. *et al.* Two Faces of CwlM, an Essential PknB Substrate, in Mycobacterium tuberculosis. *Cell Rep.* **25**, 57-67.e5 (2018).

156. Alqaseer, K. *et al.* Protein kinase B controls Mycobacterium tuberculosis growth via phosphorylation of the transcriptional regulator Lsr2 at threonine 112. *Mol. Microbiol.* (2019) doi:10.1111/mmi.14398.

157. Gaviard, C., Jouenne, T. & Hardouin, J. Proteomics of *Pseudomonas aeruginosa* : the increasing role of post-translational modifications. *Expert Rev. Proteomics* **15**, 757–772 (2018).

158. Ravichandran, A., Sugiyama, N., Tomita, M., Swarup, S. & Ishihama, Y. Ser/Thr/Tyr phosphoproteome analysis of pathogenic and non-pathogenic Pseudomonas species. *Proteomics* **9**, 2764–75 (2009).

159. Liu, L., Wang, G., Song, L., Lv, B. & Liang, W. Acetylome analysis reveals the involvement of lysine acetylation in biosynthesis of antibiotics in Bacillus amyloliquefaciens. *Sci. Rep.* **6**, 20108 (2016).

160. Reverdy, A., Chen, Y., Hunter, E., Gozzi, K. & Chai, Y. Protein lysine acetylation plays a regulatory role in Bacillus subtilis multicellularity. *PLoS One* **13**, e0204687 (2018).

Chapter 2

Structural basis for osmotic regulation of the DNA binding properties of H-NS proteins

Abstract

H-NS proteins act as osmotic sensors translating changes in osmolarity into altered DNA binding properties, thus, regulating enterobacterial genome organization and genes transcription. The molecular mechanism underlying the switching process and its conservation among H-NS family members remains elusive. Here, we focus on the H-NS family protein MvaT from *P. aeruginosa* and demonstrate experimentally that its protomer exists in two different conformations, corresponding to two different functional states. In the half-opened state (dominant at low salt) the protein forms filaments along DNA, in the fully opened state (dominant at high salt) the protein bridges DNA. This switching is a direct effect of ionic strengths on electrostatic interactions between the oppositely charged DNA binding and N-terminal domains of MvaT. The asymmetric charge distribution and intramolecular interactions are conserved among the H-NS family of proteins. Therefore, our study establishes a general paradigm for the molecular mechanistic basis of the osmosensitivity of H-NS proteins.

Introduction

Bacteria are frequently exposed to changes in their extracellular *milieu*. Key to their survival is to adapt quickly to these environmental fluctuations by adjusting their cellular machinery, enabling them to operate optimally under the new conditions, and to acquire new competencies through horizontal gene transfer (HGT) [1]. These adaptation mechanisms are regulated by the bacterial genome, the dynamic organisation of which modulates access to the genetic material to adapt and fine-tune gene expression and for incorporation of DNA of foreign origin [2].

The Histone-like nucleoid structuring (H-NS) protein is a key regulator of the dynamic bacterial genome [3,4]. The protein is conserved among enterobacteria and plays determining role in their nucleoid architecture. Generally, this protein acts as repressor of transcription, silencing the expression of many different genes and operons. Often the genes and operons targeted by H-NS family proteins are regulated by environmental factors such as osmolarity, pH and temperature (see Chapter 1) [5-7]. Additionally, H-NS family members have the unique ability to "switch off" xenogeneic genes, often in pathogens, to suppress their detrimental effect on bacterial fitness, until external conditions require expression [8-11]. To similar effect, H-NS has been shown to silence spurious transcription at intragenic promoters in *E. coli* [12].

H-NS is expressed at high levels (> 20 000 copies per cell). The protein binds non-specifically to DNA, but has a preference towards genomic regions with high AT content [10,11,13], containing specific six contiguous steps[14]. DNA binding typically initiates at such high-affinity sites on the DNA [15]. This step is followed by oligomerization of the protein, forming lateral nucleoprotein filaments [16], which stiffens DNA [17]. Under appropriate conditions the protein can mediate bridge formation between this filament and a second DNA duplex [18-22].

The current paradigm is that divalent ions drive the transition between lateral H-NS-DNA filaments and bridged DNA-H-NS-DNA complexes, without dissociation of the protein from the DNA [20,23]. This switching between the two types of complexes is believed to be the mechanistic basis of the role of H-NS proteins in bacterial nucleoid organisation and transcription regulation [20,23,24]. Nonetheless, the molecular basis that governs this phenomenon is still controversial. Previously published molecular dynamics of H-NS, indicated that the switch between the two DNA binding

modes involves a change from a half-open (also referred as a closed conformation) to an open conformation driven by $MgCl_2$ [20]. These conformational changes are modulated by the interactions between the N-terminal domain of H-NS and its C-terminal DNA binding domain (DBD). Mutagenesis at the interface of these domains generated an H-NS variant no longer sensitive to $MgCl_2$, which can form filaments and bridge DNA. Recently, these interactions were confirmed by Arold and co-workers using truncated H-NS domains [25]. However, it was claimed that these interactions could not occur unless H-NS oligomerization is abolished by temperature. These discrepancies in conclusions arise presumably from the lack of experimental structural information on the full-length protein in solution.

H-NS family members share a conserved fold topology, with a C-terminal DBD and an N-terminal domain connected via a flexible linker [26,27]. The structural unit of an H-NS nucleoprotein filament is a dimer (also called protomer) formed through the N-terminal dimerization sites of two monomers (site 1), which further oligomerize through a secondary oligomerization site (site 2) [28] (Fig. 2.1 a,b). Multiple studies have revealed the structures of H-NS truncated domains including the dimerization sites and the DBD from different bacteria [14,29-31]. Meanwhile, no structure of the full-length protein is available. The structure of the N-terminal domain oligomer (1-83) of the *S. typhimurium* H-NS C21S mutant was solved by crystallography[32]. These studies revealed a helical scaffold of a head-head and tail-tail protomer organisation, suggesting structural models involving that type of H-NS arrangement in both lateral H-NS-DNA filaments and bridged DNA-H-NS-DNA complexes.

Early studies by liquid state NMR on full length H-NS from *E. coli* and *S. typhimurium* have shown that resonances of the N-terminal domain residues were missing in the protein heteronuclear single quantum coherence (HSQC) NMR spectrum [29,33]. A similar observation was made using solid-state NMR in which case only 33% of the protein spectrum was assigned [34]. These difficulties were attributed to the inherent dynamics and structural heterogeneity of the system. Thus, owing to their flexibility and the large size of their self-assembled complexes, the characterization of the conformational landscape of full-length H-NS proteins and its contribution to functional regulation remains a challenge. In this work we have overcome these constraints by using an abridged

structural version of H-NS, MvaT from *P. aeruginosa*, in which we scrutinized its protomer structural/function relationship in response to changes in the surrounding ionic strength.

MvaT is a functional homologue of H-NS that regulates the expression of ~350 genes including the genes responsible for virulence [35] and biofilm formation [36,37]. Like other members of the H-NS family, oligomerization of MvaT along DNA is required for its gene silencing activity [38,39] and ability to stiffen and bridge DNA duplexes [19,39].

Here, we have combined integrative structural biology methods and (single-molecule) biochemical assays to decipher the structural changes in MvaT that drive the switch between its DNA stiffening and bridging activities under the influence of different salt conditions. These structural changes appear to be conserved within the H-NS family of proteins. Our studies thus provide a fundamental answer on how H-NS family members respond to changes in the osmotic environment to modulate their DNA binding modes, and hence to regulate bacterial nucleoid organisation and gene expression.

Material and Methods

Construction of expression vectors and mutagenesis

The MvaT coding gene from P. *aeruginosa* and its DBD (residues 76-124) were subcloned into pET30b vector without and with C-terminal 6×His-tag, respectively, using Gibson assembly[40]. The Gibson assembly primers were purchased from Sigma-Aldrich. Mutated MvaT derivatives were generated using the same approach. Accuracy of the cloned sequences was confirmed by DNA sequencing.

DNA substrates

All tethered particle motion and pull-down bridging assay experiments were performed using a random, AT-rich, 685 bp (32% GC) DNA substrate. The DNA substrate was generated by PCR and the products were purified using a GenElute PCR Clean-up kit (Sigma-Aldrich). If required, DNA was ^{32}P-labeled as described previously [20]. For the electrophoretic mobility shift assay an AT-rich 200 bp (32%GC) was generated using the same procedure.

The oligonucleotides to generate the 12 bp DNA duplex d(CGCATATATGCG) were purchased from Sigma Aldrich. The lyophilized oligonucleotides were solubilized in 20 mM Bis-Tris Buffer, 50 mM or 300mM KCl, pH 6, combined and hybridized by heating to 98°C for 3 min, followed by slow cooling down to room temperature. The 12 bp DNA duplex was used for NMR titration of the MvaT dimer and DBD.

Protein expression and purification

E. coli BL21 competent cells were transformed with the MvaT pET30b vector and cultured in LB medium. For ^{15}N ^{13}C or ^{15}N isotopic labelling, the transformed cells were first cultured in 2 mL LB medium and then transferred into 50 mL of inoculation culture in M9 medium (comprising the required isotopes) for incubation overnight at 37 °C. The inoculation culture was diluted in 1L M9 medium and was incubated at 37 °C until it reached an $OD_{600} \approx 0.6$. MvaT production was induced by adding 100 μM of isopropyl β-D-1-thiogalactopyranoside (IPTG) and the culture was incubated overnight at 20 °C. The next day cells were harvested by centrifugation and the pellet was resuspended in the lysis buffer (20 mM Tris, 150 mM NaCl, 10 mM EDTA, pH 7). The cells were lysed using pre-cooled French press, and the lysate was centrifuged for 20 min at 8000 rpm. Next, the supernatant was loaded on a Heparin column (from GE healthcare Life sciences) and the protein was eluted by applying a NaCl gradient from 0.15 to 1 M. The eluted fractions were checked by SDS-PAGE and the ones that contain the MvaT dimer were pooled, concentrated and buffer changed using a PD10 column to 20 mM Bis-tris, 50 mM KCl, pH 6. Next, the protein was loaded on a SP column (from GE healthcare Life sciences) and eluted by applying a NaCl gradient (from 0.15 to 1 M). The eluted fractions were also checked by SDS-PAGE and the ones that contain the MvaT dimer were pooled and concentrated to a 500 μL volume with an Amicon 10 kDa cut-off filter. The concentrated protein fractions were loaded on a GE Superdex 75 10/300 GL column and eluted with 20 mM Bis-tris, 150 mM KCl, pH 6. The collected fractions were buffer exchanged to either 20 mM Bis-tris, 50 mM KCl or 300mM KCl, 1mM EDTA, pH 6. The purity of the protein was checked by SDS-PAGE (>95%) and the concentration was determined using a bicinchoninic acid assay. The same procedure was used for the DBD over-expression and purification. The only difference in purification was in the first step where a nickel column was used

instead of a heparin column. The yield of purified MvaT dimer and DBD per liter of culture are 4 mg and 2 mg, respectively.

The Tethered Particle Motion (TPM)

The Tethered Particle Motion experiments were done as previously described [20,41] and the flow cells were prepared with minor modifications. In short, first, the flow cell was washed with 100 μl of wash buffer (10 mM Tris-HCl pH 8, 150 mM NaCl, 1 mM EDTA, 1 mM DTT, 3% Glycerol, 100 μg/ml BSA (ac)) and experimental buffer (10 mM Tris pH 8, 10 mM EDTA, 5% glycerol with different salt concentrations as indicated in the text). The flow cell was sealed after adding protein (0 nM to 1600 nM) in experimental buffer, followed by 15 minutes of incubation. The measurements were initiated 15 min after introducing protein. For each flow cell more than 200 beads were measured at a temperature of 25°C. Data analysis was done as reported previously [20,41].

Pull down bridging Assay

The DNA Bridging Assay was performed as described previously (see Chapter 5) [20,42], with minor modifications. The Streptavidin-coated Magnetic Dynabeads M280 (3 µL per sample) were resuspended in 6 µl coupling buffer (CB: 20 mM Tris-HCl pH 8.0, 2 mM EDTA, 2 M NaCl, 2 mg/mL BSA (ac), 0.04% Tween20) containing 3 µl 100 fmol biotinylated 32% GC DNA (685bp), and the bead suspensions were incubated for 20 min at 25°C on a shaker (1000 rpm). The beads were then washed twice with incubation buffer (IB: 10 mM Tris-HCl pH 8.0, 5% v/v Glycerol, 1 mM Spermidine) before resuspension in IB. Next, salt (KCl, NaCl, Kglu, $CaCl_2$, $MgCl_2$ or $MgSO_4$) was added to the desired concentration in each sample. Radioactive DNA (around 8000 cpm) was added to each sample and unlabeled 685 bp (32% GC) DNA was added to maintain a constant (2 fmol/µl) DNA concentration. MvaT or H-NS proteins were added to initiate the formation of bridged DNA-DNA complex. The mixture was incubated for 20 min (unless indicated otherwise) on the shaker at 1000 rpm at 25°C. After the incubation, the beads of each sample were washed once with its experimental buffer, before resuspension in 12 µl counting buffer (10 mM Tris pH 8.0, 1 mM EDTA, 200 mM NaCl, 0.2% SDS). The radioactive signal of samples was quantified by liquid scintillation over 5 min. Sample values recovered from the bridging assay were corrected for

background signal (from a control sample without protein). The DNA recovery was calculated based on a reference sample containing the amount of labeled ^{32}P 685 bp DNA used in each sample and expressed as 'DNA recovery (%)'. All DNA bridging experiments were performed at least in duplicate. Each experiment contained 20 mM KCl, to which additional salt (KCl, NaCl, Kglu, CaCl$_2$, MgCl$_2$ or MgSO$_4$) was added depending on the tested experimental conditions.

Electrophoretic mobility shift assay

The assay was performed on an AT-rich 200 bp DNA substrate (32%GC). Typically, 25 ng of DNA was incubated with different concentrations of the MvaT wild type or the MvaT dimer F36D/M44D in the binding buffer (10 mM Tris-HCl, 50 mM KCl, pH 7.5). The mixture was loaded on a 1% agarose gel (containing 1:10^4 dilution of Gel red DNA stain) with 1μl of 6 × loading buffer (10mM Tris-HCl pH 7.6, 0.03% bromophenol blue, 0.03 % xylene cyanol FF, 60% glycerol and 60 mM EDTA). The samples were run at 16 mA for 4 hours at 4°C in TAE standard buffer. The gels were visualized with a Bio-rad Gel Doc XR+ system.

Circular dichroism

The MvaT wild type and F36D/M44D dimer far-UV CD spectra were recorded on a Jasco 810 CD spectrometer using a 10 μM protein solution in 20 mM Bis-Tris Buffer, 150 mM KCl, pH 6. The spectra were recorded in a 0.1 cm path length quartz cuvette using four scans with a bandwidth and a wavelength step of 1 nm. The obtained spectra were background corrected and smoothed using Jasco Spectra Manager.

Isothermal titration calorimetry

ITC experiments were performed using a MicroCal VP-ITC system at 20 °C. The samples contained 20 mM Bis-Tris, pH 6 with 50 mM KCl. Typically, 10 μM of MvaT F36D/M44D was placed in the cell (1.4 mL) and titrated with 360 μM (500 μL volume) of the DNA duplex d(CGCATATATGCG), injected in 2 μL aliquots. The delay time between the injections was 60 s with a stirring speed of 307 rpm. The corresponding "protein to buffer" controls were performed for background correction. The ITC titration data were analysed using Origin 7.0 (OriginLab) provided with the instrument. Standard deviation was calculated from the fit by Origin.

Small angle X-ray scattering

All the experiments were performed at the ESRF BioSAXS beamline BM29, Grenoble, France [43]. Given the sensitivity of the batch SAXS mode for even small amounts of large soluble aggregates we used SEC-SAXS approaches to measure SAXS data only on monodisperse samples. A volume of 250 µL of protein for each MvaT sample was loaded on a GE Superdex 75 10/300 GL column *via* a high performance liquid chromatography (HPLC) system (DGU-20A5R, Shimadzu, France) attached directly to the sample-inlet valve of the BM29 sample changer. Low salt MvaT sample was measured at 11 mg/mL in 20 mM Bis-Tris, 50 mM KCl, pH 6.0, while high salt MvaT sample was measured at 9.5 mg/ mL in 20 mM Bis-Tris, 300 mM KCl, pH 6.0. The column was equilibrated with 3 column volumes to obtain a stable background signal, which was confirmed before measurement. All the SAXS data were collected at a wavelength of 0.99 Å using a sample-to-detector (PILATUS 1 M, DECTRIS) distance of 2.81 m. The scattering of pure water was used to calibrate the intensity to absolute units [44]. Data reduction was performed automatically using the EDNA pipeline [45]. Frames in regions of stable R_g were selected and averaged using PRIMUS [46] to yield a single averaged frame corresponding to the scattering of individual SEC species. Analysis of the overall parameters was carried out by PRIMUS from ATSAS 2.8.4 package [47] and by ScÅtter 3.0 software. The pair distance distribution function, P(r), and maximum diameter of the particle (D_{max}) were calculated in GNOM using indirect Fourier transform method [48]. The information on data collection and derived structural parameters is summarized in Table S2.1. The pair distance distribution functions were used to calculate *ab initio* models in P1 symmetry with DAMMIN; the models were averaged, aligned and compared using DAMAVER [47].

NMR resonance assignments

Sequential assignment of the MvaT dimer at 20 °C was performed using the triple resonances HNCACB, CBCAcoNH, HNCA, HNcoCA, HNCO and HNcaCO experiments on a ^{15}N, ^{13}C MvaT F36D/M44D NMR sample (0.5 mM in 20 mM Bis-Tris, 150 mM KCl, 1mM EDTA, pH 6). The NMR spectra were recorded on a Bruker Avance III (HD) 600 MHz spectrometer, equipped with TCI cryoprobe, processed by TopSpin 3.5 (Bruker Biospin) and analysed with Sparky software [49]. The peak list of MvaT dimer was used to assign the MvaT dimer K31C mutant HSQC spectrum. The assignments of the MvaT F36D/M44D spectra are submitted to BMRB under the entry: 28010.

NMR titration experiments

The NMR titration of the MvaT dimer and DBD with the 12 bp DNA substrate was performed on a 95 or 100 µM ^{15}N isotopically labelled protein samples, respectively, in 20 mM Bis-Tris Buffer, 50 mM KCl or 300 mM KCl, pH 6 and 6% D_2O. A series of ^{1}H-^{15}N HSQC spectra were acquired by gradually increasing the DNA:MvaT molar ratio from 0.1 or 0.2 to 1.6. The experiments were recorded at 20 °C on a Bruker Avance III (HD) 600 MHz spectrometer, equipped with TCI cryoprobe, processed by TopSpin 3.5 (Bruker Biospin) and analysed by CCPnmr software[50]. The MvaT dimer titration with KCl was conducted using the same procedure. The reference titration points were collected in a solution with 20 mM Bis-Tris, 50 mM KCl, pH 6 and the potassium chloride concentration was increased in steps to 100, 150, 200, 250 and 300 mM KCl.

The changes in peak positions and intensities were analysed by an in-house python script and the average chemical shift perturbations (CSP) were calculated using equation (1):

$$\Delta\delta_{avg} = \sqrt{\Delta\delta_H{}^2 + \frac{\Delta\delta_N{}^2}{6.25^2}} \qquad (1)$$

Line shape analysis of the titration data was performed by TITAN [51] using a two-state binding model.

Protein labelling and PRE measurement

To attach the MTS [(1-Acetyl-2,2,5,5-tetramethyl-3-pyrroline-3-methyl)-methanethiosulfonate] and MTSL [S-(1-oxyl-2,2,5,5-tetramethyl-2,5-dihydro-1H-pyrrol-3-yl)methyl methanesulfonothioate] spin labels (bio-connect Life sciences) on the MvaT dimer surface, K31 was substituted with a cysteine. A ^{15}N isotopically labelled sample of the variant MvaT K31C/F36D/K44D was produced using the procedure described above. The purified protein was first incubated for 1 hour at room temperature in the presence of 10 mM DTT to reduce disulphide bonds, followed by buffer exchange using PD10 desalting column. The protein was directly eluted into a solution of 20 times molar excess of MTS or MTSL. The mixture was incubated for 1 h stirring at 4 °C. The sample was concentrated to a volume of 500 µL with an Amicon 10 kDa cut-off filter and injected into a GE Superdex 75 10/300 GL column to remove excess spin label. Incorporation of MTSL was >95% according to mass spectrometry, and the dimeric state of the conjugated protein was checked by

analytical size exclusion chromatography. PREs were obtained using ^{1}H-^{15}N TROSY spectra of 185 μM MvaT in 20 mM Tris, pH 6 at low salt (50 mM KCl) or high salt (300 mM) and in the presence or absence of DNA, with a DNA-to-protein molar ratio of 1.6. The TROSY spectra of the diamagnetic and paramagnetic samples were processed using TopSpin 3.5 and peak intensities and line widths were extracted using CCPnmr analysis[50]. The paramagnetic contribution to the transverse relaxation rate (R2sp) was estimated from the measured intensity ratio of the paramagnetic and diamagnetic samples using equation[52] (2):

$$Ipara/Idia = \frac{R2 \exp(-R2sp*t)}{(R2+R2sp)} \quad (2)$$

where I_{para}/I_{dia} is the measured intensity ratio, R_2 is the relaxation rate estimated from the widths at the half-height of the diamagnetic sample resonances, and t is the time during which ^{1}H magnetisation is in the transverse plane during the TROSY pulse sequence (10 ms).

MvaT structure homology modelling

The full-length MvaT dimer was constructed by combining a homology model of the dimerization domain (residues 1-78) and the NMR structure of the DNA binding domain (PDB ID: 2MXE) [53] (residues 79-124), using Modeller version 9.15. The homology model for the dimerization domain was obtained by aligning residues 1-78 of MvaT to the crystal structure of the N-terminal domain of *P. putida* TurB (PDB ID: 5B52) [54].

Conjoint ensemble refinement against PRE and SAXS data

All simulations were performed in Xplor-NIH[55,56], starting from the homology model of the MvaT F36D/M44D dimer generated in this work (see text). The positions of the N-terminal domains of the MvaT dimer (residues 1-47) were fixed, the C-terminal DNA-binding domain (residues 83-122) was treated as a rigid-body group, while the intervening linker was given full degree of freedom. The computational protocol comprised an initial rigid-body simulated annealing step followed by the side-chain energy minimization as described before[57]. The energy function consisted of standard geometric (bonds, angles, dihedrals, and impropers) and steric (van der Waals) terms, a knowledge-based dihedral angle potential, and the PRE and SAXS energy terms incorporating the experimental data[58]. Truncated SAXS curves (q < 0.4 Å^{-1}) and the PRE data for the C-terminal

DNA-binding domain and the interdomain linker (residues 50-124) at each salt condition were used as the experimental input[57,58]. Multiple copies of MvaT dimers (N = 1-5) were refined simultaneously in order to simulate molecular ensembles of multiple conformers[57] (Note that this procedure allows for the atomic overlap among MvaT molecules constituting an ensemble). In each run, 100 independent calculations were performed, and 10 lowest-energy solutions were selected for further analysis.

During the simulations, the PRE contributions from both subunits were taken into account. The PRE for each residue was defined as the sum of four contributions: 1) PRE from spin label (SL) on subunit 1 to the residue on subunit 1; 2) PRE from SL on subunit 1 to the residue on subunit 2; 3) PRE from SL on subunit 2 to the residue on subunit 2; 4) PRE from SL on subunit 2 to the residue on subunit 1.

To assess the agreement between the observed PREs and the PREs back-calculated from the simulated ensembles generated in each run, we calculated the Q factor[59], equation (3):

$$Q = \sqrt{\sum_i \left(\Gamma_{2,i}^{\mathrm{obs}} - \Gamma_{2,i}^{\mathrm{calc}}\right)^2 \Big/ \sum_i \left(\Gamma_{2,i}^{\mathrm{obs}}\right)^2} \qquad (3),$$

where $\Gamma_{2,i}^{\mathrm{calc}}$ is given by equation (4):

$$\Gamma_{2,i}^{\mathrm{calc}} = \frac{1}{N} \sum_{j=1}^{N} \Gamma_{2,ij} \qquad (4),$$

where N is the ensemble size and $\Gamma_{2,ij}$ is the PRE back-calculated for the amide proton of residue (i) of the ensemble member (j).

The agreement with the experimental SAXS data in each run was assessed by calculating χ^2 with the calcSAXS helper program[57], which is part of the Xplor-NIH v 2.49 package used in this work, assuming equal conformer populations in the simulated ensembles. The lowest energy structures of the MvaT dimer obtained from the ensemble modelling were fitted into the *ab initio* molecular shapes obtained by DAMMIN using UCSF Chimera software [60]. The MvaT structural ensembles are submitted to SASDB with accession codes: SASDGS5 for MvaT (low salt) and SASDGT5 for MvaT (high salt).

Results

Fold topology and electrostatics of H-NS family proteins

Primary sequence alignments and secondary structure predictions of twelve members of the H-NS family of proteins, from different bacteria, reveal a conserved fold topology (fig. S2.1). Their C-terminal DBD contains, in most cases, two β-strands and two α-helices. The domain is connected to an N-terminal domain via a disordered linker. The N-terminal domain contains α-helices connected via random coils, but the number of helices may differ. Based on these criteria, two classes of H-NS members could be distinguished: long and short versions of H-NS. The long H-NS members have an N-terminal domain which includes four helices (α1, α2, α3 and α4), forming a dimerization site (site 1) between the H-NS monomers and an oligomerization site (site 2) between its protomers (fig. 2.1a). The crystal structure of the H-NS N-terminal domain (1-83) has shown that site 1 is formed by a "hand-shake fold" topology between α1 and α2 and part of α3. Site 1 is stabilized by a hydrophobic core and salt bridges [31,32] (fig. 2.1a). In the short members (MvaT; MvaU; TurA and TurB), these two N-terminal helices are missing (fig. 2.1b; S2.1). The crystal structure of the TurB N-terminal domain (1- 61) has revealed that site 1 is formed by a "coiled-coil motif" between the N-terminal helices α1 (corresponding to H-NS α3) of two monomers [54] (fig. 2.1b).

Using the TurB N-terminal domain crystal structure, we have built a homology model of the MvaT dimerization site which was connected via the flexible linkers to the NMR structure of the protein DNA binding domains (PDB ID: 2MXE) [53], thus obtaining a full-length structural model of the MvaT protomer (fig. 2.1b). We used this model for structural investigation.

In contrast to the differences in site 1, the oligomerisation site (site 2) fold architecture appears to be conserved between these members of the H-NS family (fig. 2.1a,b). This site is also formed by hydrophobic interactions between two α-helices (α4 and α2 for the long and short members, respectively) and stabilised by salt bridges [32,54].

One striking characteristic is a local degree of conservation of the electrostatic potential between H-NS and MvaT protomers. Their electrostatic potential surfaces show that the N-terminal domain

(helices $\alpha3$ and $\alpha1$ of H-NS and MvaT, respectively) contain negatively charged surface patches, whereas the C-terminal domain and the linker region contain positively charged regions (fig. 2.1c).

This characteristic appears to be shared between the H-NS family members, as it can be predicted from the conserved position of the negatively and positively charged residues within their primary sequences (fig. 2.1d). The five amino acid averaged charge window analysis of the primary sequences revealed that the α-helices in the N-terminal domain include predominantly negatively charged regions, while the linkers and the DNA binding domains are mostly positively charged, as they both contribute to DNA binding [61-63] (fig. 2.1d; S2.1). Additionally, α1 and α2 of the long H-NS members are positively charged in line with their contribution to the interaction with DNA [31] (fig. 2.1d; S2.1). Thus, this asymmetrical charge distribution seems to be a conserved feature between H-NS family members suggesting a specific role in their function.

In solution, it is expected that the two DNA binding domains of the H-NS protomers behave as 'beads on a flexible string', where the function of the linkers is to enable a relatively unhindered spatial search by the attached domains. Thus, electrostatic interactions between the oppositely charged domains, as suggested by earlier studies [20,25], might occur. These interactions are possibly sensitive to changes of ionic strengths in the protein environment.
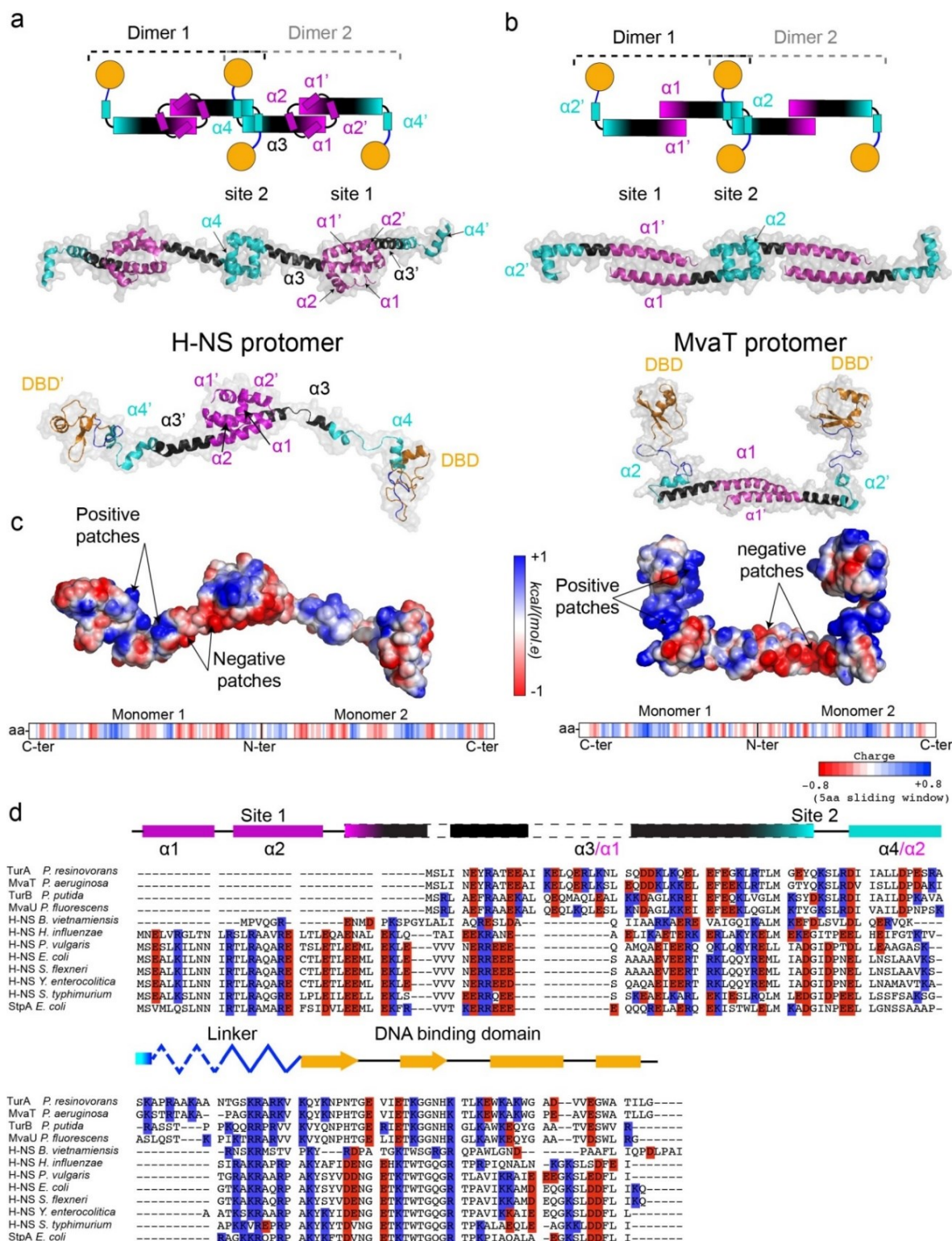
Figure 2.1: Fold topology and charged residue/charge distributions of H-NS family proteins. (a) N-terminal dimerization sites of long H-NS family members. The upper panel depicts a schematic representation of the long H-NS oligomer. The dimerization sites (site 1) are shown in magenta and the oligomerization sites (site 2) in cyan. The DNA binding domain is shown in orange sphere and the linker

region in blue. In the middle panel is the H-NS N-terminal domain crystal structure (1-83) (PDB ID: 3NR7) [32]. Site 1 and Site 2 helices are coloured and labelled as in the upper panel. In the lower panel is the H-NS protomer structural model adapted from our earlier MD simulation studies [20]. (b) N-terminal dimerization sites of short H-NS family members. The upper panel depicts a schematic representation of the short H-NS oligomer. In the middle panel is the TurB N-terminal domain crystal structure (1-64) (PDB ID: 5B52) [54]. Lower panel is the MvaT protomer structural homology model (see M&M). The colour code is as in (a). (c) The electrostatic potential surfaces of H-NS and MvaT are depicted on full-length protomer structural models of the proteins using a red/white/blue colour gradient. The negative and positive patches on the proteins' surfaces are indicated. In the lower panel is the five amino acid averaged charge window of the proteins protomers primary sequences. Positive, negative and neutral charged amino acid fragments are shown in blue, red and white bars, respectively. (d) Primary sequence alignment of selected members of the H-NS family of proteins from different bacterial organisms. The conserved positions of the charged amino acids in the protein's primary sequences are highlighted in blue (positive residues) in red (negative residues). The fold diagram of the H-NS monomer from *E. coli* is represented using the same colour code in (a). The nomenclature of the N-terminal helices is indicated in black for the long H-NS family members and in magenta for the short members.

Salt induces global conformational changes in MvaT protomer

To test our hypothesis that the MvaT protomer conformation is sensitive to changes in ionic strength of the surrounding medium, we employed a combination of circular dichroism, small-angle X-ray scattering (SAXS) and NMR spectroscopy. To this purpose, we engineered an MvaT variant in which oligomerization was abolished by substituting site 2 residues F36 and M44 with aspartic acid (D), remote from the negative charge patch of the N-terminal region. As site 1 is left unchanged, it was expected that MvaT could still form dimers, which was confirmed by size-exclusion chromatography (fig. S2.2a,b). The double mutation induces changes in the MvaT α-helical content as concluded from the overlay between the wild type and the mutant far UV CD spectra (fig. S2.2c). A similar observation was reported for H-NS from *S. typhimurium*, which was attributed to the loss of the protein oligomerization ability [33]. In the oligomeric state the helix of site 2 (α2) is locked in a helical structure by interacting with its counterpart from another MvaT dimer.

In the dimeric state this helix seems to experience exchange between extended and helical conformations (fig. 2.2d)."

The effect of the double mutation on the binding of MvaT to DNA was assessed by electrophoretic mobility shift assay (fig. S2.2d,e). Binding of the MvaT wild type caused a major reduction in DNA substrate mobility, whereas for the double mutant DNA mobility was only mildly affected. We attribute this to a lack of DNA binding cooperativity for the dimeric MvaT derivative, as confirmed by tethered particle motion (see M&M) (fig. S2.2f).

SAXS was employed to assess the effect of salt concentration on the global conformation of the MvaT F36D/M44D dimer (fig. 2.2a and Table S2.1). Under low salt conditions (50 mM KCl) the MvaT protomer adopts a relatively compact conformation as evidenced by the normalised Kratky plot and the particle's Porod exponent (3.2) (Table S2.1). Interestingly, at high salt concentrations (300 mM KCl), the MvaT protomer displays an increased flexibility, which is reflected by an increase in R_g (3.56 nm vs. 3.83 nm) and D_{max} (14.70 nm vs. 15.84 nm), a decrease in Porod exponent (3.2 vs. 2.7), and the appearance of the normalised Kratky plot (fig. 2.2a and Table S2.1).

In parallel to the SAXS analysis, we produced an isotopically labelled ^{15}N ^{13}C MvaT sample for which the ^{1}H-^{15}N HSQC NMR spectrum was assigned at 150 mM KCl. The protein spectrum shows well-dispersed resonances corresponding to residues of the DBD and multiple overlapped peaks (crowded region) centred around 8.2 ppm in the ^{1}H dimension, reporting on the helical N-terminal domain and the disordered linker (fig. 2.2b). Remarkably, the MvaT spectrum shows more resonances than expected, indicating the presence of two forms. Two resonances are observed for the amide groups of residues 45-47 and residue 53, which form the oligomerization site (site 2), and of residues 61-65 in the linker region (fig. 2.2b). Amides of the "coiled-coil" (site 1) show weak resonances and several of them could not be assigned due to broad lines (fig. 2.2b). The $C\alpha$ and $C\beta$ chemical shifts were used to predict the secondary structure probability of the MvaT dimer in solution (fig. 2.2d). Amino acid sequences of α-helix 2 (51-58), the linker (60-80) and of short stretches of α1 appear to be disordered. The presence of intrinsically disordered regions agrees with the secondary structure prediction from the far-UV CD spectrum. The deconvolution of the protein CD spectrum revealed that 40-45 % of the protein is disordered (fig. 2.2c).
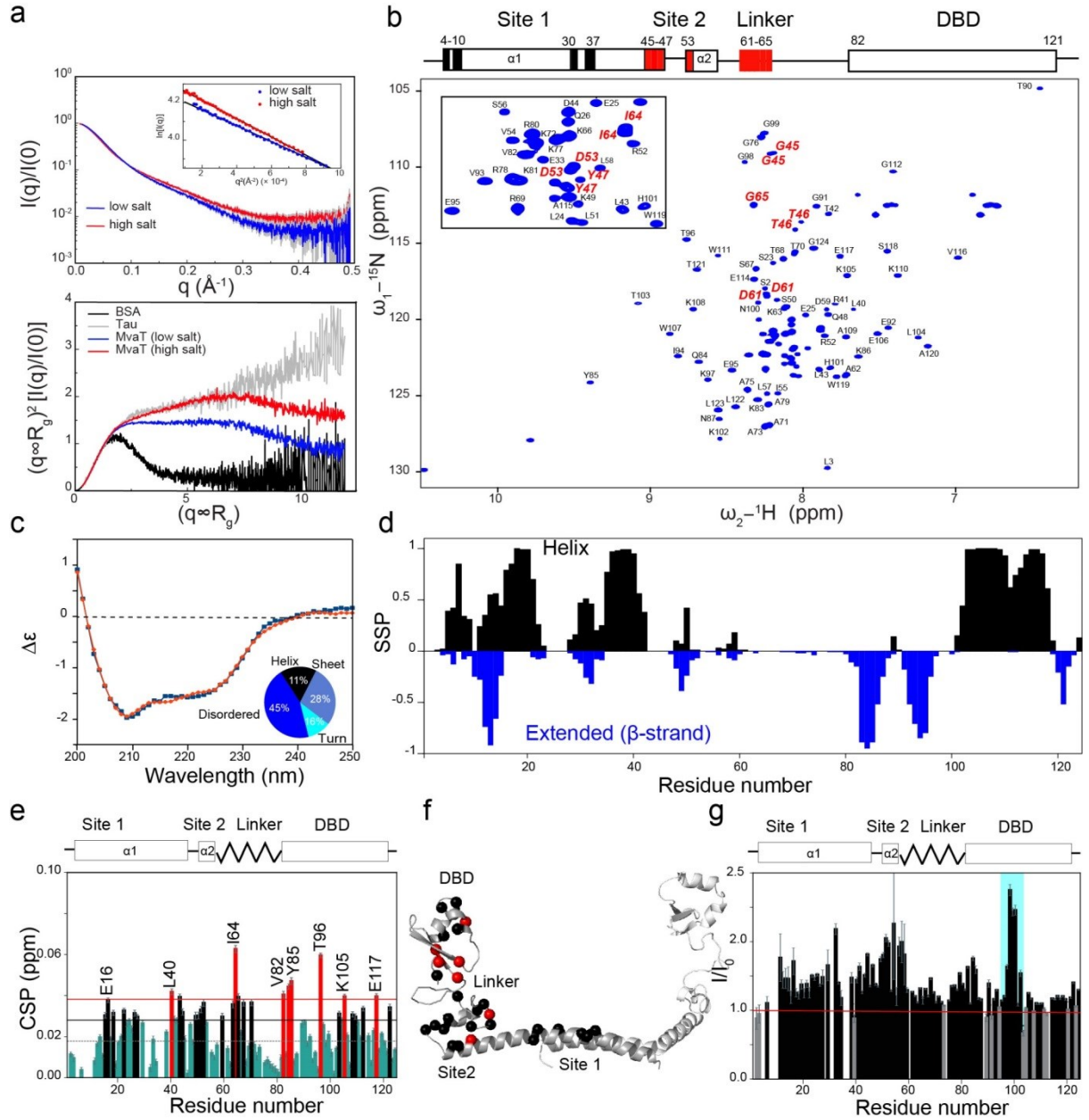
Figure 2.2: Global conformational changes in MvaT induced by salt. (a) SAXS experiments. The top panel displays the SAXS data obtained for the MvaT dimer under low salt (50 mM KCl) and high salt (300 mM KCl) conditions indicated by the blue and red curves, respectively. The error margins are coloured in grey. The inset shows the Guinier regions of both data sets. The bottom panel displays the normalised Kratky plots for the MvaT dimer under both salt conditions. An intrinsically disordered standard (Tau, grey trace) and a rigid, globular standard (BSA, black trace) are shown for comparison. (b) Assignment of the ^{1}H-^{15}N HSQC MvaT spectrum (at 150 mM KCl). Residues that appear as double peaks in the spectrum are labelled in red. Insert is a zoom in at the crowded region of the spectrum. The layout of the MvaT domains is shown above the spectrum. Residue positions with non-observable resonances in the HSQC spectrum

are marked by black rectangles. The residue positions with two observable resonances are in red. (c) Circular dichroism spectra of MvaT dimer (experimental data in blue and spectrum deconvoluted using BeStSel in red [64]). (d) Secondary structure probability (SSP) plot of the MvaT dimer derived from Cα and Cβ chemical shifts, determined by PECAN[65]. Negative values in blue bars indicate β-strand or extended secondary structures and positive values in black bars indicate α-helices. (e) Weighted average CSP of the MvaT resonances between 50 and 300 mM KCl. Resonances with CSP more than two (red line) or one (black line) standard deviation (SD) from the 10% trimmed mean (grey dashed line) are labelled and shown in red, black and green bars, respectively. (f) Residues exhibiting CSP mapped on the structural model of the MvaT dimer (see M&M). Amide nitrogens with a CSP > 1 and 2 SD trimmed mean are shown in spheres and coloured in black and red, respectively. (g) The HSQC peak intensity ratio of the MvaT dimer at 300 mM KCl (I) and 50 mM KCl (I$_0$). Grey bars indicate residues with minor peak intensity changes between the two salt conditions. Loop 95-102 of the DBD is highlighted with a cyan rectangle.

Next, we investigated the binding of potassium chloride to the MvaT protomer by NMR titration. Small chemical shift perturbations (CSP) in the fast exchange regime were observed for multiple resonances. Residues exhibiting CSP are scattered on regions of site 1, site 2, the linker and the DBD in the structural model of the MvaT dimer (fig. 2.2f), suggesting a non-specific effect due to the increase in ionic strength. Interestingly, the protein resonances show a general yet non-uniform increase of intensities at high salt compared to low salt. This suggests a decrease in the rotational correlation time of the protein folded domains (fig. 2.2g), possibly caused by the disruption of their intramolecular interactions. This observation is in line with the larger radius of gyration and the enhancement of protein flexibility derived from the SAXS data.

In conclusion, the increase in ionic strength, indeed induces global conformational changes of the MvaT dimer by shifting its conformational equilibrium from relatively compact to extended and flexible states. These structural changes are possibly due to the salt modulation of the postulated intramolecular electrostatic interactions between the oppositely charged regions of the MvaT protomer.

Salt modulation of the MvaT dimer conformational landscape

To obtain more information about the conformational changes induced by salt on the MvaT dimer, we used paramagnetic relaxation enhancement (PRE) NMR spectroscopy. PRE reports on long-range structural distances (20 to 30 Å) between a paramagnetic spin label and the amide protons of the protein [66]. Amide protons on residues within 30 Å from the spin label experience an increase in relaxation rate resulting in broadening of their NMR resonances and intensity reduction. To measure PRE on the MvaT dimer, we substituted residue K31 with a cysteine and conjugated it with either a paramagnetic (MTSL) or a diamagnetic (MTS) probe (see M&M).

Under low salt condition (50 mM KCl), strong PRE effects were observed for residues of site 1 (1-48) (fig. 2.3a). These residues were excluded from the analysis as they display weak peak intensities in the HSQC diamagnetic spectrum and sense the paramagnetic effects from spin labels on both MvaT subunits. Residues of site 2 (49-60) and the linker region (61-80) exhibit also strong PREs, indicating that the amide nuclei spend at least part of the time close the probe (fig. 2.3a). A weak PRE effect occurred for residues of the DBD, except for the loop between 95-105 that, in the DNA-bound state, is known to intercalate with the DNA minor groove [53]. The strong PRE effects within this loop suggest a rather localized interaction between the DBD and a region of the protein close to the spin label.

At 300 mM KCl, the PRE pattern is overall similar, but a decrease in PRE is observed for the site 2 residues, the linker regions and loop 95-105 of the DBD (fig. 2.3b). Under this condition, these regions could either be populating conformations in which the nuclei are further away from the spin label or spend a smaller fraction of the time in the conformation close to the spin label.

To investigate the structural states sampled by the MvaT dimer under both salt conditions, we performed ensemble calculation using an Xplor-NIH protocol which combines the PRE and SAXS data as structural restraints. For each condition, we simulated molecular ensembles of multiple conformers (N = 1-5) and assessed their agreement with the experimental data by calculating the corresponding quality metrics (PRE Q-factor and the SAXS χ^2) (see M&M). The best solutions for the low salt were obtained with N=3 (Q = 0.21; χ^2 = 1.43) (fig. 2.3c; S2.3a) and for the high salt

with N=2 (Q = 0.37; χ^2 = 1.33) (fig. 2.3d; S2.3b). The 10 lowest-energy solutions for each ensemble fit well within the molecular shapes determined by DAMMIF (fig. 2.3e,f) [67].

In agreement with the flexibility observed for MvaT in both low and high salt conditions (with a significantly more pronounced flexibility at high salt concentration), the SAXS and PRE data sets could only be described by a conformational ensemble. As expected, under low-salt conditions the MvaT ensemble is composed of rather compact conformers, while at higher salt concentrations the ensemble members adopt more extended conformations due to an increased flexibility (fig. 2.3e,f).

Based on the DBD position relative to the N-terminal domain two major species could be distinguished in both conformational ensembles: half-opened and fully-opened forms. In the half-opened states, the DBD is bound to the N-terminal domain, while the other domain is free (fig. 2.3g,h). The occupancy of the N-terminal domain with one of the DBD of the dimer appears to prevent simultaneous binding of the second DBD to the N-terminal domain due to steric hinderance. This might explain the observed asymmetrical structural configuration of the MvaT homodimer in the half-open forms.

In the fully-opened states, both DBDs are not bound to the N-terminal domain but can still be close to each other in space. Both of conformational species comprise several sub-populations with different radii of gyration (fig. 2.3e,f).

Under both salt conditions, the DBD in the major conformer of the half-opened states exhibits similar intra-subunit binding modes to the N-terminal domain, although a slight difference in orientation is observed (fig. S2.3c). The binding interface includes the positively charged loop 95-ET**K**GGN**HK**-102 (charge = 1.8, pH 6) of the DBD and the negatively charged segment 26-Q**DD**KLKKE**L**EDEE-38 (charge = -3.8, pH 6) of the N-terminal domain. In contrast, at low salt the linker appears to form closer interactions with the negatively charged patch of the N-terminal domain (26-38) compared to the high salt condition. This indicates that the linker might be involved in stabilizing the DBD-N-terminal domain complex.

In conclusion, the structural study reveals the existence of electrostatic interdomain interactions between the DBD and N-terminal domains of MvaT which are further stabilized by the linker region.

Increase in salt concentration induces delicate changes within the MvaT protomer conformational landscape by weakening these intramolecular interactions and increasing the exchange rate between the half-open and open conformers. Consequently, the protein samples a larger conformational space.
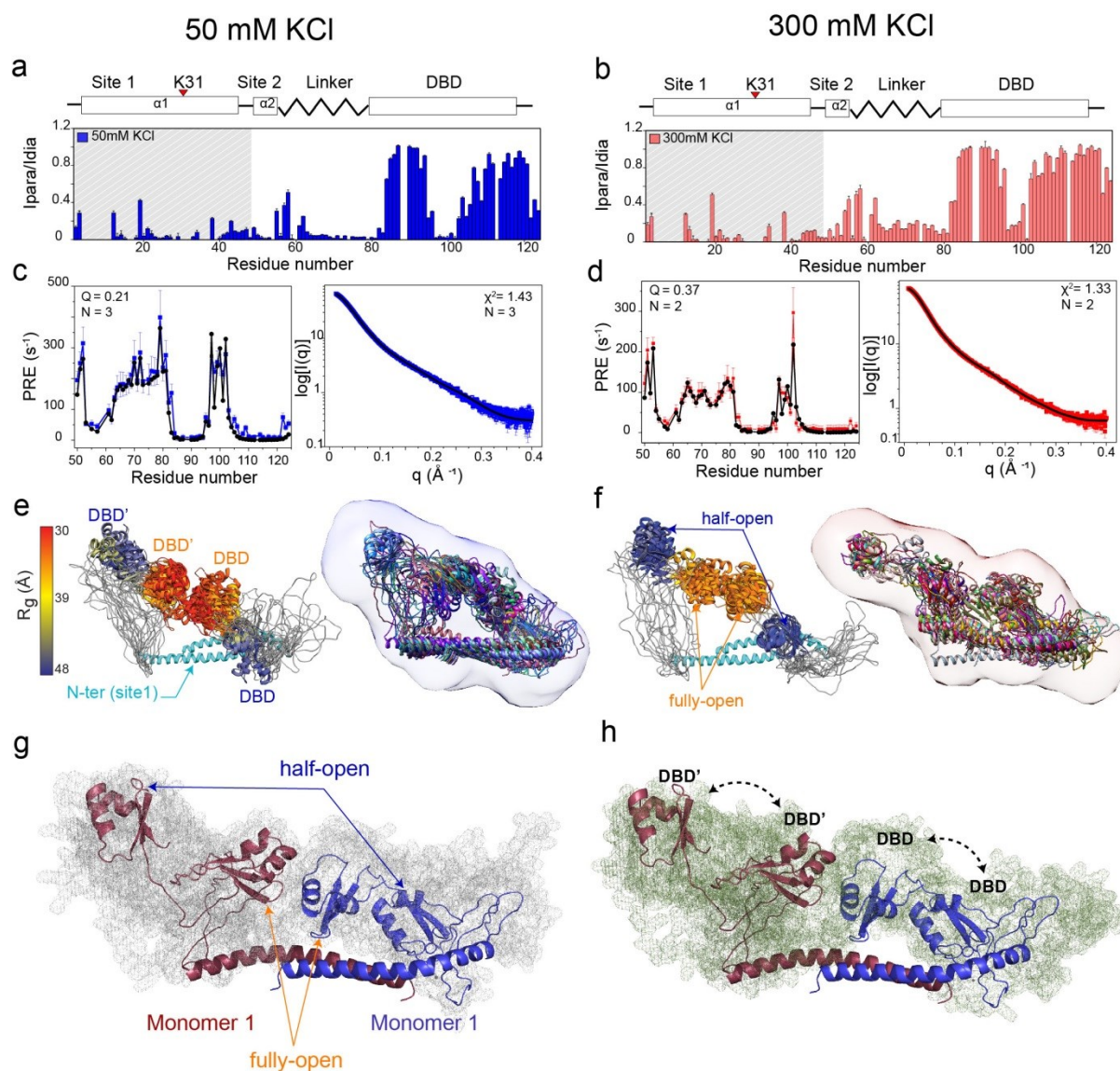

Figure 2.3: MvaT dimer structural ensembles at low and high salt conditions. (a), (b) The PRE-intensity ratio (Ipara/Idia) vs. residues number of the MvaT dimer at 50 mM KCl (blue bars) and 300 mM KCl (red bars), respectively. PRE from residues in the shaded region were excluded from the analysis. The structure of the MvaT monomer is shown schematically above the panels and the MTSL labelling position is indicated by the red triangle. The error bars are inversely proportional to the propagated signal-to-noise ratio of individual resonances. (c) and (d) The experimental PRE and SAXS curves (50 mM KCl in blue and 300

mM KCl in red) fit (black line) to the top conformers of the low and high salt ensembles, respectively. (e, f) Low (e) and high salt (f) best conformers coloured by their radius of gyration using a blue/orange gradient, respectively. The colour gradient is depicted only on the DBD of the MvaT dimer (DBD' and DBD refer to MvaT subunits 1 and 2, respectively). The best conformers are fitted into the *ab initio* molecular shapes generated by DAMMIF [67]. The low (g) and high salt (h) half-open and fully open conformers of the MvaT dimer, classified based on the position of DBDs relative to the N-terminal domain. The atomic probability distribution maps of the low and high salt ensembles are shown in grey and green meshes, respectively. The MvaT monomers are colored in red and blue. The dashed arrows indicate the exchange between the DBD configurations.

The DNA substrate contributes to the MvaT protomer conformational opening

Owing to the negative charge and specificity for the DBD it is conceivable that the DNA also modulates the interdomain interactions of the MvaT protomer. To test this hypothesis, a titration of the MvaT dimer with a 12 bp AT-rich DNA substrate at low (50 mM KCl) and high salt (300 mM KCl) concentrations, was performed using NMR. At low salt, significant CSP were observed for residues of the DBD. At the DNA:MvaT molar ratio of 1.6, a general line broadening of the DBD peaks is observed attributed to the increase of its rotational correlation time (τ_c) upon complex formation, independent of the protomer N-terminal domain (fig. S2.4a). Analysis of the titration data using a 1:1 binding model yields a $K_D = 44 \pm 5$ nM and $k_{off} = 280 \pm 5$ s^{-1} (fig. S2.4c). The affinity is too high to be deduced from this NMR titration with accuracy. Therefore, we used ITC for validation, yielding $K_D = 30 \pm 2$ nM (fig. S2.4d). No significant CSP for the N-terminal domain residues were observed, indicating that the interactions with the short DNA substrate are limited to the DBD and a few residues of the linker region (fig. 2.4a). However, a 1:1 binding model may be an oversimplification.

The ensemble structure of the MvaT dimer at 50 mM KCl revealed that interactions between the DBD and the N-terminal domain occur, with only one of the two DBD binding at any time, effectively creating two populations of DBD (fig. 2.4d). Thus, one DBD is free to bind to the DNA, whereas for the other competition for binding occurs between DNA and the N-terminal domain. The NMR spectra seem to catch this difference in the DBD forms at a DNA:MvaT molar ratio of 0.2, showing two peaks with different CSP for the DBD resonances (fig. 2.4c;2.3e). In the absence

of DNA, the DBD will be in exchange between bound and free states, and also within the bound state, it may sample multiple interactions in an encounter complex like state. Broad lines are observed for multiple amide resonances including the ones that correspond to residues of loop 95-105 (fig. S2.3d; 2.2g), suggesting that these exchange processes are intermediate to fast on the NMR time scale (i.e. the chemical shift differences between bound and free). Addition of DNA will bind the population of free DBD preferably, splitting the resonances of the two populations, provided the exchange rate between the states of DBD bound to the N-terminal domain and bound to the DNA is sufficiently slow. At higher concentrations of DNA the exchange rate is increased ($k_{ex} = k_{on}[DNA] + k_{off}$) and the exchange between the two DBD populations is too fast to result in double peaks. This model is supported by titration studies of the isolated DBD with DNA. In the absence of the N-terminal domain, the resonances of the DBD show single peaks at 0.1 and 0.2 DNA:MvaT molar ratios (fig. S2.3e).

At high salt, the interdomain interactions are weakened by the ionic strength and the exchange rates between the DBD free and bound to the N-terminal becomes fast on the NMR time scale. Therefore, the peak splitting, observed under the low salt condition, becomes invisible (fig. 2.4c,d). Interestingly, in this case smaller amplitude of CSP are observed upon DNA binding, yet with the same direction as for the low salt (fig. 2.4b). This suggests that part of the complex is in an encounter state which is in equilibrium with the specific state and does not contribute to CSP [68]. Nonetheless, a general line broadening of the DBD resonances remained observable (fig. S2.4b) and residues involved in the direct interaction with the DNA disappear. Analysis of the titration data yields a $K_D = 7.7 \pm 0.3 \ \mu M$ and a $k_{off} = 2 \pm 0.2 \times 10^3 \ s^{-1}$ (fig. S2.4b,c).

The conformational opening of the MvaT protomer induced by DNA, at low and high salt, was probed by changes in the PRE upon addition of DNA (at DNA:MvaT = 1.6). At low salt, a substantial loss in the PRE is observed for residues 60-80 of the linker region and the dimerization site 2 (fig. 2.4e). Almost no PRE effect on the DBD was observed. This indicates that the protein is adopting a fully-opened conformation in which the DNA substrate is shielding the DBD and part of the linker region from the interaction with the N-terminal domain. At high salt, this effect is less pronounced, yet DNA still reduces the PRE (fig. 2.4f). These results provide evidence that salt and DNA substrate have an additive effect on the conformational opening of the MvaT protomer.
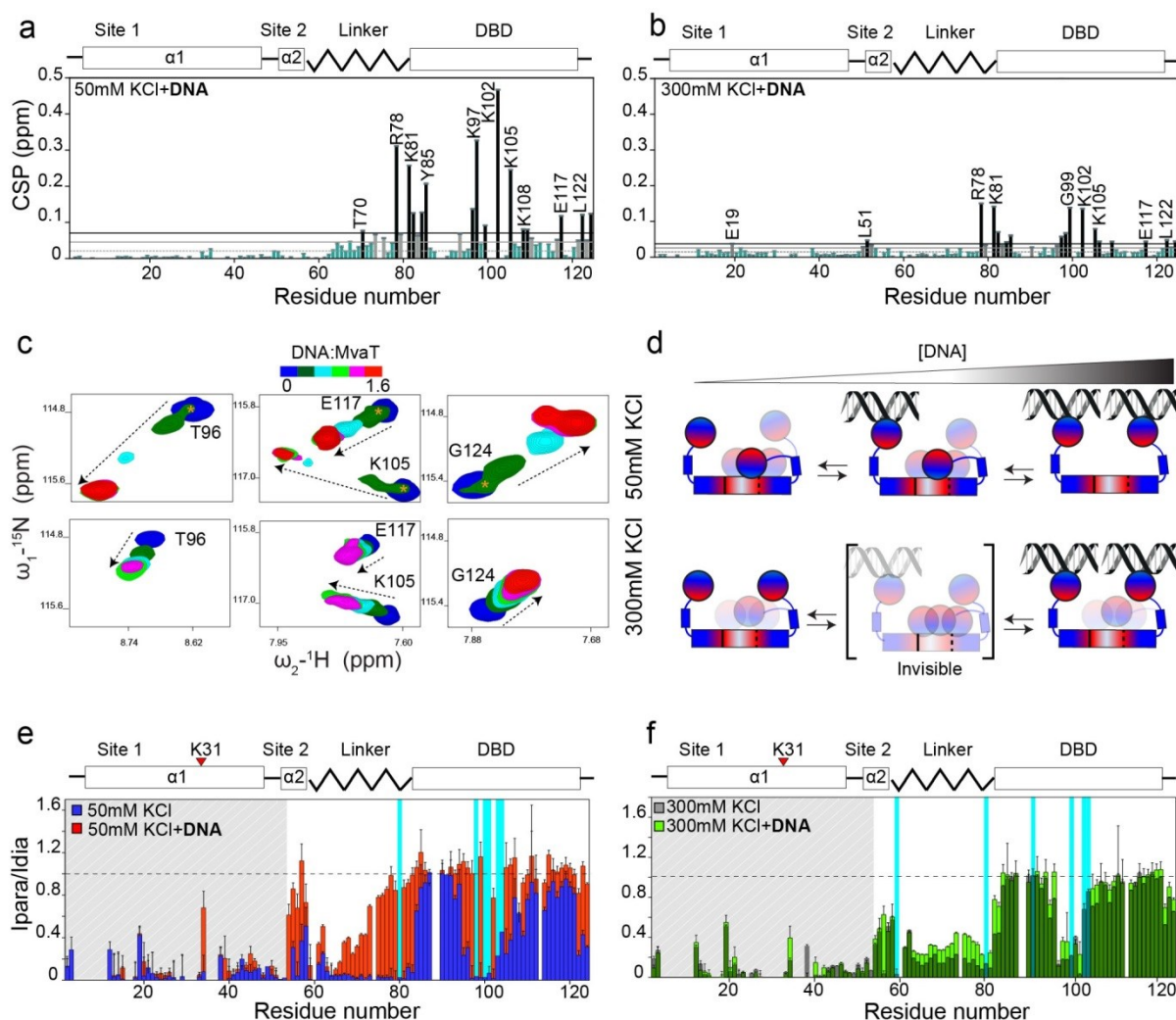
Figure 2.4: DNA modulates the conformational state of the MvaT dimer. (a) and (b) Analysis of the MvaT dimer HSQC spectra weighted average CSP at 1.6 DNA:MvaT molar ratio at 50 and 300 mM KCl, respectively. Resonances with CSP more than two (black line) or one (grey line) standard deviation (SD) from the 10% trimmed mean (grey dashed line) are labelled and shown in black, grey and green bars, respectively. (c) CSP amplitudes and directions (dashed arrows) of the DBD resonances upon titration with 12 bp DNA at 50 (upper panels) and 300 mM KCl (lower panels). The resonances that correspond to the N-terminal bound DBD are indicated by orange asterisks. (d) Schematic representation of the DNA binding mechanism to the MvaT dimer under low and high salt conditions. The electrostatic characteristics of the MvaT dimer are schematically shown by a red /white /blue colour gradient. (e) and (f) Overlay between the PRE vs. MvaT dimer residue number at low salt in the absence (blue bars) and presence of DNA (red bars) and high salt in absence (grey bars) and presence of DNA (green bars), respectively. Resonances with non-

determined PRE, due to line broadening upon DNA binding, are highlighted in cyan bars. The layout of the MvaT monomer is shown in the upper panel. The position of the spin label is indicated by the red triangle.

Modulation of MvaT electrostatic interdomain interactions by salt and DNA drives the switch between its DNA binding modes

Our structural studies have established that the MvaT dimer samples a heterogenous conformational space dominated by half open and fully open conformers. Increase in salt and DNA concentrations destabilizes the electrostatic interactions between the DBD and the N-terminal domain. Consequently, the exchange rate between the half open and fully open conformers becomes fast and the sequestration of the DBD by the N-terminal domain is diminished. Thus, the protomers can potentially interact simultaneously with two independent DNA segments.

To test whether this dynamic conformational equilibrium has implications for the structure and function of MvaT wild type-DNA complexes, we determined the modes of DNA binding under the low and high salt conditions using tethered particle motion (TPM) and bridging pull-down assay (see Chapter 5) [20,42] .

First, we investigated the effect of salt on lateral nucleoprotein formation by oligomerization of MvaT along DNA. In TPM the length and stiffness of the tethered DNA molecules is correlated to the root mean square displacement (RMS) of the attached polystyrene bead. The formation of a filament along DNA results in DNA stiffening, observed as an increase in RMS by TPM. The RMS changes of the polystyrene bead attached to a single DNA molecule (685 bp) were determined as a function of protein concentration. The experiment was performed at 50 mM KCl (low salt) and 315 mM KCl (high salt) (fig. 2.5a). Under both conditions two binding regimes were evident. At low MvaT concentration, a decrease in RMS was observed, which is attributed to the ability of MvaT to bend double stranded DNA (phase I) [53]. We propose that this regime represents a nucleation phase where MvaT protomers bind non-cooperatively to the DNA substrate (fig. 2.5c). In the second regime (II) a gradual increase in RMS occurs, which reaches a maximum of 160 nm at 1.6 μM of MvaT. This represents a phase in which the MvaT protomers gradually oligomerize along the DNA until saturation. The difference between the two salt conditions is in the first regime in which the DNA is bent by individual dimers (I). At high salt, the extent of DNA compaction resulting

from DNA bending by MvaT is reduced (fig. 2.5a). This could be due to an effect of the counterions (Cl⁻) on the DNA binding affinity of MvaT (as seen with H-NS) [20]. To minimize this potential counterion effect, we also performed the TPM experiment using potassium glutamate (Kglu) instead of KCl. Indeed, the differences in the MvaT titration curves obtained at low and high salt were much less pronounced than with KCl (fig. 2.5b).

These results suggest that the low and high salt conditions have no effect on the MvaT DNA stiffening activity. At high salt, the delicate conformational changes due to the increase in flexibility and in exchange rates between the a half-open to a fully open states of MvaT protomers have no influence on this process. Besides, the dissociation effect of the increase in ionic strength on the complex is countered by the cooperative binding of the MvaT protomers along the DNA.

Previously we have demonstrated that H-NS switches between its DNA stiffening and bridging activities as function of $MgCl_2$ by using a sensitive and quantitative bridging pull-down assay (20). Here we have used the same approach to test the effect of potassium chloride concentrations on MvaT-mediated DNA-DNA bridging. The DNA bridging efficiency (i.e. the percentage recovery of DNA from solution) as a function of KCl concentration (fig. 2.5d) revealed that at low salt concentration (50 mM KCl) the MvaT-mediated bridging activity is negligible despite the protein's ability to stiffen DNA by lateral nucleoprotein filament formation (fig. 2.5a). This agrees with our structural model in which MvaT protomers can bind to the DNA with only one of their DBDs while the other one is sequestered by the electrostatic interaction with the N-terminal domain. Under this condition the lateral nucleoprotein filaments of MvaT cannot form a bridge between two DNA duplexes.

By increasing the salt concentration, an increase of the protein bridging efficiency is observed and reaches a maximum at 315 mM KCl (Phase I'). This dependency is also observed in the presence of Kglu and NaCl (fig. 2.5d, f). The low and high salt conditions have no effect on the protein oligomerization state (fig. S2.5a).

We have also tested the effect of divalent ions on the MvaT DNA bridging activity using $MgCl_2$, $MgSO_4$ and $CaCl_2$: the DNA bridging efficiency of MvaT also depends on the tested divalent ions.

However, optimum bridging efficiency is reached at lower salt concentrations (~18 mM for $MgCl_2$ and ~20 mM for $MgSO_4$ and $CaCl_2$) (fig. 2.5e).

Previously, the switch between DNA bridging and stiffening of H-NS family members was only observed and quantitatively analysed as a function of divalent ions [20,23]. Herein we showed that the DNA bridging efficiency of MvaT also depends on monovalent ions, suggesting that the switch might not require specific ions. There are some indications that H-NS can also bridge DNA in the presence of 200 mM KCl and in absence of $MgCl_2$. While captured by AFM imaging, this observation was not corroborated by solution methods [24]. To substantiate this observation, we here determined DNA bridging efficiency of H-NS in the presence of 50-200 mM KCl. Indeed, we observe a fourfold increase in the bridging efficiency between 50 and 100 mM KCl (fig. S2.5c). These findings indicate that the switch between the DNA binding modes of H-NS proteins is independent from the type of ions and is mainly due to the increase in ionic strength. Note, however that divalent ions are more efficient (by 1 order of magnitude) in promoting bridging than monovalent ions. These differences are possibly due to the higher effective shielding of the proteins charged regions by multivalent ions.

The observed effect of ionic strength on the ability of MvaT to bridge DNA can be explained structurally. The increase in salt concentration gradually destabilizes the interdomains electrostatic interactions of the MvaT protomers. DNA has an additive contribution on the shifting of the conformational equilibrium of the MvaT protomers towards the fully opened state. In this state, MvaT exposes most of the DNA binding domains in the lateral protein filament to concurrently interact with another DNA duplex and form a bridge. Beyond a certain threshold of ionic strength, the bridged protein-DNA complex starts disintegrating because the high ionic strength will weaken the interactions between the DNA binding domain of MvaT and DNA (fig. S2.5b).

To corroborate this structure/function relationship mechanism in the context of MvaT nucleofilaments, amino acid residues located at the interface between the N-terminal and DBD domains were substituted to perturb formation of the interdomain complex. The ensemble structure calculation of the MvaT mutant dimer revealed that the interface between the two domains is formed by the negative region of the N-terminal domain (26-QDDKLKKELEDEE-38)

and the positive loop of the DBD (95-ETKGGNHK-102). Substitution of E35/E37/E38 with alanine or E33/E37 with glutamine, yielded MvaT variants capable of oligomerization in solution (data not shown) and of bridging DNA duplexes at low (100 mM) and high (300 mM) salt concentrations (fig. S2.6a,b). These MvaT variants are also able to bend and stiffen DNA, yet to a lesser extent when compared to the wild type protein (fig. S2.6c).

These macroscopic observations provide direct evidence that the electrostatic interactions of the DBD and N-terminus of MvaT change, in response to altered ionic strength, translates into altered DNA binding properties. Salt and DNA function additively to disrupt these interdomains interactions, thus inducing the required conformational changes that drive the switch between the DNA bridging and stiffening activities of the H-NS family of proteins.
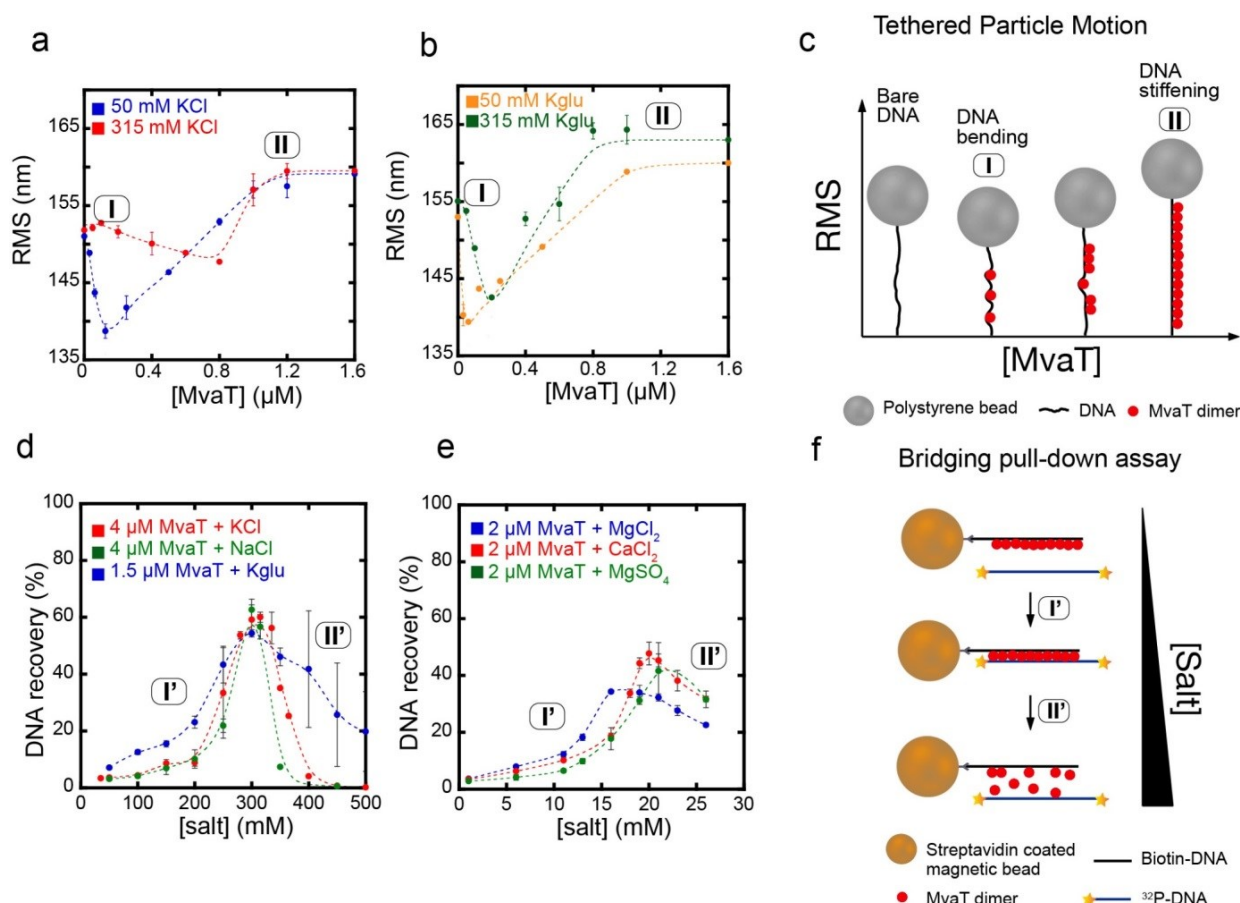

Figure 2.5: **Conformational changes of MvaT induced by salt drive the switch between its DNA stiffening and bridging activities.** (a) Root Mean Square displacement (RMS) of the tethered DNA particles as a function of MvaT concentration at 50 mM KCl (in blue) and 315 mM KCl (in red). The different regimes are labelled (I, II). (b) RMS as a function of MvaT concentration in the presence of 50 mM potassium

glutamate (KGlu) (in yellow) and 315 m KGlu (in green). (c) Schematic representation of the experimental observations using the Tethered Particle Motion technique. The different regimes observed in (a) and (b) are labelled I and II. (d) DNA bridging efficiency of the MvaT wild type as a function of monovalent ions concentration: KCl (in red); NaCl (in green); KGlu (in blue). (e) The MvaT DNA bridging efficiency as a function of divalent ion concentration: $MgCl_2$ (in blue); $CaCl_2$ (in red) and $MgSO_4$ (in green). The different regimes of MvaT DNA bridging activity are labelled (I', II'). (f) Schematic representation of the experimental observations using the DNA bridging assay. The different regimes observed in (d) and (e) are labelled I' and II'. Error bars indicate $\pm$ SD of duplicate.

Discussion

The mechanism by which H-NS family proteins sense the osmotic environment to modulate bacterial nucleoid organization and gene transcription is poorly understood. H-NS proteins form lateral nucleoprotein filaments along the DNA or bridge two DNA duplexes, resulting in DNA loops. Divalent ions drive the switch between DNA stiffening and bridging activities of the H-NS family members [17,20,23].

Our previous studies suggested that the switch between the two DNA binding modes requires H-NS protomers to experience conformational changes between an open and a closed state [20]. Although the study was based on MD simulation and supported by mutagenesis, a detailed structural description of the protein conformational landscape based on experimental evidence was missing. To test this model, we have used MvaT from *P. aeruginosa*, which we argue represents a short structural version of H-NS as a benchmark.

Analysis of the primary sequences of H-NS family members has revealed conserved positions of charged residues despite the low sequence identity. A cluster of negatively charged residues is in the N-terminal domain whereas the DNA binding domain and the linker region contain positively charged residues. Thus, we hypothesised that electrostatic interactions between the two oppositely charges domains may take place, which could be modulated by the increase in ionic strength.

By combining PREs and SAXS techniques we have modelled the conformational landscape of the MvaT dimer under low and high salt conditions. Under both conditions, the protein samples

heterogeneous conformational space where the two DNA binding domains adopt different spatial configurations. Two major conformers could be identified: a half-opened and a fully opened state. In the half-opened state, one of the DNA binding domains is interacting with the $\alpha 2$ N-terminal helix in an encounter complex like states. The interface between the two domains comprises the positively charged loop 95-ET**K**GGN**HK**-102 and the negatively charged segment 26-Q**DD**KLKK**E**L**EDEE**-38 of the DBD and the N-terminal $\alpha 2$, respectively. At low salt, these interactions prevent one of the DBDs of the MvaT protomer from forming a complex with DNA. At high salt, this electrostatic intramolecular complex is destabilized, causing an increase in exchange rate between the open and close states and thus a delicate change in the conformational space of the protein where it becomes more flexible and extended. This effect is enhanced by DNA substrate which induces the opening of the MvaT dimer by shielding the DBD from interacting with the N-terminal domain.

These findings agree with what has been proposed for H-NS. The MD simulations of the H-NS dimer in the presence of 50 mM KCl revealed interactions between its DBD and its N-terminal domain involving a negative amino acid patch in the α-helix 3 (E42-E50) and the positively charged regions 98–105 (KYSYVDENGE) and 123–129 (EQGKS) of the DBD [20]. These interactions are altered in the presence of 130 mM KCl or 10 mM MgCl$_2$. Recently, Arold and co-workers confirmed these findings by NMR titration of the N-terminal domain (2-57) with the DNA binding domain (84-137). The interdomain interactions were lost at high salt concentration. However, the authors claim that the occurrence of these interactions within the protein nucleofilament is not possible due to stereochemical restraints (as the linker is 25-30 Å from site 1) unless the oligomerization site 2 unfolds [25]. We disagree with these claims as the linker region and the DNA binding domain together have a length of more than 40 Å, which provides the DBD with enough space and degree of freedom to reach the negative residues in α-helix 3. Additionally, disruption of the H-NS interdomain interactions by mutagenesis has generated a variant that adopts an open conformational state and oligomerizes, and is able to stiffen and bridge DNA in the absence of magnesium [20]. This indicates that these interactions indeed occur in the H-NS oligomer and their modulation by salt or mutagenesis induces a switch between its DNA binding modes.

To establish structure-function relationships for the MvaT protomer we investigated the effects of salt on the DNA binding properties of MvaT using TPM and a pull-down bridging assay. MvaT, like H-NS, oligomerizes along the DNA substrate, leading to stiffening of DNA, in agreement with previous reports [38,39]. Unlike H-NS, MvaT binds to the DNA substrate and induces bending. This is due to differences between the DNA binding mechanisms of the two proteins. MvaT binds to the DNA through an 'AT-pincer' motif which causes backbone bending [53]. On the other hand H-NS binding to DNA involves an 'AT-hook like' structural motif [15,69] that intercalates within the DNA helix without perturbing its twist [70].

H-NS bridges are disrupted at lower KCl concentration compared to MvaT, indicating a higher sensitivity to the ionic strength of the surrounding medium. These differences are likely due to differences in bridge stability resulting from the difference in DNA binding mechanisms, with MvaT forming a stronger bridge than H-NS. Additionally, H-NS requires a lower amount of $MgCl_2$ compared to MvaT to reach the maximum bridging activity [20]. This could be explained by stronger electrostatic interdomain interactions within MvaT compared to H-NS, thus requiring higher KCl and $MgCl_2$ concentrations for their destabilization.

In contrast, StpA, an H-NS homologue, requires no or sub mM amounts of $MgCl_2$ to be able to bridge DNA [71,72]. The high sensitivity of StpA towards magnesium chloride is possibly due to the weaker electrostatic interdomain interactions compared to H-NS and MvaT, as concluded from the charge distribution within its primary sequence (fig. S2.1).

These three examples indicate that although the H-NS family members might structurally respond in a similar way to the increase in ionic strength to switch between their DNA stiffening and bridging activities, variations on this theme exist. These differences are due to the delicate divergence in their intrinsic charge distribution, and thus the fine-tuning of the strength of their electrostatic interdomain interactions.

The recently proposed mechanism by which H-NS senses temperature to alleviate gene repression involves unfolding of site 2, which induces an autoinhibitory conformational change within the H-NS protomer[25]. Here we propose that H-NS family proteins do not require site 2 unfolding to sense the osmotic surrounding. Their osmosensitivity is mainly mediated by the

modulation of the electrostatic interactions between their N-terminal and DNA binding domains within their nucleoprotein filaments. Altogether, we demonstrate that H-NS family proteins nucleofilaments might respond differently to the environmental changes in temperature and ionic strength.

Thus, based on the description of the conformational landscape of MvaT, we propose a general mechanism for the basic response of H-NS family proteins to changes in osmotic environment (fig. 2.6). Under low ionic strength, the H-NS protomers interact individually with AT-rich nucleation sites on the DNA. From these sites, the protein spreads cooperatively along the DNA substrate forming lateral nucleoprotein filaments where only one of the DNA binding domains of each dimer is engaged with the DNA substrate. The other domain is sequestered by electrostatic interactions with the N-terminal domain. The DNA substrate and the increase in ionic strengths additively destabilize these interactions. Consequently, the protomers release their second DNA binding domains to interact with another DNA duplex and form a bridge. Above a certain threshold of ionic strength, the bridge is dissociated due to loss of the electrostatic interactions that mediate the complex. In addition, changes in DNA topology induced by salt [73] might contribute to formation or rupture of bridges.

Although there is to date no *direct* evidence for the occurrence of such mechanism in vivo, the ions investigated in this study are present in *E. coli* at different concentrations as a function of environmental conditions [74-76]. For *P. aeruginosa*, limited information is available on the ionic composition of its intracellular milieu. However, in *E. coli* the cytosolic concentration of K^+ ranges from 30-300 mM and for Cl^- from 10-200 mM [74,75], which correlates with the condition under which the MvaT protomers experience conformational changes between half-open and fully open states.

In the present work, we have decrypted the molecular basis that governs DNA-DNA bridge formation by MvaT and proposed a structural dynamics paradigm for the osmosensitivity of H-NS family proteins. *In vivo* this mechanism is part of more extensive and complex regulatory network. Clearly this process is modulated by other regulatory factors, such as protein modulators of H-NS function, ions and their cellular concentrations, in conjunction with local DNA topology. In addition to a fundamental understanding of the activities of H-NS family proteins, our findings pave the way

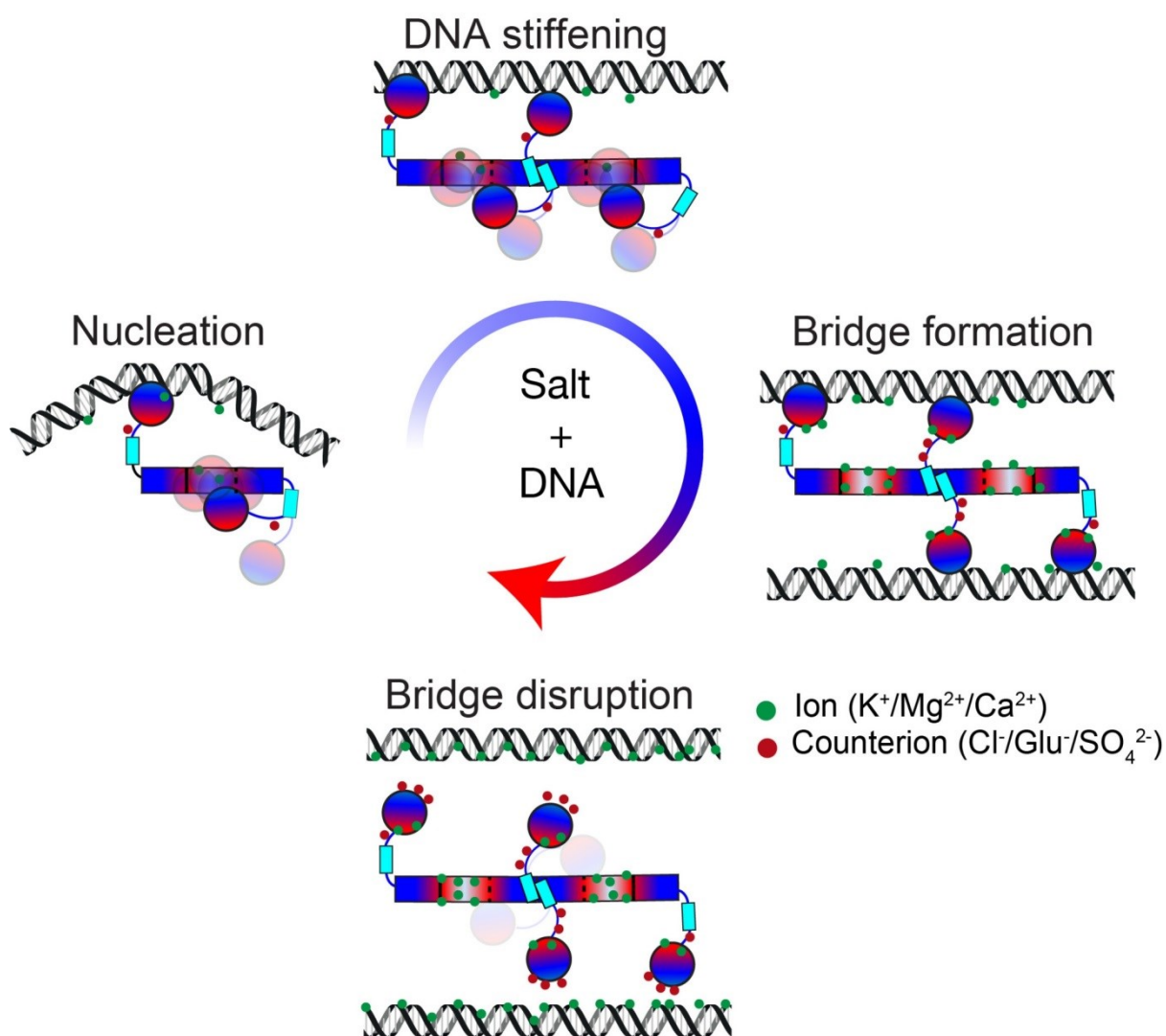for the modulation of their DNA binding modes by small chemical compounds as a new generation of antibiotics.

Figure 2.6: **General mechanism of osmoregulation of the DNA binding properties of H-NS family proteins.** The white, red and blue colours refer to neutral, negative and positive charged amino acid patch on the H-NS molecular surface.
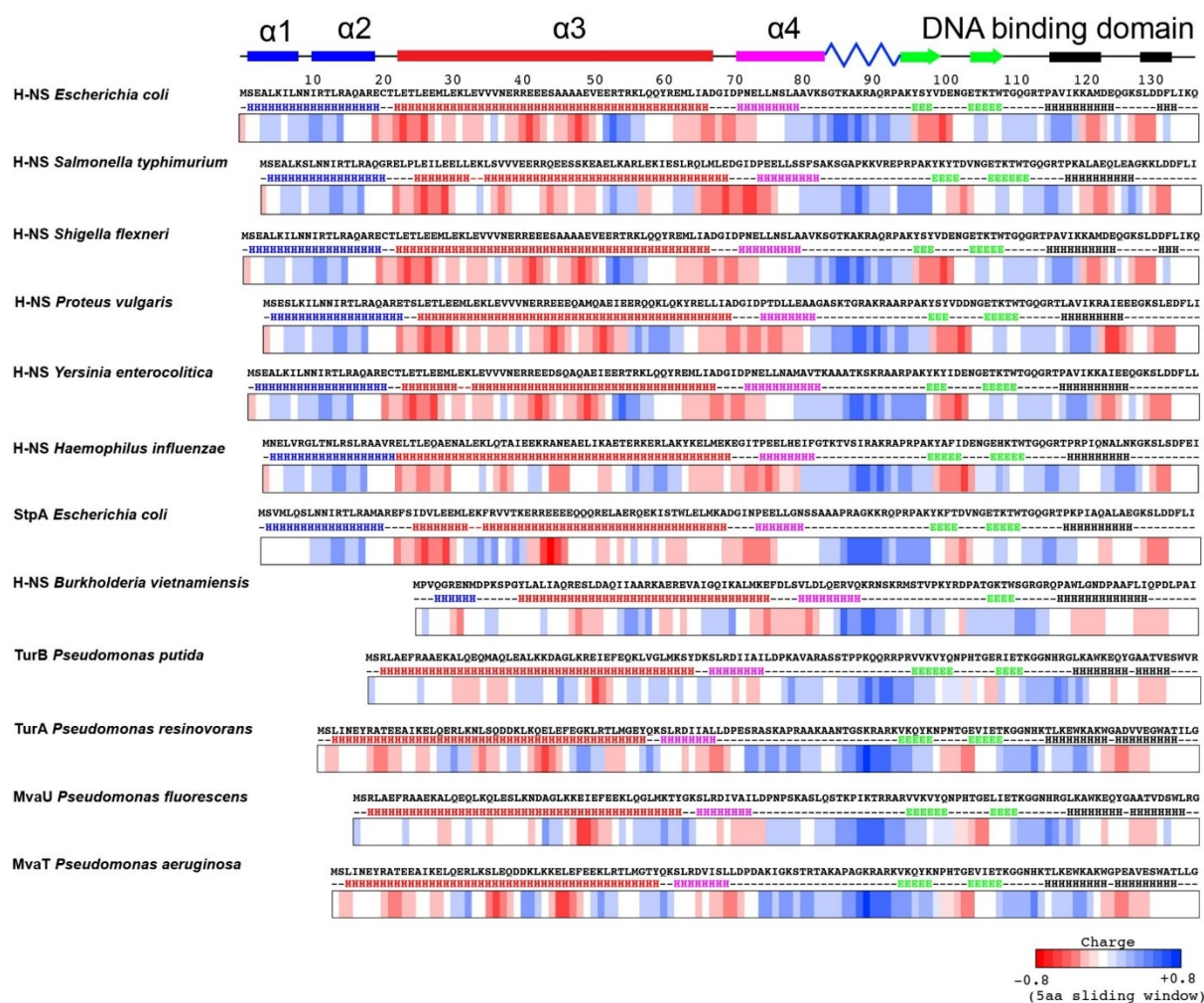
Supplementary materials

Fig. S2.1: Fold topology and charged residue/charge distributions of H-NS family proteins. Sequence alignment of twelve H-NS family proteins from different bacterial organisms was generated using Clustal omega [77]. The multi-alignment file was used to predict the secondary structures content using JPRED server [78]. (H) is for α-helices, (B) for β-sheets, (-) for random coils. A schematic of the *E. coli* H-NS secondary structure is depicted above. The lower panels represent the 5 amino acids average charge of the primary sequences of H-NS family members. Positively and negatively charged regions are colored with blue and red rectangles, respectively. The neutral amino acid patches are in white.
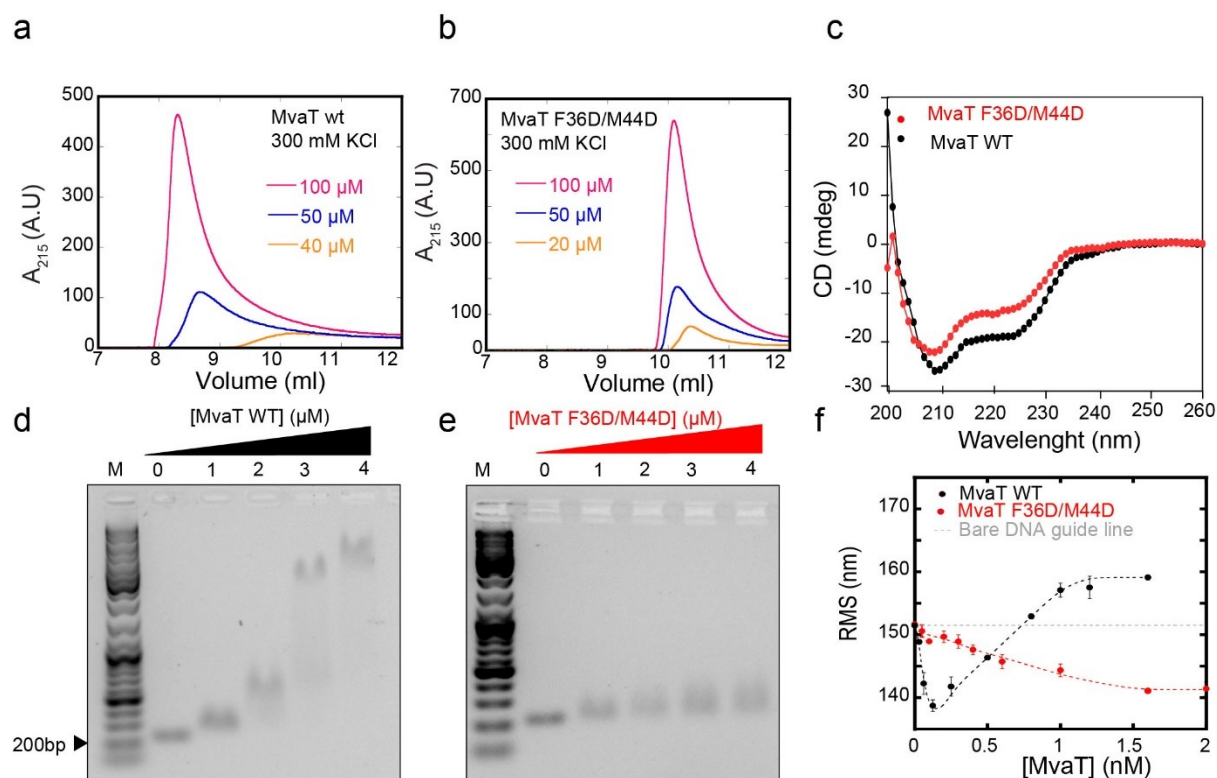
Fig. S2.2: The effects of F36D/M44D double mutations on MvaT secondary/quaternary structure and DNA binding. (a) and (b) concentration dependency of the MvaT wild type and the F36D/M44D mutant oligomerisation state in the presence of 300 mM KCl as monitored by size exclusion chromatography. (c) Overlay between the far-UV CD spectra of MvaT WT (in black) and MvaT F36D/M44D (in red). (d) and (e) Electrophoretic mobility shift assay on a 1% agarose gel of MvaT WT and MvaT F36D/M44D using a 200 bp AT-rich DNA substrate (32% GC), respectively. (f) Overlay of RMS date obtained for titration of MvaT F36D/M44D (red line) and MvaT wild type (black line) at 50 mM KCl in TPM experiments. The dashed grey line indicates the RMS of bare DNA.
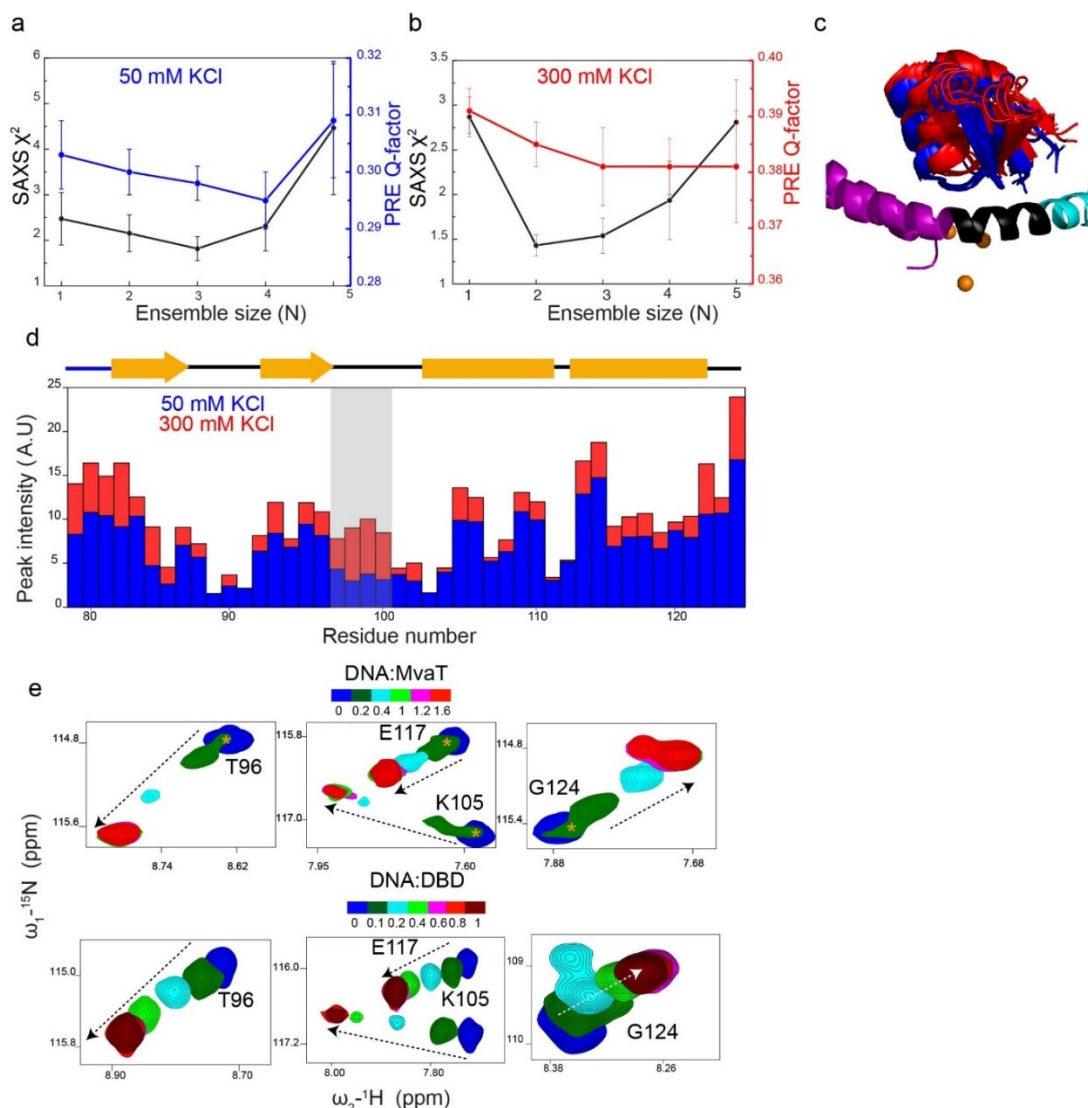
Fig. S2.3: MvaT structural ensemble calculation quality metrics and the DNA binding mechanism of the MvaT dimer and individual DBD. (a) and (b) show the variation of the SAXS χ^2 and PREs Q-factor versus the ensemble size (N) of the low and high salt MvaT structural modelling, respectively. (c) Shows the position of the DNA binding domain relative to the N-terminal domain of the lowest energy structures at low (blue cartoon) and high salt (red cartoon). The orange spheres represent the nitroxide positions determined within the ensemble structure calculation. (d) MvaT dimer DBD peak intensities at 50 mM KCl (blue bars) and 300 mM KCl (red bars). Loop 95-102 is highlighted with the grey rectangle. (e) CSP amplitudes and directions (dashed arrows) of the MvaT dimer DBD resonances (upper panels) and the individual DBD with C-terminal 6×His-tag (lower panels) upon titration with 12 bp DNA performed in 20 mM Bis-Tris, 50 mM KCl, pH 6, molar ratios are indicated. The resonances which correspond to the N-terminal bound DBD are indicated by orange asterisks.
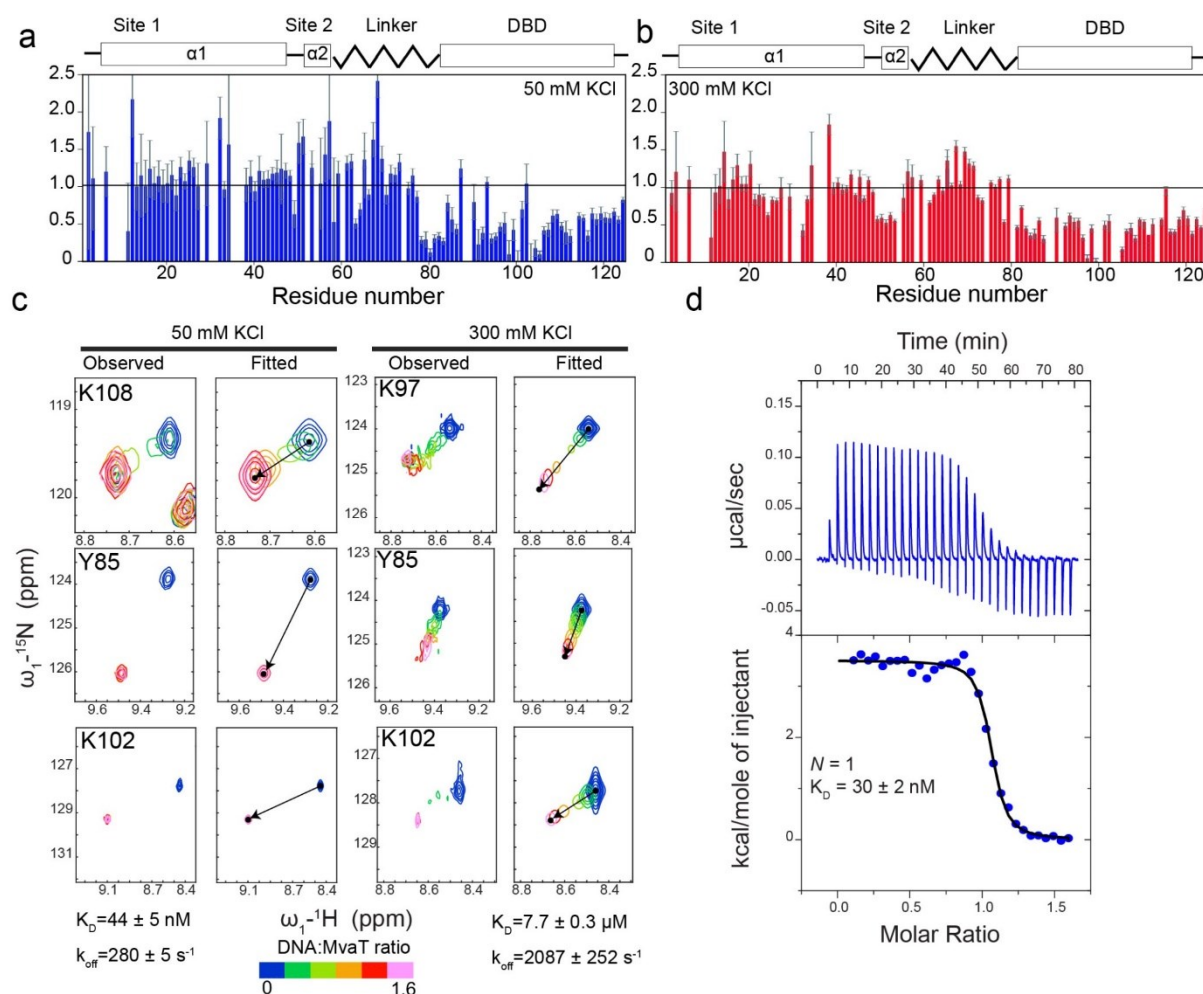
Fig. S2.4: MvaT F36D/F44D titration with 12 bp DNA AT rich DNA substrate. (a) and (b) changes in the MvaT dimer HSQC peak intensities ratio between at 1.6 DNA:MvaT molar ratio at 50 and 300 mM KCl salt concentration versus residue number, respectively. The layout of the MvaT secondary structure is shown in the upper panel. (c) MvaT dimer HSQCs line shape analysis upon titration with the 12 bp DNA substrate at low and high salt concentration. Experimental and fitted resonances of selected residues are shown. (d) ITC titration of the MvaT dimer with 12 bp DNA substrate at 50 mM. The extracted binding constant are indicated.
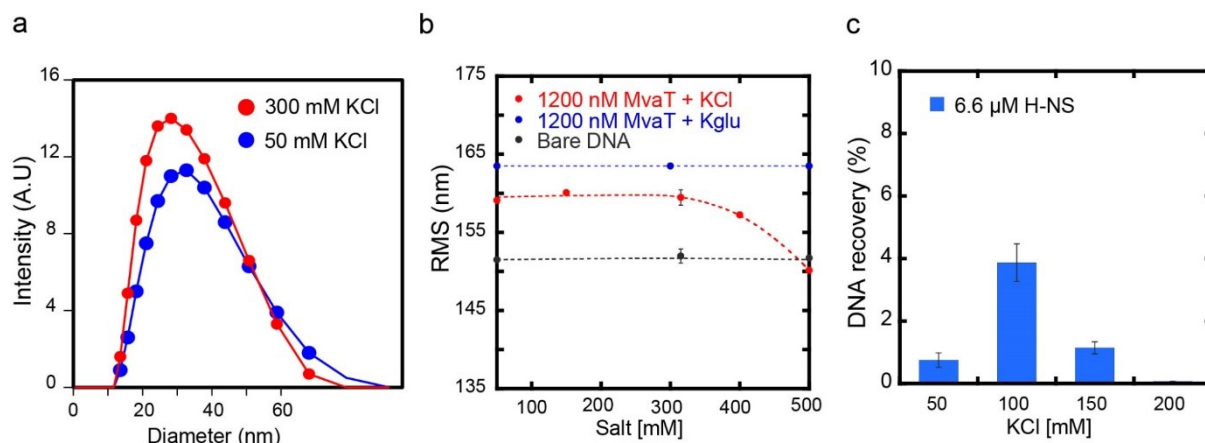
Fig. S2.5: Salt effect on H-NS protein oligomerization, stiffening and bridging activities. (a) MvaT wild type oligomer particle size at 100 μM concentration in the presence of 300 mM KCl (blue curve) and 50 mM KCl (red curve) determined by dynamic light scattering. (b) Effect of KCl (in red) and KGlu (in blue) concentration on MvaT wild type DNA stiffening activity using TPM. The effect of salt concentration on the RMS of the bare DNA is shown in black dashed line. (c) KCl concentration effect on H-NS DNA bridging efficiency using the DNA bridging assay. Error bars indicate the ± SD of duplicates.
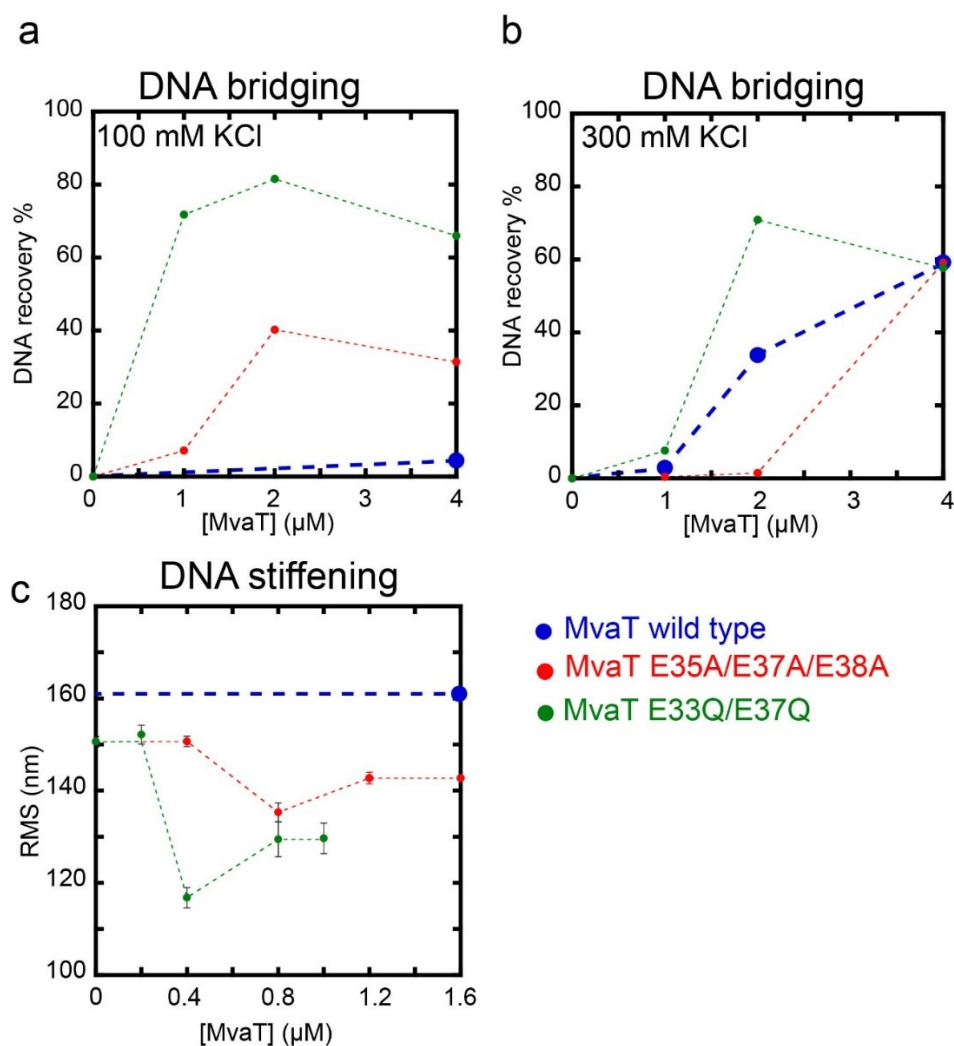
Fig. S2.6: Effect of single point mutations at the interface of the MvaT interdomain complex on MvaT-DNA complex type. (a) and (b) DNA bridging efficiency of MvaT variants at low (100mM) and high (300 mM) salt concentrations. (c) DNA stiffening activity of MvaT variants at 100 mM KCl. Note that there is an initial phase of reduction in RMS at low protein concentration (DNA bending) followed by an increase in RMS at progressively higher protein concentration (DNA stiffening). The blue dot and dashed line indicate the RMS reference point of the MvaT wild type protein at 1.6 μM concentration and at 100 mM KCl. In all panels the blue curve indicates data for the MvaT wild type, the red curve indicates data for MvaT E35A/E37A/E38A and the green curve indicates data for MvaT E33Q/E37Q.

Table S2.1. SAXS data collection and scattering-derived parameters.

	MvaT (low salt)	MvaT (high salt)
Data collection parameters		
Beam line	BM29 (ESRF)	BM29 (ESRF)
Wavelength (Å)	0.99	0.99
q range (Å^{-1})*	0.003 - 0.493	0.003 - 0.493
Concentration (mg ml^{-1}) (mode)	11 (SEC-SAXS)	9.5 (SEC-SAXS)
Buffer conditions	20 mM Bis-Tris, 50 mM KCl, pH 6.0	20 mM Bis-Tris, 300 mM KCl, pH 6.0
Temperature (°C)	20	20
Structural parameters§		
$I(0)$ (cm^{-1}) [from Guinier]	69.81 ± 0.11	74.46 ± 0.01
R_g (Å) [from Guinier]	35.63 ± 0.78	38.29 ± 0.65
$I(0)$ (cm^{-1}) [from $p(r)$]	70.31 ± 0.10	74.89 ± 0.08
R_g (Å) [from $p(r)$]	37.19 ± 0.11	39.89 ± 0.09
D_{max} (Å)	146.99	158.38
Porod volume estimate, V_p (Å^3)	47235	49908
Porod exponent	3.2	2.7
Molecular mass determination		
MM (kDa) [from *SAXSMoW* on final merged curve]	31.50 (q = 0.4 Å^{-1})	29.2 (q = 0.3 Å^{-1})
MM (kDa) [from Q_R on final merged curve]	28.09 (q = 0.4 Å^{-1})	26.45 (q = 0.3 Å^{-1})
MM (kDa) [from V_p/1.7]	27.78	29.35
Calculated MM from sequence (kDa)	28.26	28.26
Software employed		
Data processing and analysis	ATSAS, Scatter	ATSAS, Scatter
Computation of theoretical intensities and fitting	CRYSOL	CRYSOL
SASDB entry	SASDGS5	SASDGT5

Abbreviations: $I(0)$, extrapolated scattering intensity at zero angle; R_g, radius of gyration calculated using either Guinier approximation (from Guinier) or the indirect Fourier transform package GNOM [from $p(r)$]; MM, molecular mass; D_{max}, maximal particle dimension; V_p, Porod volume; V_{ex}, particle excluded volume

§Values reported are for average of frames in the peak for both MvaT samples.

*Momentum transfer $|q| = 4\pi\sin(\theta)/\lambda$

References

1   Brooks, A. N., Turkarslan, S., Beer, K. D., Yin Lo, F. & Baliga, N. S. Adaptation of cells to new environments. *Wiley Interdisciplinary Reviews: Systems Biology and Medicine* **3**, 544-561 (2011).

2   Krogh, T. J. T., Møller-Jensen, J. J. & Kaleta, C. C. Impact of Chromosomal Architecture on the Function and Evolution of Bacterial Genomes. *Frontiers in microbiology* **9**, 2019 (2018).

3   Dorman, C. J. H-NS: a universal regulator for a dynamic genome. *Nature Reviews Microbiology* **2**, 391 (2004).

4   Tendeng, C. & Bertin, P. N. H-NS in Gram-negative bacteria: a family of multifaceted proteins. *Trends in microbiology* **11**, 511-518 (2003).

5   Atlung, T. & Ingmer, H. H-NS: a modulator of environmentally regulated gene expression. *Molecular microbiology* **24**, 7-17 (1997).

6   Hurme, R. & Rhen, M. Temperature sensing in bacterial gene regulation—what it all boils down to. *Molecular microbiology* **30**, 1-6 (1998).

7   L. Qin, A. M. E., F. Ben Bdira, R. T. Dame. The architects of bacterial DNA bridges: a structurally and functionally conserved family of proteins. *Open Biology*, doi:10.1098/rsob.190223 (2019).

8   Ali, S. S., Xia, B., Liu, J. & Navarre, W. W. Silencing of foreign DNA in bacteria. *Current opinion in microbiology* **15**, 175-181 (2012).

9   Navarre, W. W., McClelland, M., Libby, S. J. & Fang, F. C. Silencing of xenogeneic DNA by H-NS—facilitation of lateral gene transfer in bacteria by a defense system that recognizes foreign DNA. *Genes & Development* **21**, 1456-1471 (2007).

10   Lucchini, S. *et al.* H-NS mediates the silencing of laterally acquired genes in bacteria. *PLoS pathogens* **2**, e81 (2006).

11   Navarre, W. W. *et al.* Selective silencing of foreign DNA with low GC content by the H-NS protein in Salmonella. *Science* **313**, 236-238 (2006).

12   Singh, S. S. *et al.* Widespread suppression of intragenic transcription initiation by H-NS. *Genes Dev.* **28**, 214-219 (2014).

13   Oshima, T., Ishikawa, S., Kurokawa, K., Aiba, H. & Ogasawara, N. Escherichia coli histone-like protein H-NS preferentially binds to horizontally acquired DNA in association with RNA polymerase. *DNA research* **13**, 141-153 (2006).

14   Gordon, B. R. *et al.* Structural basis for recognition of AT-rich DNA by unrelated xenogeneic silencing proteins. *Proceedings of the National Academy of Sciences* **108**, 10690-10695 (2011).

15   Bouffartigues, E., Buckle, M., Badaut, C., Travers, A. & Rimsky, S. H-NS cooperative binding to high-affinity sites in a regulatory element results in transcriptional silencing. *Nature Structural and Molecular Biology* **14**, 441 (2007).

16   Rimsky, S., Zuber, F., Buckle, M. & Buc, H. A molecular mechanism for the repression of transcription by the H-NS protein. *Molecular microbiology* **42**, 1311-1323 (2001).

17   Amit, R., Oppenheim, A. B. & Stavans, J. Increased bending rigidity of single DNA molecules by H-NS, a temperature and osmolarity sensor. *Biophysical journal* **84**, 2467-2473 (2003).

18   Noom, M. C., Navarre, W. W., Oshima, T., Wuite, G. J. & Dame, R. T. H-NS promotes looped domain formation in the bacterial chromosome. *Current Biology* **17**, R913-R914 (2007).

19   Dame, R. T. *et al.* DNA bridging: a property shared among H-NS-like proteins. *Journal of bacteriology* **187**, 1845-1848 (2005).

20   van der Valk, R. A. *et al.* Mechanism of environmentally driven conformational changes that modulate H-NS DNA-bridging activity. *Elife* **6**, e27369 (2017).

21   Dame, R. T., Wyman, C., Wurm, R., Wagner, R. & Goosen, N. Structural basis for H-NS-mediated trapping of RNA polymerase in the open initiation complex at the rrnB P1. *Journal of Biological Chemistry* **277**, 2146-2150 (2002).

22   Dame, R. T., Wyman, C. & Goosen, N. H-NS mediated compaction of DNA visualised by atomic force microscopy. *Nucleic Acids Res.* **28**, 3504-3510 (2000).

23   Liu, Y., Chen, H., Kenney, L. J. & Yan, J. A divalent switch drives H-NS/DNA-binding conformations between stiffening and bridging modes. *Genes & development* **24**, 339-344 (2010).

24   Winardhi, R. S., Yan, J. & Kenney, L. J. H-NS regulates gene expression and compacts the nucleoid: insights from single-molecule experiments. *Biophysical journal* **109**, 1321-1329 (2015).

25   Shahul Hameed, U. F. *et al.* H-NS uses an autoinhibitory conformational switch for environment-controlled gene silencing. *Nucleic Acids Research* (2018).

26   Dorman, C. J., Hinton, J. C. & Free, A. Domain organization and oligomerization among H-NS-like nucleoid-associated proteins in bacteria. *Trends in microbiology* **7**, 124-128 (1999).

27   Rimsky, S. Structure of the histone-like protein H-NS and its role in regulation and genome superstructure. *Curr. Opin. Microbiol.* **7**, 109-114, doi:https://doi.org/10.1016/j.mib.2004.02.001 (2004).

28   Leonard, P. G., Ono, S., Gor, J., Perkins, S. J. & Ladbury, J. E. Investigation of the self-association and hetero-association interactions of H-NS and StpA from Enterobacteria. *Molecular microbiology* **73**, 165-179 (2009).

29   Shindo, H. *et al.* Solution structure of the DNA binding domain of a nucleoid-associated protein, H-NS, from Escherichia coli. *FEBS letters* **360**, 125-131 (1995).

30   Esposito, D. *et al.* H-NS oligomerization domain structure reveals the mechanism for high order self-association of the intact protein. *Journal of molecular biology* **324**, 841-850 (2002).

31   Bloch, V. *et al.* The H-NS dimerization domain defines a new fold contributing to DNA recognition. *Nature Structural and Molecular Biology* **10**, 212 (2003).

32   Arold, S. T., Leonard, P. G., Parkinson, G. N. & Ladbury, J. E. H-NS forms a superhelical protein scaffold for DNA condensation. *Proceedings of the National Academy of Sciences* (2010).

33   Smyth, C. P. *et al.* Oligomerization of the chromatin-structuring protein H-NS. *Molecular microbiology* **36**, 962-972 (2000).

34   Renault, M., García, J., Cordeiro, T. N., Baldus, M. & Pons, M. Protein oligomers studied by solid-state NMR–the case of the full-length nucleoid-associated protein histone-like nucleoid structuring protein. *The FEBS journal* **280**, 2916-2928 (2013).

35   Westfall, L. W. *et al.* The Pseudomonas aeruginosa global regulator MvaT specifically binds to the ptxS upstream region and enhances ptxS expression. *Microbiology* **150**, 3797-3806 (2004).

36   Vallet, I. *et al.* Biofilm formation in Pseudomonas aeruginosa: fimbrial cup gene clusters are controlled by the transcriptional regulator MvaT. *Journal of bacteriology* **186**, 2880-2890 (2004).

37   Castang, S., McManus, H. R., Turner, K. H. & Dove, S. L. H-NS family members function coordinately in an opportunistic pathogen. *Proceedings of the National Academy of Sciences* **105**, 18947-18952 (2008).

38   Castang, S. & Dove, S. L. High-order oligomerization is required for the function of the H-NS family member MvaT in Pseudomonas aeruginosa. *Molecular microbiology* **78**, 916-931 (2010).

39   Winardhi, R. S. *et al.* Higher order oligomerization is required for H-NS family member MvaT to form gene-silencing nucleoprotein filament. *Nucleic acids research* **40**, 8942-8952 (2012).

40   Gibson, D. G. *et al.* Enzymatic assembly of DNA molecules up to several hundred kilobases. *Nature methods* **6**, 343 (2009).

41   van der Valk, R. A., Laurens, N. & Dame, R. T. in *The Bacterial Nucleoid: Methods and Protocols* (ed Olivier Espéli) 127-143 (Springer New York, 2017).

42   van der Valk, R. A., Qin, L., Moolenaar, G. F. & Dame, R. T. in *Bacterial Chromatin*   199-209 (Springer, 2018).

43   Pernot, P. *et al.* Upgraded ESRF BM29 beamline for SAXS on macromolecules in solution. *Journal of synchrotron radiation* **20**, 660-664 (2013).

44   Orthaber, D., Bergmann, A. & Glatter, O. SAXS experiments on absolute scale with Kratky systems using water as a secondary standard. *Journal of Applied Crystallography* **33**, 218-225 (2000).

45   Brennich, M. E. *et al.* Online data analysis at the ESRF bioSAXS beamline, BM29. *Journal of applied crystallography* **49**, 203-212 (2016).

46   Petoukhov, M. V. *et al.* New developments in the ATSAS program package for small-angle scattering data analysis. *Journal of applied crystallography* **45**, 342-350 (2012).

47   Franke, D. *et al.* ATSAS 2.8: a comprehensive data analysis suite for small-angle scattering from macromolecular solutions. *Journal of applied crystallography* **50**, 1212-1225 (2017).

48   Svergun, D. Determination of the regularization parameter in indirect-transform methods using perceptual criteria. *Journal of applied crystallography* **25**, 495-503 (1992).

49   Lee, W., Tonelli, M. & Markley, J. L. NMRFAM-SPARKY: enhanced software for biomolecular NMR spectroscopy. *Bioinformatics* **31**, 1325-1327 (2014).

50   Vranken, W. F. *et al.* The CCPN data model for NMR spectroscopy: development of a software pipeline. *Proteins: Structure, Function, and Bioinformatics* **59**, 687-696 (2005).

51   Waudby, C. A., Ramos, A., Cabrita, L. D. & Christodoulou, J. Two-Dimensional NMR Lineshape Analysis. *Scientific Reports* **6**, 24826, doi:10.1038/srep24826

https://www.nature.com/articles/srep24826#supplementary-information (2016).

52   Battiste, J. L. & Wagner, G. Utilization of site-directed spin labeling and high-resolution heteronuclear nuclear magnetic resonance for global fold determination of large proteins with limited nuclear overhauser effect data. *Biochemistry* **39**, 5355-5365 (2000).

53   Ding, P. *et al.* A novel AT-rich DNA recognition mechanism for bacterial xenogeneic silencer MvaT. *PLoS pathogens* **11**, e1004967 (2015).

54   Suzuki-Minakuchi, C. *et al.* Structural similarities and differences in H-NS family proteins revealed by the N-terminal structure of TurB in Pseudomonas putida KT2440. *FEBS letters* **590**, 3583-3594 (2016).

55   Schwieters, C. D., Kuszewski, J. J., Tjandra, N. & Clore, G. M. The Xplor-NIH NMR molecular structure determination package. *Journal of magnetic resonance* **160**, 65-73 (2003).

56   Schwieters, C. D., Kuszewski, J. J. & Clore, G. M. Using Xplor–NIH for NMR molecular structure determination. *Progress in nuclear magnetic resonance spectroscopy* **48**, 47-62 (2006).

57   Schwieters, C. D. & Clore, G. M. Using small angle solution scattering data in Xplor-NIH structure calculations. *Progress in nuclear magnetic resonance spectroscopy* **80**, 1-11 (2014).

58   Schwieters, C. D., Bermejo, G. A. & Clore, G. M. Xplor-NIH for molecular structure determination from NMR and other data sources. *Protein Science* **27**, 26-40 (2018).

59   Tang, C., Iwahara, J. & Clore, G. M. Visualization of transient encounter complexes in protein–protein association. *Nature* **444**, 383 (2006).

60   Pettersen, E. F. *et al.* UCSF Chimera—a visualization system for exploratory research and analysis. *Journal of computational chemistry* **25**, 1605-1612 (2004).

61   Gao, Y. *et al.* Charged residues in the H-NS linker drive DNA binding and gene silencing in single cells. *Proceedings of the National Academy of Sciences*, 201716721 (2017).

62   Shindo, H. *et al.* Identification of the DNA binding surface of H-NS protein from Escherichia coli by heteronuclear NMR spectroscopy. *FEBS letters* **455**, 63-69 (1999).

63   Fernández-de-Alba, C., Berrow, N. S., Garcia-Castellanos, R., García, J. & Pons, M. On the origin of the selectivity of plasmidic H-NS towards horizontally acquired DNA: linking H-NS oligomerization and cooperative DNA binding. *Journal of molecular biology* **425**, 2347-2358 (2013).

64   Micsonai, A. *et al.* BeStSel: a web server for accurate protein secondary structure prediction and fold recognition from the circular dichroism spectra. *Nucleic acids research* (2018).

65   Eghbalnia, H. R., Wang, L., Bahrami, A., Assadi, A. & Markley, J. L. Protein energetic conformational analysis from NMR chemical shifts (PECAN) and its use in determining secondary structural elements. *Journal of biomolecular NMR* **32**, 71-81 (2005).

66   Clore, G. M. & Iwahara, J. Theory, practice, and applications of paramagnetic relaxation enhancement for the characterization of transient low-population states of biological macromolecules and their complexes. *Chemical reviews* **109**, 4108-4139 (2009).

67   Franke, D. & Svergun, D. I. DAMMIF, a program for rapid ab-initio shape determination in small-angle scattering. *Journal of applied crystallography* **42**, 342-346 (2009).

68   Worrall, J. A. R. *et al.* Myoglobin and Cytochrome b5: A Nuclear Magnetic Resonance Study of a Highly Dynamic Protein Complex. *Biochemistry* **41**, 11721-11730, doi:10.1021/bi026296y (2002).

69   Gordon, B. R. *et al.* Lsr2 is a nucleoid-associated protein that targets AT-rich sequences and virulence genes in Mycobacterium tuberculosis. *Proceedings of the National Academy of Sciences*, 200913551 (2010).

70   Huth, J. R. *et al.* The solution structure of an HMG-I (Y)–DNA complex defines a new architectural minor groove binding motif. *Nature Structural and Molecular Biology* **4**, 657 (1997).

71   Lim, C. J., Whang, Y. R., Kenney, L. J. & Yan, J. Gene silencing H-NS paralogue StpA forms a rigid protein filament along DNA that blocks DNA accessibility. *Nucleic acids research* **40**, 3316-3328 (2011).

72   Boudreau, B. A. *et al.* StpA and Hha stimulate pausing by RNA polymerase by promoting DNA-DNA bridging of H-NS filaments. *Nucleic Acids Research* **46**, 5525-5546, doi:10.1093/nar/gky265 (2018).

73   Higgins, C. F. *et al.* A physiological role for DNA supercoiling in the osmotic regulation of gene expression in S. typhimurium and E. coli. *Cell* **52**, 569-584 (1988).

74   Schultz, S. G., Wilson, N. L. & Epstein, W. Cation transport in Escherichia coli. II. Intracellular chloride concentration. *J. Gen. Physiol.* **46**, 159-166, doi:10.1085/jgp.46.1.159 (1962).

75   Shabala, L. *et al.* Ion transport and osmotic adjustment in Escherichia coli in response to ionic and non-ionic osmotica. *Environ. Microbiol.* **11**, 137-148, doi:10.1111/j.1462-2920.2008.01748.x (2009).

76   Moncany, M. L. & Kellenberger, E. High magnesium content of Escherichia coli B. *Experientia* **37**, 846-847, doi:10.1007/bf01985672 (1981).

77   Sievers, F. *et al.* Fast, scalable generation of high-quality protein multiple sequence alignments using Clustal Omega. *Mol. Syst. Biol.* **7**, 539, doi:10.1038/msb.2011.75 (2011).

78   Drozdetskiy, A., Cole, C., Procter, J. & Barton, G. J. JPred4: a protein secondary structure prediction server. *Nucleic Acids Res.* **43**, W389-394, doi:10.1093/nar/gkv332 (2015).

Chapter 3

Mechanism of anti-repression of *Pseudomonas aeruginosa* H-NS family protein MvaT by the phage protein Mip

In this chapter, Fredj Ben Bdira performed and analyzed NMR experiments and performed molecular modelling. Nicholas Bowring performed and analyzed some of the TPM experiments and his-tag pull down assay.

Abstract

Bacteria and their associated bacteriophages are in a continuous battle, co-evolving defense and offense mechanisms. Bacterial xenogeneic silencers, H-NS family proteins, play important roles in bacterial phage defense and evolution by silencing incoming genes and genes acquired through horizontal gene transfer. The *Pseudomonas* phage LUZ24 encodes the Mip protein which binds the H-NS family protein MvaT of *Pseudomonas aeruginosa.* Binding of Mip was proposed to inhibit the silencing of phage LUZ24 DNA by MvaT. However, the mechanism by which Mip modulates MvaT function remains unclear. In this study we investigated how the DNA binding properties of MvaT are affected by Mip. Also, we defined how Mip interacts with MvaT and how this translates into altered DNA structuring properties. Our studies reveal that Mip interferes with the formation and stability of the bridged MvaT-DNA complex. This effect is due to interaction of Mip with both the dimerization and the DNA-binding domain of MvaT. Based on these observations we propose that binding of Mip promotes the half open - bridging incompetent - state of MvaT, resulting in relief of MvaT-mediated gene silencing.

Introduction

Bacteriophages - viruses infecting bacteria - are among the most abundant and diverse organisms on earth [1,2], found wherever bacteria exist, and they represent a constant challenge to bacteria. Bacteria and their associated bacteriophages co-evolve in a continuous battle, developing defensive and offensive strategies [3-5]. To protect themselves against bacteriophages, bacteria have evolved a variety of defense mechanisms, encoded in their genomes, including restriction modification [6], CRISPR-Cas [7] and xenogeneic silencing systems [8]. Bacterial xenogeneic silencers play important roles in bacterial evolution by recognizing and silencing foreign genes acquired through horizontal gene transfer [9,10], resulting from transformation, conjugation or transduction. The silencing of these foreign genes up to the moment that their expression is induced following an environmental cue can provide bacteria with a competitive advantage under specific conditions without compromising the integrity of global genome regulation [11]. Four types of bacterial xenogeneic silencers have been identified to date. These proteins all belong to the family of H-NS like proteins, defined by their functional similarity to the H-NS protein (see Chapter 1) [8,12-14]. Members include H-NS of *Proteobacteria* [15], MvaT of *Pseudomonas species* [16], Lsr2 of *Actinomycetes* [17] and Rok of *Bacillus species* [18]. The gene silencing mechanism of H-NS like proteins is determined by their ability to bind and spread across genes. Characteristic of H-NS family proteins is the formation of nucleofilaments along the DNA and protein-mediated DNA-DNA bridges (see Chapter 4) [19-22]. In response to bacterial xenogeneic silencing systems, bacteriophages have evolved resistance mechanisms by encoding proteins antagonizing H-NS silencing. For instance, the Gp5.5 protein of *E. coli* phage T7 is able to counteract H-NS activity in *E. coli* upon phage infection [23]. Gp5.5 binds to the central oligomerization domain of H-NS and disrupts higher-order H-NS-DNA complexes, leading to counter-silencing of genes controlled by H-NS [24,25]. Another example is the Arn protein of *E. coli* phage T4, which is a DNA mimic, which has been proposed to counteract H-NS mediated repression by targeting its DNA binding domain and thus interfering with DNA binding [26]. Bacteriophage Mu employs yet another mechanism. Binding of IHF to its site upstream of the early promoter (Pe) interferes with the formation of H-NS-DNA complexes and counteracts the H-NS-mediated repression of this promoter [27,28]. The EPV1 phage encodes H-NS on its genome, which

was proposed to repress expression of genes involved in host defense mechanisms against phage infection such as CRISPR associated proteins and a Type III restriction-modification system [29]. However, insights into the precise molecular mechanisms of inhibition are generally lacking.

The H-NS family protein MvaT of *Pseudomonas aeruginosa* plays an important role in genome organization and gene repression [16]. The *Pseudomonas* phage LUZ24 (and several related phages) encode the Mip (MvaT inhibiting protein) which binds MvaT and modulates its function. The Mip protein is one of the early phage genes expressed directly following host infection. Based on evidence that it inhibits DNA binding of MvaT, it was proposed that Mip inhibits the silencing of phage LUZ24 DNA by MvaT [30]. A number of possible mechanisms for modulation of MvaT function can be envisioned based on the nucleation-propagation-bridging assembly pathway of MvaT-DNA complexes (see Chapter 2) [13,19]. Mip may either alter 1) the DNA binding affinity of MvaT, which is important for protomer binding, 2) the multimerization properties of MvaT which determine the cooperativity of nucleoprotein filament formation or 3) the ability of MvaT to bridge DNA. In this study we investigated which of these steps in the assembly of the bridged complex is affected by Mip. Moreover, we defined how Mip interacts with MvaT and how this translates into altered DNA structuring properties. Based on this information we propose a mechanism by which Mip relieves MvaT-mediated silencing of phage genes.

Results

Mip cannot inhibit DNA binding of MvaT

It has been suggested that the Mip protein encoded on the *Pseudomonas* phage LUZ24 genome can inhibit the formation of MvaT-DNA complexes [30]. The underlying mechanism was proposed to be the inhibition of DNA binding by MvaT. However, support for such mechanism is minimal as MvaT has multiple modes of DNA binding (see introduction), which cannot be distinguished by gel electrophoresis as done in the study reporting the identification of Mip [30]. First, to verify the effect of Mip on the DNA binding of MvaT, we also performed electrophoretic mobility shift assay (EMSA). These experiments demonstrate that MvaT binds DNA (figure 3.1a), and that Mip alone does not bind to the DNA (figure 3.1b). Addition of increasing amounts of Mip from 1 to 10 µM, does not inhibit the formation of an MvaT-DNA complex (figure 3.1d), which is different from the results reported earlier [30]. To validate our observations, we next examined the effect of

Mip on the DNA binding of MvaT F36D/M44D, an MvaT mutant, that does not oligomerize and exists exclusively as dimer (see Chapter 2) [13]. Similar to MvaT wt, the DNA binding of MvaT F36DM44D was not inhibited by adding increasing amounts of Mip (figure 3.1c and 3.1e). Rather than inhibition, in both cases (figure 3.2d and 3.2e) complexes with further reduced mobility are observed upon introduction of Mip.
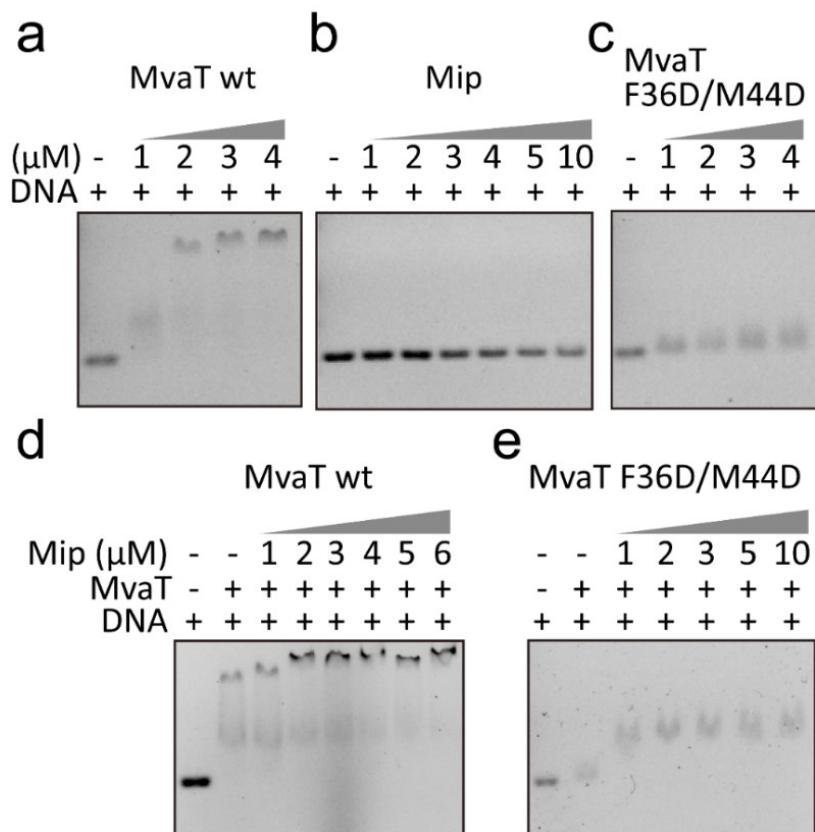

Figure 3.1. **Mip does not inhibit DNA binding of MvaT**. a) Gel electrophoretic mobility shift assay showing DNA and its binding by MvaT at concentrations of 1, 2, 3, and 4 µM. b) Gel electrophoretic mobility shift assay showing DNA and its binding by Mip at concentrations of 1, 2, 3, 4, 5, and 10 µM. c) Gel electrophoretic mobility shift assay showing DNA and its binding by MvaT F36DM44D at concentrations of 1, 2, 3, and 4 µM. Gel electrophoretic mobility shift assay showing DNA binding by d) 2 µM MvaT and e) 5 µM MvaT F36D/M44D, and the titration of the MvaT-DNA complexes with Mip at various concentrations as indicated in figure.

Mip cannot inhibit lateral MvaT-DNA complex formation

Oligomerization of MvaT is required for the formation of nucleoprotein filaments along DNA, and is essential for the function of MvaT in gene silencing [20,31]. As in our hands Mip does not inhibit

binding of MvaT to DNA, the effect of Mip on MvaT might be due to altered oligomerization behavior of MvaT along DNA. To investigate this possibility, we investigated the formation of MvaT nucleoprotein filaments and the effect of Mip on this process using Tethered Particle Motion (TPM) (see Chapter 2) [13,19]. DNA compaction, indicated by a reduction in RMS, was observed at low concentration of MvaT (figure 3.2, see Chapter 2) [13]. We attributed this effect to bending of DNA by individually bound MvaT dimers. Upon addition of increasing amounts of MvaT, the DNA was stiffened, indicated by an increase in RMS, reaching saturation level at 1200 nM. Mip alone did not alter the RMS in line with our observations that it does not bind to DNA (figure 3.1b).
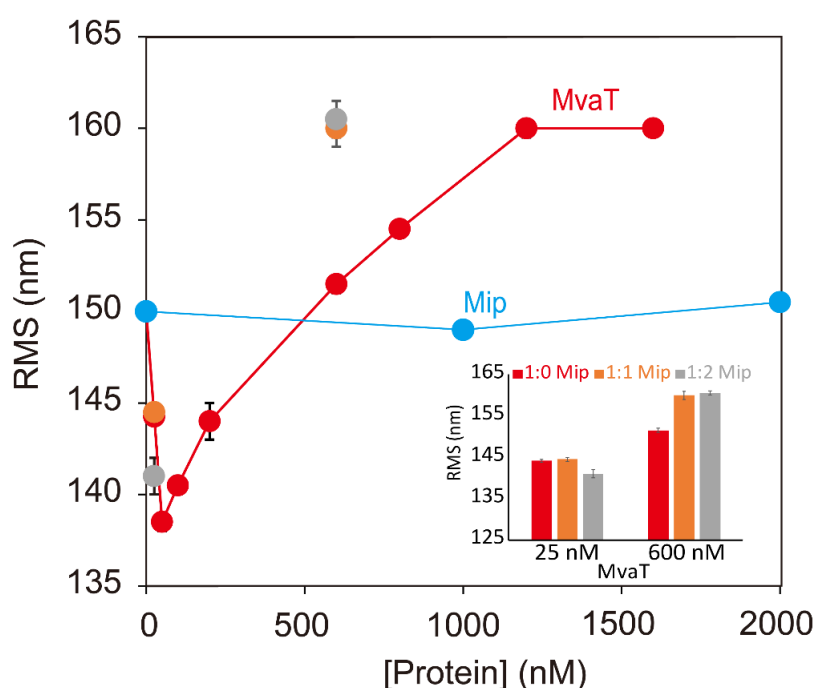

Figure 3.2. **Modulation of MvaT DNA-binding activity by Mip**. The curve (red in color) represents the RMS of DNA bound by MvaT at concentrations from 0 to 1600 nM as measured using the Tethered Particle Motion assay in the absence of Mip. The curve (blue in color) represents the RMS of DNA bound by Mip at concentrations from 0 to 2000 nM as measured using the Tethered Particle Motion assay in the absence of MvaT. The histogram indicates RMS values obtained at fixed concentrations of MvaT (25 nM and 600 nM) with varying amounts of Mip added. In the main plot, the TPM results of Mip effect on the DNA binding of MvaT at 1:1 and 1:2 ratio are indicated with orange and grey dots, respectively. The error bars represent the standard deviation of at least duplicate and some are hidden behind the data points.

To test whether Mip has an effect on the formation of the MvaT DNA filament, TPM was performed with fixed MvaT concentrations of 25 nM and 600 nM, with varying amounts of Mip added. At 25 nM MvaT addition of Mip has no or a very mild effect on the RMS of the MvaT-DNA complex. As the RMS does not return to bare DNA levels, these observations suggest that Mip does not inhibit DNA binding by MvaT in line with our observations reported in figure 3.1d. Also, at 600 nM the MvaT-DNA nucleoprotein filament is not perturbed by Mip. The increase in RMS indicates that Mip and MvaT bound together lead to a more extended nucleoprotein filament. This observation implies that Mip does not interfere with oligomerization of MvaT along DNA.

Mip interferes with the formation and stability of MvaT-DNA bridging complexes

MvaT is capable of forming nucleofilaments along DNA (see Chapter 2) [13,20] and protein-DNA bridging complexes (see Chapter 2) [13,20,32]. The DNA binding properties of MvaT are affected by the phage anti-MvaT protein Mip, while DNA binding of MvaT is not inhibited by Mip. To determine whether Mip affects the ability of MvaT to bridge DNA, we used the protein-DNA bridging assay established in earlier work (see Chapter 5) [19,33]. MvaT was found to be able to bridge DNA in the presence of divalent salt or monovalent salt at high concentration (see Chapter 2) [13]. Here we performed the experiments in the presence of $MgCl_2$. In this assay a fixed amount of MvaT (2.4 µM) is used which yields a 35% recovery of DNA in the absence of Mip. The DNA recovery decreases upon addition of increasing amounts of Mip up to 3.6 µM (figure 3.3a). Maximum inhibition of DNA recovery occurs at a Mip concentration of 1.2 µM where the Mip : MvaT molar ratio is 0.5 (figure 3.3a). Experiments carried out using an alternative divalent anion, Ca^{2+}, confirm efficient DNA bridging by MvaT, as well as perturbation of MvaT-mediated DNA bridging by Mip (figure S3.1). Our results thus clearly demonstrate that Mip interferes with the formation of bridged MvaT-DNA complexes. Next, to examine whether Mip has an effect on existing bridged MvaT-DNA complexes, we carried out a variation on the DNA bridging assay in which DNA recovery is measured over time following addition of Mip (MvaT:Mip = 1:1) at different time points during bridged MvaT-DNA complex assembly (figure 3.3c). As a control, we measured the DNA recovery promoted by MvaT over time without adding Mip. In this case DNA recovery increases over time and reaches saturation at t = ~ 600 s (figure 3.3b). When Mip is introduced at the beginning (t = 0 s), a minimal increase of DNA recovery was observed over time (up to 5%).

This observation indicates that Mip interferes with the assembly of the bridged MvaT-DNA complex. When Mip is introduced when bridged MvaT-DNA complex formation has progressed for 180 s (but has not reached saturation levels) and 1200 s (has reached saturation levels), reduction in DNA recovery is observed. This demonstrates that bridged MvaT-DNA complexes can be perturbed by Mip. Taken together, our results demonstrate that the phage protein Mip can not only interfere with the formation of bridged MvaT-DNA complexes, but also perturbs pre-assembled bridged MvaT-DNA complexes.
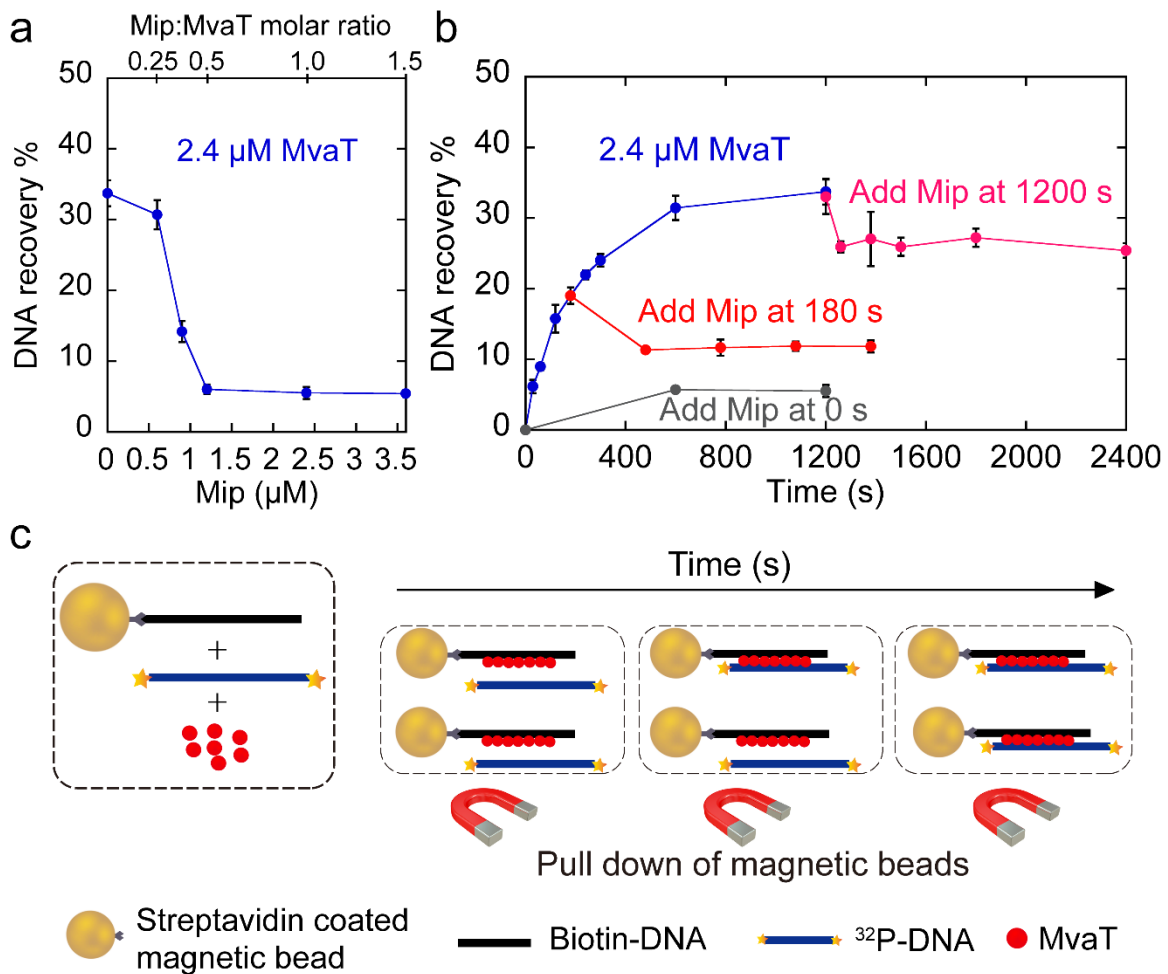

Figure 3.3. **Mip inhibits the formation of bridged MvaT-DNA complexes and perturbs existing bridged MvaT-DNA complexes.** a) Mip inhibits the formation of the bridged MvaT-DNA complex. DNA bridging efficiency (as a percentage of the input DNA) in presence of MvaT (2.4 µM), as affected by titration of Mip at concentrations up to 3.6 µM. b) Mip perturbs existing bridged DNA-MvaT-DNA complexes. The blue curve represents the kinetics of MvaT-DNA bridge formation without adding Mip. The red and pink curve represent the kinetics of MvaT-DNA bridge formation with Mip introduced at 180 s and 1200 s respectively. The grey

curve represents Mip introduced at the beginning (t = 0 s). Data are plotted as mean values and the error bars represent the standard deviation from at least 2 independent measurements. c) Experimental schematic of bridging assay over time. Magnetic beads connect to biotin labeled DNA; radioactive labeled DNA was bridged by adding MvaT; at various time points, the bridging reactions were terminated by magnetic pull down and buffer washing of beads. If required, Mip (MvaT:Mip = 1:1) was added at different time points to measure the effect of Mip on the formation of MvaT-DNA bridge complexes over time.

Mip binds the N-terminal domain of MvaT

The fold architecture of the MvaT monomer consists of an α-helical N-terminal oligomerization domain (residues 1-64) tethered to a C-terminal DNA binding domain (DBD) (residues 79-124) by a flexible linker (residues 65-78) (figure 3.4a). The structural unit of MvaT nucleofilaments is a dimer (protomer) formed by "coiled-coil" interactions between the first N-terminal α-helices of two MvaT monomers (α1: residues 1-32), dimerization site 1 (figure 3.4a). The MvaT protomers form high-order oligomers through a second dimerization site, site 2 (α2: residues 50-58). Both coiled-coils are formed by a hydrophobic core and stabilized by salt bridges (see Chapter 2) [13].

Above we have shown that the inhibitory effect of Mip on the DNA bridging activity of MvaT, is neither due to inhibition of DNA binding by MvaT nor to inhibition of oligomerization of MvaT along DNA. To define the mechanism underlying the inhibitory function of Mip, we investigated how Mip binds to MvaT. Previously, it was suggested that Mip binds to the MvaT oligomerization domain and linker region (residues 1–80) [30]. To substantiate these suggestions, here we investigated the interaction of Mip with both the N-terminal domain (residues 1-62) and the DBD (residues 79-124) of MvaT in a magnetic bead pull down assay. The results of this assay confirm that Mip binds to the N-terminal domain (residues 1-62) (figure 3.4a) and not to the DBD (residues 79-124), and also suggest that the linker region (65-80) may not be required for the Mip-MvaT complex formation.

To determine the stoichiometry of the protein-protein complex and the affinity between the two proteins, we performed isothermal titration calorimetry (ITC) of the MvaT dimer (F36D/M44D) titrated with Mip. The fit of the titration data to a 1:1 binding model yields a K_D of 170 $\pm$ 14 nM with a number of binding sites N= 0.56 (figure 3.4c). These results suggest a tight binding between the

two proteins with a stoichiometry of 1:2. Thus, the Mip-MvaT complex appears to be formed by the interaction of one molecule of Mip with two molecules of MvaT.
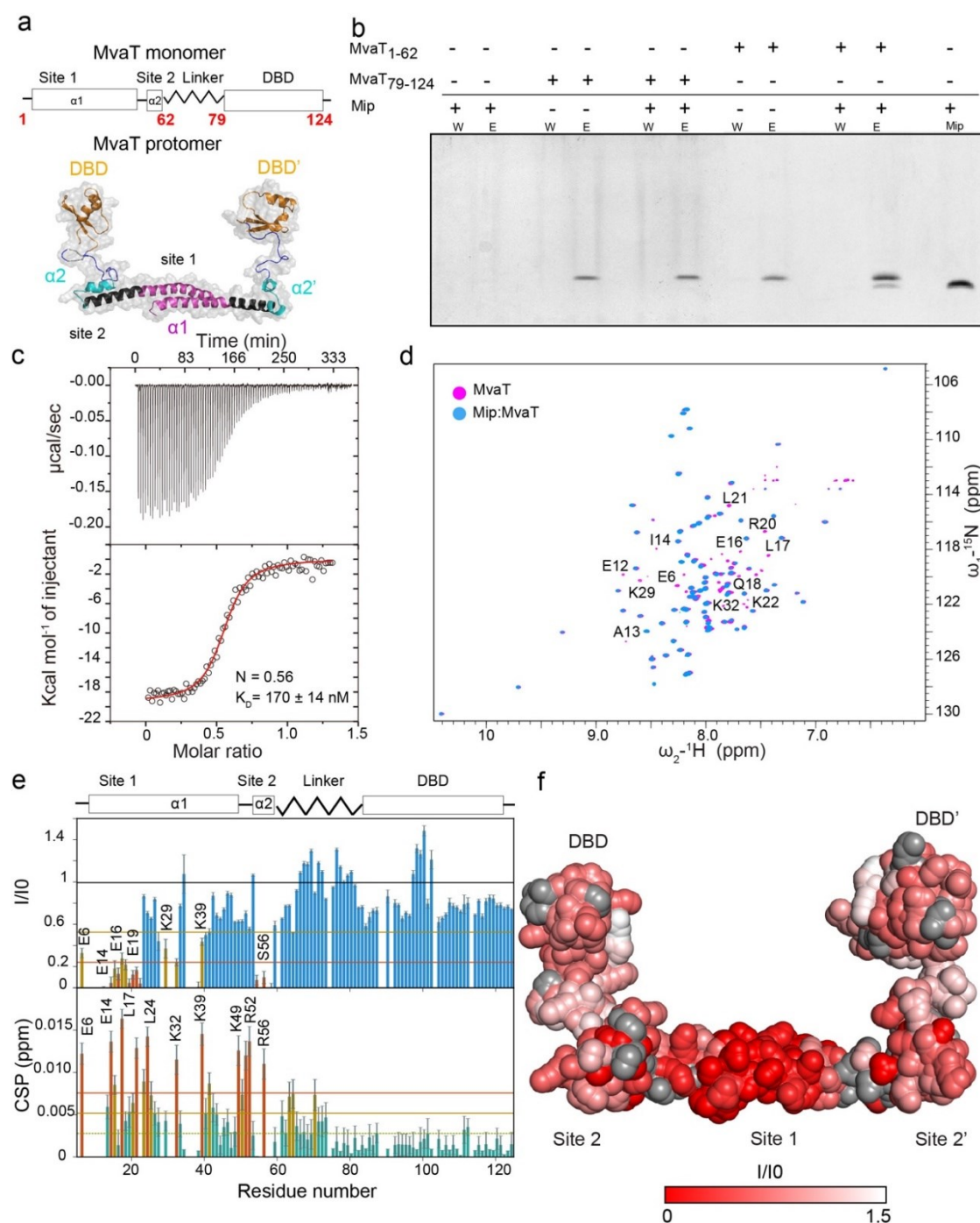

Figure 3.4. **Mip interacts with the N-terminal domain of MvaT.** a) MvaT monomer and protomer fold topology. In the lower panel is the structural model of the MvaT protomer adopted from (see Chapter 2) [13]. (b) Tricine gel analysis of the his-tag pull down assay. His-tagged MvaT truncates captured on magnetic beads were incubated with Mip. A Mip reference marker was used to identify Mip. c) ITC titration of Mip (230

μM) into MvaT (16 μM) using 2 μl of injection volume. The red line represents the best fit plot by using a 1:1 binding model. The fitting yields a K_D = 170 ± 14 nM and N = 0.56 sites. (b) Overlay between MvaT dimer ^{15}N-^{1}H HSQC spectra in the free state (magenta) and at 1.2 Mip:MvaT molar ratio (blue). Amide resonances which experience severe line broadening upon titration with Mip are labelled. (e) The upper panel depicts the ^{15}N-^{1}H HSQC spectra peak intensities ratio of MvaT in the presence of 1.2 molar ratio of Mip (I) and in the free state (I0) versus the protein residue number. Lower panel shows weighted average CSP of the MvaT resonances between the same points of titration. Resonances with CSP more than two (orange line) or one (yellow line) standard deviation (SD) from the 10% trimmed mean (green dashed line) are labelled and shown in orange, yellow and green bars, respectively. (f) Mapping of the residues with reduction in their peak intensities (red/white gradient), upon addition of Mip, on the MvaT dimer structural model surface. Residues with no data are colored in grey spheres.

As the used MvaT variant (F36D/M44D) can only form a dimer through the interaction between the two N-terminal α-helices (site1), we hypothesize that Mip is mainly interacting with site 1, to satisfy the stoichiometry of the complex. To corroborate this hypothesis, we performed a NMR titration of the MvaT dimer (F36D/M44D) with Mip using the same experimental conditions as used for the ITC titration. The ^{15}N-^{1}H HSQC spectrum of MvaT dimer was previously assigned (see Chapter 2) [13], enabling the identification of the exact region on the dimer to which Mip binds.

The addition of Mip to MvaT induced a decrease in the intensity of multiple resonances in the protein spectrum with minor changes in their chemical shift positions (figure 3.4d). Such effect is typical of a strong binding, in agreement with the ITC results (K_D= 170 ± 14 nM). At 1.2 molar ratio, the ratio between the peak's intensities of the MvaT free and bound to Mip shows that the resonances affected significantly are for residues located in the dimerization site 1 (residues 1-22) (figure 3.4e and 3.4f). A general yet non-uniform line broadening is also observed for amide resonances of the linker and the DBD (figure 3.4e). This observation might be in part explained by the increase in the rotational correlation time (τ_c) of the MvaT dimer upon complex formation with Mip. In addition, we propose that intermolecular interactions arise between Mip and MvaT DBD and linker region. These interactions are possibly too weak to be probed by the pull-down assay or ITC.

Previously we have found that at low ionic strength, the MvaT dimer exhibits intramolecular electrostatic interactions between its oppositely changed N-terminal and DBD domains, which are further stabilized by the linker region. These interactions cause line broadening in the amide's resonances of the DBD and linker. Increase in ionic strength destabilizes these intramolecular interactions and thus induces an enhancement of the peak intensities of the backbone amides of the DBD and linker (see Chapter 2) [13]. The NMR titration of MvaT with Mip was performed at high ionic strength (50 mM KCl, 16 mM MgCl$_2$), therefore it is expected that the line broadening due to electrostatic interactions between the oppositely charged domains is negligible. Therefore, we propose that the observed non-uniform lines broadening of the resonances of the residues of the linker and DBD, in the presence of Mip, is due to the formation of new intermolecular interactions between these regions and Mip.

Modeling of the Mip-MvaT complex

To understand the mechanism by which Mip modulates the DNA binding properties of MvaT we generated a molecular model of the Mip-MvaT$_2$ complex. Mip is a 46 amino acids basic protein with no tertiary structure available. The secondary structure of the Mip polypeptide chain was predicted to consist of an N-terminal (α1) and C-terminal (α2) helix connected by a flexible loop (figure 3.5a).

Next, we performed *ab initio* modelling using Rosetta [34] to predict the 3D structure of Mip. In the best structure, the two helices of Mip form a "coiled coil" motif with a hydrophobic core stabilized by a salt bridge (figure 3.5a and 3.5b). The structural models of the MvaT dimer and Mip were used to perform restrained docking with HADDOCK [35] using the NMR titration data as experimental restraints. In our modelling we only considered the binding of Mip to the MvaT dimer N-terminal domain (residues 1-22), as it appears to represent the primary interaction site between the two proteins (K$_D$ =170 $\pm$ 14 nM). Multiple structures of the Mip-MvaT$_2$ complex were obtained (figure S3.2 and M&M). The lowest energy structure of the complex is shown in figure 3.5c. The complex of the two proteins seems to be formed by electrostatic interactions between the surfaces of the positively charged Mip and the negatively charged site 1 of the MvaT dimer (figure 3.5c and 3.5d).
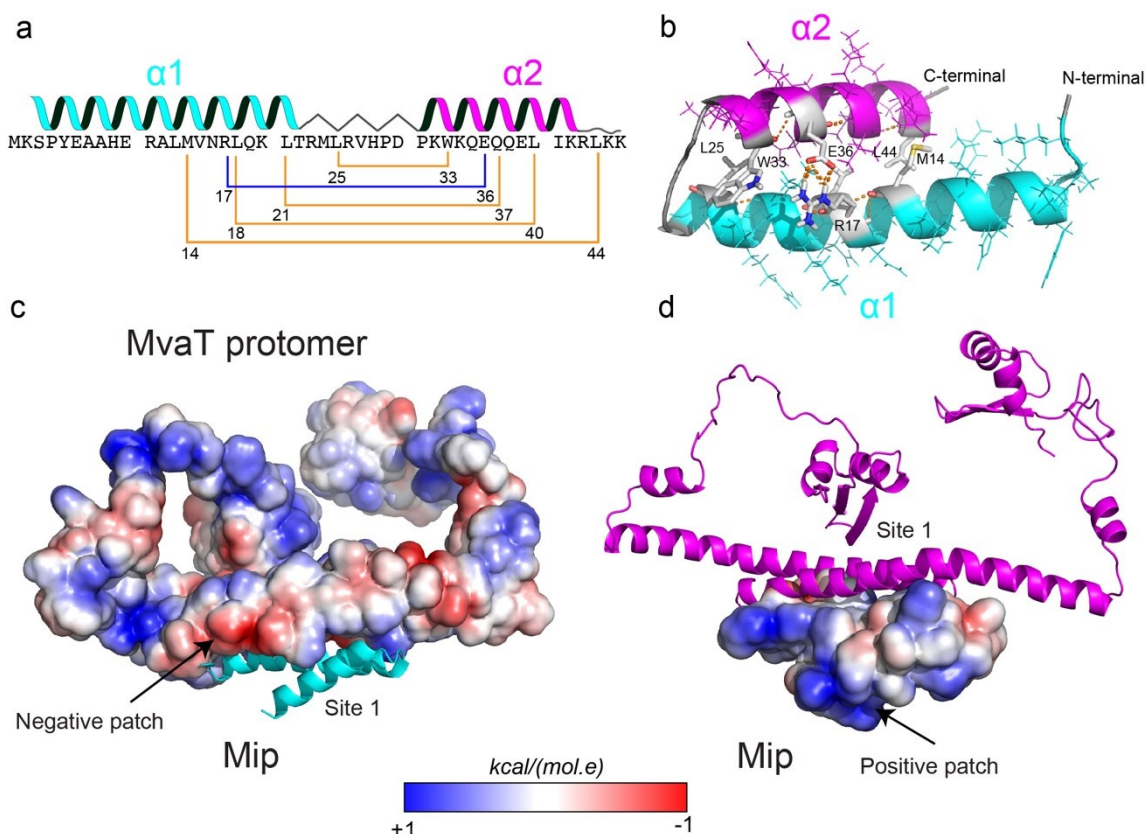
Figure 3.5. **Mip-MvaT protein complex model.** a) Mip secondary structure predicted by JPred 4 server [36]. The N-terminal helix (α1) is shown in cyan and the C-terminal helix (α2) is in magenta. (b) The lowest energy structure obtained from the *ab initio* Rosetta modeling [34].The side chains of the residues involved in the hydrophobic core of the coiled coil are shown in stick and labelled. The hydrophobic interactions are shown in (a) with yellow line and the salt bridge is shown in blue. The color code is as in (a). (c) and (d) The HADDOCK best structure of the Mip-MvaT$_2$ complex (see M&M) with the electrostatic potential surfaces of MvaT protomer and Mip, respectively.

How can our findings be structurally rationalized?

The TPM results indicate that Mip binding affects the stiffening and degree of compaction (due to bending) of DNA by MvaT. Our results show also that binding of Mip to the central dimerization domain of MvaT (site 1) can inhibit its DNA bridging activity, while DNA stiffening is not inhibited. This indicates that in the presence of Mip, despite the formation of MvaT nucleofilaments along the DNA, these filaments are unable to interact with a second DNA duplex to form a bridge. This situation resembles the low salt condition described in earlier work (see Chapter 2) [13] in which MvaT protomers adopt a half open state, in which one of the DBD's is

sequestered by intramolecular electrostatic interaction with site 1. An increase in ionic strength destabilizes these interactions and the MvaT protomers expose both of their DBD's, adopting fully open states, able to bridge two DNA duplexes (see Chapter 2) [13]. Therefore, we hypothesize that Mip counteracts the effect of the high ionic strength, used in the bridging assay condition (50 mM KCl, 16 mM $MgCl_2$), on the MvaT conformational landscape and shifts the structural equilibrium towards the half open state, similar to the low salt condition (50 mM KCl, in the absence of $MgCl_2$). This is supported by the NMR titration data which indicate that intermolecular interactions between Mip and the DBD exist. Therefore, in the presence of Mip and at high ionic strength MvaT protomers adopt a half open state that is able to stiffen, but not to bridge DNA. Further structural studies are required to validate this model.
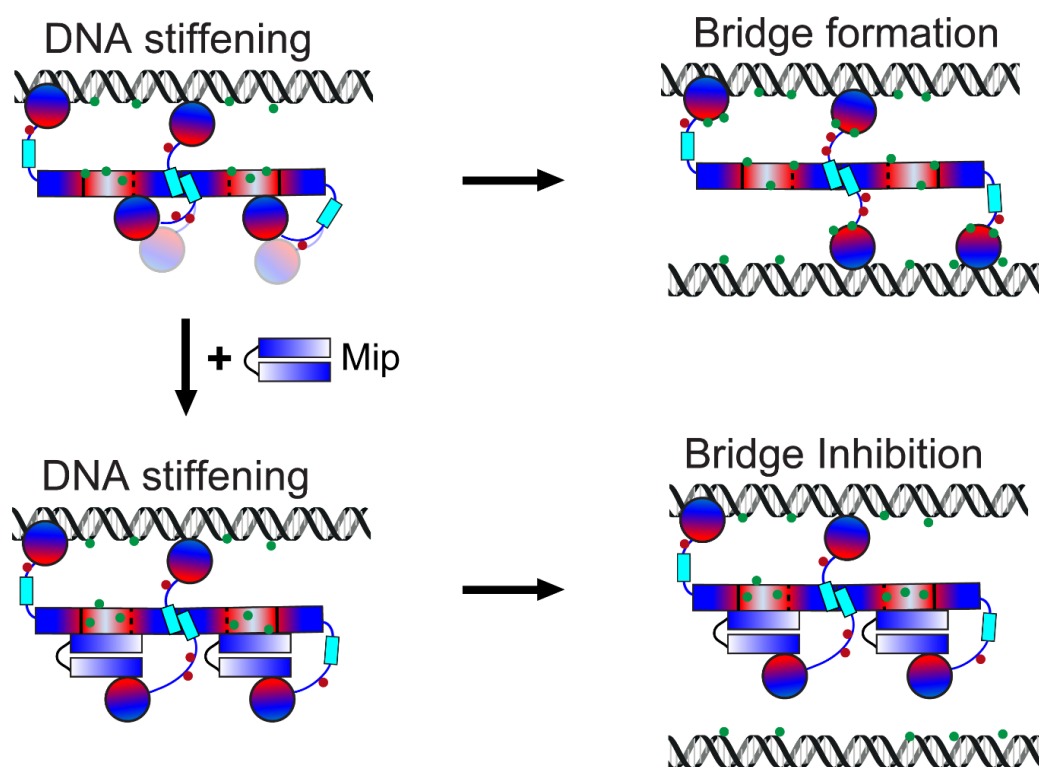

Figure 3.6. **Proposed mechanism for inhibition of MvaT DNA bridging activity by Mip.** The electrostatic surfaces of MvaT dimer and Mip are shown schematically in a red (negative)/white (neutral)/blue (positive) color gradient. Green and red dots are for ions (Mg^{2+}) and counter ions (Cl^-), respectively.

Discussion

In this work we have investigated the molecular mechanism by which the phage encoded Mip protein modulates MvaT activity. Mip interferes with the formation and maintenance of bridged MvaT-DNA complexes. This is a novel mechanism adding to the repertoire of distinct direct modulators of H-NS like protein activity [37,38]. Previously identified mechanisms involved interference with DNA binding (Arn) [26], multimerization (H-NST) [39] and stimulation of DNA bridging (Hha/YdgT) [19]. Hha/YdgT operates in strikingly similar manner as Mip: it associates with the central dimerization domain and exposes a charged surface facing outward, available for interaction with other partners. However, whereas Hha exposes a positively charged surface likely to interact with DNA and thus promoting DNA bridging, Mip exposes a positively charged surface, sequestering the DNA binding domain, shifting the structural equilibrium towards the half open state and disfavoring DNA bridging.

The interaction and co-evolution between a bacteriophage and its bacterial host play a key role in the ecological and evolutionary processes of microbial communities. Successful bacteriophage infection requires coping with bacterial resistance systems. One such bacterial resistance systems is that executed by H-NS-like proteins which cause xenogeneic silencing. To mitigate the effects of such H-NS-like proteins, bacteriophages encode proteins counteracting gene silencing by H-NS-like proteins. Our results show that the phage protein Mip is capable of inhibiting the DNA bridging activity of H-NS-like protein MvaT without inhibiting the DNA stiffening activity of the protein. DNA bridging is believed to be crucial in gene silencing [40,41]. To enhance the activity of H-NS proteins in gene silencing, bacteria themselves also encode proteins that modulate what type of H-NS-DNA complex is formed. Binding of Hha to H-NS exposes a positively charged surface [42] and stimulates its DNA bridging activity [19], which facilitates H-NS-mediated silencing of foreign genes in bacteria [43]. The Hha family protein YdgT also enhances DNA bridging [19]. YdgT, however, stimulates DNA bridging by enhancing the cooperativity of filament formation, the step preceding bridged H-NS-DNA complex formation [19].

In general, a better understanding of how viral proteins counteract H-NS proteins is important for design of proteins or molecules countering phage infection. Potential applications of such molecules can be envisioned in biotechnology, where phage infections are a threat to large

scale culturing, or in phage therapy where they may aid in enhancing the ability to infect and kill their host. Moreover, due to their global role in gene regulation in bacteria H-NS-like proteins are potential drug targets to mitigate bacterial infections. Understanding at the molecular mechanistic level how H-NS activity is modulated is key to such developments.

Materials and Methods

Construction of plasmids

The plasmids encoding MvaT of *P. aeruginosa* (pRD228), its derivatives (MvaT F36D/M44D (pRD277), MvaT 1-62-His (pRD360) and MvaT 79-124-His (pRD361)) and Mip of Pseudomonas phage LUZ24 (pRD232) were constructed using pET30b as vector by Gibson assembly [44]. The cloned sequences were verified by DNA sequencing.

DNA substrates

All tethered particle motion and bridging assay experiments were performed using a random, AT-rich, 685 bp (32% GC) DNA substrate used in previous research (see Chapter 2) [13,19]. The DNA substrate was generated by PCR and the products were purified using a GenElute PCR Clean-up kit (Sigma-Aldrich). If required, DNA was ^{32}P-labeled as described previously [19]. For the electrophoretic mobility shift assay an AT-rich 200 bp (31%GC) was generated using the same procedure.

Protein expression and purification

BL21 (DE3) pLysS cells transformed with (pRD228, pRD277, pRD360, pRD361 and pRD232) were grown in 2l of LB supplemented with kanamycin (100 µg/ml) at 37°C to an OD600 of ~0.6. Protein expression was induced with 0.5 mM isopropyl β-D-1-thiogalactopyranoside (IPTG) overnight at 18°C. Cells were centrifuged at 7000 × g for 15 min at 4°C. MvaT and MvaT F36D/M44D were purified as described previously (see Chapter 2) [13]. MvaT 1-62-His and MvaT 79-124-His were purified with modifications. The harvested cells were lysed by sonication in a lysis buffer containing 20 mM Tris-HCl (pH 8.0), 1 M NaCl. The lysate was cleared by centrifugation at 37 000 × g for 30 min at 4°C. Next, the supernatant was loaded on a HisTrap HP

5ml column (GE healthcare Life sciences) and the protein was eluted by applying an imidazole gradient from 0 to 1 M. The eluted fractions were checked by SDS-PAGE and the fractions that contain the target protein were pooled, concentrated and buffer exchanged using a PD10 column to 20 mM tris-HCl pH 7, 100 mM KCl. Next, the MvaT 1-62-His and MvaT 79-124-His were loaded on a HiTrap Q HP 5ml and HiTrap SP HP 5ml column (GE healthcare Life sciences) respectively and eluted by applying a NaCl gradient (from 0.1 to 1 M). The eluted fractions were also checked by SDS-PAGE and the pooled fractions were concentrated to a 500 μl volume with an Amicon 10 kDa cut-off filter. The concentrated protein fractions were loaded on a GE Superdex 75 10/300 GL column and eluted with 20 mM Tris-HCl pH 8, 300 mM KCl, 10% Glycerol. For the purification of Mip, the harvested cells were lysed by sonication in a lysis buffer containing 20 mM Tris-HCl (pH 7.0), 100 mM NaCl. Next, the supernatant was loaded on a HiTrap SP HP 5ml column (GE healthcare Life sciences) and the protein was eluted by applying a NaCl gradient from 0.1 to 1 M. The eluted fractions were checked by SDS-PAGE and the fractions that contain the target protein were pooled, concentrated and loaded into a GE Superdex 75 10/300 GL column and eluted with 20 mM Tris-HCl pH 8, 300 mM KCl, 10% Glycerol. The purity of the protein was checked by SDS-PAGE and the concentration was determined using a Pierce BCA protein assay kit (Thermo Scientific).

His-tag pull down assay

120 μl of the High-Density Nickel Agarose (Jena Bioscience) suspension was pipetted into an Eppendorf tube. The beads were prepared by changing the solution to binding buffer (100 mM NaCl, 10 mM tris-HCl pH 7.2, 50 mM imidazole, 20 mM $MgCl_2$). The nickel beads were then centrifuged at 7000 rpm for 2 minutes and the supernatant was removed. 250 μl of the desired combination of MvaT 79-124-His (40 μM), His-MvaT 1-62 (40 μM) and/or Mip (40 μM), in binding buffer, was added to the prepared nickel beads. This was incubated for 30 minutes while being shaken at 1000 rpm. After incubation the samples were centrifuged at 3000 rpm for 2 minutes. The supernatant was removed, and the pellet was carefully resuspended in 250 μl of binding buffer. This was referred to as a washing step and was repeated a total of six times. Following the final washing step, 250 μl of elution buffer (100 mM NaCl, 10 mM tris HCl pH 7.2, 1.5 M imidazole, 20 mM $MgCl_2$) was added to the beads instead of binding buffer to elute any protein bound to the

bead. The samples were centrifuged at 3000 rpm for 2 minutes and the supernatant was collected. 10 µl of the supernatant was run on a tricine gel.

Tethered Particle Motion

Tethered Particle Motion experiments were performed as described previously (see Chapter 2) [13] and the flow cells were prepared with minor modifications. In short, first, the flow cell was washed with 100 ml of wash buffer (10 mM Tris-HCl pH 8, 150 mM NaCl, 1 mM EDTA, 1 mM DTT, 3% Glycerol, 100 µg/ml BSA (ac)) and experimental buffer (10 mM Tris pH 8, 50 mM KCl, 10 mM EDTA, 5% glycerol). The flow cell was sealed after adding protein (MvaT alone or MvaT-Mip mixure) in experimental buffer, followed by 10 minutes of incubation. The measurements were initiated 15 min after introducing protein. For each flow cell more than 200 beads were measured at a temperature of 25°C.

Electrophoretic mobility shift assay

The assay was performed on an AT-rich 200 bp DNA substrate (31% GC). DNA (25 ng) was incubated with different concentrations of the desired combination of MvaT, MvaT F36D/M44D and Mip in the binding buffer (10 mM Tris-HCl, 60 mM KCl, pH 8.0). The mixture was loaded on a 1% agarose gel (containing 1:10^4 dilution of Gel red DNA stain) with loading buffer (10 mM Tris-HCl, pH 7.6, 0.03% bromophenol blue, 0.03 % xylene cyanol FF, 60% glycerol and 60 mM EDTA). The samples were run at 4°C in TAE standard buffer. The gels were visualized with a Bio-rad Gel Doc XR+ system.

Isothermal Titration Calorimetry

Isothermal Titration Calorimetry experiments were performed as described previously (see Chapter 2) [13] with modifications. Briefly, ITC experiments were performed using a MicroCal VP-ITC system at 20 °C. The protein samples were dialyzed to a buffer containing 20 mM Bis-Tris, pH 6, 50 mM KCl, 16 mM MgCl$_2$. Typically, 20 µM of MvaT F36D/M44D was placed in the cell (1.4 ml) and titrated with 300 µM (500 µl) of the Mip, injected in 2 µl aliquots. The delay time between the injections was 60 s with a stirring speed of 307 rpm. The corresponding "protein to buffer" controls were performed for background correction. The ITC titration data were analysed using

Origin 7.0 (OriginLab) provided with the instrument. Standard deviation was calculated from the fit by Origin.

Bridging assay

The bridging assay was performed as described previously (see Chapter 2) [13] with modifications. To start the bridging reaction, MvaT was added, followed by 2 µl of Mip to different final concentrations. The samples were incubated while shaking at 1000 rpm at 25°C. The reactions were stopped and washed at certain time with buffer (10 mM Tris-HCl, pH 8, 65 mM KCl, 5% glycerol, 1 mg/ml BSA(ac), 1 mM spermidine, 20 mM $CaCl_2$, 0.02% Tween 20), followed by resuspension in 12 µl denaturing buffer (10 mM tris pH 8, 200 mM NaCl, 1 mM EDTA, 0.2% SDS (10%)). Scintillation was used to determine the final radioactivity of each sample. 2 µl of radioactive DNA was used as a reference to calculate the bridging efficiency (DNA recovery %).

NMR titration

The NMR titration of the MvaT dimer with Mip was performed on a 150 µM ^{15}N isotopically labelled protein sample, in 20 mM Bis-Tris Buffer, 50 mM KCl, 16 mM $MgCl_2$, pH 6 and 6% D_2O. A series of ^{1}H-^{15}N HSQC spectra were acquired by gradually increasing the Mip:MvaT molar ratio from 0.2 to 1.2. The experiments were recorded at 20 °C on a Bruker Avance III (HD) 600 MHz spectrometer, equipped with TCI cryoprobe, processed by TopSpin 3.5 (Bruker Biospin) and analysed by Sparky software [45]. The changes in peak positions and intensities were analysed by an in-house python script and the average chemical shift perturbations (CSP) were calculated using equation (1):

$$\Delta\delta_{avg} = \sqrt{\Delta\delta_H{}^2 + \frac{\Delta\delta_N{}^2}{6.25^2}} \qquad (1)$$

Modelling

The prediction of Mip 3D structure was performed using an *Ab initio* Rosetta modelling approach implemented in Robetta server (http://new.robetta.org). Prediction of the Mip-MvaT$_2$ complex was performed by HADDOCK2.2 server (https://milou.science.uu.nl/services/HADDOCK2.2) [35] using default setting parameters. The data from the NMR titration of the MvaT dimer with Mip was used to restrain the docking. The best *ab initio* model of Mip and the homology model of MvaT dimer

(see Chapter 2) [13] were used. Only the amino acids of site 1 of the MvaT dimer were classified as *active* in the docking settings. As no experimental information is available on which residues of Mip are involved in the complex formation, the full protein amino acid sequence was classified as *active*. Amino acid residues indirectly involved in complex formation (passive residues) were automatically identified by the server. HADDOCK clustered 138 structures in 16 clusters, which represents 69.0 % of the water-refined models HADDOCK generated. The statistics of the top cluster are shown in the table below. The top cluster is the most reliable according to HADDOCK. The reported scores and energies are averages calculated over the top four members of a cluster. The HADDOCK score is defined as: HADDOCK-score = $1.0*E_{VDW}+0.2*E_{ELEC}+1.0*E_{Desolvation}$

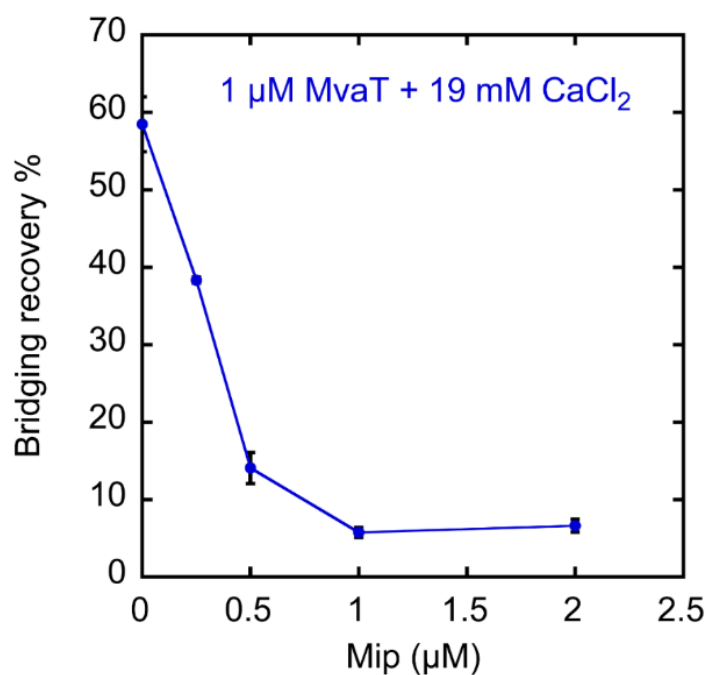| Cluster 3	
HADDOCK score	-103.3 +/- 14.3
Cluster size	11
RMSD from the overall lowest-energy structure	1.0 +/- 0.6
Van der Waals energy	67.0 +/- 7.6
Electrostatic energy	-360.2 +/- 63.5
Desolvation energy	-5.0 +/- 7.0
Restraints violation energy	407.9 +/- 78.85
Buried Surface Area	2369.2 +/- 90.2
Z-Score	-2.0

Supplementary information

Figure S3.1. **Mip inhibits the formation of a bridged DNA-MvaT-DNA complex.** DNA bridging efficiency (as a percentage of the input DNA) of MvaT (2.4 µM) as affected by titration of Mip at concentrations from 0 to 2.5 µM as measured by the DNA bridging pull down assay in the presence of 19 mM $CaCl_2$.
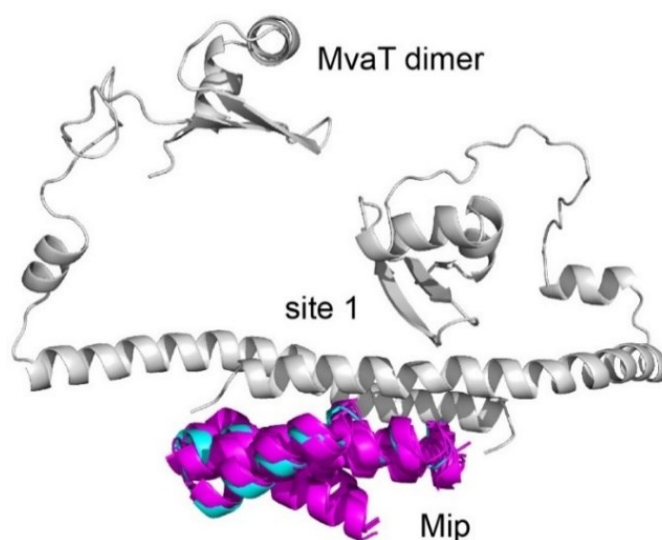

Figure S3.2: **HADDOCK best cluster of Mip-MvaT$_2$ complex**. The different orientations of Mip are shown in magenta cartoon and MvaT dimer in grey cartoon. The lowest energy structure of Mip within the complex is shown is cyan cartoon.

References

1   Bergh, O., Borsheim, K. Y., Bratbak, G. & Heldal, M. High abundance of viruses found in aquatic environments. *Nature* **340**, 467-468, doi:10.1038/340467a0 (1989).

2   Wommack, K. E. & Colwell, R. R. Virioplankton: viruses in aquatic ecosystems. *Microbiol. Mol. Biol. Rev.* **64**, 69-114, doi:10.1128/mmbr.64.1.69-114.2000 (2000).

3   Stern, A. & Sorek, R. The phage-host arms race: shaping the evolution of microbes. *Bioessays* **33**, 43-51, doi:10.1002/bies.201000071 (2011).

4   Chibani-Chennoufi, S., Bruttin, A., Dillmann, M.-L. & Brüssow, H. Phage-Host Interaction: an Ecological Perspective. *J. Bacteriol.* **186**, 3677, doi:10.1128/JB.186.12.3677-3686.2004 (2004).

5   Stone, E., Campbell, K., Grant, I. & McAuliffe, O. Understanding and Exploiting Phage-Host Interactions. *Viruses* **11**, 567, doi:10.3390/v11060567 (2019).

6   Enikeeva, F. N., Severinov, K. V. & Gelfand, M. S. Restriction-modification systems and bacteriophage invasion: who wins? *J. Theor. Biol.* **266**, 550-559, doi:10.1016/j.jtbi.2010.07.006 (2010).

7   Dupuis, M. E., Villion, M., Magadan, A. H. & Moineau, S. CRISPR-Cas and restriction-modification systems are compatible and increase phage resistance. *Nat Commun* **4**, 2087, doi:10.1038/ncomms3087 (2013).

8   Pfeifer, E., Hünnefeld, M., Popa, O. & Frunzke, J. Impact of Xenogeneic Silencing on Phage–Host Interactions. *J. Mol. Biol.*, doi:https://doi.org/10.1016/j.jmb.2019.02.011 (2019).

9   Flores-Rios, R., Quatrini, R. & Loyola, A. Endogenous and Foreign Nucleoid-Associated Proteins of Bacteria: Occurrence, Interactions and Effects on Mobile Genetic Elements and Host's Biology. *Comput Struct Biotechnol J* **17**, 746-756, doi:10.1016/j.csbj.2019.06.010 (2019).

10   Navarre, W. W. The Impact of Gene Silencing on Horizontal Gene Transfer and Bacterial Evolution. *Adv. Microb. Physiol.* **69**, 157-186, doi:10.1016/bs.ampbs.2016.07.004 (2016).

11   Huttener, M., Paytubi, S. & Juarez, A. Success in incorporating horizontally transferred genes: the H-NS protein. *Trends Microbiol.* **23**, 67-69, doi:10.1016/j.tim.2014.12.009 (2015).

12   Singh, K., Milstein, J. N. & Navarre, W. W. Xenogeneic Silencing and Its Impact on Bacterial Genomes. *Annu. Rev. Microbiol.* **70**, 199-213, doi:10.1146/annurev-micro-102215-095301 (2016).

13   Qin, L. *et al.* Structural basis for osmotic regulation of the DNA binding properties of H-NS proteins. *Nucleic Acids Res.*, doi:10.1093/nar/gkz1226 (2020).

14   Qin, L., Erkelens, A. M., Ben Bdira, F. & Dame, R. T. The architects of bacterial DNA bridges: a structurally and functionally conserved family of proteins. *Open Biol* **9**, 190223, doi:10.1098/rsob.190223 (2019).

15   Navarre, W. W., McClelland, M., Libby, S. J. & Fang, F. C. Silencing of xenogeneic DNA by H-NS-facilitation of lateral gene transfer in bacteria by a defense system that recognizes foreign DNA. *Genes Dev.* **21**, 1456-1471, doi:10.1101/gad.1543107 (2007).

16   Castang, S., McManus, H. R., Turner, K. H. & Dove, S. L. H-NS family members function coordinately in an opportunistic pathogen. *Proc Natl Acad Sci U S A* **105**, 18947-18952, doi:10.1073/pnas.0808215105 (2008).

17   Gordon, B. R., Imperial, R., Wang, L., Navarre, W. W. & Liu, J. Lsr2 of Mycobacterium represents a novel class of H-NS-like proteins. *J. Bacteriol.* **190**, 7052-7059, doi:10.1128/jb.00733-08 (2008).

18   Smits, W. K. & Grossman, A. D. The transcriptional regulator Rok binds A+T-rich DNA and is involved in repression of a mobile genetic element in Bacillus subtilis. *PLoS Genet.* **6**, e1001207, doi:10.1371/journal.pgen.1001207 (2010).

19   van der Valk, R. A. *et al.* Mechanism of environmentally driven conformational changes that modulate H-NS DNA-bridging activity. *Elife* **6**, doi:10.7554/eLife.27369 (2017).

20   Winardhi, R. S. *et al.* Higher order oligomerization is required for H-NS family member MvaT to form gene-silencing nucleoprotein filament. *Nucleic Acids Res.* **40**, 8942-8952, doi:10.1093/nar/gks669 (2012).

21   Qu, Y., Lim, C. J., Whang, Y. R., Liu, J. & Yan, J. Mechanism of DNA organization by Mycobacterium tuberculosis protein Lsr2. *Nucleic Acids Res.* **41**, 5263-5272, doi:10.1093/nar/gkt249 (2013).

22   Qin, L., Erkelens, A. M., Markus, D. & Dame, R. T. The B. subtilis Rok protein compacts and organizes DNA by bridging. *bioRxiv*, 769117, doi:10.1101/769117 (2019).

23   Liu, Q. & Richardson, C. C. Gene 5.5 protein of bacteriophage T7 inhibits the nucleoid protein H-NS of Escherichia coli. *Proc Natl Acad Sci U S A* **90**, 1761-1765, doi:10.1073/pnas.90.5.1761 (1993).

24   Ali, S. S., Beckett, E., Bae, S. J. & Navarre, W. W. The 5.5 protein of phage T7 inhibits H-NS through interactions with the central oligomerization domain. *J. Bacteriol.* **193**, 4881-4892, doi:10.1128/jb.05198-11 (2011).

25   Zhu, B., Lee, S. J., Tan, M., Wang, E. D. & Richardson, C. C. Gene 5.5 protein of bacteriophage T7 in complex with Escherichia coli nucleoid protein H-NS and transfer RNA masks transfer RNA priming in T7 DNA replication. *Proc Natl Acad Sci U S A* **109**, 8050-8055, doi:10.1073/pnas.1205990109 (2012).

26   Ho, C. H., Wang, H. C., Ko, T. P., Chang, Y. C. & Wang, A. H. The T4 phage DNA mimic protein Arn inhibits the DNA binding activity of the bacterial histone-like protein H-NS. *J. Biol. Chem.* **289**, 27046-27054, doi:10.1074/jbc.M114.590851 (2014).

27   Kano, Y., Yasuzawa, K., Tanaka, H. & Imamoto, F. Propagation of phage Mu in IHF-deficient Escherichia coli in the absence of the H-NS histone-like protein. *Gene* **126**, 93-97, doi:10.1016/0378-1119(93)90594-s (1993).

28   van Ulsen, P., Hillebrand, M., Zulianello, L., van de Putte, P. & Goosen, N. Integration host factor alleviates the H-NS-mediated repression of the early promoter of bacteriophage Mu. *Mol. Microbiol.* **21**, 567-578, doi:10.1111/j.1365-2958.1996.tb02565.x (1996).

29   Skennerton, C. T. *et al.* Phage Encoded H-NS: A Potential Achilles Heel in the Bacterial Defence System. *PLOS ONE* **6**, e20095, doi:10.1371/journal.pone.0020095 (2011).

30   Wagemans, J. *et al.* Antibacterial phage ORFans of Pseudomonas aeruginosa phage LUZ24 reveal a novel MvaT inhibiting protein. *Frontiers in Microbiology* **6**, 1242, doi:10.3389/fmicb.2015.01242 (2015).

31   Castang, S. & Dove, S. L. High-order oligomerization is required for the function of the H-NS family member MvaT in Pseudomonas aeruginosa. *Mol. Microbiol.* **78**, 916-931 (2010).

32   Dame, R. T. *et al.* DNA bridging: a property shared among H-NS-like proteins. *J. Bacteriol.* **187**, 1845-1848, doi:10.1128/jb.187.5.1845-1848.2005 (2005).

33   van der Valk, R. A., Qin, L., Moolenaar, G. F. & Dame, R. T. Quantitative Determination of DNA Bridging Efficiency of Chromatin Proteins. *Methods Mol Biol* **1837**, 199-209, doi:10.1007/978-1-4939-8675-0_12 (2018).

34   Bradley, P., Misura, K. M. & Baker, D. Toward high-resolution de novo structure prediction for small proteins. *Science* **309**, 1868-1871, doi:10.1126/science.1113801 (2005).

35   van Zundert, G. C. P. *et al.* The HADDOCK2.2 Web Server: User-Friendly Integrative Modeling of Biomolecular Complexes. *J. Mol. Biol.* **428**, 720-725, doi:10.1016/j.jmb.2015.09.014 (2016).

36   Drozdetskiy, A., Cole, C., Procter, J. & Barton, G. J. JPred4: a protein secondary structure prediction server. *Nucleic Acids Res.* **43**, W389-394, doi:10.1093/nar/gkv332 (2015).

37   van der Valk, R. A., Vreede, J., Cremazy, F. & Dame, R. T. Genomic looping: a key principle of chromatin organization. *J. Mol. Microbiol. Biotechnol.* **24**, 344-359, doi:10.1159/000368851 (2014).

38   Stoebel, D. M., Free, A. & Dorman, C. J. Anti-silencing: overcoming H-NS-mediated repression of transcription in Gram-negative enteric bacteria. *Microbiology* **154**, 2533-2545, doi:10.1099/mic.0.2008/020693-0 (2008).

39   Williamson, H. S. & Free, A. A truncated H-NS-like protein from enteropathogenic Escherichia coli acts as an H-NS antagonist. *Mol. Microbiol.* **55**, 808-827, doi:10.1111/j.1365-2958.2004.04421.x (2005).

40   Boudreau, B. A. *et al.* StpA and Hha stimulate pausing by RNA polymerase by promoting DNA–DNA bridging of H-NS filaments. *Nucleic Acids Res.* **46**, 5525-5546, doi:10.1093/nar/gky265 (2018).

41   Kotlajich, M. V. *et al.* Bridged filaments of histone-like nucleoid structuring protein pause RNA polymerase and aid termination in bacteria. *eLife* **4**, e04970, doi:10.7554/eLife.04970 (2015).

42   Ali, S. S. *et al.* Structural insights into the regulation of foreign genes in Salmonella by the Hha/H-NS complex. *J. Biol. Chem.* **288**, 13356-13369, doi:10.1074/jbc.M113.455378 (2013).

43   Ueda, T. *et al.* Functions of the Hha and YdgT proteins in transcriptional silencing by the nucleoid proteins, H-NS and StpA, in Escherichia coli. *DNA Res.* **20**, 263-271, doi:10.1093/dnares/dst008 (2013).

44   Gibson, D. G. *et al.* Enzymatic assembly of DNA molecules up to several hundred kilobases. *Nat. Methods* **6**, 343-345, doi:10.1038/nmeth.1318 (2009).

45   Lee, W., Tonelli, M. & Markley, J. L. NMRFAM-SPARKY: enhanced software for biomolecular NMR spectroscopy. *Bioinformatics* **31**, 1325-1327, doi:10.1093/bioinformatics/btu830 (2015).

Chapter 4

The *B. subtilis* Rok protein compacts and organizes DNA by bridging

This chapter is based on the following manuscript:

Abstract

Rok from *Bacillus subtilis* is an abundant DNA binding protein similar in function to H-NS-like proteins found in many proteobacteria. Rok binds across the genome with a preference for A/T rich DNA. Such DNA often contains genes of foreign origin that are silenced due to Rok binding. Rok also has been implied in global organization of the *B. subtilis* genome. However, how Rok binds to DNA and how it represses transcription is unclear. Also, it is unknown whether Rok-mediated gene repression can be induced or relieved following changes in physico-chemical conditions, as noted for H-NS-like proteins. Here we investigate the DNA binding properties of Rok and determine the effects of physico-chemical conditions on these properties. We demonstrate that Rok is a DNA bridging protein similar to H-NS like proteins from *E. coli* (H-NS), *Pseudomonas sp.* (MvaT) and *Mycobacteria* (Lsr2). Strikingly, unlike these proteins, the ability of Rok to bridge DNA is not affected by changes in physico-chemical conditions. Not being a direct sensor of such changes sets Rok apart from other H-NS like proteins. It implies the existence of other (protein-mediated) mechanisms to relieve Rok-mediated gene silencing in response to changes in environmental conditions.

Introduction

The bacterial genome, like that of eukaryotic cells, is both functionally organized and compactly folded. Nevertheless, genes need to be accessible for the transcription machinery or need to be made accessible if environmental conditions so require: the nucleoid is dynamically organized and re-organized [1,2]. Many factors contribute to the compact shape of the nucleoid, including DNA supercoiling, macromolecular crowding and nucleoid-associated proteins (NAPs) [3-5]. The Histone-like nucleoid structuring protein (H-NS), one of the main NAPs in *Escherichia coli*, plays important roles in both genome organization and gene regulation [6]. H-NS non-specifically binds DNA across the genome, but has a preference for AT-rich DNA. DNA acquired via horizontal gene transfer (HGT) is often AT-rich and is recognized as xenogeneic DNA by H-NS [7,8]. Although genes acquired via HGT are key to the evolution of bacteria by conferring new genetic traits, inappropriate expression of newly acquired genes can lead to loss of competitive fitness of bacteria. H-NS family proteins including H-NS of *E. coli*, MvaT of *Pseudomonas sp.* and Lsr2 of *Mycobacteria*, function as xenogeneic silencers, silencing foreign DNA until an environmental signal leads to relief of repression.

Akin to H-NS, MvaT and Lsr2 are also regulators of global gene expression. Although by sequence the proteins are not homologous, they are similar in DNA binding properties and function, due to their similar organization in functional domains. Structural studies have revealed that H-NS, Lsr2 and MvaT have an N-terminal oligomerization domain consisting of two dimerization sites, a C-terminal DNA binding domain and a flexible linker region [7,9-12]. Due to their ability to dimerize and oligomerize, these proteins can bind along DNA forming a nucleoprotein filament, which stiffens DNA [13-15]. Under appropriate physico-chemical conditions the proteins also can bridge remote segments along a DNA duplex [16-18], yielding DNA loops. The bridging activity of H-NS and MvaT can be modulated by both monovalent (Na^+, K^+) and divalent (Mg^{2+}, Ca^{2+}) salt (see Chapter 2) [19-22], while for Lsr2 it remains unclear whether ionic conditions affect its binding properties. The DNA binding activity of H-NS family proteins (either the formation of nucleoprotein filaments or bridged protein-DNA complexes) is sensitive to temperature, pH and salt, which contributes to adaptation of cells to environmental challenges, mediated by the bacterial genome [2,6,23]. Both filament formation and DNA bridging activity of H-NS family proteins have been suggested to account for gene regulation [20]. However, as only the DNA bridging activity can be switched on or

off by small changes in physicochemical condition, this might be the mode of binding essential to regulation of environmentally regulated genes [24].

Rok of *Bacillus subtilis* was recently proposed to be a functional homolog of H-NS based on the observation that Rok binds extended regions along the genome, which are preferentially AT-rich and have been acquired via horizontal gene transfer. Rok contributes to silencing of the genes within such regions [25]. The ability of Rok to silence genes on DNA of foreign origin classifies it as a xenogeneic silencer like H-NS, MvaT and Lsr2. Rok is also found associated with a large subset of chromosomal domain boundaries in *B. subtilis* [26], which suggests it contributes to genome organization of *B. subtilis*. However, how Rok binds to DNA and how it silences genes remains unknown. In addition, it is unknown whether gene silencing by Rok can be modulated by changes in physico-chemical growth conditions such as temperature, pH and salt.

Results

Rok compacts DNA

All H-NS family proteins (H-NS, MvaT and Lsr2) exhibit two modes of binding to DNA: filament formation along DNA and DNA bridging (see Chapter 2) [14,15,17-19,22]. Both lateral nucleoprotein filament complex formation and DNA bridging are suggested to be important for the function of these proteins in gene silencing. To probe whether Rok, like H-NS family proteins, exhibits DNA stiffening activity (reflecting the formation of a protein filament along DNA) or not, we investigated the effect of Rok binding on the conformation of DNA by using Tethered Particle Motion (TPM) [27,28]. Here, the Root Mean Square displacement (RMS) of a bead (exhibiting thermal motion) at the extremity of a DNA substrate attached to a glass surface, gives a readout of DNA conformation. If a protein stiffens DNA, the RMS will increase following the binding of proteins. If a protein softens, bends, or bridges DNA, a reduction in RMS will take place. We investigated the interaction between Rok and an AT-rich (32%GC) DNA substrate, which we used earlier in studies of the DNA-binding properties of H-NS [21] and MvaT (see Chapter 2) [22]. We determined the effect of Rok on DNA conformation by titration from 0-10 nM (Figure 4.1a). Bare DNA has an RMS of 150 ± 2 nm. Upon addition of increasing amounts of Rok, a second unique population at an RMS of about 80 nm appears. Saturation of Rok binding is achieved at 8 nM; at this concentration only the population with reduced RMS is observed (Figure 4.1b). The observed reduction of RMS is an

indication of DNA compaction by binding of Rok; it implies that Rok does not form filaments along DNA as observed for other H-NS-family proteins under similar conditions [14,15,19] (Figure 4.1c). The fact that compaction occurs at low protein concentration and that the structural transition is abrupt is suggestive of cooperative behavior. The reduction in RMS can be attributed either to DNA bending as observed for HU (Figure 4.1c) or to DNA bridging.
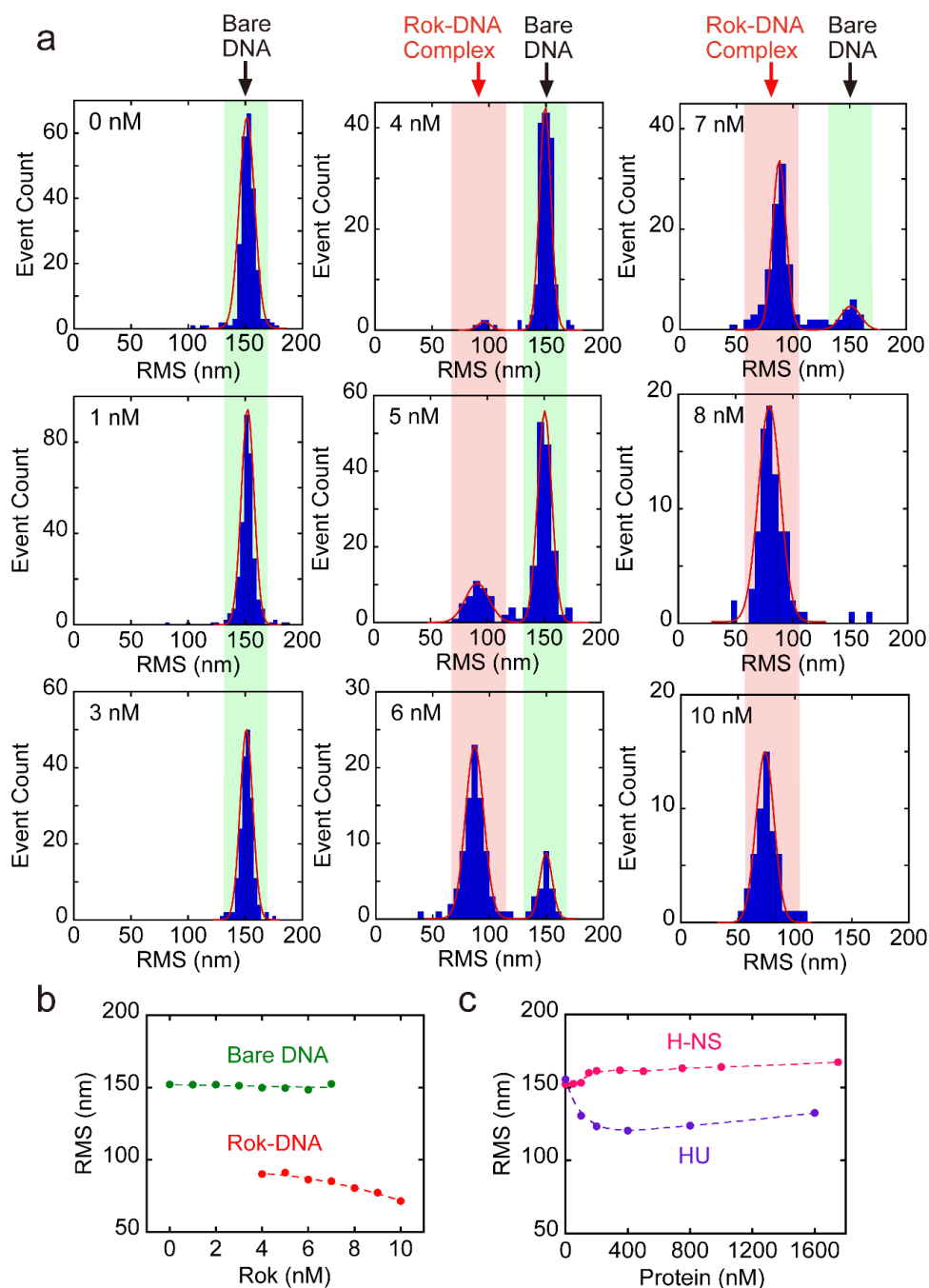

Figure 4.1. *B. subtilis* **Rok compacts DNA.** a) Histograms of Root Mean Square (RMS) obtained for 32%GC DNA as a function of Rok at concentrations of 0, 1, 3, 4, 5, 6, 7, 8, and 10 nM as measured by TPM

in the presence of 50 mM KCl. The histograms were fitted to Gaussian distributions, in which the RMS value at around 150 nm represents bare DNA and the population of RMS at around 80 nM represents DNA bound by Rok. The bare DNA and Rok-DNA complex populations are highlighted with a light green and red box, respectively. The data for each concentration is the combination of three independent measurements and the RMS for each concentration was obtained by fitting the combined data to a Gaussian distribution. b) RMS values obtained for 32%GC DNA as a function of Rok at concentrations from 0 nM to 10 nM. Green and red dots represent the average RMS resulted from fitting with a Gaussian distribution, where green dots and red dots represent bare DNA and Rok-DNA complexes, respectively. Error bars represent the standard error of the mean; due to their small size they are hidden behind the data points. How the RMS values are distributed among the two populations is not taken into account in this representation. c) RMS as a function of protein concentration of *E. coli* H-NS and HU. Error bars represent the standard error of the mean; due to their small size they are hidden behind the data points. The Rok coding gene from *B. subtilis* was cloned into pET30b using Gibson Assembly [29] resulting in vector pRD231. Following overproduction in Rosetta™ (DE3) pLysS, cells were lysed and the lysate was centrifuged for 30 min at 37000 rpm. The supernatant was filtered with a 0.22 µm Millex-GP Syringe Filter. Next, the protein was purified using a HiTrap Heparin HP 1 mL affinity column (GE Healthcare), a HiTrap SP HP 1 mL column (GE Healthcare) and a GE Superdex 75 10/300 GL column. The purified protein was checked by mass spectrometry. The concentration was determined using a Pierce™ BCA Protein Assay Kit (Thermo Scientific). The DNA used for Tethered Particle Motion (TPM) experiments is a random, AT-rich (32% GC), 685 bp DNA substrate [21,30]. Measurements were performed as previously described [21] with minor modifications. Briefly, the flow cell was washed with 100 µL experimental buffer (10 mM Tris-HCl pH 8, 10 mM EDTA, 5% glycerol, 50 mM KCl) to remove excess beads and 100 µL protein diluted in experimental buffer is flowed in and incubated for 5 minutes. Next, the flow cell was washed with protein solution one more time, sealed with nail polish and incubated for 5 minutes. After incubation, the flow cell was directly transferred to the holder and incubated for 5 more minutes to stabilize the temperature at 25°C for the measurement. For each flow cell more than 200 beads were measured and measurements for each concentration were performed in triplicate.

Rok is able to bridge DNA

In order to determine the structural basis of the observed DNA compaction, we next investigated the ability of Rok to bridge DNA in a quantitative biochemical DNA bridging assay, which we used earlier to evaluate the impact of buffer conditions on the DNA bridging efficiency of H-NS and MvaT (see Chapter 2) [21,22]. In this assay biotinylated DNA is bound to streptavidin-coated beads and radioactively labeled DNA offered in trans can be recovered by magnetic pull-down of beads when bridged by protein. The radioactive signal of the DNA pulled down is a proxy of DNA bridging efficiency. To determine whether Rok bridges DNA we carried out a titration with Rok from 0 - 0.5 µM. The DNA (685 bp, 32% GC) used in the bridging assay is same as the DNA used in TPM experiments. In the absence of Rok, no radioactive DNA was recovered. DNA recovery increases upon addition of increasing amounts of Rok. Saturation of DNA recovery occurs at a Rok concentration of 0.3 µM (figure 4.2). These data unambiguously show that Rok is a DNA bridging protein. Rok has a similar DNA bridging efficiency as H-NS, yet reaches this efficiency at 10 times lower concentration (0.3 µM vs 3 µM) [21], which is attributed to the high cooperativity in DNA binding by Rok.
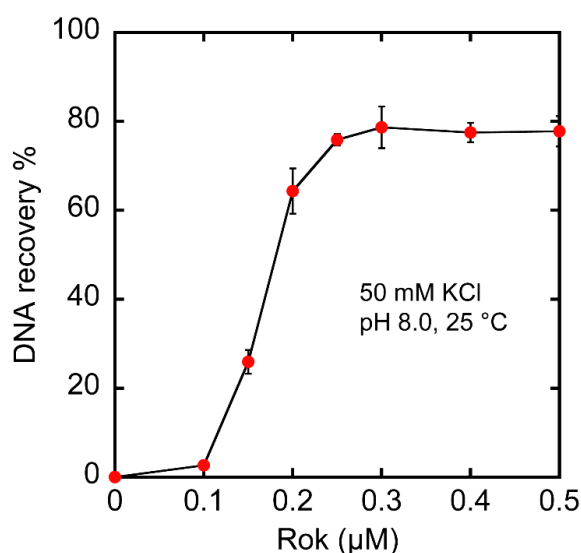
Figure 4.2. Rok bridges DNA. A) DNA recovery (as a percentage of the input DNA) as a function of Rok concentration from 0 to 0.5 µM as measured by the DNA bridging assay in the presence of 50 mM KCl at 25 ºC. Data are plotted as mean values and the error bars represent the standard deviation from independent triplicate measurements. The DNA used for the bridging assay, the same as that used for TPM, was ^{32}P-labeled as described previously [31]. The DNA bridging assay was performed as previously described

(see Chapter 5) [21,32] with minor modifications. Streptavidin-coated Magnetic M-280 Dynabeads (Thermo Fisher) were resuspended in buffer (20 mM Tris-HCl pH 8.0, 2 mM EDTA, 2 M NaCl, 2 mg/mL BSA (ac), 0.04% Tween 20) containing 100 fmol biotinylated 32% GC DNA (685 bp) and incubated at 1000 rpm for 20 min at 25°C. The beads with associated DNA were washed twice before resuspension in buffer (10 mM Tris-HCl, pH 8.0, 5% v/v Glycerol, 1 mM Spermidine). Radioactive ^{32}P-labeled DNA and unlabeled DNA were combined to maintain a constant (2 fmol/µL) concentration and a radioactive signal around 8000 cpm, and then added to each sample. Next, Rok was added (concentration as indicated) to initiate formation of bridged protein-DNA complexes. The samples were incubated for 20 min at 1000 rpm at 25°C. After the incubation, the beads were washed with the same experimental buffers before resuspension in counting buffer (10 mM Tris-HCl, pH 8.0, 1 mM EDTA, 200 mM NaCl, 0.2% SDS). The radioactive signal of DNA was quantified by liquid scintillation and was used for the calculation of protein DNA bridging efficiency (%) based on a reference sample containing the same amount of labeled ^{32}P 685 bp DNA used in each sample. All DNA bridging experiments were performed at least in triplicate.

DNA bridging activity of Rok is not sensitive to environmental conditions (temperature, pH and salt).

Bacteria adapt to environmental changes and environmental cues have a direct effect on the function of H-NS-like proteins. This is suggestive of environment-sensory activity of these proteins at H-NS-regulated environment-responsive genes. The DNA bridging activity of H-NS is sensitive to environmental conditions, such as salt [19]. Adaptation of *B. subtilis* to osmotic up- and downshift is a frequent challenge, which is also essential for growth and survival in its natural living environment [33]. To determine whether Rok's DNA bridging activity is also sensitive to salt condition, we investigated the effect of changing monovalent and divalent salt concentration. An increase in concentration of KCl from 50 mM to 300 mM has no significant effect on the DNA bridging activity of Rok. Nevertheless, at higher concentration of KCl the formation of bridged complexes is abolished (figure 4.3a). A similar result was obtained for titration with MgCl$_2$ in the range from 0 mM to 90 mM (figure 4.3b). Only beyond a certain ionic strength, the bridged Rok-DNA complexes start disintegrating and this ionic strength is likely not physiologically relevant anymore. It has been reported that the bridging activity of H-NS and MvaT can be modulated by both monovalent (K$^+$) and divalent (Mg^{2+}) salt (see Chapter 2) [19-22]. However, unlike H-NS and MvaT, the formation of

bridged Rok-DNA complexes requires neither Mg^{2+} nor a high concentration of K^+. These results indicate that DNA bridging activity of Rok neither requires nor is inhibited by salt at biologically relevant concentrations.

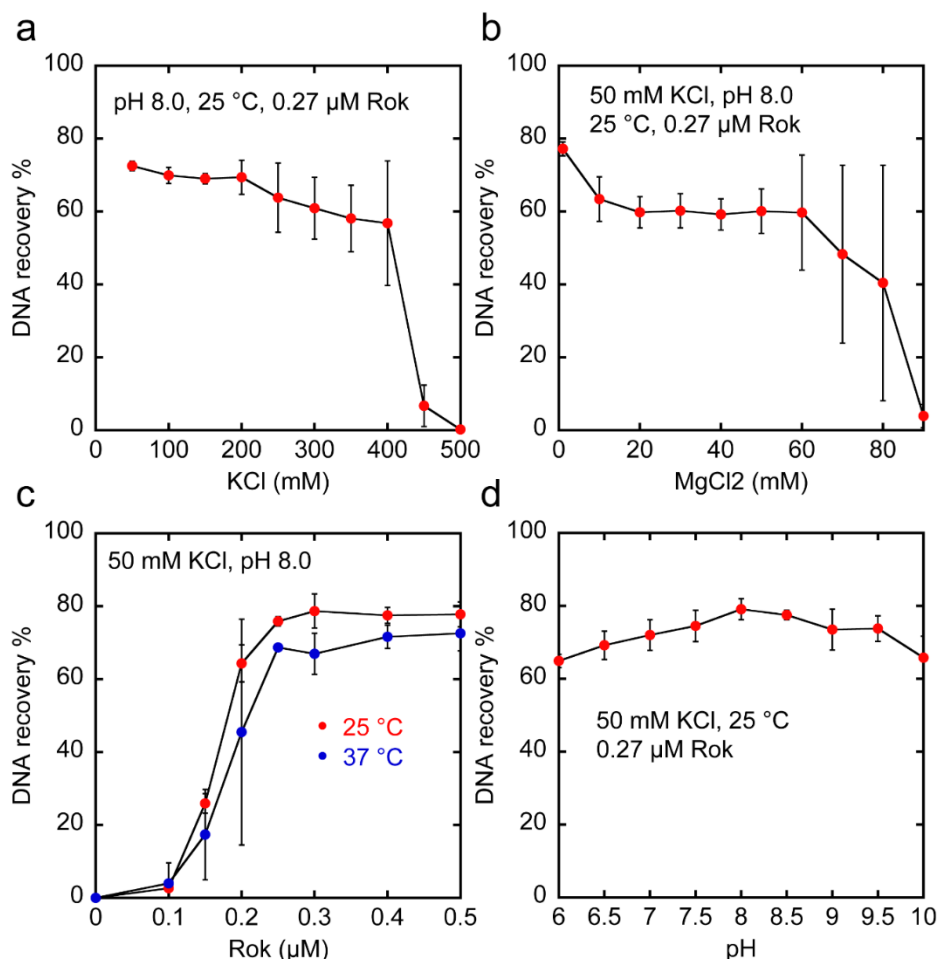**Figure 4.3. DNA bridging activity of Rok is not sensitive to temperature, pH and salt.** A) DNA recovery (as a percentage of the input DNA) as a function of KCl concentration from 50 to 500 mM measured by the DNA bridging assay in the presence of 0.27 µM Rok at 25 °C. b) DNA recovery as a function of $MgCl_2$ concentration from 1 to 90 mM in the presence of 0.27 µM Rok at 25 °C. c) DNA recovery as a function of Rok concentration from 0 to 0.5 µM at 25 °C (red) and 37 °C (blue), respectively. d) DNA recovery as a function of pH from 6 to 10 in the presence of 0.27 µM Rok at 25 °C. Data are plotted as mean values and the error bars represent the standard deviation from three independent measurements. The experiment was carried out in the same way as described for figure 4.2. Salt concentration (KCl or $MgCl_2$), protein concentration, temperature and pH were varied in line with the experiments. For pH 6 and 6.5 MES (2-morpholinoethanesulfonic acid) was used instead of Tris-HCl and for pH 9, 9.5 and 10 CHES (*N*-Cyclohexyl-2-aminoethanesulfonic acid) was used.

B. subtilis, found in soil and the gastrointestinal tract of ruminants and humans, can live at different temperatures and pH conditions. Therefore, we investigated the effect of temperature on DNA bridging efficiency. An increase in temperature from 25 ºC to 37 ºC has no significant effect on the DNA bridging activity of Rok (figure 4.3c). Next, we also investigated the effect of pH. Across a range from 6 to 10, pH has no effect on the DNA bridging activity of Rok (figure 4.3d). Strikingly, even crossing the pI of Rok (9.31) did not interfere with its capacity of DNA bridging. Taken together, all these results indicate that the DNA bridging activity of Rok is not affected by changes in physico-chemical conditions, which is unexpectedly different from H-NS, MvaT and Lsr2.

We have studied the DNA binding properties of Rok. We found that Rok is a DNA bridging protein and evaluated its DNA bridging capacity under various physiologically relevant conditions. The protein is remarkably insensitive to changes in physico-chemical conditions. Although Rok has low sequence similarity with H-NS, MvaT or Lsr2, they have similar domain organization: the N-terminal dimerization and oligomerization domain, a C-terminal DNA binding domain and a flexible linker in between. H-NS, MvaT and Lsr2 can oligomerize along DNA, which causes DNA stiffening. Such a stiffening effect was not observed for Rok. Instead, only DNA compaction was observed in our study. Because we demonstrated that Rok is a DNA bridging protein, we attribute the observed DNA compaction to bridging by Rok. Based on our results and the known properties of Rok, we propose that Rok bridges DNA, without associating into nucleoprotein filaments, but employing dimeric Rok as bridging units (Figure 4.4). The Rok dimers cluster cooperatively due to high local DNA concentration upon initiation of bridging, but earlier studies suggest that the protein forms oligomers in solution [34], while our study does not provide evidence for Rok oligomers along DNA. Unexpectedly, Rok-DNA bridging activity is not affected by changes in physico-chemical conditions, which sets the protein apart from H-NS, MvaT and Lsr2. It implies the presence of other (protein-mediated) mechanisms to relieve Rok-mediated gene silencing in response to changes in environmental conditions. An example of a Rok antagonist is ComK which can relieve gene repression mediated by Rok at the *comK* promotor [35]. Based on the robustness of Rok in binding to DNA we expect the existence of similar antagonistic factors operating at other sites across the genome.
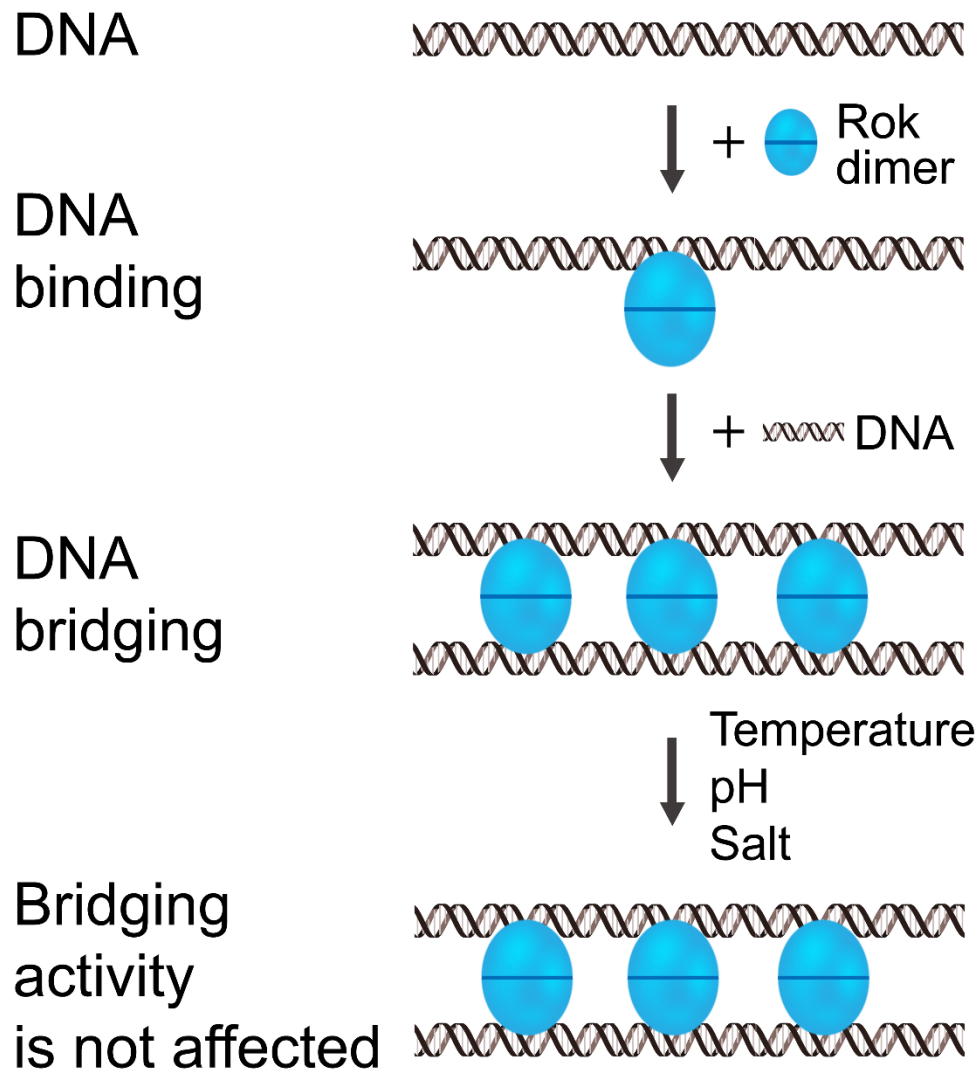
Figure 4.4. The proposed mechanisms of DNA binding by Rok. Rok binds DNA as a dimer without associating into nucleoprotein filaments. Dimeric Rok acts as bridging unit. Rok dimers cluster cooperatively in between two DNA duplexes, not due to dimer-dimer interactions, but due to high local DNA concentration which drives association and bridging by additional dimers. The DNA bridging activity of Rok is not sensitive to changes in physico-chemical conditions (temperature, pH and salt).

References

1   Badrinarayanan, A., Le, T. B. & Laub, M. T. Bacterial chromosome organization and segregation. *Annu. Rev. Cell. Dev. Biol.* **31**, 171-199 (2015).

2   Dorman, C. J. H-NS: a universal regulator for a dynamic genome. *Nat. Rev. Microbiol.* **2**, 391-400, doi:10.1038/nrmicro883 (2004).

3   Dame, R. T. The role of nucleoid-associated proteins in the organization and compaction of bacterial chromatin. *Mol. Microbiol.* **56**, 858-870, doi:10.1111/j.1365-2958.2005.04598.x (2005).

4   Luijsterburg, M. S., Noom, M. C., Wuite, G. J. & Dame, R. T. The architectural role of nucleoid-associated proteins in the organization of bacterial chromatin: a molecular perspective. *J Struct Biol* **156**, 262-272, doi:10.1016/j.jsb.2006.05.006 (2006).

5   Stuger, R. *et al.* DNA supercoiling by gyrase is linked to nucleoid compaction. *Mol. Biol. Rep.* **29**, 79-82 (2002).

6   Dillon, S. C. & Dorman, C. J. Bacterial nucleoid-associated proteins, nucleoid structure and gene expression. *Nat. Rev. Microbiol.* **8**, 185-195, doi:10.1038/nrmicro2261 (2010).

7   Gordon, B. R. *et al.* Structural basis for recognition of AT-rich DNA by unrelated xenogeneic silencing proteins. *Proc Natl Acad Sci U S A* **108**, 10690-10695, doi:10.1073/pnas.1102544108 (2011).

8   Dorman, C. J. H-NS-like nucleoid-associated proteins, mobile genetic elements and horizontal gene transfer in bacteria. *Plasmid* **75**, 1-11, doi:10.1016/j.plasmid.2014.06.004 (2014).

9   Summers, E. L. *et al.* The structure of the oligomerization domain of Lsr2 from Mycobacterium tuberculosis reveals a mechanism for chromosome organization and protection. *PLoS One* **7**, e38542, doi:10.1371/journal.pone.0038542 (2012).

10   Arold, S. T., Leonard, P. G., Parkinson, G. N. & Ladbury, J. E. H-NS forms a superhelical protein scaffold for DNA condensation. *Proc Natl Acad Sci U S A* **107**, 15728-15732, doi:10.1073/pnas.1006966107 (2010).

11   Suzuki-Minakuchi, C. *et al.* Structural similarities and differences in H-NS family proteins revealed by the N-terminal structure of TurB in Pseudomonas putida KT2440. *FEBS Lett.* **590**, 3583-3594, doi:10.1002/1873-3468.12425 (2016).

12   Ding, P. *et al.* A Novel AT-Rich DNA Recognition Mechanism for Bacterial Xenogeneic Silencer MvaT. *PLoS Pathog* **11**, e1004967, doi:10.1371/journal.ppat.1004967 (2015).

13   Lim, C. J., Lee, S. Y., Kenney, L. J. & Yan, J. Nucleoprotein filament formation is the structural basis for bacterial protein H-NS gene silencing. *Sci Rep* **2**, 509, doi:10.1038/srep00509 (2012).

14   Qu, Y., Lim, C. J., Whang, Y. R., Liu, J. & Yan, J. Mechanism of DNA organization by Mycobacterium tuberculosis protein Lsr2. *Nucleic Acids Res.* **41**, 5263-5272, doi:10.1093/nar/gkt249 (2013).

15   Winardhi, R. S. *et al.* Higher order oligomerization is required for H-NS family member MvaT to form gene-silencing nucleoprotein filament. *Nucleic Acids Res.* **40**, 8942-8952, doi:10.1093/nar/gks669 (2012).

16   Dame, R. T., Wyman, C. & Goosen, N. H-NS mediated compaction of DNA visualised by atomic force microscopy. *Nucleic Acids Res.* **28**, 3504-3510, doi:10.1093/nar/28.18.3504 (2000).

17   Dame, R. T. *et al.* DNA bridging: a property shared among H-NS-like proteins. *J. Bacteriol.* **187**, 1845-1848, doi:10.1128/jb.187.5.1845-1848.2005 (2005).

18   Chen, J. M. *et al.* Lsr2 of Mycobacterium tuberculosis is a DNA-bridging protein. *Nucleic Acids Res.* **36**, 2123-2135, doi:10.1093/nar/gkm1162 (2008).

19   Liu, Y., Chen, H., Kenney, L. J. & Yan, J. A divalent switch drives H-NS/DNA-binding conformations between stiffening and bridging modes. *Genes Dev.* **24**, 339-344, doi:10.1101/gad.1883510 (2010).

20   Winardhi, R. S., Yan, J. & Kenney, L. J. H-NS Regulates Gene Expression and Compacts the Nucleoid: Insights from Single-Molecule Experiments. *Biophys. J.* **109**, 1321-1329, doi:10.1016/j.bpj.2015.08.016 (2015).

21   van der Valk, R. A. *et al.* Mechanism of environmentally driven conformational changes that modulate H-NS DNA-bridging activity. *Elife* **6**, doi:10.7554/eLife.27369 (2017).

22   Qin, L. *et al.* Structural basis for osmotic regulation of the DNA binding properties of H-NS proteins. *Nucleic Acids Res.*, doi:10.1093/nar/gkz1226 (2020).

23   Atlung, T. & Ingmer, H. H-NS: a modulator of environmentally regulated gene expression. *Mol. Microbiol.* **24**, 7-17, doi:10.1046/j.1365-2958.1997.3151679.x (1997).

24   Boudreau, B. A. *et al.* StpA and Hha stimulate pausing by RNA polymerase by promoting DNA-DNA bridging of H-NS filaments. *Nucleic Acids Res.* **46**, 5525-5546, doi:10.1093/nar/gky265 (2018).

25   Smits, W. K. & Grossman, A. D. The transcriptional regulator Rok binds A+T-rich DNA and is involved in repression of a mobile genetic element in Bacillus subtilis. *PLoS Genet.* **6**, e1001207, doi:10.1371/journal.pgen.1001207 (2010).

26   Marbouty, M. *et al.* Condensin- and Replication-Mediated Bacterial Chromosome Folding and Origin Condensation Revealed by Hi-C and Super-resolution Imaging. *Mol. Cell* **59**, 588-602, doi:10.1016/j.molcel.2015.07.020 (2015).

27   van der Valk, R. A., Laurens, N. & Dame, R. T. Tethered Particle Motion Analysis of the DNA Binding Properties of Architectural Proteins. *Methods Mol Biol* **1624**, 127-143, doi:10.1007/978-1-4939-7098-8_11 (2017).

28   Henneman, B., Heinsman, J., Battjes, J. & Dame, R. T. Quantitation of DNA-Binding Affinity Using Tethered Particle Motion. *Methods Mol Biol* **1837**, 257-275, doi:10.1007/978-1-4939-8675-0_14 (2018).

29   Gibson, D. G. *et al.* Enzymatic assembly of DNA molecules up to several hundred kilobases. *Nat. Methods* **6**, 343-345, doi:10.1038/nmeth.1318 (2009).

30   Laurens, N. *et al.* Alba shapes the archaeal genome using a delicate balance of bridging and stiffening the DNA. *Nat Commun* **3**, 1328, doi:10.1038/ncomms2330 (2012).

31   Wagner, K., Moolenaar, G. F. & Goosen, N. Role of the insertion domain and the zinc-finger motif of Escherichia coli UvrA in damage recognition and ATP hydrolysis. *DNA Repair* **10**, 483-496 (2011).

32   van der Valk, R. A., Qin, L., Moolenaar, G. F. & Dame, R. T. Quantitative Determination of DNA Bridging Efficiency of Chromatin Proteins. *Methods Mol Biol* **1837**, 199-209, doi:10.1007/978-1-4939-8675-0_12 (2018).

33   Hoper, D., Bernhardt, J. & Hecker, M. Salt stress adaptation of Bacillus subtilis: a physiological proteomics approach. *Proteomics* **6**, 1550-1562, doi:10.1002/pmic.200500197 (2006).

34   Duan, B. *et al.* How bacterial xenogeneic silencer rok distinguishes foreign from self DNA in its resident genome. *Nucleic Acids Res.* **46**, 10514-10529, doi:10.1093/nar/gky836 (2018).

35   Smits, W. K., Hoa, T. T., Hamoen, L. W., Kuipers, O. P. & Dubnau, D. Antirepression as a second mechanism of transcriptional activation by a minor groove binding protein. *Mol. Microbiol.* **64**, 368-381, doi:10.1111/j.1365-2958.2007.05662.x (2007).

Chapter 5

Quantitative determination of DNA bridging efficiency of chromatin proteins

This chapter is based on the following chapter:

van der Valk, R. A., Qin, L., Moolenaar, G. F., & Dame, R. T. (2018). Quantitative determination of DNA bridging efficiency of chromatin proteins. In Bacterial Chromatin (pp. 199-209). Humana Press, New York, NY.

The chapter was jointly written by R.v.d.V. and L.Q.

Abstract

DNA looping is important for genome organization in all domains of life. The basis of DNA loop formation is the bridging of two separate DNA double helices. Detecting DNA bridge formation generally involves the use of complex single-molecule techniques (atomic force microscopy, magnetic or optical tweezers). Although DNA bridging can be qualitatively described, quantification of DNA bridging and bridging dynamics using these techniques is challenging. Here we describe a novel biochemical assay capable of not only detecting DNA bridge formation, but also allowing for quantification of DNA bridging efficiency and the effects of physico-chemical conditions on DNA bridge formation.

1. Introduction

Three-dimensional organization of genomes affects and is affected by DNA transactions such as transcription regulation, replication, and recombination. In cells, a family of DNA-binding proteins, called chromatin proteins, is involved in the organization of the genome. These proteins wrap DNA around themselves, bend it, or bridge DNA, forming loops. DNA loops play a variety of roles in genome organization. These loops may operate locally with regulatory functions at specific single genes [1,2], or over longer distances, enabling the organism to co-regulate genes that are in terms of genomic position far apart [3,4]. Although studies involving DNA looping have a rich history [3,5-12], in recent years, numerous new insights have become available through the application of new biochemical and biophysical techniques.

Classically, DNA loops (DNA bridges) were studied through the use of electron microscopy and atomic force microscopy [13-16]. These techniques permit visualization of DNA bridges. But, these static images are incapable of resolving the formation of DNA bridges or its modulation. The advent of biophysical techniques such as magnetic and optical tweezers have made it possible to stretch bridged DNA molecules by applying force [17,18] and determine biophysical properties of the DNA bridges, but it is difficult to quantitate the protein(s)-DNA bridging efficiency.

Here we describe a novel method for the quantification of protein-DNA bridging efficiency and its modulation by environmental conditions and other proteins. In this "bridging assay", we use streptavidin coated paramagnetic beads coupled to 5' biotin-labeled DNA (bait DNA). The DNA-coated beads are then incubated in the presence of ^{32}P radioactively labeled DNA and a DNA bridging protein (or any di- or multivalent DNA binding ligand). The beads are pulled down by using their magnetic properties and the amount of recovered ^{32}P radiolabeled DNA (prey DNA) is detected through liquid scintillation. The recovered ^{32}P radiolabeled DNA is a direct measurement of the amount of DNA bridges formed under these conditions.

2. Materials

Prepare all solutions using ultrapure water (prepared by purifying deionized water, to attain a sensitivity of 18 MΩ-cm at 25 °C) and analytical grade reagents. Prepare and store all reagents at -20 °C (unless indicated otherwise). You also need access to some routine biochemical techniques [19].

2.1 Stock solutions

The following stock solutions are required to perform this experiment

- Phosphate buffered saline (PBS): 12 mM $NaPO_4$ pH 7.4, 137 mM NaCl
- Renaturation buffer 10x (RB 10x): 200 mM Tris*HCl pH 9.5, 10 mM Spermidine, 1 mM EDTA
- Labeling buffer (LB): 500 mM Tris-HCl pH 9.5, 100 mM $MgCl_2$, 40 % Glycerol
- Coupling buffer (CB): 20 mM Tris-HCl pH 8.0, 2mM EDTA, 2M NaCl, 2mg/ml Acetylated BSA, 0.04% Tween20
- Incubation buffer 10x (IB 10x): 100 mM Tris-HCl pH 8.0, 0.2% Tween20, 10 mg/ml Acetylated BSA
- DNA storage buffer: 10 mM Tris-HCl pH 8.0, 50 mM KCl, 10 mM $MgCl_2$
- Stop buffer: 10 mM Tris-HCl pH 8.0,1 mM EDTA, 200 mM NaCl, 0.2% SDS

2.2 Generation of DNA substrates using PCR

To generate a DNA substrate for TPM, it is advised to use Polymerase Chain Reaction. This reaction requires:

- a DNA template containing the sequence of interest (see Note 1)
- a Forward primer
- a Reverse primer
- Dream-Taq DNA polymerase 5U/µL
- 2 mM Deoxyribose Nucleotide Triphosphate (dNTP)
- 10x Dream Taq-polymerase reaction buffer
- Gene Elute PCR cleanup kit (Sigma-Aldrich)
- Eppendorf® PCR tubes

- Biorad T100 Thermocycler or any other available PCR machine

- 1% agarose gel in 1x TBE

- Nanodrop® (Thermo Fisher)

- DNA ladder

2.3 Bridging assay equipment

- Magnetic Eppendorf rack

- Eppendorf shaker

- Eppendorf rack

- Eppendorf pipettes

- Streptavidin coated Dynabeads

2.4 Quantifying DNA bridging through radioactivity

- Liquid scintillator (HIDEX 300SL)

- Counting vials

- 37 °C heat block

- 80 °C water bath

- Eppendorf® PCR tubes

- ATP, gamma ^{32}P

- Tabletop Eppendorf centrifuge

- T4 Polynucleotide Kinase 10 U/μL

- Mini G50 columns (GE Healthcare)

3. Methods

3.1 Generation of DNA substrates using PCR

These reagents are combined in an Eppendorf® PCR tube according to the scheme below. These reactions must be done for both the standard and biotinylated primers.

Reagent	Final quantity
DNA template	1 ng
Forward primer	10 pmol
Reverse primer	10 pmol
2 mM dNTP	5 µL
10x Taq Polymerase buffer	5 µL
5 U/µL Dream Taq Polymerase	0.2 µL
H$_2$O	Add to total volume of 50 µL

1. Keep this reaction mix on ice as much as possible and initiate the PCR using the following protocol (see Note 2).

	Cycles	Temperature	Duration
Initial denaturation	1	95° C	5 minutes
Denaturation	35	95° C	30 seconds
Annealing		62° C	30 seconds
Elongation		72° C	4 minutes
Final elongation	1	72° C	10 minutes
	1	15° C	∞

2. Purify the PCR product using the GeneElute PCR cleanup kit.
3. Load 2 µL of the purified PCR product on a 1% agarose gel in TBE buffer alongside a DNA molecular weight marker for verification that a product of the expected length is formed. An example of a successful PCR and purification of the obtained PCR product is shown in **Figure 5.1**.
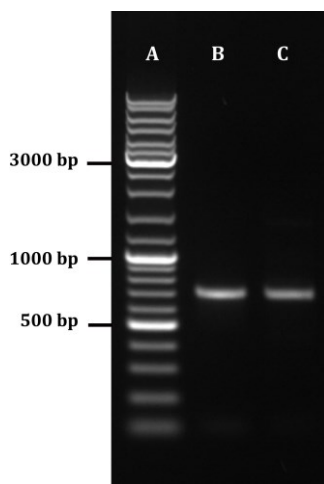
Figure 5.1: **Visualization of PCR product size by agarose gel electrophoresis.** (A) 2 µL of the GeneRuler DNA molecular weight marker. (B) 2 µL of the purified PCR-generated unlabeled DNA (685 bp, ready for ^{32}P labeling). (C) 2 µL of the purified PCR-generated biotin-labeled DNA (685 bp).

4. Finally, the concentration of purified PCR-generated DNA needs to be determined accurately. Determine the concentration of the purified DNA by measuring UV absorbance at 260 nm and 280 nm (see Note 3). If no other method is available the concentration of DNA can also be approximated using a DNA dilution series run on an agarose gel compared to a reference marker. Store the DNA solution at -20 °C.

3.2 Radiolabeling DNA

1. Add 1.5 µL of RB 10x to 2 pmol of the purified DNA and fill to a final volume of 15 µL using H_2O

2. Prepare the Kinase mix according to the following scheme:

Kinase mix component	Added volume per DNA labeling (µL):
LB 10x	2.5
50 mM DTT	2.5
ATP, gamma ^{32}P	2
10 U/µL Polynucleotide Kinase	1
H_2O	2

3. Incubate the DNA mix at 80°C for 2 minutes and immediately put the sample on ice (see Note 4)

4. Add 10 µL of the Kinase mix to the DNA sample and incubate at 37°C for 30 minutes

5. Stop the reaction by adding 1 µL of 0.5M EDTA. Incubate the sample at 75°C for 15 minutes to deactivate the kinase

6. Quickly spin the sample down using a tabletop centrifuge.

7. Prepare the mini G50 column by pre-incubating it in DNA storage buffer as described by the column manual.

8. Purify the labeled DNA using the G50 column

9. Assess the volume of the purified DNA and fill it to 100 µL using DNA storage buffer. The DNA should now have a final concentration of approximately 20 pmol/µL.

10. Fill a counting vial with 7 ml of H_2O

11. Prepare 2 µL of the labeled DNA for liquid scintillation, by transferring it to a PCR tube and submerging it in the counting vial.

12. Determine the amount of counts per minute per vial.

13. Quantify the counts per µL of labeled DNA

3.3 Bridging assay

The DNA bridging assay relies on the immobilization of bait DNA on magnetic microparticles and the capture and detection of ^{32}P labeled prey DNA if DNA-DNA bridge formation occurs (see **Figure 5.2** for a schematic depiction of the assay).
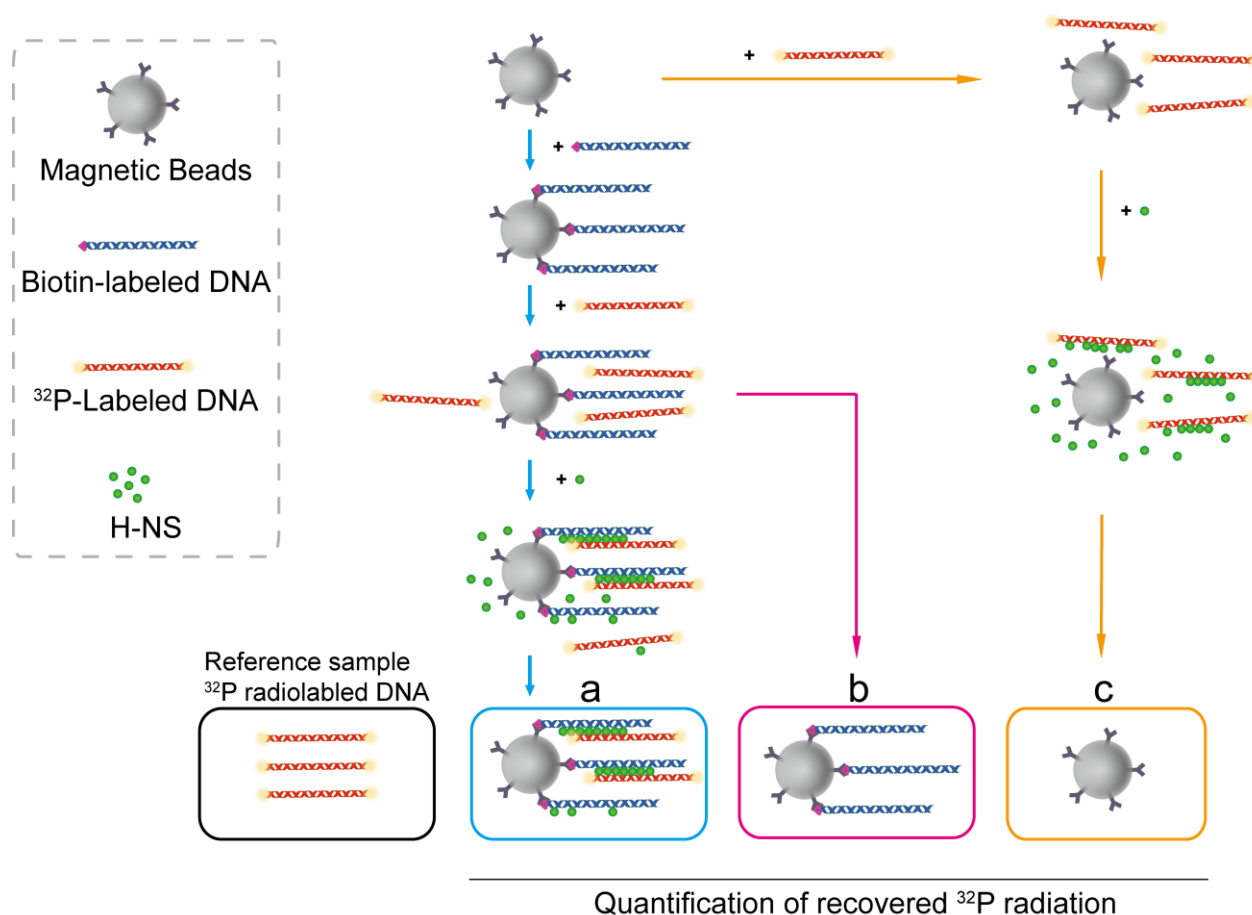
Figure 5.2: **Schematic depiction of the DNA bridging assay with the H-NS DNA bridging protein.** A standard DNA bridging assay is shown by the blue arrows. Here streptavidin coated paramagnetic beads are coupled to the bait DNA, 5' labeled with biotin. The beads bound with DNA are then incubated in the presence of ^{32}P radiolabeled DNA strand and H-NS. Next, using a magnetic rack, the beads are pulled down and the amount of recovered ^{32}P radiolabeled DNA (prey DNA) is quantified based on a reference ^{32}P radiolabeled DNA sample. (b) The pink arrows indicate a standard negative control for the DNA bridging assay, in which no H-NS is added. This control checks the stability of both prey and bait DNA. No ^{32}P radiolabeled DNA should be recovered for this sample (see Note 5 if this is the case). (c) The orange arrows indicate a standard negative control for the assay in which the DNA bridging assay is performed in the absence of the bait DNA to test the stability of the protein. No ^{32}P radiolabeled DNA should be recovered for this assay (see Note 6 if this is the case).

1. Wash 3 µL of streptavidin coated paramagnetic beads (henceforth referred to as "beads") per condition you wish to test with 50 µL of PBS on the magnetic rack (see Note 7)

2. Wash the beads with 50 µL of CB twice

3. Resuspend the beads in 3 µL of CB

4. Dilute 100 pmol of biotinylated DNA in a total volume of 3 µL using DNA storage buffer (one per sample)

5. Add the biotinylated DNA solution to the washed and resuspended beads

6. Gently vortex the sample to ensure that the beads are resuspended

7. Incubate the samples at 25°C for 20 mins in the Eppendorf shaker at 1000 RPM.

8. Wash the beads with 16 µL of 1x IB twice

9. Resuspend the beads in 16 µL of 1x IB

10. Add 2 µL of radiolabeled DNA (with a minimum of 5000 counts per minute)

11. Add 2 µL of the protein of interest

12. Gently vortex the sample to ensure that the beads are resuspended

13. Incubate the samples at 25°C for 20 mins in the Eppendorf shaker at 1000 RPM.

14. Gently wash the beads with bridged protein-DNA complexes with 20 µL of IB

15. Resuspend the beads in Stop buffer

16. Transfer the sample to the liquid Cherenkov-scintillation counter

4. Results

4.1 DNA bridging efficiency as a function of protein concentration.

The protein concentration used in the assay determines the amount of DNA bridging observed. It is therefore essential to test a range of protein concentrations whenever a previously uncharacterized DNA bridging protein is investigated using the bridging assay. Here, we show an example (**Figure 5.3**) from our recent study investigating the DNA bridging efficiency of the Histone-like Nucleoid Structuring (H-NS protein) [20]. Using this assay, it was demonstrated that the DNA bridging efficiency of H-NS is highly dependent on protein concentration.
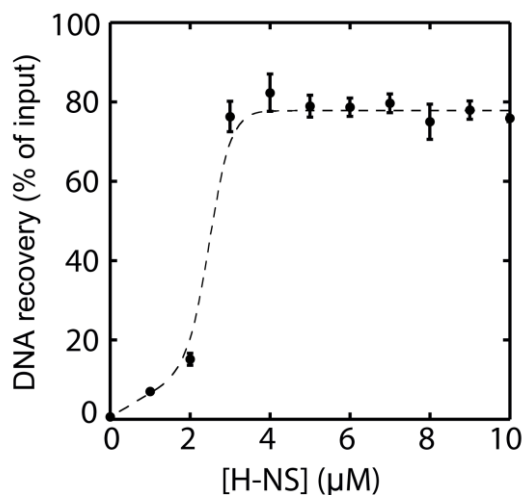
Figure 5.3: **DNA bridging as a function of H-NS concentration** [20]. The experiments were performed in the presence of 10 mM Tris-HCl pH 8.0, 50 mM KCl, 10 mM MgCl$_2$, 5% (w/v) glycerol. Error bars indicate the standard deviation of a triplicate of experiments.

4.2 DNA bridging efficiency of H-NS as a function of physico-chemical conditions

The DNA bridging assay allows for facile testing of the effect of altered physico-chemical conditions. It has been shown previously that H-NS-mediated DNA bridging is strongly modulated by environmental factors such as osmotic stress [17,20]. The DNA bridging assay revealed that increasing the amount of KCl in the buffer indeed effectively abolishes DNA bridging by H-NS (**Figure 5.4**) [20].

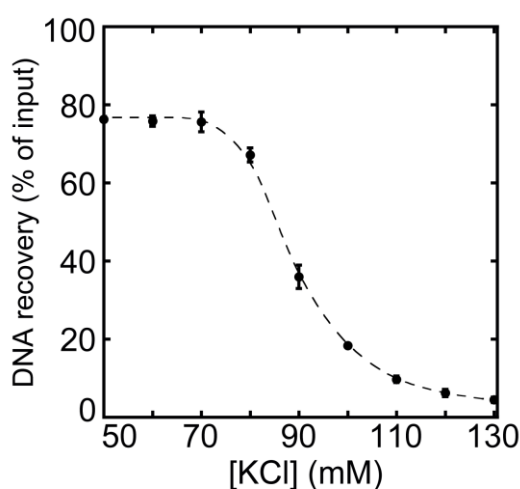**Figure 5.4**: **Modulation of H-NS-DNA bridging by [K$^+$]** [20]. The experiments were performed with 3,3 µM H-NS in 10 mM Tris-HCl pH 8.0, 10 mM MgCl$_2$, 5% w/v glycerol. Error bars indicate the standard deviation of a triplicate of experiments

This strong dependence of H-NS activity on environmental factors underlines the necessity to test different buffer conditions when testing new proteins. It is, however, important to verify that the DNA binding activity of the protein is still intact under conditions that no DNA bridging is observed (see Note 8).

Notes:

1. The length of the DNA substrate used can affect the efficiency of the assay. A 685 base pair DNA substrate was used in the experiments described here.

2. This PCR protocol was optimised for a 685 bp DNA substrate using a Biorad T100 Thermocycler. Some optimization may be required for different thermocyclers or substrates of different length.

3. When determining the concentration of the DNA it may be advantageous to use a Nanodrop® as this technique requires a very small volume.

4. Snap-chilling your DNA before labeling the DNA remains single-stranded and increases the efficiency of the Kinase

5. Recovery of ^{32}P labeled DNA in the absence of DNA bridging proteins may be an indication of DNA aggregation. In these cases, it is best to:

   a. Check the integrity of DNA on a 1% agarose gel.

   b. Re-evaluate the experimental buffer as the absence of salt may cause larger DNA substrates to aggregate. Similar effects may occur at extreme pH's.

   c. Use new beads as the streptavidin coating may decay over time, leading to inconclusive experiments.

6. If ^{32}P Labeled DNA is recovered in the absence of biotin labeled DNA, and not in the situation described in Note 5, it is likely caused by precipitation or aggregation of the protein. In these cases it is best to:

   a. Optimize the experimental buffer. Some proteins precipitate in sub-optimal conditions. The conditions can vary greatly from protein to protein so it is best to test a wide array of conditions (ion concentrations, pH, ion composition, etc) and detergents until a suitable buffer has been found.

      b. Use new beads, see Note 5c

7. When washing the beads on the magnetic rack pay attention to the following:

      a. Keep the Eppendorf tubes in the magnetic rack and incubate for at least 1 min to ensure that the beads are pelleted.

      b. When removing the supernatant make sure to pipette slowly and not to disturb the pelleted beads with the pipette tip.

      c. Use a 0.5-10 Eppendorf micropipette to ensure that all liquid is removed from the sample.

      d. Gently pipette the new liquid onto the pelleted beads

8. DNA binding of proteins is best confirmed with additional solution based experiments such as Microscale thermophoresis [21] or Tethered particle motion [22].

Reference

1   Besse, M., von Wilcken-Bergmann, B. & Müller-Hill, B. Synthetic lac operator mediates repression through lac repressor when introduced upstream and downstream from lac promoter. *The EMBO Journal* **5**, 1377-1381 (1986).

2   Becker, N. A., Peters, J. P., Lionberger, T. A. & Maher, I. I. I. L. J. Mechanism of promoter repression by Lac repressor–DNA loops. *Nucleic Acids Res.* **41**, 156-166, doi:10.1093/nar/gks1011 (2013).

3   Schleif, R. DNA Looping. *Annu. Rev. Biochem.* **61**, 199-223, doi:10.1146/annurev.bi.61.070192.001215 (1992).

4   Rao, Suhas S. P. *et al.* A 3D Map of the Human Genome at Kilobase Resolution Reveals Principles of Chromatin Looping. *Cell* **159**, 1665-1680, doi:https://doi.org/10.1016/j.cell.2014.11.021 (2014).

5   Matthews, K. S. DNA looping. *Microbiol Rev* **56**, 123-136 (1992).

6   Rippe, K., von Hippel, P. H. & Langowski, J. Action at a distance: DNA-looping and initiation of transcription. *Trends Biochem. Sci.* **20**, 500-506 (1995).

7   Schleif, R. Regulation of the L-arabinose operon of Escherichia coli. *Trends Genet.* **16**, 559-565 (2000).

8   Chambeyron, S. & Bickmore, W. A. Does looping and clustering in the nucleus regulate gene expression? *Curr. Opin. Cell Biol.* **16**, 256-262, doi:10.1016/j.ceb.2004.03.004 (2004).

9   Saiz, L. & Vilar, J. M. DNA looping: the consequences and its control. *Curr. Opin. Struct. Biol.* **16**, 344-350, doi:10.1016/j.sbi.2006.05.008 (2006).

10   Dorman, C. J. & Kane, K. A. DNA bridging and antibridging: a role for bacterial nucleoid-associated proteins in regulating the expression of laterally acquired genes. *FEMS microbiology reviews* **33**, 587-592, doi:10.1111/j.1574-6976.2008.00155.x (2009).

11   van der Valk, R. A., Vreede, J., Cremazy, F. & Dame, R. T. Genomic looping: a key principle of chromatin organization. *Journal of molecular microbiology and biotechnology* **24**, 344-359, doi:10.1159/000368851 (2014).

12   Cairns, J. *et al.* CHiCAGO: robust detection of DNA looping interactions in Capture Hi-C data. *Genome Biology* **17**, 127, doi:10.1186/s13059-016-0992-2 (2016).

13   Lyubchenko, Y. L., Shlyakhtenko, L. S., Aki, T. & Adhya, S. Atomic force microscopic demonstration of DNA looping by GalR and HU. *Nucleic Acids Res.* **25**, 873-876, doi:10.1093/nar/25.4.873 (1997).

14   Dame, R. T., Wyman, C. & Goosen, N. H-NS mediated compaction of DNA visualised by atomic force microscopy. *Nucleic Acids Res.* **28**, 3504-3510, doi:10.1093/nar/28.18.3504 (2000).

15   Dame, R. T. *et al.* DNA bridging: a property shared among H-NS-like proteins. *Journal of bacteriology* **187**, 1845-1848, doi:10.1128/JB.187.5.1845-1848.2005 (2005).

16   Murugesapillai, D. *et al.* DNA bridging and looping by HMO1 provides a mechanism for stabilizing nucleosome-free chromatin. *Nucleic Acids Research* **42**, 8996-9004, doi:10.1093/nar/gku635 (2014).

17   Liu, Y., Chen, H., Kenney, L. J. & Yan, J. A divalent switch drives H-NS/DNA-binding conformations between stiffening and bridging modes. *Genes Dev.* **24**, 339-344, doi:10.1101/gad.1883510 (2010).

18   Dame, R. T., Noom, M. C. & Wuite, G. J. Bacterial chromatin organization by H-NS protein unravelled using dual DNA manipulation. *Nature* **444**, 387-390, doi:10.1038/nature05283 (2006).

19   Sambrook, J., Fritsch, E. F. & Maniatis, T. *Molecular cloning: a laboratory manual*. (Cold spring harbor laboratory press, 1989).

20   van der Valk, R. A. *et al.* Mechanism of environmentally driven conformational changes that modulate H-NS DNA-bridging activity. *Elife* **6**, doi:10.7554/eLife.27369 (2017).

21   Corbeski, I. *et al.* Microscale Thermophoresis Analysis of Chromatin Interactions. *Methods Mol Biol* **1837**, 177-197, doi:10.1007/978-1-4939-8675-0_11 (2018).

22   Henneman, B., Heinsman, J., Battjes, J. & Dame, R. T. Quantitation of DNA-Binding Affinity Using Tethered Particle Motion. *Methods Mol Biol* **1837**, 257-275, doi:10.1007/978-1-4939-8675-0_14 (2018).

Chapter 6

Unravelling the biophysical properties of chromatin proteins and DNA using Acoustic Force Spectroscopy

This chapter is based on the following chapter:

Lin, S. N., Qin, L., Wuite, G. J., & Dame, R. T. (2018). Unraveling the biophysical properties of chromatin proteins and DNA using acoustic force spectroscopy. In Bacterial Chromatin (pp. 301-316). Humana Press, New York, NY.

The chapter was jointly written by S.N.L. and L.Q..

Abstract

Acoustic Force Spectroscopy (AFS) is a single-molecule micromanipulation technique that uses sound waves to exert force on surface-tethered DNA molecules in a microfluidic chamber. As large numbers of individual protein-DNA complexes are tracked in parallel, AFS provides insight into the individual properties of such complexes as well as their population averages. In this chapter, we describe in detail how to perform AFS experiments specifically on bare DNA, protein-DNA complexes, and how to extract their (effective) persistence length and contour length from force-extension relations.

1. Introduction

Sound waves can be used to exert forces on objects; this concept is key to the application of controlled forces on surface-tethered microparticles using a method called acoustic force spectroscopy (AFS) [1,2]. By applying force on the microparticle, force is exerted on the tether, DNA or a protein-DNA complex [1,2]. The experimental layout for studying protein-DNA complexes is similar to that used for tethered particle motion (TPM) [3] and magnetic tweezers (MT) [4]: one end of a DNA substrate is labeled with DIG to bind the anti-DIG on the sample carrier or flow chamber surface, while the other end of the DNA is labeled with biotin to bind on the silica or magnetic beads. In AFS, force is applied vertically to microspheres attached to surface-tethered DNA molecules as is the case for MT. The x-y motion of the bead is monitored and its diffraction pattern is used to determine its z-position from a look-up table (LUT) of radial profiles [1]. The z-position of the bead (minus the bead radius) corresponds to the end-to-end distance of the DNA tether.

Acoustic pressure is generated by a vibrating piezo element attached to the bottom or top of the flow cell. The acoustic pressure transfers potential energy into the medium in the flow cell chamber and forms a standing wave. Particles, in this case, polystyrene or silica microspheres 1-5 μm in diameter (with a volume V), are forced to align at the nodes of the standing wave. By increasing the voltage (changing the amplitude of the wave), beads will experience a larger force (F) towards the wave node [5,6]. The effective force applied on each bead is described by Equation (1).

$$F = -V\nabla \left[\frac{1-\kappa^*}{4} \kappa_m P^2 - \frac{(\rho^*-1)}{1+2\rho^*} \rho_m v^2 \right] \quad \cdots\cdots (1)$$

in which P is the acoustic pressure (energy gradient), v is the velocity of particles, and ρ^* (=ρ_p / ρ_m) and κ^* (= κ_p/κ_m) are the density ratio and compressibility ratio between the particle and the fluid, respectively [5]. The magnitude of the force applied to a bead is determined by the material and size of the bead, the medium inside the flow cell, and the vibration of the piezo. We routinely apply forces up to ~70 pN to achieve DNA overstretching and protein unfolding, with polystyrene microspheres, 4.5 μm in diameter.

Here, we describe the assembly of an acoustic force spectroscopy instrument around a commercial inverted microscope and explain how to perform experiments on DNA molecules and protein-DNA complexes. In addition, we demonstrate how structural and mechanochemical properties of protein-DNA complexes can be extracted from AFS data.

2. Materials

Prepare all solutions by using ultrapure water (prepared by purifying deionized water, to attain a sensitivity of 18 MΩ-cm at 25 °C; MilliQ). Prepare solutions at room temperature (RT) and store at 4 °C.

2.1 Stock solutions and beads

2.1.1 Buffer for analysis by agarose gel electrophoresis (see section 3.1)

TAE: 40 mM Tris (pH 7.6), 20 mM acetic acid and 1 mM EDTA.

2.1.2 Solutions for reference bead preparation (see section 3.2)

1. Buffer A: 100 mM $Na_2B_4O_7$, 150 mM NaCl, 0.05 % w/v Pluronics (pH 8.3) (BASF), 30 µM Digoxigenin-NHS ester (Sigma-Aldrich).
2. Buffer B: 10 mM HEPES (pH 7.5).
3. Buffer C: 10 mM HEPES (pH 7.5) with 0.1% Pluronics.

2.1.3 Solutions for cleaning protocol (see section 3.4 and 4.5)

1. Bleach solution: 0.7 M NaClO.
2. Sodium thiosulfate solution: 10 mM $Na_2S_2O_3$.

2.1.4 Solutions for passivation of the flow cell (see section 3.6)

1. Phosphate Buffered Saline (PBS, pH 7.4): 150 mM NaCl and 10 mM phosphate. 1 mM EDTA and 10 mM NaN_3 are added to prevent bacterial growth in the buffer.
2. Anti-digoxigenin solution: 200 µg/ml anti-DIG (Roche) in PBS.
3. Buffer D: 0.2 % (w/v) BSA (Sigma-Aldrich) in PBS.
4. Buffer E: 0.5 % (w/v) Pluronics (Sigma-Aldrich) in PBS.
5. Buffer F: 0.02 % (w/v) Casein (Roche) and 0.02 % (w/v) Pluronics in PBS.

2.1.5 Solutions for passivation of the flow cell (see section 3.2 and 3.6)

1. 1.9 µm Streptavidin-coated bead (Kisker Biotech) in PBS.

2. 4.5 µm Streptavidin-coated bead (Kisker Biotech) in PBS.

2.2 DNA substrates

DNA substrates for AFS experiments are generated via Polymerase Chain Reaction (PCR) using 5' biotinylated and 5' Digoxygenin-labeled primers [Note 1]. The length of DNA is designed to be in the range significantly shorter than the distance from the surface to the wave node. AFS is capable to measure DNA substrates as short as 1 kbp and as long as 45.5 kbps [10]. Table 6.1 and section 3.1.2 summarizes oligonucleotides used to generate our toolbox of DNA of different lengths (2000-8000 bp) and sequence content (32% and 50%) by PCR. All DNA substrates are stored at -20°C after purification and concentration determination.

1. A DNA template contains the sequence of interest; plasmid pKYBI (8393 bp, New England Biolabs) and plasmid pRD227 are used as the templates for 8000 bp DNA substrate with 50% GC content and 2000 bp DNA substrate with 32% GC content, respectively.

2. 5' biotin-labeled reverse primer (see Table 6.1)

3. 5' Digoxygenin-labeled forward primer (see Table 6.1)

4. 100% DMSO (New England Biolabs)

5. Recombinant *Taq* DNA polymerase (5 U/µl) (Thermo Scientific)

6. Deoxyribose Nucleotide Triphosphate (dNTP mix) (Thermo Scientific, 2mM)

7. *Taq* DNA polymerase reaction buffer (Thermo Scientific, 10X)

8. GenElute ™ PCR cleanup kit (Sigma-Aldrich)

9. Biorad T100 Thermocycler PCR or any other available PCR machine.

10. 1% agarose gel in 1x TAE

11. Nanodrop® (Thermo Scientific)

12. GeneRuler DNA ladder (ThermoFisher Scientific)

Table 6.1. Primer sequences

Primer name	Sequence (5' - 3')	Modification
32% GC AFS General forward primer	G**T**GTG**T**GTGTG**T**GGTG**T**GTGGTGG ATACATATGCAACTTGAACGGCGTAAAAGAGG	5' Digoxygenin
2000 bp 32% GC AFS reverse primer	G**T**G**T**G**T**G**T**GTGTGGTGTGTGGTGG TCCCTCACTAGTTTAGTACATGAACTG	5' Biotin
50% GC AFS general forward primer	C**T**CTC**T**CTCTC**T**TCTC**T**CTTCTCT GAATTCGCGGCCGCCGTC	5' Digoxygenin
2000 bp 50% GC AFS reverse primer	C**T**C**T**C**T**C**T**CTCTTCTCTCTTCTCT CAGTGGGAACGATGCCCTC	5' Biotin
4000 bp 50% GC AFS reverse primer	C**T**C**T**C**T**C**T**CTCTTCTCTCTTCTCT CAGCGGTGGTTTGTTTGCCG	5' Biotin
6000 bp 50% GC AFS reverse primer	C**T**C**T**C**T**C**T**CTCTTCTCTCTTCTCT CGATCCCCGGCAAAACAGC	5' Biotin
8000 bp 50% GC AFS reverse primer	C**T**C**T**C**T**C**T**CTCTTCTCTCTTCTCT GGTACCAATGTTTTAATGGCGGATG	5' Biotin
T = Modified T		

2.3 AFS Instrument

The AFS system is built around a commercially available inverted microscope combined with commercially available electronics and a commercially available AFS chip (see Fig. 6.1).

1 Microscope: Inverted microscope (Nikon, TE200) with condenser (Nikon, LWD lens), CFI Achromat 40x air objective (Nikon, NA= 0.65).

2 Illumination: Collimated LED (ThorLabs, 660 nm, 1200 mA). [Note2]

3 CMOS camera (Thorlabs, monochrome, pixel size 5.3 µm, 60 fps) connects to the computer.

4 Stage: Z-axis piezo translation stage (PI, MCLS03200), driven by Nano-Drive controller system (MCL, Nano-Drive, MCLC03200) which connects to the computer.

5 Function generator (Keysight, 33220A).

6 Power supply (Voltcraft, VSP 1410).

7 Amplifier (Mini-Circuits, LZY-22+).

8 TMC Vibracontrol clean top isolation table.

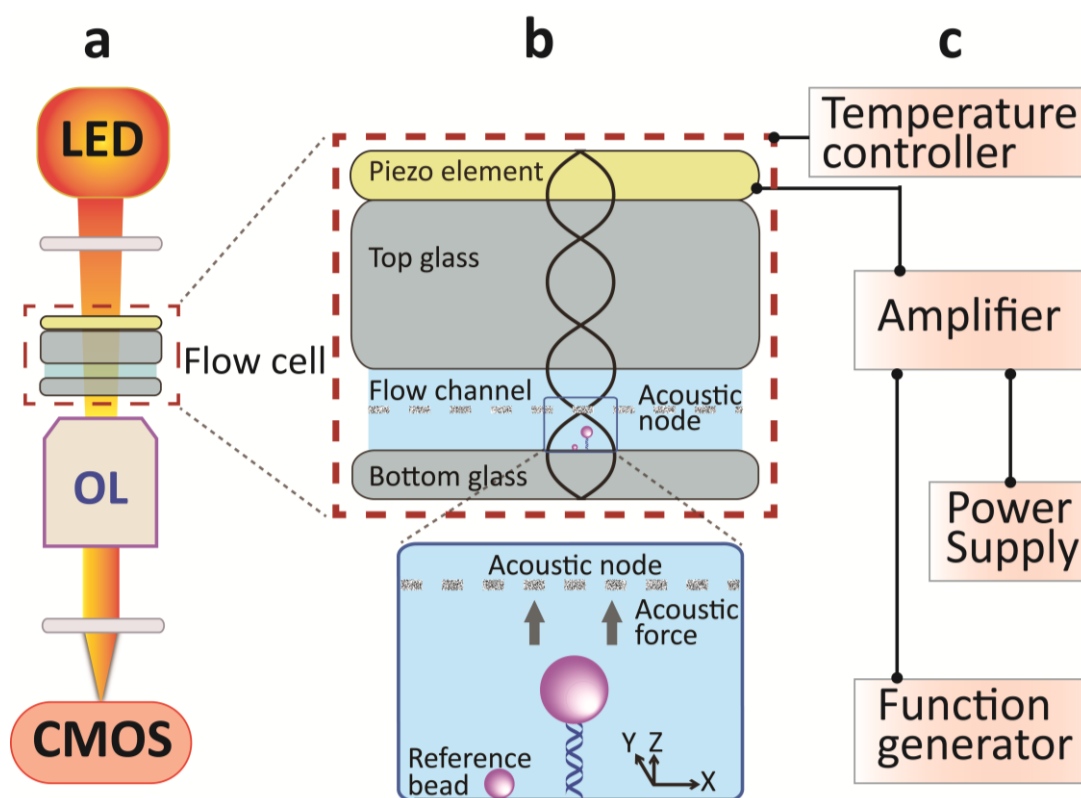9   Computer: "Advanced AFS workstation"   (LUMICKS B.V., AFS-CPU).

Figure 6.1: **Illustration of the principle of Acoustic Force Spectroscopy.** (a) The acoustic force spectroscopy instrument consists of a flow cell, an inverted microscope visualizing targets with objective lens (OL), temperature controller connected to the AFS-Chip holder, a CMOS digital camera and 660 nm LED light source. (b) AFS flow cell consists of the piezo element and two glass slides with a fluidic channel in between. The acoustic wave generated by the piezo travels through the top glass to the bottom glass and the bottom glass as a reflector reflects the acoustic wave, producing the standing wave over the flow cell. The acoustic standing waves carry pressure profile, which generate acoustic forces. The tethered particles in the flow channel exposed to the acoustic force are driven in the direction of the acoustic pressure node. (c) The temperature controller independently connects to the AFS-Chip metal holder. Both power supply and function generator connect to the amplifier, which controls the piezo element.

10 AFS-chip (LUMICKS B.V., AFS-CH2). (see Fig. 6.2)

11 AFS-chip temperature control holder. (see Fig. 6.3)

12 Custom pressure system. Syringes contain samples and buffers are connected to a gas pressure container. (see Fig. 6.3)
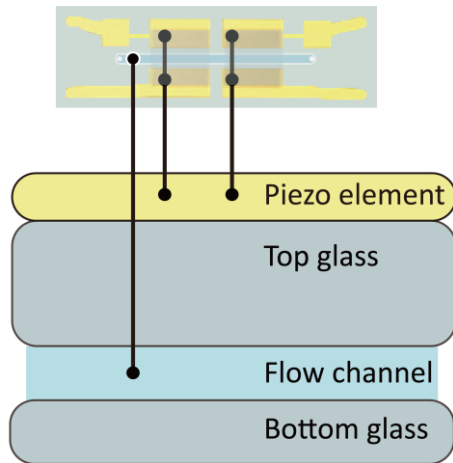
Figure 6.2: Schematic representation of an AFS-chip. The AFS flow cell consists of the piezo element, top glass slide and bottom glass slide with a flow channel in between.
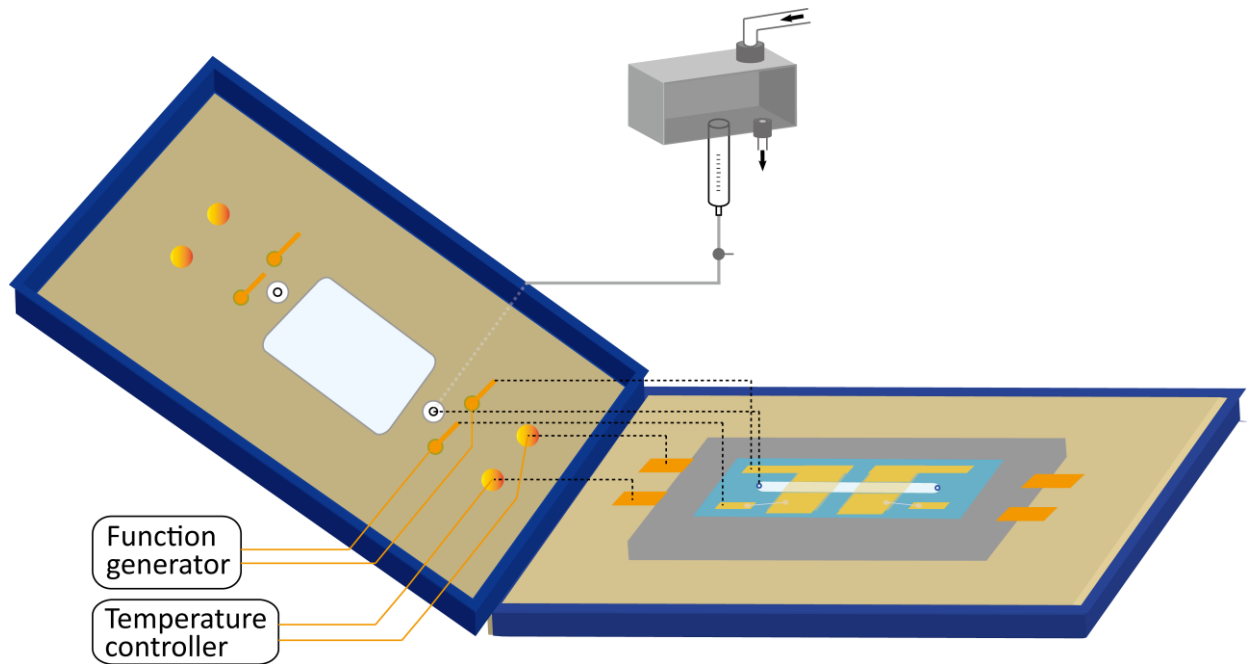

Figure 6.3: Schematic representation of the temperature control holder. The AFS-chip fits into the temperature control metal holder (grey) and this metal holder fits into the flow cell holder (light brown and navy blue) that consists of lid and base. When the lid closed, the metal points on the lid, connected to the function generator and temperature controller, will connect to their counterparts (metal regions) on the piezo and the metal holder (grey), and the holes on the lid, connected to the pressure can by thin tube, will connect to their counterparts (holes) on the AFS-chip.

2.4 Particle tracking, control and analysis

Three programs, a bead tracking program (see section 3.6), a data analysis program (see section 3.7.1), and an extensible worm-like-chain (eWLC) fitting program (see section 3.7.2) are used during the measurement and data analysis process.

1. The tracking program is written in LabVIEW [1] and available online http://figshare.com/articles/AFS_software/1195874. A detailed manual is also provided with the software. It is used to:

1) Control output frequency and output power of vibration. Apply a linear force ramp mode, the voltage is ramped with a square-root function.

2) Create a template image of a bead (imaged via a LED with a camera) to track bead position using a template-matching algorithm.

3) Track the x, y movements of tethered beads and record a look-up-table (LUT) in z direction for each bead. Routinely, the z-stage is moved in 80 nm steps through the LUT range of 0 - 8000 nm. The z-distance range of the LUT has to be larger than the maximal extension of the DNA molecule.

4) Calibrate force-voltage relationship.

2. The data analysis program is also written in LabVIEW [1] and available online via the same link as indicated under 2.4.1). It is used to:

1) Perform real-time acquisition of three-dimensional bead position in the flow cell.

2) Determine anchor points of all the tracked beads.

3) Correct for drift (see **note 3**) based on positions of the surface attached reference beads.

4) Generate force-extension (force-distance, FD) curves.

3. The WLC model fitting program is written in MatLab [7] and available online https://github.com/onnodb/FDFIT/tree/AFSFitting. It is used to:

1) Fit FD curves exported from data analysis program to the eWLC model.

2) Extract values of parameters reflecting the physical characteristics of bare DNA and protein-DNA complexes.

3. Methods

3.1 Generation of DNA substrate using PCR

1. DNA substrates for AFS experiments are generated by PCR. Carefully mix the reagents below in a PCR tube. Keep the enzymes in a -20°C cold block and dNTP stocks on ice when taken outside the freezer.

Reagent	Quantity
dNTP mix (2mM)	5 µL
Forward primer (10 pmol)	1 µL
Reverse primer (10 pmol)	1 µL
Taq Polymerase buffer (10X)	5 µL
DNA template (10 ng)	1 µL
Taq DNA Polymerase (5U/ µL)	0.2 µL
DMSO (100%)	1.25 µL
MilliQ	Add to 50 µL total volume

2. Use the program below to perform PCR (optimized for use in a Biorad T100 Thermocycler).

	Temperature	Duration	Cycle
Initialization	95	5 min	1
Denaturation	95	30 sec	
Annealing	65	30 sec	35
Extension/Elongation	72	4 min	
Final Elongation	75	10 min	1
Final hold	15	∞	1

3. Load 5 µL of each PCR product on a 1% agarose gel in TAE buffer, alongside a DNA marker for size estimation of the PCR product. Purify the PCR products with GeneElute PCR cleanup kit. See figure 6.4 for an example of the purified PCR products.

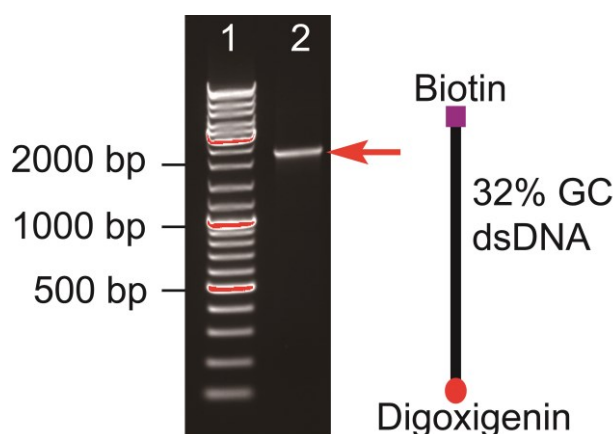4. Use Nanodrop® to measure the concentration of PCR products. Store the purified DNA products in MilliQ at -20°C.

Figure 6.4: **Visualization of PCR product size by agarose gel electrophoresis.** (1) 2 µL of the GeneRuler DNA marker. (2) 2 µL of the purified PCR product, and it is ready for use in Acoustic Force Spectroscopy experiments. The schematic representation of PCR-generated 5' digoxigenin and 3' biotin modified-DNA.

3.2 Preparation of reference beads

1. Mix 8 µl of 0.5% (w/v) 1.9 µm polystyrene beads into 1 ml of buffer A.

2. To coat polystyrene beads with DIGs, incubate the bead solution with DIG-NHS at RT for 3 hours with tumbling.

3. Centrifuge the bead solution at 2000 x g for 1 minute, and discard the supernatant.

4. Remove the free DIG-NHS by washing the bead solution with 1 ml buffer C. Centrifuge at 2000 x g for 1 minute and discard the supernatant. Repeat the wash twice.

5. Resuspend the beads in 1 ml buffer B. The beads can be used immediately or stored at 4°C.

3.3 Preparation of tether beads

1. To exchange the storage buffer of the commercial beads with PBS, dilute 20 µl of the bead solution in 500 µl PBS.

2. Vortex the sample thoroughly.

3. Centrifuge at 2000 x g for 2 minutes and discard the supernatant, but avoid discarding beads. Resuspend the beads in 500 µl PBS.

4. Repeat steps 2 and 3, carefully discard ~450 µL of supernatant, leaving ~50 µl in tube.

5. Add 4 µl of the reference beads to the 50 µl solution from step 4 and resuspend by vortexing.

3.4 Flow cell and tubing cleaning

The tubing and the flow cell are used repeatedly in our system; we replace the syringe before each experiment.

1. Install the flow cell chip into its holder. The holder is connected to tubing (see Fig 6.3).

2. Introduce 0.2 ml of bleach into the flow cell through the tubing and incubate for 10 minutes.

3. Rinse the tubing and the flow cell with MilliQ.

4. Introduce 0.2 ml $Na_2O_2N_3$ into the flow cell via the tubing and incubate for 10 minutes.

5. Flush 0.5 ml MilliQ into flow cell through the tubing.

3.5 Preparation of flow cell and bead tethers

To minimize waste of materials, in steps 1, 5, and 7, the sample is manually pipetted into the flow cell without using the syringe. However, all the buffers for passivation are introduced through the syringe so the syringe and tubing are also passivized. All preparations are at RT.

1. Inject 20 µl of anti-digoxigenin solution into the flow chamber and incubate for 20 minutes.

2. To prevent air bubbles flowing into the flow chamber, introduce 0.5 ml of buffer D into the syringe and flush out the air present in the tubing before connecting the tubing to the holder. Place the chip in holder, leave drops at the two holes in the flow cell and clamp the holder gently. [8]

3. Inject 0.1 ml of buffer D and incubate for 30 minutes for the first time passivation. Discard the residual of buffer D in syringe.

4. Add 0.5 ml buffer E into the syringe, flush in 0.1 ml of buffer E and incubate for 30 minutes for the second time passivation. Discard the residual of buffer E in the syringe.

5. Take out the chip to introduce 30 µl of DNA solution in the flow chamber and incubate for 20 minutes. Place the chip back into the holder and clamp the holder gently.

6. Add 0.5 ml buffer F into the syringe. Flush in 0.1 ml buffer F to remove free DNA.

7. Take out the chip to introduce 20 µl bead solution in the flow chamber. Place the chip back into the holder, clamp the holder gently and incubate for 30 minutes.

8. Add 0.5 ml measuring buffer in the syringe.

9. The flow cell is ready for measurement.

3.6 Measurements

1. Switch on the illumination and bring the bottom-tethered beads into focus. (see Fig. 6.2)

2. Start the bead tracking program in LabView.

3. Select the frequency for the piezo. The piezo frequency is given by provider (LUMICKS). Each piezo has a specific impedance, in other words, there is deviation of vibration frequency from chip to chip. More details have been described previously [11].

4. Remove untethered beads by flushing the flow cell with the measurement buffer at a flow rate of 0.2 µl/min until such beads are no longer observed in the region of interest (ROI).

5. Select the tethered beads in the ROI.

   Generate a LUT for each ROI, applying a constant force (≈10 pN) to the tethers to minimize bead motion. The "Create LUT" botton in the program starts to move the sample stage (or objective) and record the ring patterns at different z-positions. We collect the LUT at 60 Hz with a camera exposure time in 16.6 ms, each stage moving step is 80 nm throughout a range of 0 - 8000 nm.

6. Start to record the tracking of the selected tethered beads.

7. Record the x-y motions of the tethered beads in the absence of force, the x-y motions are used for determination of the single tethered beads in data analysis. The time required to sample all conformations depends on bead size; for beads with a diameter of 4.5 µm, a 10 minute recording is sufficient.

8. To calibrate the force-voltage relationship of each tethered beads, apply a series of different forces on the tethered particles. To collect sufficient data for power spectra fitting (see section 3.7.1), perform 2 minutes of z-position recording for each forces.

9. Apply low force (~10 pN) and slow flowing rate (0.2 µl/min) while introducing protein solution. The flow in the flow chamber will result in a drag force on the tethered beads.

10. Apply a constant rate force ramp (120 ms between each force steps) to generate FD curves of bare DNA and protein-DNA complexes.

3.7 Data analysis

3.7.1 Generate FD curves

1. Load the data into the analysis program in LabView.

2. Determine the single tethered beads and reference beads data by the root mean squared (RMS) displacement values and anisotropic ratio (s) from the x-y motions of each tethers.

   In Subheading 3.6, step 7, tethered beads randomly move around their anchor points without force applied. In AFS, RMS is used to quantify the degree of the tether motions in two dimensions over a period of time, t:

   $$RMS = \sqrt{\langle (x - \bar{x})^2 + (y - \bar{y})^2 \rangle_t} \quad \cdots (2)$$

   In which $\bar{x}$ and $\bar{y}$ are the average positions of the tethered bead over time t.

   Usually, not all tethered microspheres are attached to the surface via a single tether. Calculation of the anisotropic ratio (**s**) allows separation of single-tethered microspheres from stuck and multiple-tethered microspheres.

   $$s = \frac{\lambda_{major}}{\lambda_{minor}} \quad \cdots (3)$$

   In which λ_{major} and λ_{minor} represent the maximum and minimum value along the axes of the x-y-scatter plot respectively.

   Single-tethered microspheres are expected to exhibit a perfectly symmetrical motion and to have an anisotropic ratio of 1. In our studies we use s < 1.3 as a threshold to discard multiple-tethered or poorly tracked particles. The particles that match the selection criterium are used for further analysis.

3. Remove the drift from the measured data by calculating the average drift of the stuck beads. Stuck beads are selected based on their X and Y motions. In our studies we use RMS < 200 / s ≈ 1 (see **Note 4**].

4. Determine the anchor points of the tethers by selecting the x-y motion trace without force applied during the measurement. Use "Anchor point" function in the program to determine the end-to-end length of the DNA molecule by Pythagoras calculation and the anchor point in data analysis program.

5. Calibrate the force-voltage relationship by selecting the voltage-time plot in the program where constant voltages were applied. Generate and fit power spectrum. [Note 5]

6. Generate FD curves by selecting the time period which force ramp was applied. Export FD curves in text file with 'Export function' in the program for eWLC fitting. (See 3.7.2)

3.7.2 Extensible worm-like chain model (eWLC) model Fitting

The extensible worm-like-chain model in formula (4) describes the behavior of elastic polymers such as DNA and protein-DNA complexes [8].

$$\frac{z}{L_c} = 1 - \frac{1}{2}\left(\frac{k_B T}{F L_p}\right)^{\frac{1}{2}} + \frac{F}{K_0} \qquad \cdots\cdots (4)$$

In which z is the extension and F is the external force, k_B is the Boltzmann constant, T is the absolute temperature, K_0 is the stretch modulus, Lp is the persistence length and Lc is contour length. A typical value for the stretch modulus of double-stranded DNA is about 1000 pN [9].

1. Run the fitting program in MatLab software.
2. Import FD curves in MatLab program.
3. Select the data point of the FD curves which are taken below 30 pN.
4. Determine persistence length (Lp), contour length (Lc), and stretch modulus (K_0).

4. Analysis of protein-DNA complexes using AFS

Architectural proteins bind to DNA via minor or major groove interactions and result in wrapping, bending, or bridging of the DNA. By applying force to protein-DNA complexes, the effect of proteins on DNA conformation and the binding behavior of these proteins can be investigated. Here we discuss the effects of two types of DNA binding proteins, HU and H-NS.

4.1 Force-Extension curves of HU-DNA complex

HU protein compacts and stiffens DNA in protein concentration dependent manner. In our experimental system, DNA was compacted at the concentration below 400 nM. Above 400 nM, DNA was extended by the filament of HU proteins (See Fig. 6.5).
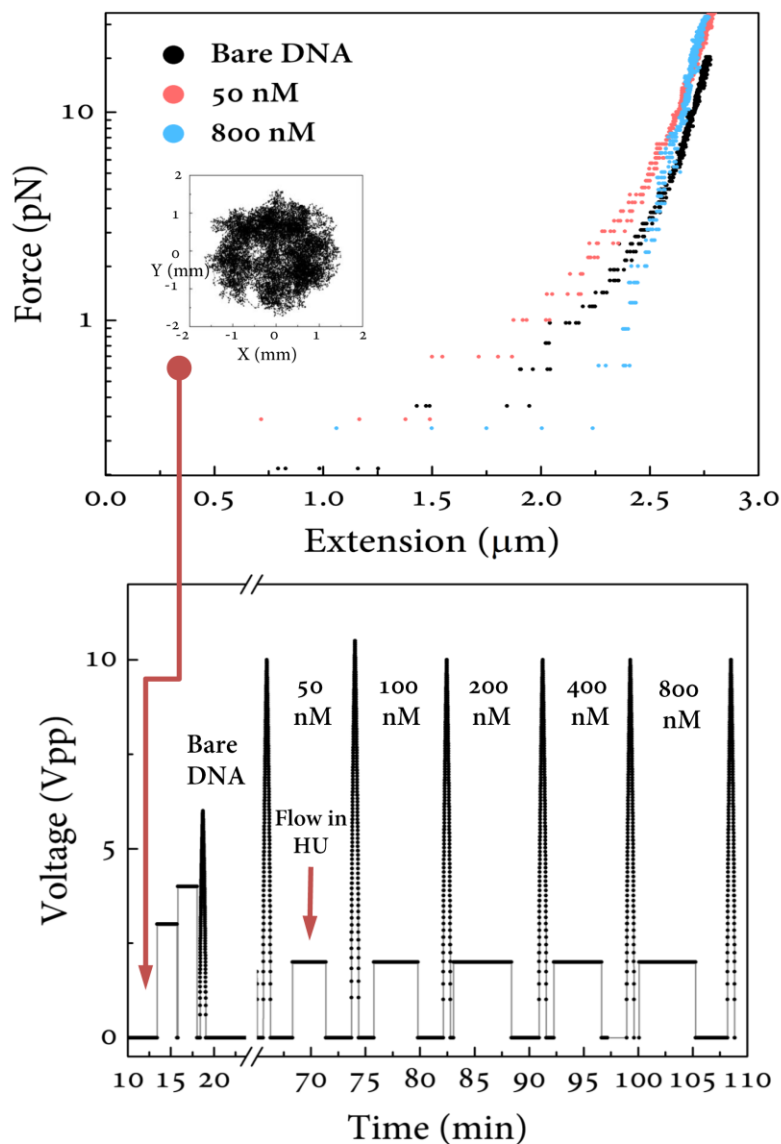

Figure 6.5. Stretched HU-DNA complex and the flow chart of force application. The top figure shows three force-extension curves at HU absent (black), low concentration (red), and high concentration (blue). Top inside is the freely movement of a tether bead (symmetry in 1.2). Bottom plot shows the force v.s. time. Low force ~2 pN was applied while introducing proteins.

4.2 Pulling of DNA and DNA-H-NS complex

Histone-like nucleoid-structuring (H-NS) protein is a bacterial protein that plays a key role in chromosome organization and regulation. DNA and DNA-H-NS complex was studied by using AFS system (see Fig. 6.6). It shows that DNA was stiffened by H-NS at 2000 nM, which is in agreement with previous study [10,11].
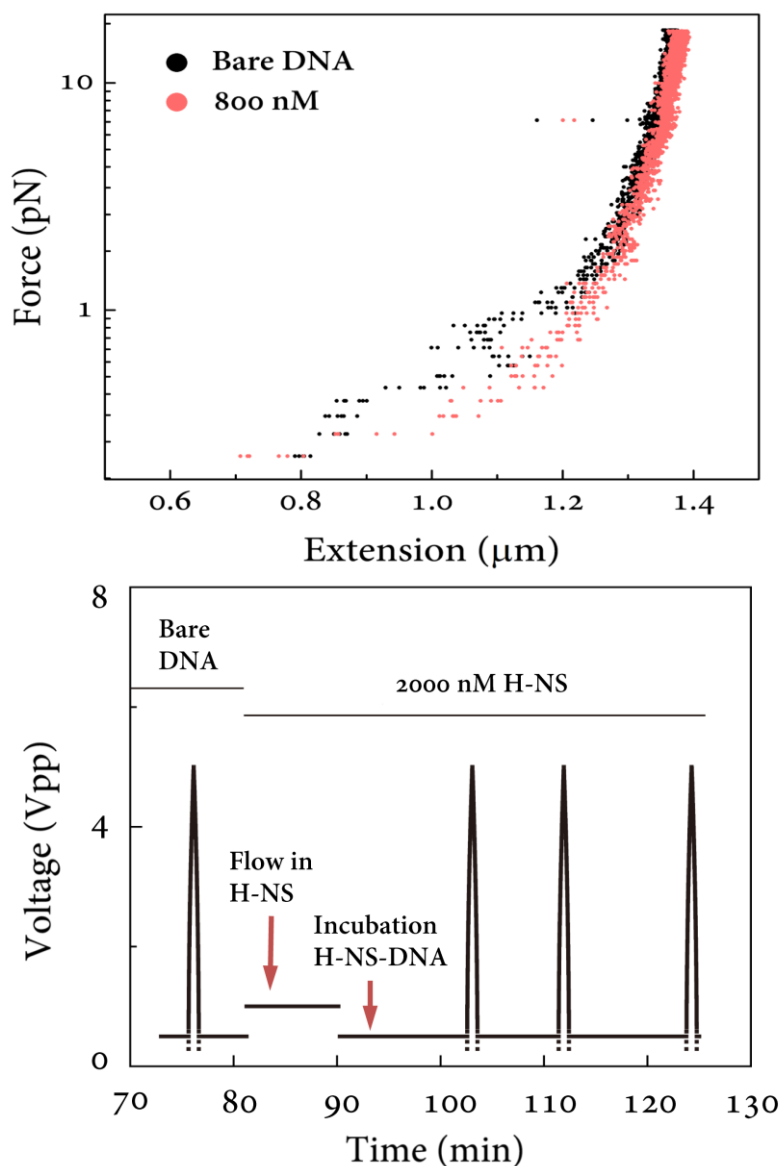

Figure 6.6. Stretched H-NS-DNA complex and the flow chart of force application. Top plot shows force-extension curves of 4000 bp bare DNA (red) and H-NS-DNA complex (blue). Bottom plot shows the applied voltage v.s. time. Low force 0.8 pN was applied while introducing proteins and 0.2 pN was applied while incubating H-NS-DNA complex.

Notes

1. DNA substrates can also be prepared by other approaches, e.g. by filling in Digoxigenin/Biotin at two ends of cut plasmid or by ligating modified oligos/dsDNAs.

2. Diffraction ring patterns are required for accurate bead tracking. The light source needs to be monochromatic and aligned in parallel. To obtain collimated light, either a point source or an iris conjugated to your condenser is required. For monochromatic illumination a LED of defined wavelength or band-pass filter in the illumination path is suggested.

3. Movement of the machine or heat created by piezo vibration causes drift in the flow cell. A highly efficient piezo results in minimal heating of the system.

4. To correct drift signal, the program subtracts the displacements from x, y, z on the average traces of the selected stuck beads. The average displacement of the stuck beads is as a starting point, 0.

5. The force power spectrum fitting is described in Norrelykke and Flyvbjerg [12]. Two important parameters are obtained from the fitting are the frequency at the corner of the spectrum and the diffusion coefficient. The diffusion coefficient dependence can also be predicted from the bead size and the distance from the surface [13]. Nevertheless, the microsphere size varies in the same batch. Checking whether the theoretical value is overlaps with the fitted value gives a reference of the error. This function is already included in the AFS data analysis program. Lorentzian formula and importance-weighted least squares fitting generate the force power spectra fitting [14,15]:

$$P(f) = \frac{D/(2\pi^2)}{f^2 + \left(k/\left(2\pi \times \gamma_{fax}\right)\right)^2}$$

where $D = k_B T / \gamma_{fax}$ is the microsphere diffusion constant, k_B *is* the Boltzmann constant, *T is* the temperature, γ_{fax} *is* the effective drag coefficient, *f is* the frequency and *k is* the stiffness of a Hooke spring acting on the microsphere. $k = F / (L_{ext} + R)$; in the expression

of k, F is the force, L_{ext} is the measured extension of the DNA and R is the radius of the microsphere.

References

1   Sitters, G. *et al.* Acoustic force spectroscopy. *Nat. Methods* **12**, 47-50, doi:10.1038/nmeth.3183 (2015).

2   Kamsma, D., Creyghton, R., Sitters, G., Wuite, G. J. & Peterman, E. J. Tuning the Music: Acoustic Force Spectroscopy (AFS) 2.0. *Methods* **105**, 26-33, doi:10.1016/j.ymeth.2016.05.002 (2016).

3   van der Valk, R. A., Laurens, N. & Dame, R. T. Tethered Particle Motion Analysis of the DNA Binding Properties of Architectural Proteins. *Methods Mol Biol* **1624**, 127-143, doi:10.1007/978-1-4939-7098-8_11 (2017).

4   Brouwer, T. B., Kaczmarczyk, A., Pham, C. & van Noort, J. Unraveling DNA Organization with Single-Molecule Force Spectroscopy Using Magnetic Tweezers. *Methods Mol Biol* **1837**, 317-349, doi:10.1007/978-1-4939-8675-0_17 (2018).

5   Settnes, M. & Bruus, H. Forces acting on a small particle in an acoustical field in a viscous fluid. *Phys Rev E Stat Nonlin Soft Matter Phys* **85**, 016327, doi:10.1103/PhysRevE.85.016327 (2012).

6   Gor'Kov, L. in *Soviet Physics Doklady.* 773.

7   Broekmans, O. D., King, G. A., Stephens, G. J. & Wuite, G. J. DNA Twist Stability Changes with Magnesium(2+) Concentration. *Phys Rev Lett* **116**, 258102, doi:10.1103/PhysRevLett.116.258102 (2016).

8   Odijk, T. Stiff Chains and Filaments under Tension. *Macromolecules* **28**, 7016-7018, doi:10.1021/ma00124a044 (1995).

9   Wang, M. D., Yin, H., Landick, R., Gelles, J. & Block, S. M. Stretching DNA with optical tweezers. *Biophys. J.* **72**, 1335-1346, doi:10.1016/S0006-3495(97)78780-0 (1997).

10   Lim, C. J., Lee, S. Y., Kenney, L. J. & Yan, J. Nucleoprotein filament formation is the structural basis for bacterial protein H-NS gene silencing. *Sci Rep* **2**, 509, doi:10.1038/srep00509 (2012).

11   van der Valk, R. A. *et al.* Mechanism of environmentally driven conformational changes that modulate H-NS DNA-bridging activity. *Elife* **6**, doi:10.7554/eLife.27369 (2017).

12   Nørrelykke, S. F. & Flyvbjerg, H. Power spectrum analysis with least-squares fitting: amplitude bias and its elimination, with application to optical tweezers and atomic force microscope cantilevers. *Review of Scientific Instruments* **81**, 075103 (2010).

13   Schäffer, E., Nørrelykke, S. F. & Howard, J. Surface forces and drag coefficients of microspheres near a plane surface measured with optical tweezers. *Langmuir* **23**, 3654-3665 (2007).

14   te Velthuis, A. J., Kerssemakers, J. W., Lipfert, J. & Dekker, N. H. Quantitative guidelines for force calibration through spectral analysis of magnetic tweezers data. *Biophys. J.* **99**, 1292-1302, doi:10.1016/j.bpj.2010.06.008 (2010).

15   Berg-Sørensen, K. & Flyvbjerg, H. Power spectrum analysis for optical tweezers. *Review of Scientific Instruments* **75**, 594-612, doi:10.1063/1.1645654 (2004).

Chapter 7

Summary and Prospects

Bacteria often experience external challenges, such as changes in environmental conditions or attacks by bacteriophages. To cope with these challenges, bacteria need to be able to adapt quickly to the challenges. Key to the survival of bacteria is to be able to adapt to environmental stresses, to acquire new genetic characteristics through horizontal gene transfer to remain competitive and to silence these foreign genes as long as they do not provide any benefits. These mechanisms of adaptation are controlled via the structure of the bacterial genome, which is dynamically compacted and organized.

The Histone-like nucleoid structuring (H-NS) protein is a key regulator of the dynamic bacterial genome. The protein is conserved among enterobacteria and plays a determinant role in the architecture of their nucleoid acting as a global genome organizer and gene regulator. H-NS generally acts as repressor of transcription, silencing the expression of many genes and operons. The gene organization and silencing mechanism of H-NS is determined by its ability to bind and spread across genes. Characteristic of H-NS is the formation of nucleofilaments along the DNA and protein-mediated DNA-DNA bridges. Functional analogs of H-NS have been found in other bacterial species: MvaT in *Pseudomonas* species, Lsr2 in actinomycetes and Rok in *Bacillus* species. These proteins complement *hns⁻* phenotypes and have similar DNA-binding properties, despite their lack of sequence homology. These H-NS like proteins are widely distributed in the genome and prefer to bind and repress AT rich DNA acquired through horizontal gene transfer, which makes them bacterial xenogeneic silencers. Structurally, they have overall similar domain organization: the N-terminal domain functions in dimerization and oligomerization, the C-terminal domain binds DNA and the two are connected by a flexible linker. Attributed to their delicate domain arrangement, the four proteins are all capable of bridging DNA duplexes, which is believed to be crucial in gene silencing. The structural and functional characteristics of these four architectural proteins (H-NS, MvaT, Lsr2 and Rok) are summarized in **Chapter 1**.

Stress-responsive regulatory proteins in bacteria, particularly H-NS like proteins, function as gene silencers and as sensors of environmental changes. The bacterial genome operates as an information processing machine, translating environmental cues into altered transcription of specific genes required for adaptation and survival. Key to this process is the dynamic organization of the bacterial genome driven by such cues. The genes targeted by H-NS family proteins are

often regulated by environmental factors such as osmolarity, pH and temperature. H-NS proteins are able to bridge DNA duplexes, which is key to gene regulation and their responding to changing conditions in the environment. Divalent ions have been shown to be able to drive the transition between lateral H-NS-DNA filaments and bridged DNA-H-NS-DNA complexes. This switching between the two types of complexes is believed to be the mechanistic basis of the role of H-NS proteins in bacterial nucleoid organization and transcription regulation. Earlier Molecular Dynamics simulation studies of H-NS, indicated that the switch between the two DNA binding modes involves a change from a half-open (also referred as a closed conformation) to an open conformation driven by $MgCl_2$. However, the molecular basis that governs this phenomenon remains poorly elucidated. In **Chapter 2,** we used an abridged structural version of H-NS, MvaT from *P. aeruginosa*, in which we scrutinized its protomer structural/function relationship in response to changes in the surrounding ionic strength. We have combined integrative structural biology methods and biochemical assays to decipher the structural changes in MvaT that drive the switch between its DNA stiffening and bridging activities under different salt conditions. These structural changes appear to be conserved within the H-NS family of proteins: analysis of the primary sequences of H-NS family members revealed conserved positions of charged residues despite the low sequence identity. This suggests that their osmosensitivity is mediated by the modulation of the electrostatic interactions between their N-terminal and DNA binding domains within their nucleoprotein filaments.

Bacteriophages are among the most abundant and diverse organisms on planet, found wherever bacteria exist, and they represent a constant challenge to bacteria. Bacteria and their associated bacteriophages co-evolve in a continuous battle, developing defensive and offensive mechanisms. The interaction and co-evolution between a bacteriophage and its bacterial host play a key role in the ecological and evolutionary processes of microbial communities. Successful bacteriophage infection requires coping with bacterial resistance systems. Bacterial xenogeneic silencers, H-NS family proteins, play important roles in bacterial phage defense and evolution by silencing incoming genes and genes acquired through horizontal gene transfer. To mitigate the effects of such H-NS-like proteins, bacteriophages encode proteins counteracting gene silencing by H-NS-like proteins. The *Pseudomonas* phage LUZ24 encodes the Mip protein which binds the H-NS

family protein MvaT of *Pseudomonas aeruginosa.* Binding of Mip was earlier proposed to inhibit the silencing of phage LUZ24 DNA by MvaT. However, the mechanism by which Mip modulates MvaT function remained unclear. In **Chapter 3**, we investigated how the DNA binding properties of MvaT are affected by Mip. Also, we defined how Mip interacts with MvaT and how this translates into altered DNA structuring properties. Our studies reveal that Mip interferes with the formation and stability of the bridged MvaT-DNA complex. This effect is due to interaction of Mip with both the dimerization and the DNA-binding domain of MvaT. Based on these observations we propose that binding of Mip promotes the half open - bridging incompetent - state of MvaT, resulting in relief of MvaT-mediated gene silencing.

Rok from Bacillus subtilis is an abundant DNA binding protein similar in function to H-NS-like proteins found in many proteobacteria. Rok binds across the genome with a preference for A/T rich DNA. Such DNA often contains genes of foreign origin that are silenced due to Rok binding. Rok also has been implied in global organization of the B. subtilis genome. However, how Rok binds to DNA and how it represses transcription is unclear. Also, it is unknown whether Rok-mediated gene repression can be induced or relieved following changes in physico-chemical conditions, as noted for H-NS-like proteins. In **Chapter 4**, we investigated the DNA binding properties of Rok and determined the effects of physico-chemical conditions on these properties. We demonstrate that Rok is a DNA bridging protein similar to H-NS like proteins from E. coli (H-NS), Pseudomonas sp. (MvaT) and Mycobacteria (Lsr2). Strikingly, unlike these proteins, the ability of Rok to bridge DNA is not affected by changes in physico-chemical conditions. Not being a direct sensor of such changes sets Rok apart from other H-NS like proteins. It implies the existence of other (protein-mediated) mechanisms to relieve Rok-mediated gene silencing in response to changes in environmental conditions.

In **Chapter 5** and **Chapter 6**, we have described two methods well-suited to the analysis of the interaction between H-NS family proteins: a DNA bridging assay and Acoustic Force Spectroscopy (AFS). These techniques are also helpful in understanding how proteins or molecules interfere with the DNA binding functionality of H-NS family proteins. For instance, the bridging assay can be used as a method to identify proteins or molecules that alter the DNA bridging activity of H-NS proteins which is crucial in gene silencing. Single molecule technique, like AFS, Optical Tweezers

and Magnetic Tweezers, can help in studying mechanisms underlying H-NS mediated effects on gene transcription by RNAP.

Prospects

It is a long journey to understand the (dynamic) chromosome organization of bacteria, however, advances in genome-scale approaches over the past few decades have improved our understanding of bacterial genome folding. Bacterial DNA-bridging proteins play important role in genome organization and gene regulation due to their binding at distinct regions throughout the genome. DNA bridging and modulation of DNA bridging seems to be functionally conserved across species. This provides new opportunities to understand how genomes are dynamically organized by comparative functional and evolutionary analyses of functionally conserved DNA-bridging proteins from different species. A key in understanding genome organization and an important current challenge is to better define local changes in DNA folding in response to environmental challenges and to understand how these affect other nucleic acid transactions within living cells. For instance, biophysical and biochemical techniques have identified structures of H-NS proteins interacting with nucleic acids and have shown how these interactions are modulated by environmental changes *in vitro*, but it is unclear how these affect transcription *in vivo*. Furthermore, although we understand how a single nucleoid-associated protein organizes DNA, it is not obvious how the joint efforts of multiple NAPs combine within cells In addition to the environmental conditions and protein partners, post translational modification can also contribute to modulating the DNA binding properties/functions of bacterial nucleoid-associated proteins. This aspect needs more extensive research which would promote our understanding of the dynamic chromosome organization of bacteria.

Proteins from bacteria and bacteriophages have been shown to be able to interfere with the function of H-NS proteins. Such interference can occur at any of the steps towards assembly of the bridged H-NS-DNA complex i.e. during initial DNA binding, multimerization or the stage of DNA bridging. In general, a better understanding of how viral proteins counteract H-NS proteins is important for design of proteins or molecules countering phage infection. Potential applications of such molecules can be envisioned in biotechnology, where phage infections are a threat to large scale culturing, or in phage therapy where they may aid in enhancing the ability to infect and

kill their host. Moreover, due to their global role in gene regulation in bacteria H-NS-like proteins are potential drug targets to mitigate bacterial infections. Understanding at the molecular mechanistic level how H-NS proteins activity is modulated is key to such developments.

Hoofdstuk 7

Samenvatting en vooruitzichten

Bacteriën komen veelvuldig externe uitdagingen tegen in de vorm van veranderingen in omgevingsfactoren of aanvallen van bacteriofagen. Om hiermee om te kunnen gaan, moeten bacteriën zich snel aanpassen aan deze uitdagingen. Belangrijke strategiën om te overleven zijn het aanpassen aan stressfactoren uit de omgeving met name door veranderingen in genexpressie en het verkrijgen van nieuwe genetische eigenschappen door horizontale overdracht van vreemde genen die uitgeschakeld blijven zolang ze geen voordeel bieden, maar essentieel zijn voor competitieve fitheid in specifieke omgevingscondities. Deze adaptatiemechanismen worden aangestuurd vanuit het bacteriële genoom, dat dynamisch opgevouwen en functioneel georganiseerd is.

Het histon-achtige nucleoïde-structurerende eiwit (H-NS) is een belangrijke regulator van structuur en functie van het bacteriële genoom. Het eiwit is geconserveerd in enterobacteriën. In het algemeen opereert H-NS als een repressor van transcriptie die de expressie van vele genen en operons onderdrukt. De onderdrukking van genexpressie door H-NS is een gevolg van binding van H-NS langs (delen van) genen en operonen. Karakteristiek voor de werking van H-NS is de vorming van nucleofilamenten langs DNA en door het eiwit gevormde DNA-DNA bruggen. Functionele analogen van H-NS zijn gevonden in andere bacteriesoorten: MvaT in de *Pseudomonas*-familie, Lsr2 in actinomyceten en Rok in de *Bacillus*-familie. Deze eiwitten zijn in staat om te compenseren voor de afwezigheid van H-NS in een *hns*- stam als gevolg van vergelijkbare DNA-bindende eigenschappen. Deze eiwitten verschillen in sequentie, maar zijn functioneel homoloog. H-NS-achtige eiwitten zijn wijdverspreid. Bij voorkeur binden ze aan AT-rijk DNA dat is verkregen door horizontale gen-overdracht en schakelen dat uit. Voor wat betreft hun structuur beschikken ze over een vergelijkbare organisatie in functionele domeinen: een N-terminaal domein dat verantwoordelijk is voor dimerisatie en oligomerisatie, een C-terminaal domein dat aan DNA bindt en een 'linker' die de twee domeinen met elkaar verbindt. Als gevolg van deze specifieke domeinorganisatie, is elk van deze vier eiwitten in staat tot brugvorming tussen twee DNA-duplexen. Vermoedelijk is dit noodzakelijk voor de rol van het eiwit in

genregulatie. De structurele en functionele eigenschappen van deze vier architectonische eiwitten (H-NS, MvaT, Lsr2 en Rok) zijn samengevat in **Hoofdstuk 1**.

Regulerende eiwitten die reageren op stress in bacteriën, vooral H-NS-achtige eiwitten, hebben een functie in het uitschakelen van genen; zij treden op als sensoren die reageren op veranderingen in omgevingscondities. Het bacteriële genoom functioneert als een machine die informatie verwerkt in de vorm van signalen uit de omgeving en deze vertaalt in veranderingen in transcriptie van bepaalde genen die nodig zijn voor aanpassing en overleving. Belangrijk in dit proces is de dynamische organisatie van het bacteriële genoom die verandert in reactie op zulke signalen. De expressie van genen die gereguleerd worden door eiwitten uit de H-NS-achtige eiwitfamilie, wordt vaak bepaald door omgevingsfactoren zoals osmolariteit, pH en temperatuur. H-NS-achtige eiwitten kunnen DNA-duplexen bruggen, wat belangrijk is voor genregulatie en het reageren op veranderende omgevingsfactoren. Er is aangetoond dat divalente ionen kunnen zorgen voor de transitie tussen H-NS-DNA-filamenten gevormd langs DNA en gebrugde DNA-H-NS-DNA-complexen. Het schakelen tussen deze twee soorten complexen vormt vermoedelijk de mechanistische basis voor de functie van H-NS-eiwitten in de organisatie van het bacteriële nucleoïde en de regulatie van transcriptie. De resultaten van simulaties van de moleculaire dynamiek van H-NS in eerdere studies suggereren dat de overgang tussen de twee manieren van DNA binden een gevolg is van een conformatieverandering en wel een overgang van een half-open (ook wel gesloten conformatie genoemd) naar een open conformatie onder invloed van van $MgCl_2$. De precieze moleculaire basis van dit fenomeen is echter nog niet duidelijk. In **Hoofdstuk 2** hebben wij een structureel verkorte versie van H-NS, MvaT van *P. aeruginosa*, gebruikt om de relatie tussen structuur en functie in het kader van veranderingen in omgevingsfactoren te onderzoeken. We hebben methoden uit de structuurbiologie en biochemische assays gecombineerd om de veranderingen in structuur van MvaT te onderzoeken, die de overgang van filamentvorming langs DNA naar DNA-bruggende activiteit onder verschillende zout condities aansturen. Deze structuurveranderingen lijken geconserveerd te zijn in de familie van H-NS-achtige eiwitten: een analyse van de primaire structuur van leden van de H-NS-achtige eiwitfamilie

laten zien dat geladen residuen in specifieke gebieden zitten, ondanks de lage overeenkomst in sequentie. Dit suggereert dat de gevoeligheid voor zout wordt veroorzaakt door elektrostatische interacties tussen de N-terminale en DNA-bindende domeinen.

Bacteriofagen komen voor op elke plek waar bacteriën leven. Daarmee vormen ze een constante bedreiging voor bacteriën. Bacteriën en hun bijbehorende bacteriofagen co-evolueren in een constante strijd, waarbij ze van beide kanten verdedigende en aanvallende mechanismes ontwikkelen of aanpassen. De interactie en co-evolutie tussen een bacteriofaag en zijn bacteriële gastheer spelen een belangrijke rol in de ecologische en evolutionaire processen van microbiologische gemeenschappen. Voor succesvolle infectie van een bacterie door een bacteriofaag moet deze zich kunnen verdedigen tegen de afweermechanismes van de bacterie. Bacteriële repressoren van vreemd DNA, zoals H-NS-achtige eiwitten, spelen een belangrijke rol in de verdedigingtegen fagen en in de evolutie van bacteriële genomen door het onderdrukken van de expressie van inkomende genen en genen opgenomen door horizontale genoverdracht. Om de effecten van deze H-NS-achtige eiwitten tegen te gaan codeert het genoom van bacteriofagen voor eiwitten die de uitschakeling van genen door H-NS-achtige eiwitten te niet doen. De *Pseudomonas* faag LUZ24 codeert voor het eiwit Mip dat bindt aan het H-NS-achtige eiwit MvaT van *Pseudomonas aeruginosa.* Voorheen werd aangenomen dat het binden van Mip leidde tot het tegen gaan van de onderdrukking van genen op het LUZ24 faag-DNA door MvaT te remmen. Het mechanisme waarmee Mip de functie van MvaT moduleert was echter nog onduidelijk. In **Hoofdstuk 3** beschrijven we studies aan de DNA-bindende eigenschappen van MvaT en de wijze waarop deze worden beïnvloed door Mip. Ook verduidelijken we hoe Mip en MvaT aan elkaar binden en hoe dat zich vertaalt in veranderingen in het type complexen gevormd tussen MvaT en DNA. Dit onderzoek maakt duidelijk dat Mip een negatieve invloed heeft op de vorming en stabiliteit van het gebrugde MvaT-DNA complex. Dit effect wordt veroorzaakt door de interactie van Mip met zowel het dimerisatie, als het DNA-bindende domein van MvaT. Op basis van deze waarnemingen postuleren we dat het binden van Mip de half-open, niet-bruggende

conformatie van MvaT induceert, wat tot het opheffing leidt van MvaT-gemedieerde onderdrukking van genexpressie.

Rok is een DNA-bindend eiwit dat in hoge concentratie aanwezig is in *Bacillus subtilis* en functionele gelijkenissen vertoont met de H-NS-achtige eiwitten die in veel proteobacteriën voorkomen. Rok bindt langs het hele genoom, met een voorkeur voor A/T-rijk DNA. Dit DNA bevat vaak genen van andersoortige oorsprong, die worden uitgeschakeld door het binden van Rok. Rok lijkt ook betrokken te zijn bij de globale organisatie van het *B. subtilis* genoom. Hoe Rok aan DNA bindt, en op welke manier dit leidt tot het onderdrukken van transcriptie is echter nog onduidelijk. Het is ook nog onbekend of Rok-gemedieerde genonderdrukking geïnduceerd of verminderd kan worden door veranderingen in fysisch-chemische leefcondities, zoals aangetoond voor H-NS-achtige eiwitten. In **Hoofdstuk 4** onderzochten we de DNA-bindingseigenschappen van Rok en bepaalden het effect van fysisch-chemische condities op die eigenschappen. We laten ziet dat Rok een DNA-bruggend eiwit is, vergelijkbaar met de H-NS-achtige eiwitten van *E. coli* (H-NS), *Pseudomonas sp.* (MvaT) en Mycobacteria (Lsr2). Opvallend is dat, ondanks deze gelijkenis, het vermogen van Rok om DNA te bruggen niet afhangt van veranderingen in fysisch-chemische condities. Niet kunnen dienen als een directe sensor van veranderingen in zulke condities onderscheidt Rok van andere H-NS-achtige eiwitten. Dit impliceert het bestaan van andere (eiwit-gemedieerde) mechanismen die gen-uitschakeling door Rok kunnen opheffen, als reactie op veranderingen in fysisch-chemische leefcondities..

In **Hoofdstuk 5** en **Hoofdstuk 6** beschreven we twee methoden die zeer geschikt zijn om de interactie tussen H-NS-achtige eiwitten te analyseren: een DNA-bruggingstest en akoestische krachtspectroscopie (AFS). Deze technieken kunnen helpen bij het verduidelijken van het mechanisme waarme eiwitten of andere moleculen de DNA-bruggende eigenschappen van H-NS-achtige eiwitten moduleren. De DNA-bruggingstest kan bijvoorbeeld gebruikt worden om dit soort eiwitten en andere moleculen te identificeren.

Vooruitzichten

Het ontrafelen van de (dynamische) organisatie van chromosomen in bacteriën is een lange reis. De afgelopen paar decennia zijn er echter technieken ontwikkeld die op de schaal van een volledig genoom ons begrip over bacteriële genoomvouwing verbeteren. Bacteriële DNA-bruggende eiwitten spelen een belangrijke rol in genoomorganisatie en genregulatie doordat zij binden aan bepaalde regionen verspreid over het gehele genoom. De vorming van DNA-DNA-bruggen en de modulatie hiervan, lijken geconserveerd over verschillende soorten. Dit biedt ons nieuwe mogelijkheden om te begrijpen hoe genomen dynamisch georganiseerd worden door vergelijkende functionele en evolutionaire analyses op functioneel geconserveerde DNA-bruggende eiwitten van verschillende soorten. Het belang van het begrijpen van genoomorganisatie en een belangrijke uitdaging ligt in het beter bepalen van de effecten van omgevingsfactoren op lokale vouwing van DNA en het begrijpen hoe deze veranderingen andere nucleïnezuurtransacties beïnvloeden in levende cellen. Vooralsnog zijn door gebruik van biofysische en biochemische technieken structuren bepaald van H-NS en H-NS-DNA-complexen. Dit verduidelijkt *in vitro* hoe deze interacties worden gemoduleerd door lokale veranderingen in fysisch-chemische condities. Het blijft echter nog onduidelijk hoe dit transcriptie *in vivo* beinvloedt. Hoewel we inmiddels begrijpen hoe een enkel nucleïnezuur-associërend eiwit DNA kan organiseren, is het nog niet duidelijk hoe meerdere van dit soort eiwitten tezamen functioneren in de cel. Naast omgevingsfactoren en eiwitpartners, kunnen ook post-translationele modificaties een rol spelen in het moduleren van DNA-bindende eigenschappen en functies van bacteriële nucleïnezuur-associërende eiwitten. Dit aspect van ons begrip over de dynamische organisatie van het bacteriële genoom behoeft echter meer uitgebreid onderzoek.

Het is aangetoond dat bacteriële eiwitten en bacteriofagen kunnen interfereren met de functie van H-NS-eiwitten. Deze interferentie kan gebeuren tijdens elke stap in het proces van vorming van een gebrugd H-NS-DNA complex, oftewel tijdens het initiële binden van DNA, de multimerisatie langs DNA, of het proces van DNA-brugging. Een beter begrip van hoe virale eiwitten H-NS kunnen tegenwerken is nodig om eiwitten of andere moleculen te kunnen ontwerpen die een

faaginfectie kunnen tegengaan. Potentiële toepassingen van zulke moleculen zijn te vinden in de biotechnologische sector, waar faaginfecties een bedreiging vormen voor grootschalige culturen, of in faagtherapie, waar zij voor een verbetering kunnen zorgen in het vermogen van fagen om hun bacteriële gastheer te doden. Door hun brede rol in genregulatie in bacteriën, vormen H-NS-achtige eiwitten potentiële targets voor medicijnen tegen bacteriële infecties. Om zulke ontwikkelingen te realiseren is het van belang om goed te begrijpen hoe de activiteit van H-NS-achtige eiwitten wordt gemoduleerd op een moleculair en mechanistisch niveau.

LIST OF PUBLICATIONS

1. **Qin, L**, Ben Bdira, F. & Dame, R. T. Mechanism of anti-repression of *Pseudomonas aeruginosa* H-NS family protein MvaT by the phage protein Mip. *Manuscript in preparation*.

2. **Qin, L.**, Erkelens, A. M., Markus, D. & Dame, R. T. (2019). The *B. subtilis* Rok protein compacts and organizes DNA by bridging. *bioRxiv*, 769117.

3. **Qin, L**, Ben Bdira, F., Sterckx, Y. G., Volkov, A. N., Vreede, J., Giachin, G., van Schaik, P., Ubbink, M. & Dame, R. T. (2020). Structural basis for osmotic regulation of the DNA binding properties of H-NS proteins. *Nucleic Acids Research*, 48(4), 2156-2172.

4. **Qin, L**, Erkelens, A. M., Ben Bdira, F. & Dame, R. T. (2019). The architects of bacterial DNA bridges: a structurally and functionally conserved family of proteins. *Open Biology*, 9(12), 190223.

5. Paiva, A. M. O., Friggen, A. H., **Qin, L.**, Douwes, R., Dame, R. T. & Smits, W. K. (2019). The bacterial chromatin protein HupA can remodel DNA and associates with the nucleoid in *Clostridium difficile*. *Journal of Molecular Biology*, *431*(4), 653-672.

6. Lin, S. N.*, **Qin, L.***, Wuite, G. J. & Dame, R. T. (2018). Unraveling the Biophysical Properties of Chromatin Proteins and DNA Using Acoustic Force Spectroscopy. In Bacterial Chromatin (pp. 301-316). Humana Press, New York, NY. (Co-first author).

7. van der Valk, R. A., **Qin, L.**, Moolenaar, G. F. & Dame, R. T. (2018). Quantitative Determination of DNA Bridging Efficiency of Chromatin Proteins. In Bacterial Chromatin (pp. 199-209). Humana Press, New York, NY.

8. Boudreau, B. A., Hron, D. R., **Qin, L**., van der Valk, R. A., Kotlajich, M. V., Dame, R. T. & Landick, R. (2018). StpA and Hha stimulate pausing by RNA polymerase by promoting DNA–DNA bridging of H-NS filaments. *Nucleic Acids Research*, *46*(11), 5525-5546.

9. van der Valk, R. A., Vreede, J., **Qin, L.**, Moolenaar, G. F., Hofmann, A., Goosen, N. & Dame, R. T. (2017). Mechanism of environmentally driven conformational changes that modulate H-NS DNA-bridging activity. *Elife*, 6, e27369.

10. **Qin, L.**, Wu, Y., Liu, Y., Chen, Y. & Zhang, P. (2014) Dual Effects of Alpha-Arbutin on Monophenolase and Diphenolase Activities of Mushroom Tyrosinase. *PLOS ONE* 9(10): e109398.

CURRICULUM VITAE

Born in Liaoning province, China   24 March 1990

Bachelor of Science: Bioengineering and Technology   2008-2012

Dalian Polytechnic University - Liaoning, China

Master of Science: Chemical Engineering and Technology, Biochemistry   2012-2015

Beijing University of Chemical Technology - Beijing, China

Ph.D.: Molecular Biology and Biochemistry   2015-2019

Under supervision of Dr. Remus Th. Dame

Dynamic organization of bacterial chromatin by DNA bridging proteins

Leiden University – The Netherlands